Role of apolipoprotein MIC26 in mitochondrial and metabolic disorders

Inaugural-Dissertation

zur Erlangung des Doktorgrades
der Mathematisch-Naturwissenschaftlichen Fakultät
der Heinrich-Heine-Universität Düsseldorf

vorgelegt von

Melissa Lubeck
aus Recklinghausen

Düsseldorf, März 2024

aus dem Institut für Biochemie und Molekularbiologie I
der Heinrich-Heine-Universität Düsseldorf

Gedruckt mit der Genehmigung der
Mathematisch-Naturwissenschaftlichen Fakultät der
Heinrich-Heine-Universität Düsseldorf

Berichterstatter:

1. Prof. Dr. rer. nat. Andreas S. Reichert
2. Prof. Dr. rer. nat. Hadi Al-Hasani

Tag der mündlichen Prüfung: 15.05.2024

When you open the door
toward openness and
transparency a lot of people
will follow you through.

KIRSTEN GILLIBRAND

Table of contents

1 Summary 6
2 Abbreviations 7
3 Introduction 8
3.1 Mitochondria - the hubs of cellular metabolism 8
3.2 Metabolic diseases, the metabolic syndrome, and insulin resistance 9
3.2.1 Metabolism and its diseases 9
3.2.2 Insulin resistance 10
3.2.3 Insulin signaling and cellular mechanisms inducing insulin resistance 10
3.3 Mitochondrial energy generation and the contribution to disease development 13
3.3.1 Oxidative phosphorylation 13
3.3.2 TCA cycle and the three major mitochondrial fuels 14
3.3.3 Defects of mitochondrial catabolic processes in metabolic pathophysiology 16
3.4 Mitochondrial dynamics and their influence on cellular energy balance 18
3.4.1 Mitochondrial fusion and fission 18
3.4.2 Mitochondrial dynamics in cellular fuel adaptation 20
3.4.3 Mitochondrial dynamics and metabolic diseases 21
3.5 Mitochondrial ultrastructure and intramitochondrial dynamics 23
3.5.1 Unique features of mitochondrial ultrastructure and their regulators 23
3.5.2 Defective mitochondrial ultrastructure and diseases 24
3.6 Mitochondrial MICOS complex in disease development 26
3.6.1 MICOS complex and its role in mitochondrial ultrastructure maintenance 26
3.6.2 Role of the MICOS complex in metabolic disease development 27
3.6.3 Identification of apolipoprotein MIC26 with contradicting observations 28
3.6.4 The biological role of MIC26 and its involvement in metabolic diseases 29
4 Aim of the project 32
5 Results 33
5.1 MIC26 and MIC27 are bona fide subunits of the MICOS complex in mitochondria and do not exist as glycosylated apolipoproteins 33
5.2 A X-linked nonsense APOO/MIC26 variant causes a lethal mitochondrial disease with progeria-like phenotypes 58
5.3 Mitochondrial Apolipoprotein MIC26 is a metabolic rheostat regulating central cellular fuel pathways 69
6 Discussion 140
6.1 MIC26 regulates key cellular metabolic pathways 140
6.2 Loss of MIC26 reduces cellular glutamine usage 141
6.3 MIC26 mediates the glycolytic switch 142
6.4 MIC26 induces nutrient dependent rewiring of lipid and cholesterol biosynthesis 144
6.5 MIC26 abnormalities are detrimental for human health 147
6.6 Conclusion and outlook 150

7 References 152
8 Publications 171
8.1 Lubeck *et al.*, 2023a 171
8.2 Peifer-Weiß *et al.*, 2023 171
8.3 Lubeck *et al*., 2023b 171
9 Acknowledgements 172
10 Eidesstattliche Versicherung 173

1 Summary

Abnormal functioning and regulation of the human metabolism is implicated in the onset of severe life hampering diseases including type 2 diabetes or non-alcoholic fatty liver disease. Mitochondria are pivotal for essential metabolic functions including cellular lipid metabolism, energy generation and fuel utilization. Malfunctioning mitochondria result in disease development and progression. As the primary metabolic hub mitochondria utilize the majority of cellular nutrients and orchestrate their conversion or storage in form of energy. Moreover, mitochondrial dysfunction has a prominent role in obesity and insulin resistance. Mitochondrial ultrastructure and intra- as well as intermitochondrial dynamics are essential features for proper mitochondrial functionality. Mitochondrial ultrastructure, especially in terms of cristae formation, maintenance, and dynamics, are dependent on the MICOS complex, comprising seven mammalian subunits: MIC60, MIC10, MIC13, MIC19, MIC25, MIC27 and MIC26. MIC26, hypothesized to have a dual cellular localization within the mitochondrial MICOS complex and the cellular secretory pathway, has been implicated to play a role in diabetes and lipid metabolism.

This dissertation aimed to elucidate the cellular localization, function of MIC26 and its contribution to metabolic diseases. Using multiple biochemical assays, cell and tissue models, including *MIC26* KO cell lines, MIC26 overexpression, along with immunoblot analysis and mass spectrometry, we demonstrate that MIC26 is exclusively present as a 22 kDa protein in the mitochondria. Additionally, we showed that MIC26 plays an essential physiological role. Patients, harboring a $MIC26^{E178X}$ mutation, inducing protein truncation, developed progeria-like phenotypes, resulting in lethality. Biological evaluation unveiled mitochondrial ultrastructure defects, abnormalities in mitochondrial dynamics and protein instability. To elucidate the functional role of MIC26 regulating cellular metabolism under nutritional overload conditions, a multi-omics study supported by validation using various assays in wildtype and *MIC26* KO cells under normo- and hyperglycemia, was conducted. We identified MIC26 to be a crucial cellular regulator of mitochondrial metabolite usage. MIC26 exerts a suppressive influence on glycolysis, cholesterol, and lipid metabolism under normoglycemic conditions, with opposing effects under hyperglycemia. Deleting *MIC26* resulted in nutritional independent rewiring of cellular glutamine usage and oxidative phosphorylation. Overall, we identified MIC26 as a metabolic rheostat, maintaining mitochondrial ultrastructure, leading to stability of several mitochondrial metabolite transporters while it directly impacts lipid and cholesterol metabolism by harboring a lipid binding domain, resulting in alterations of lipid metabolism. We hypothesize that balanced MIC26 levels and functionality are required to prevent excess fat accumulation under normal nutrient conditions and to mediate energy storage under nutrient overload. Thus, we propose MIC26 to be essential to prevent obesity and the development of metabolic diseases.

2 Abbreviations

AA	Amino acids
AMP/ADP/ATP	Adenosinmono-/di-/triphosphate
Apo	Apolipoprotein
BAT	Brown adipose tissue
Cer	Ceramide
CJ	Crista junction
CI-CV	Complex I – Complex V
CL	Cardiolipin
CM	Cytoplamic mitochondria
CoA	Coenzyme A
DAG	Diacylglycerides
DNA	Desoxyribonucleic acid
ER	Endoplasmic reticulum
ETC	Electron transport chain
$FADH_2$	Flavin adenine dinucleotide
FAO	Fatty acid oxidation
FBS	Fetal bovine serum
FFA	Free fatty acids
H	Hyperglycemia
HFD	High fat diet
HGPS	Hutchinson-Gilford Progeria Syndrome
IBM	Inner boundary membrane
IM	Inner membrane
IMS	Intermembrane space
IR	Insulin resistance
KG	Ketoglutarate
KI	Knockin
KO	Knockout
LD	Lipid droplets
MELAS	Mitochondrial encephalopathy, lactic acidosis and stroke like episodes
MetS	Metabolic syndrome
MIB	Mitochondrial intermembrane space bridging complex
MICSO	Mitochondrial contact site and cristae organizing system
mRNA	Messenger RNA
mtDNA	Mitochondrial DNA
N	Normoglycemia
NADH	Nicotinamide adenine dinucleotide
NAFLD	Non-alcoholic fatty liver disease
OA	Oleic acid
OAA	Oxaloacetate
OM	Outer membrane
OXPHOS	Oxidative phosphorylation
PDM	Peridroplet mitochondria
RET	Reverse electron transfer
RNA	Ribonucleic acid
ROS	Reactive oxygen species
SkM	Skeletal muscle
TAG	Triacylglycerides
TCA cycle	Tricarboxylic acid cycle
T2D	Type 2 Diabetes
VLDL	Very low-density lipo particles
WAT	White adipose tissue
WT	Wildtype

3 Introduction

3.1 Mitochondria - the hubs of cellular metabolism

Mitochondria are organelles fulfilling a diversity of cellular functions in a tissue- and cell-type-dependent manner. Besides the most known mitochondrial function, oxidative phosphorylation (OXPHOS), mitochondria are involved in amino acid (AA) metabolism, cellular calcium homeostasis, heat generation, iron-sulfur (Fe/S) cluster synthesis, steroidogenesis, lipid oxidation and synthesis, reactive oxygen species (ROS) formation, apoptotic signaling and several more.

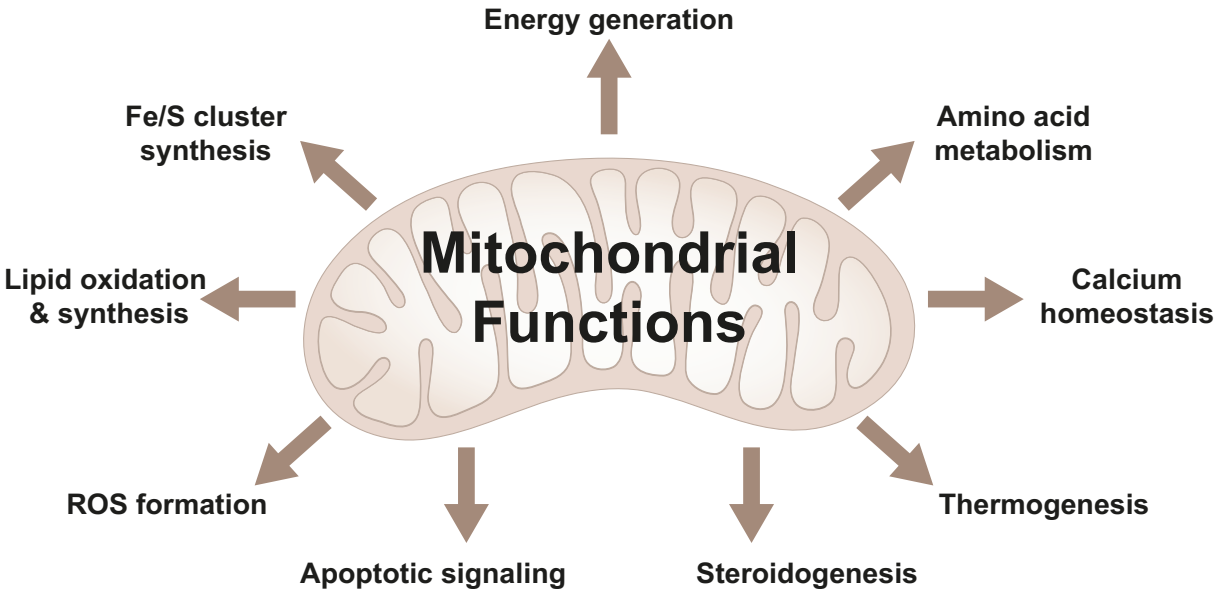

Figure 1: Mitochondria fulfill a diverse range of essential cellular metabolic functions. The most prominent role is mitochondrial energy generation via OXPHOS. Among others, they are involved in cellular anabolic and catabolic pathways, cellular signaling (e.g. via ROS formation) cellular apoptosis or thermogenesis.

Mitochondria harbor a unique structure comprised of a double membrane consisting of an outer membrane (OM) and an inner membrane (IM). The IM can be distinguished in the inner boundary membrane (IBM) running parallel to the OM and cristae, which are invaginations of the IM. Mitochondria are inter- and intramitochondrial highly dynamic organelles (Kondadi & Reichert, 2024). Multiple mitochondria within a cell form a dynamic network through fusion and fission processes. These highly dynamic features are essential for maintaining mitochondrial quality control, including the clearance of damaged mitochondria (termed mitophagy) and the distribution of mitochondrial content. Additionally, mitochondria exhibit dynamic behavior with cristae merging and splitting within a single mitochondrion (Kondadi et al., 2020). Moreover, mitochondria directly interact with other cellular organelles (interorganellar dynamics) such as the endoplasmic reticulum (ER) and lipid droplets (LD). Due to their essential role in key

metabolic pathways, mitochondrial dysfunction is associated with various diseases like diabetes, metabolic syndrome (MetS), and cardiovascular disorders. A major contribution to these disease developments is the impairment of the highly interconnected mitochondrial metabolic functions, dynamics, and ultrastructure.

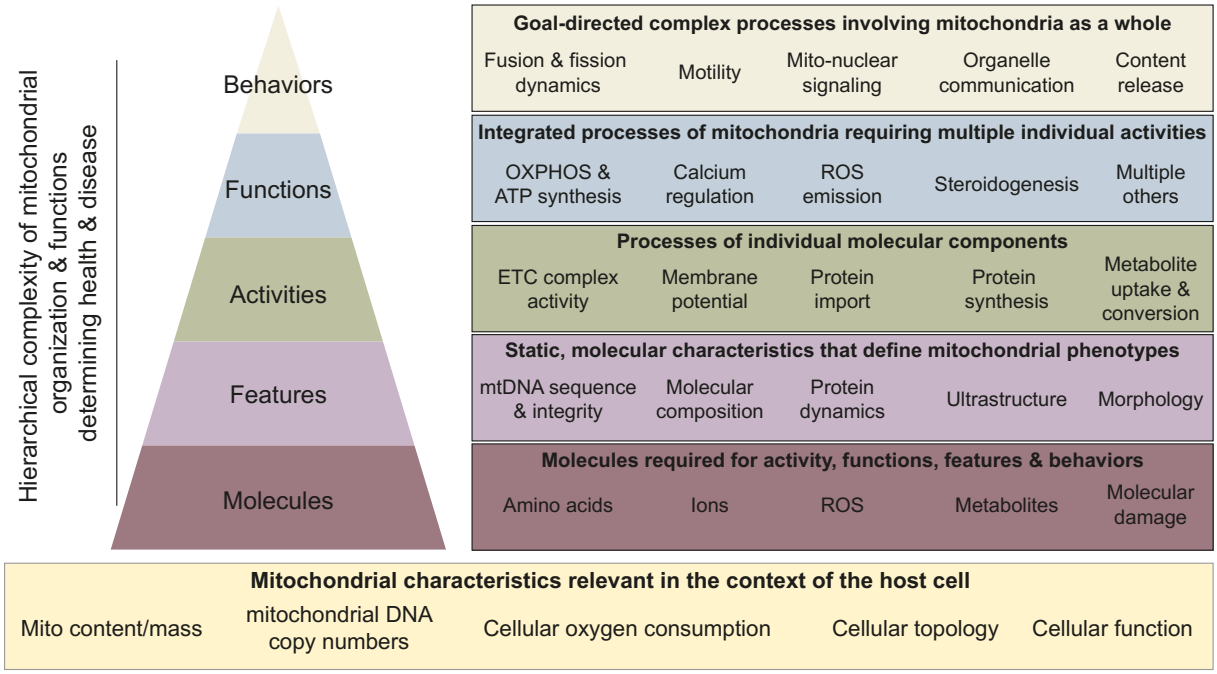

Figure 2: Hierarchical complexity of mitochondrial organization, including behaviors, functions, activities, features, and molecules as well as cell type dependent characteristics, that are required for proper cellular functioning. Malfunctioning of these highly interconnected processes lead to severe disease development. Figures adapted and modified from (Monzel et al., 2023).

3.2 Metabolic diseases, the metabolic syndrome, and insulin resistance

3.2.1 Metabolism and its diseases

Metabolic diseases are a major burden of public health causing several million deaths annually. Over the last two decades, the global prevalence of these diseases has risen, with the highest spikes observed in countries with a high socio-demographic index (Chew et al., 2023). Metabolic diseases are generally classified as disorders affecting different processes of the body's metabolism. Metabolism comprises a cluster of whole-body biochemical processes that utilize food to convert and produce energy, to preserve life and normal body functioning. Metabolism can be categorized into anabolism and catabolism. Anabolism defines the buildup of macromolecules such as proteins, lipids, or polysaccharides, while catabolism breaks down polymers into their simpler forms, providing building blocks for cell growth, repair, and energy generation (Judge & Dodd, 2020). Consequently, metabolic diseases lead to either the accumulation or the deficiency of crucial metabolites and macromolecules, disrupting energy generation and overall body functioning. Metabolic diseases can be distinguished into inherited

or acquired dysfunctions of metabolism. Inherited metabolic disorders often manifest in newborns and children, while acquired metabolic diseases typically appear in adults (Essig, 2020). A prevalent acquired metabolic disorder is MetS also known as syndrome X. MetS is attributed to various metabolic abnormalities, including insulin resistance (IR), hyperinsulinemia, hypertension, dyslipidemia, and central obesity (Saklayen, 2018). In addition to epigenetic and genetic factors, high-risk behaviors such as overeating diets rich in uncomplex sugars and saturated free fatty acids (FFA) coupled with a lack of physical activity contribute to the development of MetS. An un-intervened progression of the MetS often leads to the development of type-2-diabetes (T2D) and cardiovascular diseases. Among the various complex mechanisms driving MetS development, chronic inflammation, neurohormonal activation, and IR were identified as essential players in disease progression (Fahed et al., 2022).

3.2.2 Insulin resistance

IR is classified as an impaired response of the target tissue to stimulation with insulin. Insulin, an endocrine peptide hormone, is produced and secreted by pancreatic β-cell islets. In a healthy organism, food intake stimulates insulin secretion from pancreatic β-cell, followed by the stimulation of primary target tissues to regulate the body's glucose homeostasis. The primary tissues involved include the liver, skeletal muscle (SkM), and white adipose tissue (WAT). In WAT and the SkM insulin binding to the insulin receptor (InsR) stimulates glucose uptake from the bloodstream, converting it to energy or storing it as glycogen for later fasting periods. In the liver, insulin binding to its receptor mediates the downregulation of glycogenolysis and gluconeogenesis, preventing the production and secretion of glucose. In the WAT lipogenesis is induced by insulin stimulation while lipolysis is inhibited. Upon IR the previously described actions of insulin are hampered, leading to increased blood glucose levels and compensatory overproduction of insulin (hyperinsulinemia) to counteract hyperglycemia (M. Li et al., 2022). Nowadays, based on the complexity of interorgan crosstalk and its involvement in several cellular metabolic pathways, the development of IR is not fully understood. However, an increasing epidemiology of people suffering from IR has increased scientific research interest in the last few decades.

3.2.3 Insulin signaling and cellular mechanisms inducing insulin resistance

After insulin is secreted from the pancreatic β-cells, it can bind to the α-subunit of the target tissue plasma membrane-localized InsR, which belongs to the class of receptor tyrosine kinases. Upon binding and receptor dimerization, tyrosine residues in the intracellular chain of the β-subunit undergo autophosphorylation (Kasuga et al., 1982; Yunn et al., 2023). This process sequentially recruits and activates downstream target proteins, including insulin

receptor substrate isoforms (IRS), phosphatidylinositol-3-phosphate kinase (PI3K), and protein kinase B isoforms (PKB/AKT). AKT has more than 100 described cellular substrates, which is contributing to the diversification of tissue-dependent pathway activations in insulin signaling (M. Li et al., 2022). For example, phosphorylation of AKT can induce GLUT4 translocation to the plasma membrane in SkM and WAT, directly affecting cellular glucose uptake (Wang et al., 1999). It further stimulates glycogen production by blocking glycogen synthase kinase 3 (GSK3), and thus indirectly activating glycogen synthase (GS), mainly occurring in the liver and SkM but also in WAT at lower rates (Cross et al., 1997; Summers et al., 1999). Additionally, AKT directly activates the transcription factor forkhead box O1 (FOXO1), leading to the inhibition of hepatic gluconeogenesis under insulin stimulatory conditions (Dong et al., 2008; Puigserver et al., 2003). *De novo* lipogenesis is induced by AKT via the activation of the sterol regulatory element binding protein 1c (SREBP-1c) and the phosphorylation of ATP citrate lyase (ACLY) (Li et al., 2010; Martinez Calejman et al., 2020). Further, lipolysis is suppressed by AKT through insulin-dependent activation of phosphodiesterase 3B (PDE3B) and increased cyclic AMP (cAMP) to AMP conversion. Decreased cAMP levels reduce PKA activity, leading to increased activation of hormone-sensitive lipase (HSL) activity and thus suppressed lipolysis (DiPilato et al., 2015; Lindh et al., 2007).

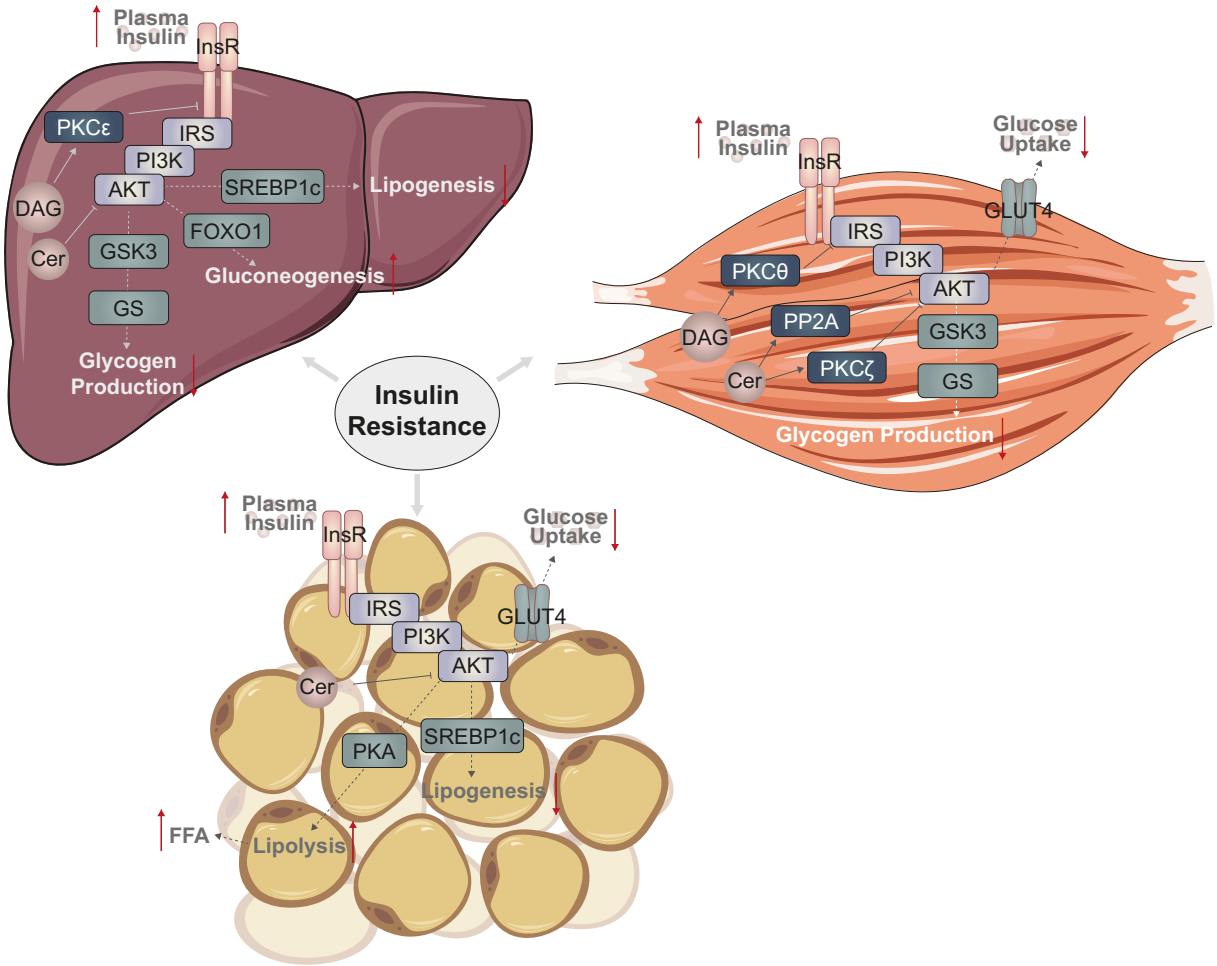

Figure 3: Model of IR associated metabolic defects in liver, SkM, and WAT. Red arrows indicate metabolic changes upon IR. Adapted and modified from (da Silva Rosa et al., 2020).

However, under IR conditions, insulin stimulation is unable to induce the previously described signaling pathways. This results in decreased glucose uptake in SkM and WAT, increased gluconeogenesis in the liver, and increased lipolysis in WAT, among other metabolic dysregulations (Petersen & Shulman, 2018).

One of the leading factors in the pathogenesis of IR is cellular lipotoxicity. Lipotoxicity is defined as the ectopic accumulation of lipids and lipid derivatives such as FFA, diacylglycerides (DAGs), triacylglycerides (TAGs), and ceramides. Early studies in this research field showed a correlation between the accumulation of DAG, plasma membrane translocation of protein kinase Cθ (PKCθ) in SkM, and PKCε and PKCθ in the liver, and IR or T2D in mice and patients (Petersen & Shulman, 2018). Different genetically modified animal models showed that PKCε/PKCθ translocation is indeed dependent on the cellular level of *sn*-1,2-DAG. Mice models with a hepatic deletion of phosphatidic acid phosphatase lipin-1 or lipin-2, responsible for the formation of *sn*-1,2-DAG from phosphatidic acid reduced hepatic DAG formation and ameliorated hyperglycemia and IR (Ryu et al., 2009; Ryu et al., 2011). Conversely, overexpression of lipin-2 in the liver impaired glucose tolerance and increased DAG and TAG content (Ryu et al., 2011), while SkM lipin-1 transgenic mice developed obesity and IR (Phan & Reue, 2005). Subsequent investigations showed a direct inhibitory phosphorylation site of IRS for PKCθ (Li et al., 2004) and InsR for PKCε (Petersen et al., 2016) linking the accumulation of *sn*-1,2-DAG levels to the downregulation of insulin signaling.

In addition to the interference posed by the accumulation of DAGs on insulin signaling, there have been reports indicating a correlation between elevated ceramide levels and IR. Ceramide is a sphingolipid that plays an essential role in forming the epidermal permeability barrier and is one of the major lipids in the cell membrane. Furthermore, ceramides play an essential role in signal transduction (Alrbyawi et al., 2019). Total ceramide accumulation was shown to induce IR, prompting different studies to investigate specific effects on the liver, SkM, and WAT (Holland et al., 2007). In a large study comparing obese and lean human subcutaneous as well as visceral WAT biopsies, different ceramide species, including C14:0, C16:0, C16:1, C18:1, and others, as well as the expression of ceramide synthase 6 (CerS6) but not CerS1-5, were significantly upregulated. A *CerS6* knockout (KO) mouse model showed improved whole-body glucose metabolism upon a high fat diet (HFD) feeding, with reduced serum insulin concentrations, improved insulin sensitivity, and glucose tolerance compared to respective littermates (Turpin et al., 2014). A further study showed that several species of ceramides were upregulated comparing lean to obese people but only C16-ceramide species were significantly higher comparing obese patients with T2D to obese humans without diabetes in subcutaneous WAT. This was referred to an upregulation of the *de novo* pathway generating C16-ceramides (Chathoth et al., 2022). However, further studies showed that in SkM, C18:0 ceramide species were the predominant form induced by HFD in mice. This correlated with an increased

expression in CerS1, which catalyzes C18:0 ceramides synthesis. In line, *CerS1* deficiency protected from diet-induced obesity and IR pathogenesis (Turpin-Nolan et al., 2019). In the liver, it was shown that ceramide content increases with IR in obese patients (Razak Hady et al., 2019). Different studies provided mechanistic insight into the interference of ceramides with insulin signaling cascade proteins. Already in 2000, it was shown that the accumulation of ceramides can cause reduced AKT S473 phosphorylation (Schubert et al., 2000). Studies showed that ceramides can directly interact with PP2A and also stimulate the dissociation of PP2A and I2PP2A, leading to PP2A plasma membrane translocation, which, in turn, can then lead to the dephosphorylation of AKT (Bharath et al., 2015; Dobrowsky et al., 1993). On the other hand, it was shown that AKT plasma membrane translocation is blocked via ceramide activation of PKCζ (Powell et al., 2003).

In summary, IR induced by e.g. lipotoxicity from DAG or ceramide accumulation contributes to the development of several severe diseases, such as the onset of T2D with fasting and postprandial hyperglycemia and non-alcoholic fatty liver disease (NAFLD) (M. Li et al., 2022). Consequently, investigating how IR develops on a cellular mechanistic level has become a crucial research topic. A major target of interest in the pathogenesis of IR and other metabolic diseases is mitochondrial dysfunction.

3.3 Mitochondrial energy generation and the contribution to disease development

3.3.1 Oxidative phosphorylation

OXPHOS is the mitochondrial process that converts and stores energy in the form of adenosine triphosphate (ATP) using a multimeric system consisting of the electron transport chain (ETC) complexes I-IV (CI - CIV) and the F_1F_O-ATP synthase (ATPase/complex V), primarily located in the cristae. The ETC transfers electrons from NADH and $FADH_2$ to oxygen and simultaneously pumps protons from the mitochondrial matrix to the mitochondrial intermembrane space (IMS) to establish an electrochemical gradient. This gradient drives the ATPase activity, transporting protons back to the matrix and simultaneously producing ATP from adenosine diphosphate (ADP). In detail, CI or NADH dehydrogenase is a large enzyme complex with 44 subunits encoded by nuclear as well as mitochondrial DNA (mtDNA). It assembles with the help of various assembly factors first into six main modules, termed N, Q, ND1, ND2, ND4, and ND5 modules, and subsequently forms a L-shaped 1 MDa complex (Baradaran et al., 2013; Guerrero-Castillo et al., 2017). CI transfers two electrons per NADH molecule to ubiquinone (Coenzyme Q/CoQ), resulting in the pumping of four protons from the mitochondrial matrix to the IMS (Galkin et al., 1999). CII or succinate dehydrogenase (SDH) contains out of four subcomplexes with two hydrophilic head subunits facing the mitochondrial matrix named SDHA and SDHB, and two hydrophobic IM anchored subunits termed SDHC

and SDHD (Du et al., 2023). CII is involved in the oxidation of succinate to fumarate in the tricarboxylic acid (TCA) cycle and transfers electrons from $FADH_2$ to ubiquinone during OXPHOS. However, CII has no proton pumping activity. Following, ubiquinol (reduced ubiquinone) travels from CI or CII to CIII, referred to as Cytochrome *c* (Cyt*c*) reductase. CIII activity requires the assembly of dimers ($CIII_2$). After dimerization $CIII_2$ simultaneously reduces two Cyt*c* molecules by transferring two electrons delivered from ubiquinol to each Cyt*c*. The electron translocation from CoQ to Cyt*c* goes along with the shift of four protons from the mitochondrial matrix to the IMS and is termed the Q-cycle. CIV or Cytochrome *c* oxidase (COX) transfers in total four electrons from four Cyt*c* molecules to one O_2 molecule. The reduced oxygen reacts with two protons, forming water. Simultaneously, four protons are pumped to the IMS (Osellame et al., 2012). CV or the F_1F_O-ATP synthase was shown to assemble in rows of dimeric supercomplexes at the tips of mitochondrial cristae, contributing to their membrane curvature (Strauss et al., 2008). It consists of the F_1-subcomplex located in the mitochondrial matrix and the membrane bound F_0-subcomplex, while both subunits are connected by a peripheral stalk (Signes & Fernandez-Vizarra, 2018). The F_O-subunit has a barrel like structure that allows protons to travel from the IMS to the F_1-subunit down their electrochemical gradient. These protons force the rotation of the turbine-like F_1-subunit which catalyzes the binding of ADP and phosphate, subsequently converting it to ATP (Strauss et al., 2008).

Overall, mitochondria use the OXPHOS machinery comprised of five large complexes to produce energy in the form of ATP by transforming NADH, $FADH_2$, and O_2. NADH and $FADH_2$ are mainly supplied via the TCA cycle.

3.3.2 TCA cycle and the three major mitochondrial fuels

The TCA cycle, also called the citric acid cycle or Krebs cycle, is a mitochondrial multistep process that converts metabolites via a series of chemical reactions to release NADH and $FADH_2$. Therefore, it serves as the metabolic hub for energy generation via aerobic cellular respiration (OXPHOS) (Alabduladhem & Bordoni, 2023). In addition to delivering molecules for ATP production during phases of energy demand and thus contributing to cellular catabolism, TCA cycle intermediates can also serve as important precursors for the biosynthesis of cellular macromolecules such as lipids or proteins, but also cholesterol, and hence contribute to cellular anabolism (MacLean et al., 2023). The TCA cycle consists of eight enzymes, most of which are capable of performing reversible conversions. In brief, the TCA cycle starts with the reaction that combines acetyl-coenzyme A (CoA) with oxaloacetate (OAA) using citrate synthase to produce citrate. Following this, aconitase converts citrate to its isomers, first aconitate and then isocitrate. The subsequent reaction performed by isocitrate dehydrogenase, generates α-ketoglutarate (α-KG) and releases one carbon dioxide (CO_2) molecule. Furthermore, this step reduces NAD^+ to NADH + H^+, which fuels mitochondrial CI.

Next, α-KG is converted to succinyl-CoA again under the generation of NADH + H^+ and CO_2. This conversion also requires one molecule of CoA, which is, however, directly released again in the next step by converting succinyl-CoA to succinate by succinyl-CoA synthetase. The reaction from succinate to fumarate is mediated by the enzymes of CII succinate dehydrogenase (Chapter 3.3.1). Fumarate is then converted to malate via the enzyme fumarase. The last step is again a NADH-generating reaction forming malate to OAA via malate dehydrogenase. OAA can then, together with acetyl-CoA, start a new cycle (Alabduladhem & Bordoni, 2023). However, not all TCA cycle intermediates are continuously converted into their respective subsequent intermediates. They are also used as precursors for cataplerotic processes (Inigo et al., 2021). OAA, for example, can be used mainly in the liver to generate glucose via gluconeogenesis in fasting phases. Citrate can be exported from mitochondria and converted to acetyl-CoA, which serves as a precursor for lipid anabolism or cholesterol biosynthesis. OAA and α-KG can be converted to aspartate or glutamate, respectively, and serve as metabolites for AA or nucleotide production (Alabduladhem & Bordoni, 2023). On the other hand, also different intermediates than OAA and acetyl-CoA can feed the TCA cycle. Glutamine has been shown to be an essential source of the majority of carbon atoms in different TCA cycle metabolites (DeBerardinis et al., 2007; Fan et al., 2013). Glutamine is first converted to glutamate via glutaminase (GLS) and then produces α-KG. AA catabolism can also fuel the TCA cycle via fumarate or succinyl-CoA and acetyl-CoA. OAA and acetyl-CoA can both be generated from pyruvate. Pyruvate is the end product of cellular glycolysis, which uses glucose as a starting material, is the anaerobic form of cellular energy production (Arnold & Finley, 2023). Pyruvate is transferred into mitochondria via the mitochondrial pyruvate carrier 1 and 2 (MPC1/2). Following this, pyruvate carboxylase can generate OAA in an ATP-dependent reaction. Acetyl-CoA is generated from pyruvate by the pyruvate dehydrogenase complex. Acetyl-CoA is also derived from mitochondrial β-oxidation, the process that degrades fatty acids. Long-chain fatty acid oxidation requires active mitochondrial import via the carnitine shuttle. Firstly, fatty acyl-carnitine is formed by the OM enzyme carnitine acetyltransferase I (CPT1) and transported into the mitochondrial matrix via the carnitine translocase protein (CACT). There, CPT2 catalyzes the reconversion to fatty acyl-CoA. CPT1 was shown to be the rate-limiting step of mitochondrial β-oxidation, and the regulation of CPT1 occurs on the one hand at a transcriptional level via the peroxisome proliferator activated receptors (PPAR) or allosterically via inhibition through the fatty acid synthesis intermediate malonyl-CoA (Lopez-Vinas et al., 2007). After the import of acyl-CoA, mitochondrial β-oxidation orchestrates the degradation of FFA in a sequential and iterative manner, ultimately yielding acetyl-CoA molecules. Initially, acyl-CoA are transformed into trans-2-enoyl-CoA through the enzymatic activity of acyl-CoA dehydrogenase, while simultaneously converting FAD to $FADH_2$. Subsequently, enoyl-CoA hydratase catalyzes the

formation of L-3-hydroxyacyl-CoA. This compound serves as the substrate for the subsequent reaction, where L-3-hydroxyacyl-CoA dehydrogenase facilitates the generation of 3-ketoacyl-CoA and NADH. In the final step of the process, β-ketothiolase cleaves off an acetyl-CoA molecule, which is then directed into the TCA cycle. Meanwhile, the remaining FFAs, shortened by two carbon units, can enter further cycles of β-oxidation, culminating in the complete metabolic conversion of the entire FFA into acetyl-CoA (Adeva-Andany et al., 2019). Defects of mitochondrial energy production have a range of tremendous effects on pathophysiology of metabolic diseases.

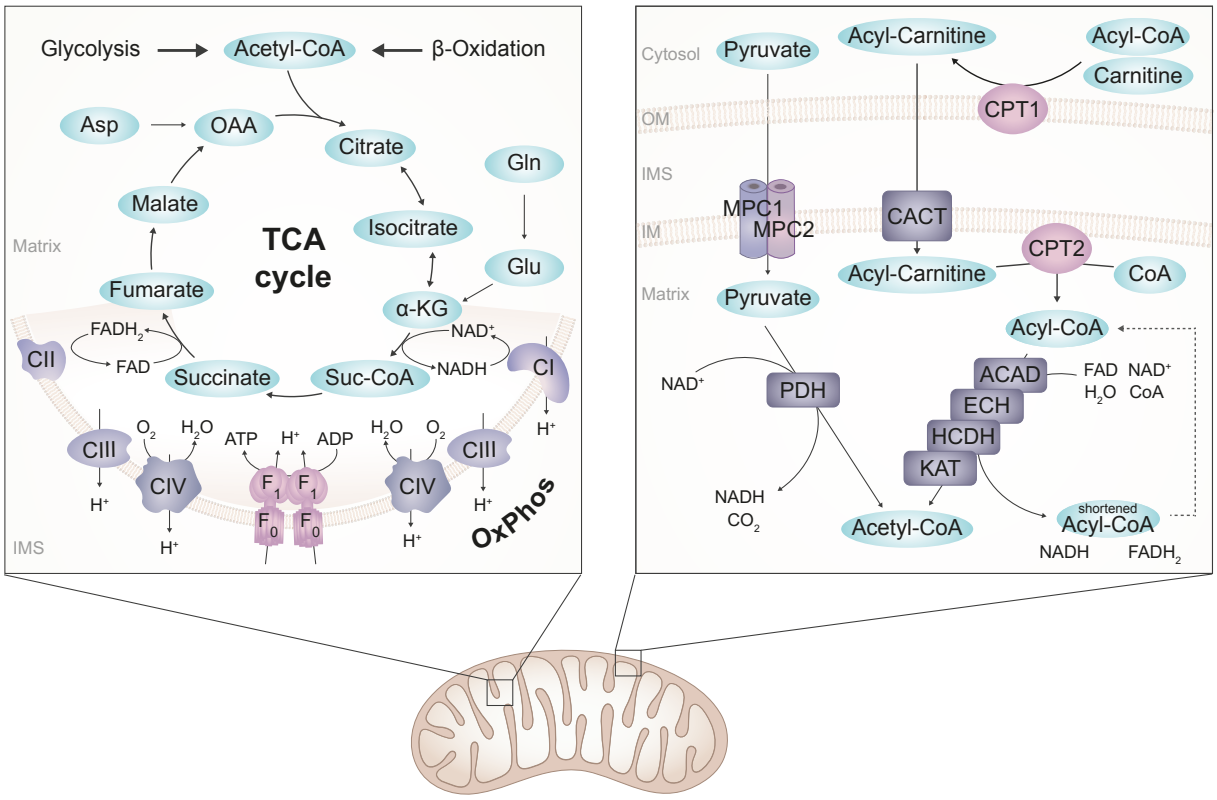

Figure 4: Mitochondrial catabolic processes for energy generation. Left panel representing mitochondrial energy conversion starting from acetyl-CoA undergoing conversion through the TCA cycle and producing NADH and $FADH_2$ which fuel mitochondrial respiration via the electron transport chain complexes leading to generation of an electrochemical gradient which drives the F_0F_1-ATPase that produces ATP. Right panel shows the generation of TCA cycle starting material acetyl-CoA from pyruvate and FFA through mitochondrial β-oxidation. Adapted and modified from (Martinez-Reyes & Chandel, 2020).

3.3.3 Defects of mitochondrial catabolic processes in metabolic pathophysiology

Defective mitochondrial energy generation is a common feature of the pathophysiology of metabolic diseases. The number of identified genes linked to energy generation disorders has extensively increased in the last decades and has either a direct effect on mitochondrial energy generation, inducing a disruption in the generation of the OXPHOS complexes, or a secondary

effect by an upstream effect that feeds mitochondrial OXPHOS (Frazier et al., 2019). The metabolic consequences of defective mitochondrial catabolic processes include a reduction of cellular energy, an increase in cellular ROS, or an accumulation or lack of essential cellular metabolites (Smeitink et al., 2006). ROS is a collective term defining oxygen-containing highly reactive species, including, for example, superoxide (O_2^-), hydrogen peroxide (H_2O_2), or hydroxyl radicals ($OH^\cdot$), with diverse effects on cell biology defined as oxidative stress (Li et al., 2016). Physiological levels of oxidative stress are required for cellular signaling, while immense oxidative stress leads to cellular oxidative damage to biomolecules such as DNA or lipids (Sies et al., 2017). Mitochondria are a major source of ROS generation. Here, ROS is generated via ETC CI and CIII by leakage of electrons during electron transfer to molecular oxygen (Hinkle et al., 1967; Kussmaul & Hirst, 2006; Turrens et al., 1985). Also, reverse electron transfer (RET) due to decreased activity of e.g., CIII and CIV or a highly reduced CoQ pool with a high proton motive force (Δp) leads to a backflow of electrons to CI, which in turn produces superoxide (Murphy, 2009). In general, impaired mitochondrial function is highly associated with increased formation of ROS (Guo et al., 2013). Consequently, resulting oxidative damage has been shown to be an underlying cause of multiple metabolic disorders including neurodegeneration (e.g., Parkinson's or Alzheimer's disease), cancer, or IR and T2D (Lennicke & Cocheme, 2021). Obese and insulin resistant humans, as well as animal models, represented higher SkM H_2O_2 levels, suggesting a role in the development of IR (Anderson et al., 2009; Bonnard et al., 2008). The underlying consequences are presumably relatable to increased metabolic flux and reduced expression of antioxidant enzymes leading to unphysiological ROS formation (Rosen et al., 2001). Excess nutrient conditions force leakage of electrons during OXPHOS (Han, 2016). On a cellular level, different mechanisms of how ROS interferes with insulin signaling have been reported. Firstly, high ROS levels can activate c-Jun amino-terminal kinase (JNK) (Shen & Liu, 2006), which has been shown to negatively regulate insulin action on IRS1 (Aguirre et al., 2000; Lee et al., 2003). Thus, mice with *JNK1* depletion were protected from HFD-induced obesity, inflammation, and IR (Hirosumi et al., 2002). Furthermore, I kappa B kinase beta (IKK beta) and the NF-kappa B pathway (Lingappan, 2018) are reported to be activated in inflammatory and oxidative stress conditions, which also lead to the pathogenesis of IR (Cai et al., 2005; Shoelson et al., 2003; Sinha et al., 2004; Yuan et al., 2001).

Besides that, ROS is known to induce damage by oxidizing essential biomolecules, leading to increased formation of dysfunctional mitochondria and improper function of mitochondria to meet cellular energy demand and deal with overload of cellular fuels (Sangwung et al., 2020). To further validate the effect of ROS on insulin signaling inhibition, several studies used antioxidants to reduce cellular ROS levels and, by that, were able to prevent HFD-induced obesity (Anderson et al., 2009; Bonnard et al., 2008). Besides ectopic ROS level generation,

dysfunction of mitochondrial lipid conversion was correlated to the development of lipotoxicity and thus connected to IR development via cellular development of lipotoxicity. Mitochondria are the primary cellular hub that breaks down FFA to acetyl-CoA and converts them to energy via the TCA cycle. An elevation of plasma FFA due to nutritional overload or dysfunction of storing capacity in WAT leads to increased FFA uptake into e.g., SkM or liver. If mitochondria cannot fully compensate increased supplementation of FFA using FAO, either due to an overload of other nutrients or due to malfunctioning of mitochondria, FFA accumulate and lead to increased lipid storage or increased formation of DAGs and ceramides, which have a direct inhibitory effect on cellular insulin signaling as described before (Chapter 3.2.3) (Zhang et al., 2010). On a cellular level, studies extensively investigated the effect of CPT1 on the development of IR. CPT1 protein activity is the rate limiting step for mitochondrial β-oxidation, (Chapter 3.3.2). Studies showed that deletion of *CPT1* or etomoxir-induced inhibition of CPT1 (Dobbins et al., 2001; Kim et al., 2014) led to increased lipid accumulation and pathology of IR, while overexpression of CPT1 could prevent lipid-induced IR (Bruce et al., 2009; Perdomo et al., 2004). Also, reducing cellular malonyl-CoA level by hepatic overexpression of malonyl-CoA decarboxylase (MCD), leading, on the one hand, to decreased lipid content, and on the other hand, to a reduced feedback inhibition of CPT1, increased FAO and ameliorated whole-body IR (An et al., 2004). However, improving FAO to rescue IR is under high debate. Assuming that mitochondria switch fuel preferences in order to meet fuel availability and maintain energy demand, upregulation of FFA usage could lead to a decrease in glucose consumption and, thus, cellular glucose uptake, which would further promote blood hyperglycemia (Randle, 1998; Randle et al., 1963; Roden, 2004). Also, it was shown that inhibiting FAO by e.g., the reduction of MCD promoted glucose oxidation and IR (Bouzakri et al., 2008; Koves et al., 2008). Also, contradicting the previously reported observations, different studies reported an enhanced FAO rate in hearts of commonly used insulin-resistant and obesity-prone mouse models termed db/db and ob/ob mice (Buchanan et al., 2005; Mazumder et al., 2004) and Wistar rats (Turner et al., 2007). An increased FAO was recently attributed to a fragmented mitochondrial phenotype contributing to an increased activity of CPT1 (Ngo et al., 2023).

3.4 Mitochondrial dynamics and their influence on cellular energy balance

3.4.1 Mitochondrial fusion and fission

Mitochondria are highly dynamic cellular organelles that undergo continuous fusion and fission events to adapt to cellular and mitochondrial demands (Westermann, 2012). The term ‘fusion’ describes the process where two mitochondria merge their content and membranes, resulting in one mitochondrion, while ‘fission’ describes the opposing mechanism where one mitochondrion segregates into two separate mitochondria (Scott & Youle, 2010).

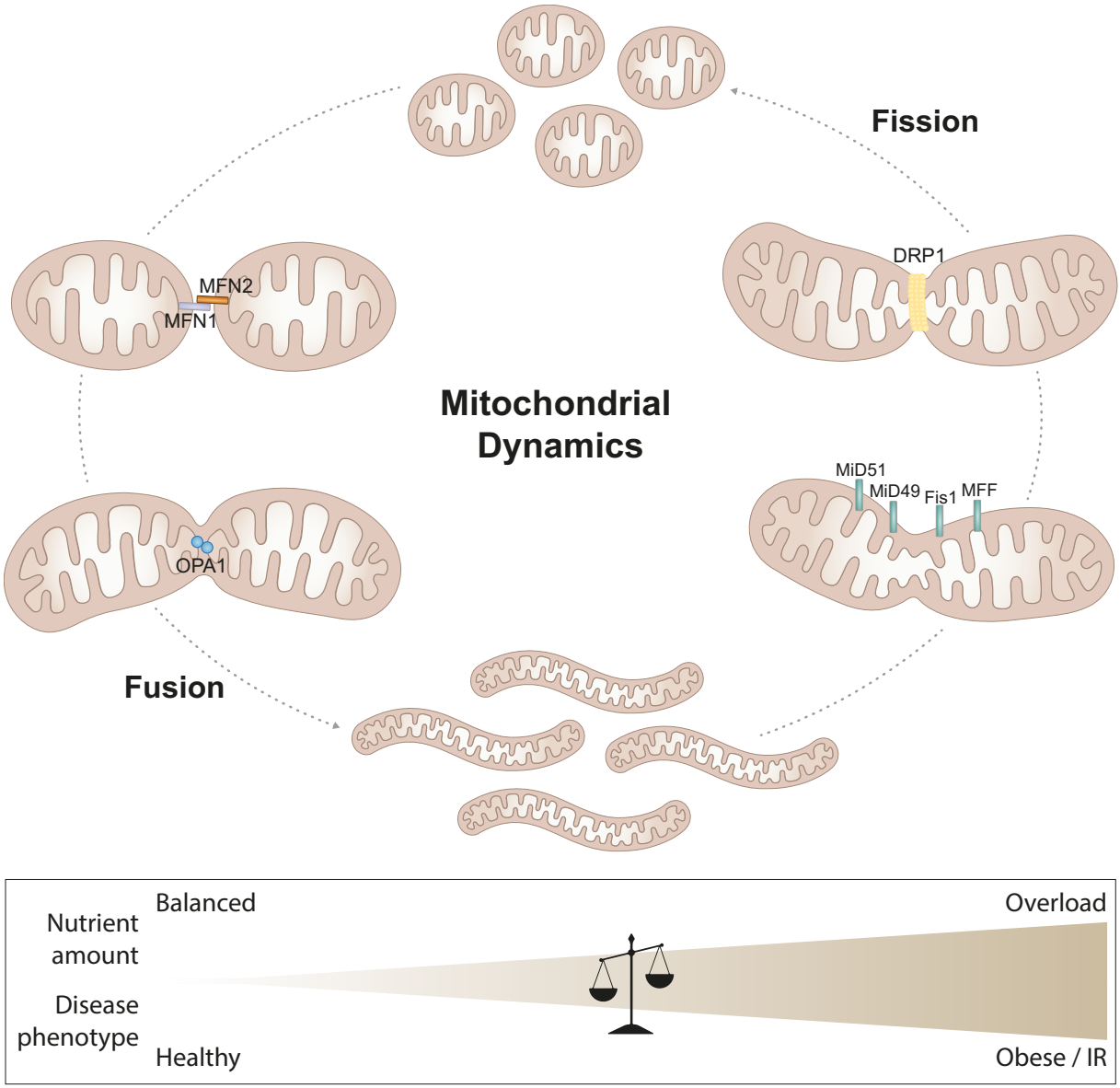

Figure 5: Mitochondrial dynamics describes the cellular process of mitochondrial fusion and fission mediated via MFN1/2 and OPA1 or MiD49, MiD51, MFF, Fis1 and DRP1 respectively. Nutrient overload as well as obese and IR phenotypes have been associated with shifting the balance of fusion and fission to an increased fragmented mitochondrial phenotype.

Mitochondrial dynamics depends on and contributes to multiple physiological circumstances. Nutritional load has been shown to shift the balance between fragmented and elongated mitochondrial phenotypes, while malfunctioning of the essential key regulators mediating fusion or fission has been attributed to disease development (Kondadi & Reichert, 2024).

The key regulators of mitochondrial fusion and fission are members of the dynamin GTPase protein family. To undergo mitochondrial fission, mammalian dynamin-related protein 1 (DRP1) localizes to the mitochondrial OM. This localization and recruitment have been shown to be mediated by a series of OM bound adapter proteins, including fission 1 (Fis1) (Mozdy et al., 2000; Yoon et al., 2003), the mitochondrial fission factor (MFF) (Otera et al., 2010) and the

mitochondrial dynamics proteins of 49 kDa and 51 kDa (MiD49 and MiD51) (Dikov & Reichert, 2011; Loson et al., 2013; Palmer et al., 2011). Following this, DRP1 oligomerizes at the mitochondrial OM and forms a spiral- and ring- like structure tying off the mitochondrion (Basu et al., 2017). Subsequently, DRP1 orchestrates scission using GTP hydrolysis (Michalska et al., 2018).

Mitochondrial fusion is regulated by mitofusin 1 and 2 (MFN1, MFN2) and optic atrophy-1 (OPA1) in mammals. MFN1 and MFN2 have been shown to have diverse but also redundant functions (Chen et al., 2003; Eura et al., 2003), including the mediation of OM fusion. Here, they tether two mitochondria by binding to another MFN protein from an adjacent mitochondrion and enable fusion via GTP hydrolysis (Tilokani et al., 2018). IM fusion is mediated via OPA1, which is active in multiple forms containing high molecular weight isoforms termed long-OPA1 (L-OPA1) and different cleavage products, resulting from YMEL1 and OMA1 proteolytic activity, called short-OPA1 (S-OPA1) (Anand et al., 2014; Duvezin-Caubet et al., 2007; Tilokani et al., 2018).

3.4.2 Mitochondrial dynamics in cellular fuel adaptation

Mitochondrial fusion and fission have been demonstrated to be essential in mitochondrial content exchange, specific disposal of damaged mitochondrial sections (mitophagy), and adaptation to cellular fuels and energy demands (Chan, 2020). A network consisting mainly of elongated and interconnected mitochondria is termed a tubular mitochondrial morphology, while shortened and separate mitochondria are referred to as a fragmented mitochondrial morphology. A shift to a fragmented mitochondrial phenotype can occur either through genetic abnormalities in mitochondrial proteins or the previously described fusion and fission mediators, or due to excess nutrient conditions.

Starving conditions lead to a more elongated and tubular mitochondrial network (Liesa & Shirihai, 2013). While increased fragmentation, as a consequence of genetically induced mitochondrial defects, is presumably an effect to induce damage control of dysfunctional mitochondria, excess nutrient conditions also induce mitochondrial fragmentation but do not increase mitophagy (Bach et al., 2005; Galloway et al., 2014; Molina et al., 2009). Hence, obesity has been linked to a more fragmented mitochondrial phenotype. Initially, mitochondrial fragmentation was considered to be a phenotype of exclusively malfunctioning mitochondria. However, a recent study connected increased mitochondrial fragmentation as a cellular mechanism to induce increased FAO rates and, hence, a physiological adaptive relevance (Ngo et al., 2023). Mitochondrial fragmentation results in increased membrane curvature, inducing conformational changes in CPT1. These rearrangements decrease malonyl-CoA binding ability and, thus, the blocking capability of the protein, increasing the rate-limiting step reaction of FAO (Ngo et al., 2023).

In conclusion, mitochondrial morphology has been attributed to fuel oxidation capacity. However, cellular fuel status can also influence mitochondrial morphology. Consequently, mitochondrial dynamics and nutrient availability have been attributed to play a crucial role in metabolic disease pathophysiology.

3.4.3 Mitochondrial dynamics and metabolic diseases

Alterations of mitochondrial dynamics mainly increased mitochondrial fission or decreased mitochondrial fusion deriving from variations in protein abundances of the mitochondrial dynamics' regulators have been extensively reported in disease development (Chen et al., 2023; Yapa et al., 2021). An overview of investigated deletion phenotypes of fusion and fission proteins in mice is listed in table 1.

Table 1: Summary of phenotypes linked to gene deletion of fusion and fission mediators adapted from (Kondadi et al., 2019).

Gene deletion	Function	Model System	Phenotype
Mfn1 & *Mfn2* DKO	OM fusion	Whole body KO in mice	Embryonic lethality
Mfn1 KO, *Mfn2* KO, *Mfn1* & *Mfn2* DKO	OM fusion	Mammalian cell lines	Decreased growth rate, reduced oxygen consumption & membrane potential
Mfn1 & *Mfn2* DKO	OM fusion	SkM specific KO in mice	Growth defects and lethality after 6-8 weeks, mtDNA depletion
Mfn1 & *Mfn2* DKO	OM fusion	Cardiac specific KO in mice	Cardiomyopathy
Drp1 KO	OM fission	Whole body KO in mice	Embryonic lethality
Drp1 KO	OM fission	Mammalian cell lines	Apoptosis delayed, membrane potential and ATP levels reduces
Drp1 KO	OM fission	SkM and heart specific KO in mice	Neonatal lethality due to dilated cardiomyopathy
Opa1 KO	IM fusion	OPA1 heterozygous mice	Decreased cardia output, onset of blindness
Opa1 KO	IM fusion	Inducible SkM specific KO	Reduced body weight, muscle atrophy and weakness
Mff KO	OM fission	Whole body KO	Lethality after 13 weeks of age, heart failure due to cardiomyopathy

In detail, increased DRP1 activity was associated with NAFLD (Galloway et al., 2014), Parkinson's, Alzheimer's or Huntington's disease (Cho et al., 2009; Feng et al., 2021) (Shirendeb et al., 2012), IR, and diabetes (Galloway et al., 2012; Jheng et al., 2012), and cancer (Ferreira-da-Silva et al., 2015; Kashatus et al., 2015). Decreased expression or altered activity of MFN1, MFN2, or OPA1 was related to heart failure (Wai et al., 2015), cardiomyopathy (Hu et al., 2019), Alzheimer's or Huntington's disease (Shirendeb et al., 2011; Wang et al., 2009), autosomal dominant optic atrophy (Lenaers et al., 2012), cancer (S. Li et al., 2022; Zhang et al., 2013), Charcot-Marie-Tooth disease (Braathen et al., 2010), or also obesity (Bach et al., 2003). Especially, alterations in MFN2 were reported in several studies to induce IR or being altered in T2D. In muscle biopsies from obese and T2D patients, MFN2 mRNA and protein levels were decreased (Bach et al., 2005; Hernandez-Alvarez et al., 2010). Chronic exercise led to an upregulation of MFN2 protein levels in healthy subjects, while this effect did not occur in T2D patients (Hernandez-Alvarez et al., 2010). In mice, liver-specific depletion of *Mfn2* caused expected mitochondrial fragmentation and showed impaired glucose and insulin tolerance in standard and HFD fed mice, in line with decreased insulin signaling in the liver and the SkM. Detailed investigations correlated *Mfn2* deficiency to increased ROS generation as well as extensive ER stress, which led to interference with insulin signaling (Sebastian et al., 2012). In WAT from HFD fed WT mice *Mfn2* mRNA levels were monitored over a time period of 12 weeks and represented a constant diminishing trend compared to a standard diet fed mice (Mancini et al., 2019). Also, in WAT biopsies comparing obese to healthy subjects *Mfn2* mRNA level were significantly reduced. Adipose specific *Mfn2* deletion caused increased adiposity, increased plasma leptin and blood glucose level and IR upon HFD feeding. Increased fat mass accumulation upon *Mfn2* KO and HFD feeding was in line with increased PPAR-γ mRNA, which is reported to induce storage of FFA and promotes adipogenesis. *Vice versa*, they represented that pharmacologically induced PPAR-γ downregulation increased MFN2 expression, again giving evidence for a bilaterally regulated link between overnutrition and mitochondrial dynamics. Overexpression of MFN2 in rats fed a HFD was able to improve SkM IR by increased GLUT4 plasma membrane translocation presumably induced via increased activation of AMP-activated protein kinase (AMPK) (Kong et al., 2013). A further study overexpressing MFN2 in rats' liver also observed improved insulin signaling and related the observed effects to decreased suppressor of cytokine signaling 3 (SOCS3) activity, which was further demonstrated to inhibit insulin signaling (Gan et al., 2013; Kawaguchi et al., 2004; Rui et al., 2002).

In conclusion, mitochondrial dynamics within a cell is crucial for the maintenance of cellular metabolic pathway regulations and is highly sensitive to either nutritional status or genetic changes in key regulators of mitochondrial fusion and fission. However, altered mitochondrial dynamics is often observed and linked to models of mitochondrial ultrastructure abnormalities.

3.5 Mitochondrial ultrastructure and intramitochondrial dynamics

3.5.1 Unique features of mitochondrial ultrastructure and their regulators

Mitochondrial ultrastructure is a unique cellular architecture with highly different phenotypes depending on cell and tissue type, cellular energy requirements, or nutritional conditions. The two parallel running mitochondrial phospholipid membrane bilayers, termed OM and IM, have different properties and functions. The smooth OM displays a barrier between the mitochondrial IMS and the cellular cytosol and is rich in phosphatidylcholine (PC), phosphatidylinositol (PI), sphingomyelin (SM), and cholesterol (Horvath & Daum, 2013). The OM contains several protein(complexes) that enable the diffusion of ions, small molecules, and metabolites, such as porins and voltage-dependent anion channels (VDACs), import of proteins e.g., translocase of the outer membrane (TOM) complex or mitochondrial signaling e.g. MFNs (Vitali et al., 2020), and others.

The IM, consisting of the IBM and the cristae, separates the IMS and mitochondrial matrix and mainly contains phosphatidylethanolamine (PE), phosphatidylglycerol (PG), and cardiolipin (CL) (Horvath & Daum, 2013). The IBM contains e.g., several transporters, including the nucleotide exchanger e.g., adenine nucleotide transporters (ANTs), essential metabolite exchanger e.g., citrate/malate exchanger CIC or AA transporters e.g., the glutamate/aspartate exchanger ARALAR (Ruprecht & Kunji, 2020). Cristae house the OXPHOS complexes (Vogel et al., 2006), which have been described to be stabilized through the high content of cardiolipin within the mitochondrial IM (Pfeiffer et al., 2003; Zhang et al., 2002). The OM and IM are connected via the mitochondrial intermembrane space bridging complex (MIB), while the formation of cristae from the IBM is induced, maintained, and regulated via the mitochondrial contact site and cristae organizing system (MICOS) complex (Huynen et al., 2016). The mammalian MIB complex includes the proteins metaxins (MTX1/2/3), sorting and assembly machinery 50 (SAMM50), and the DnaJ heat shock protein family member C11 (DNAJC11), as well as MIC60 and MIC19. The MICOS complex was first discovered in yeast and includes seven proteins in the mammalian organism, with two described subcomplexes: MIC60/MIC25/MIC19 and MIC10/MIC26/MIC27, with MIC13 stabilizing the MIC10 subcomplex (Anand et al., 2016; Harner et al., 2011; Hoppins et al., 2011; Naha et al., 2023; Rabl et al., 2009; von der Malsburg et al., 2011).

The MICOS complex is located at the neck of the cristae leading to the formation of pore like structures termed cristae junctions (CJs) with an average diameter of 28 nm (Frey & Mannella, 2000). Depletion of MICOS subunits has been shown to result in the loss of CJs (Anand et al., 2020; Kondadi et al., 2020a; Koob et al., 2015b; Stephan et al., 2020). CJs are proposed to act as diffusion barriers for proteins, metabolites, and ions (Frey et al., 2002; Mannella et al., 2013). Cristae have been shown to be able to possess different membrane potentials within one mitochondrion and have an overall higher membrane potential compared to the IBM (Wolf

et al., 2019). Like mitochondrial dynamics (Chapter 3.4), intramitochondrial dynamic processes have been described (Kondadi et al., 2020). Using live-cell-stimulated emission depletion (STED) super-resolution nanoscopy, dynamics between individual cristae, termed cristae merging and splitting events, have been shown (Kondadi et al., 2020a; Kondadi et al., 2020b). These continuous cycles of membrane remodeling are highly dependent on the MICOS complex subunits as well as the mitochondrial bioenergetic state with a prominent role of ADP/ATP metabolite exchange (Golombek et al., 2024).

Consequently, the maintenance of proper mitochondrial ultrastructure is an essential requirement to fulfill mitochondrial and cellular metabolic functions.

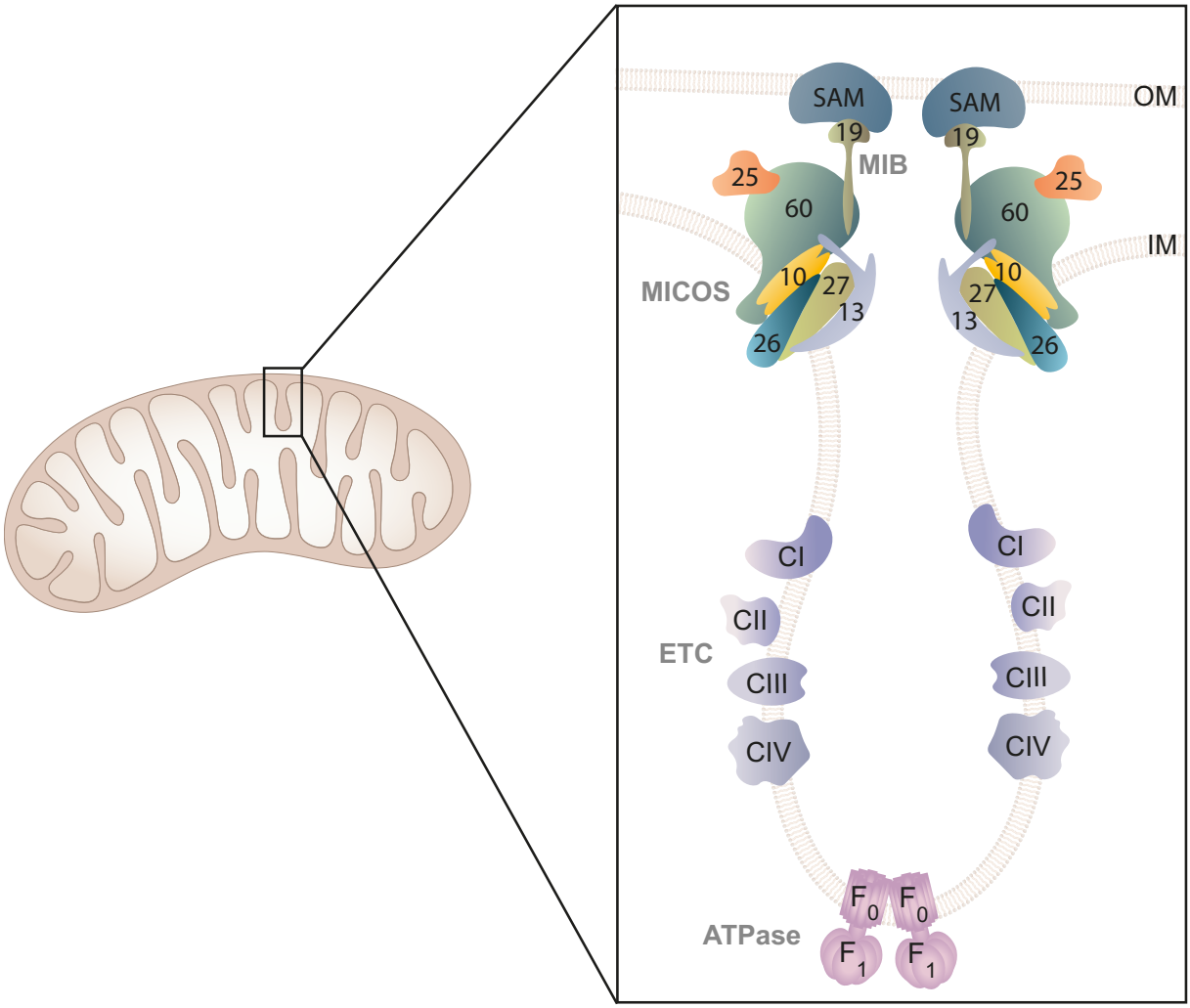

Figure 6: Formation and maintenance of mitochondrial cristae, which harbor the OXPHOS is mediated by the MICOS complex including the seven mammalian subunits MIC13, MIC10, MIC26, MIC27, MIC25, MIC19 and MIC60. Further MIC19 and MIC60 are involved in establishing mitochondrial IM and OM contact sites with SAM (MIB complex).

3.5.2 Defective mitochondrial ultrastructure and diseases

Aberrances in mitochondrial ultrastructure have been described to occur in a range of different diseases. These mitochondrial ultrastructure abnormalities can derive from both changes in

mitochondrial and nuclear-encoded proteins, alterations in phospholipid composition, and cellular nutritional status (Acehan et al., 2007; Brandt et al., 2017; Gao et al., 2010; Habersetzer et al., 2013; Perez-Hernandez et al., 2022). Reported diseases with defective mitochondrial ultrastructure include heart failure (Bugger et al., 2010), liver dysfunction (Meroni et al., 2022), mitochondrial encephalopathy, lactic acidosis, and stroke-like episodes (MELAS) (Takemura et al., 2016), Barth syndrome (Acehan et al., 2007), Huntington's, Alzheimer's, and Parkinson's diseases (Barsoum et al., 2006; Nakamura et al., 2011; Vanisova et al., 2022), as well as obesity and diabetes (Choo et al., 2006; Li et al., 2014; Vanhorebeek et al., 2005).

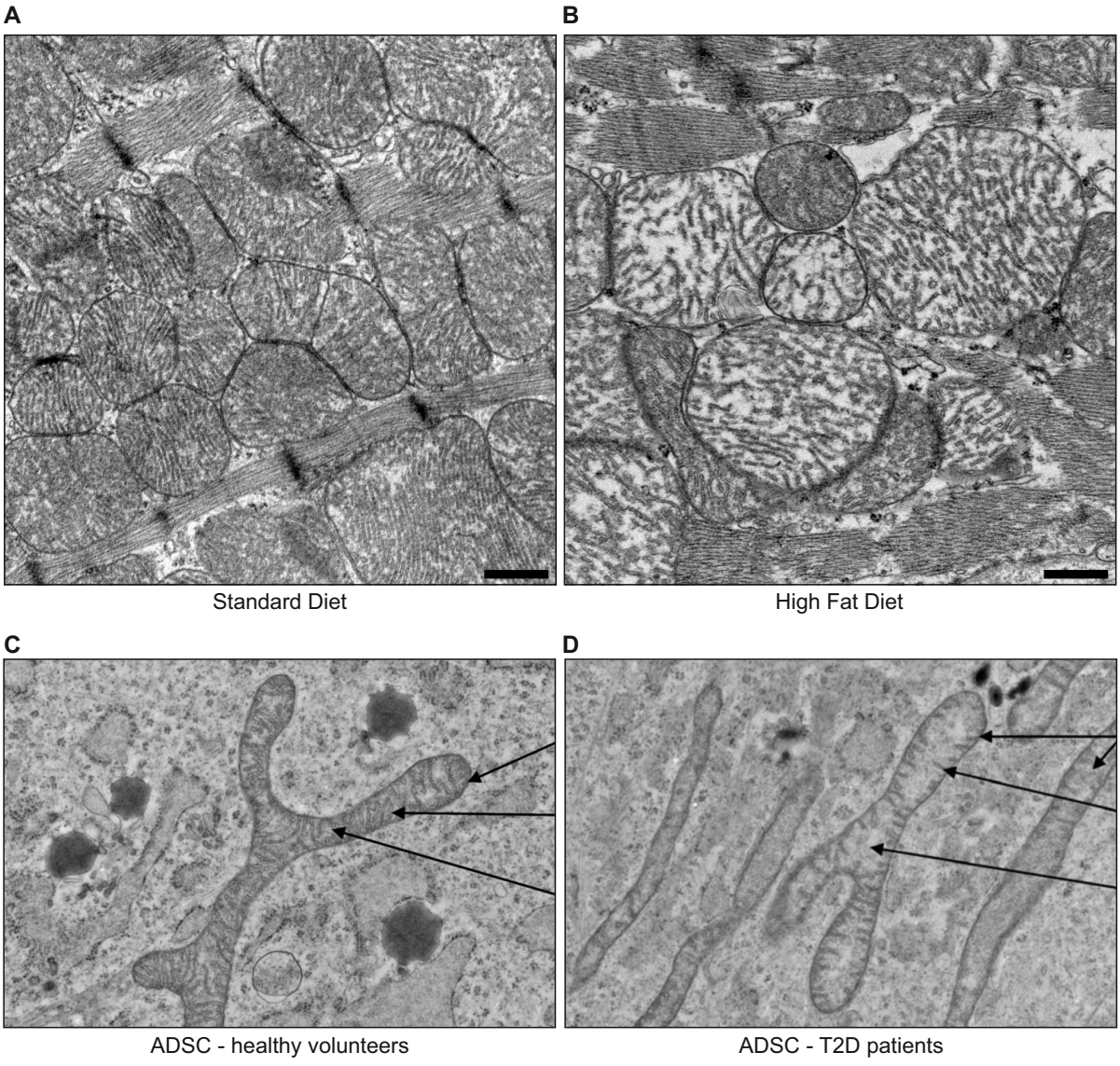

Figure 7: Electron microscopy images of heart mitochondria from standard diet (A) and HFD (B) fed C57BL/6J mice (tissue samples fixed with 3 % glutaraldehyde) representing mitochondrial ultrastructural changes induced by nutritional overload. Scale bar represents 500 nm. Unpublished data, EM accomplished by Andrea Borchardt. Electron microscopy images from adipose derived mesenchymal stem cells (ADSC) from healthy volunteers (C) and patients with T2D (D) from (Horiguchi et al., 2021).

In detail, diabetic mice show a phenotype of swollen mitochondria, with decreased electron density in electron micrographs and shortened and reduced number of cristae (Shao et al., 2023). The reduction of cristae and CJs directly affects mitochondrial OXPHOS and presumably leads to changes in ADP/ATP generation, ROS formation and in general cellular metabolism. Thus, a functional MICOS complex, responsible for the formation and maintenance of cristae and CJs, is an interesting target to study for cellular metabolism, overall mitochondrial function, and disease development.

3.6 Mitochondrial MICOS complex in disease development

3.6.1 MICOS complex and its role in mitochondrial ultrastructure maintenance

The MICOS complex is highly conserved throughout different species and includes the seven mammalian subunits: MIC60/IMMT, MIC19/CHCHD3, MIC25/CHCHD6, MIC13/QIL1, MIC10/MINOS1, MIC27/APOOL, and MIC26/APOO (Anand et al., 2021). Among several cell lines and tissues, depletion of MIC60 and MIC10 represented the strongest phenotypes of loss of CJs and abnormal cristae formation (Kondadi et al., 2020a; Rabl et al., 2009; Stephan et al., 2020). Depletion of MIC60 leads to a loss or reduction of all other MICOS subunits. Loss of MIC10 and MIC13 results in reduced steady state protein levels of the MIC10/MIC26/MIC27 subcomplex and abrogates proper MICOS assembly. However, depletion of the protease YMEL1 has been able to rescue MICOS assembly and CJ formation in *MIC13* KO cell lines, suggesting a protective function of MIC13 from proteolytic MIC10 degradation (Naha et al., 2023). MIC27 and MIC26 are part of the MIC10 subcomplex and share 37 % amino acid identity in humans. Double deletion of MIC27 and MIC26 in the mammalian HAP1 cell line as well as deletion of the *Dmel* gene which shares sequence homology with mammalian MIC26 and MIC27 in Drosophila, caused severe mitochondrial ultrastructure changes, while single deletions had cell-type-specific effects (Anand et al., 2020; Wang et al., 2020). HeLa *MIC26* or *MIC27* knockdown and KO did not affect cristae morphology and mitochondrial ultrastructure (Ott et al., 2015; Stephan et al., 2020). However, in HAP1 and 143B depleted cell lines, strong mitochondrial abnormalities have been observed (Anand et al., 2020; Koob et al., 2015b; Weber et al., 2013). Furthermore, an antagonistic protein level regulation of MIC26 and MIC27 has been proposed upon depletion of the respective other protein in different cell lines, which was, however, cell-type-dependent as well (Anand et al., 2020; Koob et al., 2015b; Lubeck et al., 2023). On a functional level, a study proposed MIC10 oligomerization to be regulated via MIC26 and MIC27 in an antagonistic manner with a destabilizing effect of MIC26 and an opposing stabilizing effect of MIC27 (Rampelt et al., 2018). Additionally, MIC27 has been shown to directly bind CL, and *MIC26* deletion caused CL level reduction with a pronounced effect in *MIC26/MIC27* DKO cells (Anand et al., 2020; Weber et al., 2013). Here, the reduction of CL levels was attributed to result in decreased OXPHOS complex assembly and

mitochondrial respiration, showing a direct effect of *MIC26/MIC27* deletion on cellular bioenergetics (Anand et al., 2020). MIC19 has been reported to directly interact with SAMM50 in the OM and MIC60 in the IM and thus is indispensable for the IM and OM contact and stability of mitochondrial structure and function (Tang et al., 2020). MIC25, like MIC19, is a family member of CHCHD proteins and a member of the MIC60 subcomplex. However, MIC25 is not required for MIB complex formation and does not interact with SAMM50 (Utsumi et al., 2018). Loss of MIC25 does not lead to changes in mitochondrial CJs formation and general mitochondrial ultrastructure (Stephan et al., 2020). However, loss of *MIC25* has been described to reduce mitochondrial area and perimeter and increase ROS levels in stem cell derived cardiomyocytes (Hinton et al., 2023).

Overall, nearly all MICOS subunits have been attributed to the mammalian deficiency of CJ formation and proper mitochondrial ultrastructure. Consequently, there is a range of reported and associated metabolic diseases attributed to MICOS subunit defects.

3.6.2 Role of the MICOS complex in metabolic disease development

Aging has been reported to lead to a sequential reduction over time of mRNA levels of MIC60, MIC19, and MIC25 in the cardiac mouse muscle, in line with a highly disrupted mitochondrial ultrastructure (Hinton et al., 2023). Different clinically reported mutations in MIC13/Qil1 have been suggested to cause a severe phenotype of mitochondrial encephalopathy with recurrent liver disease at an early fatal onset (Guarani et al., 2016; Kishita et al., 2020; Russell et al., 2019). Characterization of patient derived SkM and fibroblast biopsies revealed a decrease in protein level of all other MICOS complex subunits compared to healthy control samples, impaired respiratory function, and highly abnormal mitochondrial ultrastructure (Guarani et al., 2016). It was further found that a mutation in MIC13 was correlated with mitochondrial DNA depletion (Kishita et al., 2020).

A further study linked MIC10 to cellular response to bacterial infection with L. monocytogenes (Carvalho et al., 2020). Here, infection caused host cell mitochondrial fragmentation, which was abolished after depletion of MIC10. Patient derived fibroblast with Barth syndrome, having reduced levels of CL caused by mutations in *tafazzin* (*Taz*), showed increased MICOS assembly level (Chatzispyrou et al., 2018). Recently, it was shown that mice with increased expression of MIC19 are protected against obesity and T2D resulting from increasing energy expenditure (Sohn et al., 2023). CD-1 mice showed increased MIC19 protein levels and, in line, increased mitochondrial cristae formation and CI and CII activity in the fasted compared to the fed state, inducing an adaptive mechanism against hepatic steatosis development. Further, mice overexpressing MIC19 showed promoted mitochondrial cristae formation, OXPHOS and FAO, as well as decreased body weight, liver TAG accumulation, and improved fasting blood glucose levels. This shows, on the one hand, that nutrient overload can lead to

abnormal mitochondrial ultrastructure and function but, on the other hand, a possible role of MIC19 MICOS subunit in regulating mitochondrial nutrient-dependent mechanisms with a possible protective effect on disease development. The MICOS subunit MIC60 has been linked to multiple different metabolic diseases among them neurodegenerative diseases such as Parkinson's disease (Deng et al., 2021; Myung et al., 2003; Van Laar et al., 2016; Wang et al., 2008), mitochondrial encephalopathy (Dong et al., 2023), and diabetes (Thapa et al., 2015). Further is has been reported that whole body deletion of *MIC60* is lethal to mice (Feng et al., 2023). Cardiac interfibrillar mitochondria from streptozotocin (STZ) induced diabetic mice showed a significant decrease in MIC60 peptide abundances from proteomics analysis (Baseler et al., 2011). Transgenic MIC60 mice were able to rescue the STZ induced diabetic phenotype and showed improved mitochondrial ultrastructure, decreased ROS levels, increased membrane potential, and decreased lipid peroxidation by-products (Thapa et al., 2015). In mice with IR induced by 16 weeks HFD feeding, proteomics analysis revealed an upregulation of MIC60 and MIC19 in the liver (Guo et al., 2013).

In conclusion, most of the MICOS subunits have been shown to induce metabolic diseases upon protein alterations. Especially a connection to the development of diabetes has been observed in MIC60 and MIC19. Furthermore, a link between abnormalities MIC26 protein level and diabetes and obesity has been described.

3.6.3 Identification of apolipoprotein MIC26 with contradicting observations

MIC26 initially termed apolipoprotein O (ApoO) was first identified in 2003 in the cardiac transcriptome of a dog nutritional model of obesity (Philip-Couderc et al., 2003). Sequence analysis revealed high conservation throughout different mammalian species. A specific polypeptide signature of 22 AA residue repeats forming a pair of α-helices was identified to overlap with the signature of apolipoprotein A1/A4/E family. Subsequently, the newly discovered protein was termed apolipoprotein O in a chronological manner of apolipoprotein nomenclature. In contradiction to a calculated molecular mass of 22.284 Da, immunoblotting using a homemade antibody revealed a 55 kDa protein in different sera from mice, humans, and dogs as well as different cell lines. Recombinant expression in bacteria and mammalian cell lines, however, led to the expression of a 20-22 kDa protein. An increased molecular weight was explained by *O*-linked glycosylation of MIC26 based on partial sensitivity of the 55 kDa band to treatment with the deglycosylation enzyme chondroitinase ABC. Within this study, MIC26 was associated with mainly high-density lipoprotein (HDL) localization in the plasma. Hence, MIC26 was thought to be a novel classical apolipoprotein presumably involved in myocardial lipid homeostasis and cholesterol transport (Lamant et al., 2006). In the following years, research presumed MIC26 to exclusively function as a 55 kDa protein in association with lipoprotein metabolism. However, in 2013, complexome analysis revealed MIC26 to be a

putative MICOS subunit (Weber et al., 2013). Subsequent characterization indeed identified MIC26 to be a mitochondrial protein, exclusively located in the mitochondrial IM and to interact with MIC60, MIC27 and MIC10 (Koob et al., 2015b; Ott et al., 2015; Turkieh et al., 2014). Here, it was also reported that mitochondrial MIC26 is a 22 kDa form, concluding a dual modified protein existence, once in a mitochondrial 22 kDa form and a 55 kDa form involved in lipoprotein secretion and located in the secretory pathway organelles (Koob et al., 2015b; Ott et al., 2015). Following studies mainly focused on the function of mitochondrial MIC26 (Anand et al., 2020; Beninca et al., 2021; Guo et al., 2023; Rampelt et al., 2018; Tian et al., 2017). However, contradicting results have been reported about the sensitivity of the 55 kDa protein to downregulation experiments, which, however, revealed a successful suppression of the 22 kDa protein expression (Beninca et al., 2021; Koob et al., 2015a). Recently, the first study combining *MIC26* KO cell lines and focusing on both presumed MIC26 forms revealed that an appearing 55 kDa protein derives from unspecific immuno-reactivity of MIC26 antibodies, and identified that MIC26 is exclusively existing in a 22 kDa form in the mitochondria (Lubeck et al., 2023). Hence, the following sections summarizing current knowledge about the biological role of MIC26 will exclude conclusions that have been drawn from an unspecifically detected 55 kDa protein.

3.6.4 The biological role of MIC26 and its involvement in metabolic diseases

Initially, it has been reported that MIC26 mRNA levels are increased in the hearts of diabetic patients and have been suggested to execute a protective function against lipoapoptosis (Lamant et al., 2006). Microarray analysis of MIC26 siRNA cell lines reported an involvement of MIC26 in cellular lipid signaling and inflammation (Chen-Lu Wu, 2013). A role of MIC26 in lipid metabolism has also been reported in a transgenic mouse model, stating that MIC26 expression induced lipotoxicity. Increasing MIC26 mRNA levels correlated with the increasing presence of IR-inducing DAG but not TAG species in the human and mouse heart, as well as the transcription factors PPARα and PGC1α. Furthermore, MIC26 overexpression induced mitochondrial respiration and led to abnormal mitochondrial ultrastructure (Turkieh et al., 2014). In line, a different study using MIC26 overexpressing HeLa and MIC26 downregulated 143B cells reported that both up- and downregulation of MIC26, impaired basal and maximal mitochondrial respiration, as well as mitochondrial ultrastructure (Koob et al., 2015a, 2015b). MIC26 overexpression in the liver of HFD fed mice induced TAG accumulation in the liver and plasma with a common downregulation of multiple genes involved in fatty acid metabolism. These mice also showed a severe mitochondrial ultrastructure phenotype (Tian et al., 2017). Further, in mice adipose tissue specific deletion of MIC26 caused increased adiposity, brown adipose tissue (BAT) whitening, disrupted mitochondrial ultrastructure, impaired respiration, and a shift to glycolytic metabolism (Guo et al., 2023). Recently MIC26 has been reported to

be regulated via the small non-coding microRNA (miR) miR-200c (Mostofa et al., 2022). The miR-200 family microRNAs have been shown to regulate T2D-associated pancreatic beta cell survival (Belgardt et al., 2015) and have been involved in nonalcoholic steatohepatitis. Exposure to ethanol as a model of alcoholic hepatic steatosis induces miR-141 and miR-200c levels and promotes liver TAG accumulation, while miR-141/200c KO mice were resistant to ethanol induced TAG accumulation. Overexpression of miR-200c but not miR-141 in mice liver, as well as ethanol treatment in WT mice, significantly reduced MIC26 expression. Following, induction of miR-200c via e.g., alcohol exposure reduces MIC26 expression and hence leads to mitochondrial dysfunction, reduced FAO, and increased TAG accumulation and hepatic steatosis (Mostofa et al., 2022).

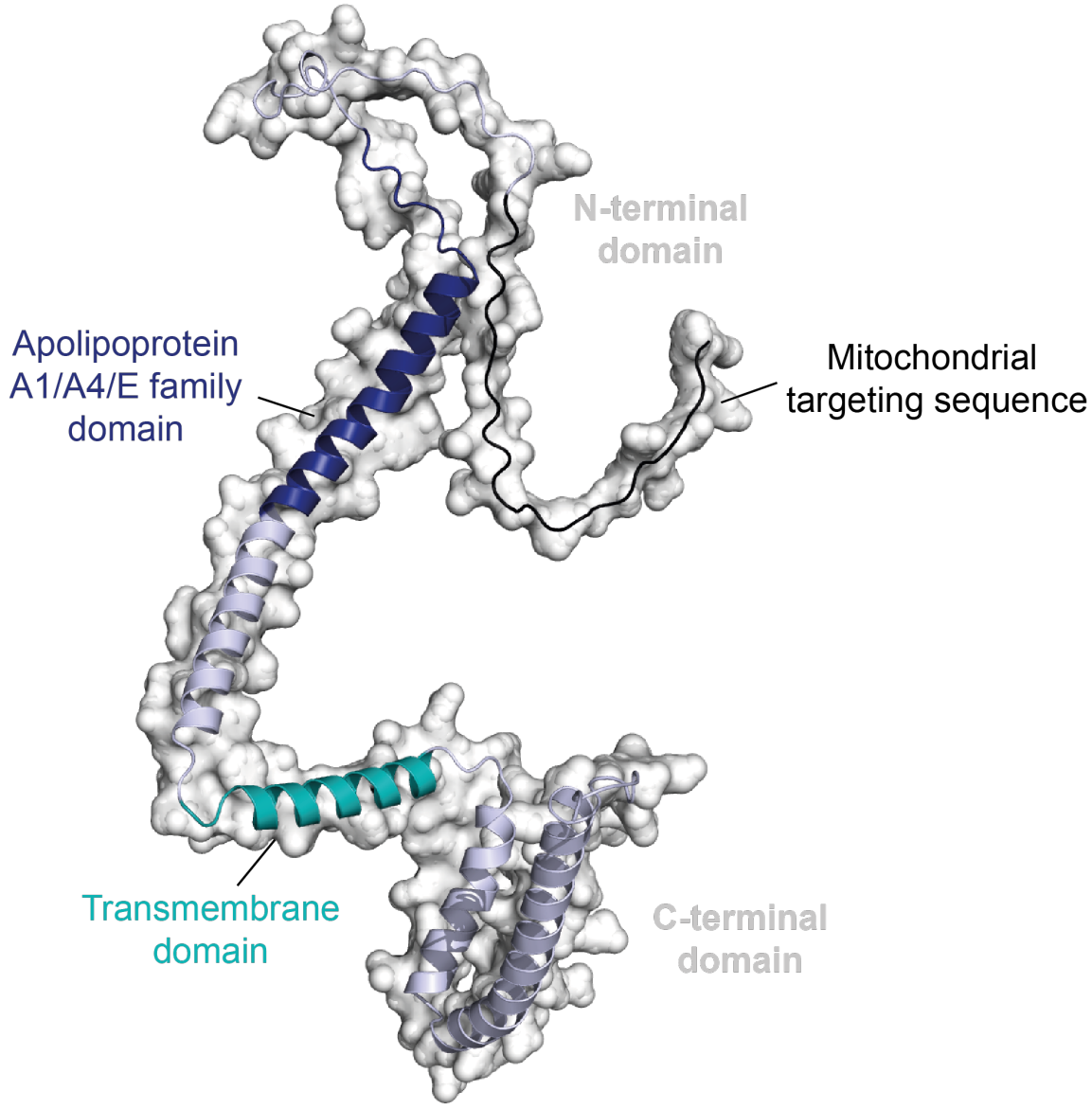

Figure 8: Predicted protein structure of MIC26 including a mitochondrial targeting sequence, the apolipoprotein A1/A4/E family domain and a transmembrane domain. Structure was acquired from AlphaFold and visualization was performed using Pymol.

Besides ethanol, also HFD feeding reduced MIC26 expression revealing a sensitivity to cellular nutritional stressors (Guo et al., 2023). Furthermore, a clinically occurring pathogenic mutation MIC26^{I117T} was reported to lead to severe lactic acidosis, muscle weakness, cognitive impairment, and autistic features (Beninca et al., 2021). Biochemical evaluation of this mutant in mammalian cell lines, yeast and *Drosophila* revealed impaired MICOS assembly, altered number of cristae, and CJ. Overall, abnormal protein levels of MIC26, down as well as upregulated, have been shown to be detrimental for mitochondrial ultrastructure and function. Furthermore, MIC26 is an essential component in the regulation of lipid metabolism throughout different species, tissue, and cell types.

Conclusively, MIC26 dysregulation is an essential target to be investigated in the pathophysiology of metabolic diseases including the metabolic syndrome, obesity, IR, T2D, and NAFLD.

4 Aim of the project

Mitochondria possess a unique ultrastructure consisting of an outer membrane and an inner membrane, the latter being further distinguished into an inner boundary membrane and cristae. Several studies have established that the MICOS complex, situated at the neck of the cristae, plays a pivotal role in cristae formation and maintenance. Variations in the levels of the apolipoprotein and MICOS subunit, MIC26, have been associated with diabetes and lipotoxicity development. Additionally, MIC26 has been postulated to exist in a mitochondrial 22 kDa form and an *O*-glycosylated 55 kDa form, which is undergoing secretion. However, to the beginning of this dissertation, little has been known about the regulation and interaction of both forms. Especially, the selective contribution of the different MIC26 forms to the observed mitochondrial and cellular abnormalities like lipotoxicity has not been elucidated. Moreover, to the beginning of this study, all available in vivo investigations have exclusively looked at overexpression of MIC26, while consequences of in vivo depletion of MIC26 function remains unexplored.

This dissertation aims to elucidate the roles of both reported forms of MIC26 in the regulation of cellular metabolic processes. Specifically, it seeks to understand the cellular localization, functions, and regulation of each form, and to discern which form contributes to reported abnormalities in cellular lipid metabolism. MIC26 is a subunit of the MICOS complex that has been shown to be depleted upon loss of several other MICOS subunits, including MIC10, MIC13, MIC60 and MIC19, however it does not lead to the loss of the aforementioned subunits. To further understand the contribution of MIC26 to effects that have been observed with the loss of the above-mentioned MICOS subunits, we aim to explore the loss of MIC26 function on both a cellular and in vivo level. To understand a possible role of MIC26 alone or in the integrity of the MICOS complex in the development of lipotoxicity and diabetes, we aim to investigate a nutrient-dependent regulation of MIC26. In this context, we aim to decipher the regulatory function of MIC26 on central metabolic fuel pathways including glycose, lipid and glutamine metabolism, which will give insights into the effects of altered MIC26 level caused by e.g. nutritional impact on disease development.

The objectives of this dissertation have been addressed in the publications in Chapter 5.1, 5.2, and 5.3. The publication 5.1 investigates the two postulated MIC26 forms, while the publication in Chapter 5.2 explores the first described in vivo patient mutation causing a loss of function MIC26 phenotype. Chapter 5.3 focuses on the mechanisms underlying the observed phenotypes of MIC26 protein level abnormalities and their effect on regulating key metabolic pathways, as previously described in Chapter 5.2.

5 Results

5.1 MIC26 and MIC27 are bona fide subunits of the MICOS complex in mitochondria and do not exist as glycosylated apolipoproteins

PLOS ONE

RESEARCH ARTICLE

MIC26 and MIC27 are bona fide subunits of the MICOS complex in mitochondria and do not exist as glycosylated apolipoproteins

Melissa Lubeck[1], Nick H. Derkum[1], Ritam Naha[1], Rebecca Strohm[1], Marc D. Driessen[2], Bengt-Frederik Belgardt[3,4], Michael Roden[4,5,6], Kai Stühler[2,7], Ruchika Anand[1], Andreas S. Reichert[1], Arun Kumar Kondadi[1]*

1 Medical Faculty and University Hospital Düsseldorf, Institute of Biochemistry and Molecular Biology I, Heinrich Heine University Düsseldorf, Düsseldorf, Germany, **2** Medical Faculty and University Hospital, Institute of Molecular Medicine, Protein Research, Heinrich Heine University Düsseldorf, Düsseldorf, Germany, **3** Institute for Vascular and Islet Cell Biology, German Diabetes Center (DDZ), Leibniz Center for Diabetes Research at Heinrich Heine University, Düsseldorf, Germany, **4** German Center for Diabetes Research (DZD e.V.), Partner Düsseldorf, Neuherberg, Germany, **5** Medical Faculty and University Hospital Düsseldorf, Department of Endocrinology and Diabetology, Heinrich Heine University, Düsseldorf, Germany, **6** Institute for Clinical Diabetology, German Diabetes Center, Leibniz Center for Diabetes, Heinrich Heine University, Düsseldorf, Germany, **7** Molecular Proteomics Laboratory, BMFZ, Heinrich Heine University Düsseldorf, Düsseldorf, Germany

* kondadi@hhu.de

OPEN ACCESS

Citation: Lubeck M, Derkum NH, Naha R, Strohm R, Driessen MD, Belgardt B-F, et al. (2023) MIC26 and MIC27 are bona fide subunits of the MICOS complex in mitochondria and do not exist as glycosylated apolipoproteins. PLoS ONE 18(6): e0286756. https://doi.org/10.1371/journal.pone.0286756

Editor: Benedetta Ruzzenente, Imagine Institute for genetic diseases, FRANCE

Received: December 8, 2022

Accepted: May 23, 2023

Published: June 6, 2023

Peer Review History: PLOS recognizes the benefits of transparency in the peer review process; therefore, we enable the publication of all of the content of peer review and author responses alongside final, published articles. The editorial history of this article is available here: https://doi.org/10.1371/journal.pone.0286756

Data Availability Statement: All relevant data are within the manuscript and its Supporting information files.

Abstract

Impairments of mitochondrial functions are linked to human ageing and pathologies such as cancer, cardiomyopathy, neurodegeneration and diabetes. Specifically, aberrations in ultrastructure of mitochondrial inner membrane (IM) and factors regulating them are linked to diabetes. The development of diabetes is connected to the 'Mitochondrial Contact Site and Cristae Organising System' (MICOS) complex which is a large membrane protein complex defining the IM architecture. MIC26 and MIC27 are homologous apolipoproteins of the MICOS complex. MIC26 has been reported as a 22 kDa mitochondrial and a 55 kDa glycosylated and secreted protein. The molecular and functional relationship between these MIC26 isoforms has not been investigated. In order to understand their molecular roles, we depleted *MIC26* using siRNA and further generated *MIC26* and *MIC27* knockouts (KOs) in four different human cell lines. In these KOs, we used four anti-MIC26 antibodies and consistently detected the loss of mitochondrial MIC26 (22 kDa) and MIC27 (30 kDa) but not the loss of intracellular or secreted 55 kDa protein. Thus, the protein assigned earlier as 55 kDa MIC26 is nonspecific. We further excluded the presence of a glycosylated, high-molecular weight MIC27 protein. Next, we probed GFP- and myc-tagged variants of MIC26 with antibodies against GFP and myc respectively. Again, only the mitochondrial versions of these tagged proteins were detected but not the corresponding high-molecular weight MIC26, suggesting that MIC26 is indeed not post-translationally modified. Mutagenesis of predicted glycosylation sites in MIC26 also did not affect the detection of the 55 kDa protein band. Mass spectrometry of a band excised from an SDS gel around 55 kDa could not confirm the presence of any peptides derived from MIC26. Taken together, we conclude that both

Funding: 1) Funded by the Deutsche Forschungsgemeinschaft (DFG) Graduiertenkolleg VIVID RTG 2576 to ASR (www.dfg.de) 2) DFG Grant KO 6519/1-1 to AKK 3) DFG Grant AN 1440/3-1 to RA The funders had no role in study design, data collection and analysis, decision to publish, or preparation of the manuscript.

Competing interests: The authors have declared that no competing interests exist.

MIC26 and MIC27 are exclusively localized in mitochondria and that the observed phenotypes reported previously are exclusively due to their mitochondrial function.

Introduction

Mitochondria are essential double-membrane-enclosed organelles required for a myriad key cellular functions including ATP conversion, iron-sulfur cluster biogenesis, programmed cell death, calcium buffering, vital metabolic processes and inflammatory responses. The mitochondrial inner membrane (IM) is spatially heterogenous and composed of the inner boundary membrane (IBM), parallel to the outer membrane (OM), and the cristae membrane (CM) extending as invaginations towards the mitochondrial matrix. CMs house the electron transport chain (ETC) complexes [1,2] and are responsible for ATP generation. Cristae exist in a variety of shapes and sizes depending on the cell, tissue type and bioenergetic status of the cell [3,4]. Aberrant cristae are found in a wide variety of pathologies like diabetic cardiomyopathy, neurodegeneration and mitochondrial myopathy [5–7]. The IBM and CM are separated by distinct pore-like structures which are around 25 nm in diameter and termed crista junctions (CJs) [8,9]. CJs were proposed as a diffusion barrier for various metabolites, membrane and soluble proteins [10–13]. In congruence, it was shown that there was differential localisation of various proteins in the IM: The IBM predominantly contains proteins involved in mitochondrial fusion and protein import while the CMs are enriched with proteins belonging to mitochondrial protein synthesis, iron-sulfur cluster biogenesis and ETC complexes [1,2]. In fact, the CJs give rise to heterogenous membrane potential of the individual cristae [14]. Therefore, CJs are an important structural and functional constituent of the IM.

The MICOS (Mitochondrial contact site and cristae organising system) complex is a multiprotein complex comprising of seven *bona fide* proteins which resides at the CJs. The MICOS complex was discovered in *Saccharomyces cerevisiae* by independent groups [15–17]. The proteins of the MICOS complex include two subcomplexes: MIC60/MIC25/MIC19 and MIC10/MIC26/MIC27 which are bridged by MIC13 [18,19] using its conserved GxxxG and WN motifs [20]. The MICOS complex present in the IM is in turn connected via MIC60 to SAM50 present in the OM through MIC19 contributing to the formation of a 2 mega Dalton MIB (Mitochondrial intermembrane space bridging) complex [21,22]. Thus, the MIB complex mediates the IM and OM contacts. The MICOS complex correlates with the presence of cristae. In fact, a very recent study showed that Mic60 is involved in the development of intracytoplasmic membranes in alphaproteobacteria [23]. Mic60 is conserved from alphaproteobacteria to virtually all eukaryotes, whereas Mic10 is widely distributed in the later domain of life [24,25]. However, there is a difference w.r.t Mic10 and Mic60 in organisms which are opisthokonts and not, like *Trypansoma brucei*. TbMic60 lacks a conserved mitofilin domain while there are two TbMic10 proteins inconsistent with opisthokonts [26]. Other MICOS proteins display inconsistent phylogenetic distribution. For instance, MIC26 and MIC27 are paralogs which are only present in opisthokonts [24,25]. The MICOS complex proteins play a wide range of roles in bending the IM, formation of contact sites, protein import, mtDNA organisation, lipid metabolism, cristae dynamics, mitochondrial motility, integrity of the respiratory chain super complexes and the F_1F_O-ATP synthase [3,17,27–34]. Consequently, it is well established that proteins of the MICOS complex are associated with various pathologies [35,36]. Mutations in *MIC60* were shown to be present in Parkinson's disease patients [37]. A recent report showed that homozygous mutations in *MIC60* led to developmental encephalopathy, optic atrophy, dystonia and nystagmus [38]. *MIC13* mutations cause mitochondrial

encephalopathy and hepatic disorders [39]. It is also known that mutations in *MIC26* cause mitochondrial myopathy, cognitive defects and lactic acidosis [40]. Further, there is an intricate connection between MICOS proteins and diabetes. Interfibrillary cardiac mitochondria showed a decreased amount of MIC60 in type I diabetic hearts indicating mitochondrial dysfunction contributes to diabetic cardiomyopathy [41]. When control and transgenic mice, overexpressing *Mic60*, were treated with streptozotocin to induce diabetes, the transgenic mice displayed improved mitochondrial ultrastructure and cardiac contractile functions compared to control mice [42]. Hence, increased amount of MIC60 is beneficial to overcome at least some cellular abnormalities in diabetes. Regarding other MICOS proteins, hearts of diabetic patients showed an upregulation of *MIC26* mRNA pointing to a close link between diabetes and the mitochondrial apolipoprotein MIC26 [43]. Overexpression of *Mic26* in murine liver resulted in steatosis where the effects were more pronounced in mice fed with high-fat diet compared to normal diet [44]. Further, triglyceride content was increased in liver upon *Mic26* overexpression when mice were fed with normal as well as high-fat diet while the effects were pronounced with high-fat diet. In addition, the mRNA expression of genes involved in fatty acid metabolism was altered.

Complexome profiling of purified bovine mitochondria resulted in the identification of two homologous apolipoproteins, MIC26/APOO and MIC27/APOOL, as a part of mammalian MICOS complex [45]. Accordingly, an altered mitochondrial ultrastructure and function was observed in cells depleted for MIC26 and MIC27 [31,46] as well as in cells including cardiac myoblasts overexpressing *MIC26* and *MIC27* [45,47]. Other studies have demonstrated the structural, functional and pathological importance of MIC26 localized to the mitochondria [31,40,46,48,49] which we designate as $MIC26_{22kDa}$ throughout this manuscript. Before MIC26 was shown to be present in mitochondria as a 22 kDa protein [46–48], it was observed that the MIC26 apolipoprotein was O-glycosylated and present as a 55 kDa protein, termed $MIC26_{55kDa}$ from now on [43]. In fact, MIC26 was initially found as a protein of unknown function while studying cardiac transcriptome in dogs fed with hypercaloric high-fat diet in an obesity-related hypertension model [50]. This protein of unknown function which contained a couple of amphipathic α-helices, a common feature of apolipoprotein family, was enriched in high-density lipoproteins and therefore identified as an apolipoprotein and given the name ApoO in chronological succession [43]. A protein band at 55 kDa was observed in human, dog and murine serum as well as in human auricle and HepG2 cells. However, the recombinant protein resulted in a size of 22 kDa. In order to explain the discrepancy between the observed 55 kDa and the 22 kDa recombinant protein, the authors predicted MIC26 is glycosylated and found that $MIC26_{55kDa}$ was sensitive to chondroitinase ABC (cABC) deglycosylation releasing a maximum of 50% of the protein at 22 kDa [43]. This was validated by preventing the MIC26 glycosylation by using *p*-nitrophenyl-*β*-D-xyloside which increased the 22 kDa protein in modest amounts. Following this characterisation, it was deemed to be an original glycoprotein. $MIC26_{55kDa}$ was increased around two-fold in plasma of patients suffering from acute coronary syndrome [51]. When HepG2 cells were depleted for MIC26, microarray analysis revealed genes involved in fatty acid metabolism and inflammatory responses were differentially expressed [52]. Transgenic overexpression of *Mic26* mice fed with a high-fat diet resulted in alterations of mitochondrial ultrastructure, cardiac and metabolic functions in that there was an enhanced accumulation of diglycerides in *Mic26* overexpressing mice [47]. Other reports immediately after this showed that $MIC26_{22kDa}$ was conclusively localized to the mitochondria [46,48]. Hence, a dual role of MIC26 as a mitochondrial as well as glycosylated protein emerged into prominence. However, studies in chicken after the discovery of the mitochondrial $MIC26_{22kDa}$ still focussed exclusively on the so-called $MIC26_{55kDa}$ secreted version [53,54]. Therefore, it is important to study both the $MIC26_{22kDa}$ and $MIC26_{55kDa}$

together. Although it is clear that increased amounts of MIC26 in mice lead to defects at the cellular and organismal level [47], the significance and relevance of the $MIC26_{55kDa}$ is not clearly understood. In fact, to the best of our knowledge, the 55 kDa protein of MIC26 was not studied in *MIC26* knockouts (KOs). In addition, MIC26 was not found to be a part of high-density lipoprotein (HDL)-associated proteins in a proteomic study where other major apolipoproteins could be detected [55]. Therefore, there are considerable inconsistencies regarding $MIC26_{55kDa}$. In this manuscript, we focussed to solve this conundrum. In fact, in light of multiple experiments, we consider that the recognised 55 kDa protein band is nonspecific and must be treated with caution in future research endeavours.

Materials and methods

Cell culture and downregulation using siRNA

HEK293 and HeLa cells were maintained in 1 g/L glucose DMEM (PAN-Biotech) supplemented with 10% fetal bovine serum (FBS, Capricorn Scientific), 2 mM GlutaMAX (Gibco), 1 mM sodium pyruvate (Gibco) and penstrep (PAN-Biotech, penicillin 100 U/mL and 100 μg/mL streptomycin). HepG2 cells were cultured in 1 g/L glucose DMEM (PAN-Biotech) supplemented with 10% FBS (Capricorn Scientific), 2 mM GlutaMAX (Gibco) and penstrep (PAN--Biotech). C2C12 cells were cultured in 4.5 g/L DMEM (Pan-Biotech) supplemented with 10% FBS (Capricorn Scientific) and penstrep (PAN-Biotech), whereas HAP1 cells were maintained in Iscove's modified DMEM medium (IMDM, Sigma-Aldrich) supplemented with 20% FBS, 2 mM GlutaMAX (Gibco) and penstrep (PAN-Biotech). All the above-mentioned cells were grown at 37˚C supplied with 5% CO_2. For downregulation of *MIC26*, the cells were transfected with Lipofectamine™ RNAiMAX reagent (Invitrogen) according to the manufacturer's protocol. Downregulation was done for 48 h with 10 nM of siRNA. Negative control medium GC duplex (Invitrogen, cat no: 462001) was used as control along with following siRNA sequences (Thermo Fischer Scientific):

1. *MIC26* # 1 (ID30917 targeting exon 6 and 7): 5'-GGAUAUAUAGUCAUAGAAGTT-3'; 5'-CUUCUAUGACUAUAUAUCCTC-3'
2. *MIC26* # 2 (ID127368 targeting exon 3 and 4): 5'-GGAAACGUACUCCCAAACUTT-3'; 5'-AGUUUGGGAGUACGUUUCCTG-3'
3. *MIC26* # 3 (ID127366 targeting exon 2): 5'-CCUCCCAAAAAUUCCGUGATT-3'; 5'-UCACGGAAUUUUUGGGAGGTG-3'

Generation of *MIC26* and *MIC27* KOs using the CRISPR/Cas method

MIC26 and *MIC27* KOs in HepG2, HeLa and HEK293 cells were generated using the double nickase method. This CRISPR/Cas KO system consists of two plasmids where each plasmid contained a sgRNA sequence and a reporter (either GFP or puromycin resistance) for positive selection of cells. The plasmid mix was commercially available (Santa Cruz Biotechnology): MIC26: double nickase plasmid sc-413137-NIC and MIC27 double nickase plasmid sc-414464-NIC. Cells were seeded on 35 mm dishes and transfected one day later with 1 μg of the respective plasmid mix using GeneJuice (Novagen) reagent according to the manufacturers protocol. Two days after transfection, single cells were sorted by FACS (Beckman Coulter) using GFP fluorescence into a 96-well plate (Greiner) containing respective conditioned media to obtain homogeneous KO cell populations from single cells. HAP1 *MIC26* and *MIC27* KO cells were custom-made by Horizon (UK) as described before [31].

Molecular cloning/Plasmids & Constructs

MIC26-GFP was generated by cloning human MIC26 in to the pEGFP-N1 vector, using the Kpn1 and Age1 restriction enzymes which was followed by ligation. MIC26^{S34A}-GFP, MIC26^{S41A}-GFP and MIC26^{S50A}-GFP mutant variants of MIC26-GFP were generated using the Q5 site-directed mutagenesis kit (New England Biolabs). pMSCV-MIC26 plasmid, generated in a previous study [31], was used as a template for making pMSCV-MIC26-myc plasmid using the Q5 site-directed mutagenesis kit (New England Biolabs) according to manufacturer's protocol with the following primers:

1. myc-tag forward:
   5'-GAACAAAAACTCATCTCAGAAGAGGATCTCTAGCGAATTCTACCGGGTAG-3'
2. myc-tag reverse:
   5'-CCCAGATCCCTTAGTTCCAGGTGAATTCTTCACA-3'

For generating triple mutant MIC26$^{S34A/S41A/S50A}$-myc plasmid, insertion of myc-tag and triple amino acid mutations from serine to alanine (S34, S41 and S50) were generated using the following primers:

3. MIC26-S34/41/50A forward:
   5'-CTACTCAG-TTCCTGAGGGTCAAGCGAAGTATGTGGAGGAGGCA-3'
4. MIC26-S34/41/50A reverse:
   5'-AGTGC-AAGCTCATCAACCTTCACGGCATTTTTGGGAGGTGAGTC-3'

In order to express MIC26-GFP and MIC26-myc variants, HEK293 cells were seeded onto 35 mm plates and transfected with 1 μg of corresponding plasmid using GeneJuice (Novagen) reagent according to the manufacturer's protocol and grown for 48 h until harvest.

SDS gel electrophoresis and Western Blotting

Cellular proteins were harvested from a corresponding number of cells after washing them three times with 2 mL DPBS (PAN-Biotech) followed by scraping and resuspending the cells in an appropriate volume of lysis buffer (210 mM mannitol, 70 mM sucrose, 1 mM EDTA, 20 mM HEPES, 1 x protease inhibitor (Sigma-Aldrich)) or RIPA buffer (150 mM NaCl. 0.1% SDS, 0.05% DOC. 1% Triton-X-100. 1 mM EDTA, 1mM Tris, pH 7.4, 1 x protease inhibitor (Sigma-Aldrich)). Following the incubation of cells for 10 min on ice, they were mechanically disrupted using a 20G canula by repetitive strokes. In order to harvest secreted proteins, cells were seeded into 35 mm plates containing 2 mL standard growth medium. After 24 h incubation, cells were carefully washed three times with 2 mL DPBS (PAN-Biotech) and grown for another 24 h in the corresponding medium lacking FBS. The culture medium was collected and separated from detached cells by centrifugation for 5 min at 1000g and 4˚C. Next, proteins in cell culture media were precipitated by the addition of 10% trichloroacetic acid (TCA) for 40 min on ice. The precipitated proteins were pelleted by centrifugation for 10 min at 16,000 g, 4˚C and washed twice with 2 mL ice-cold acetone. The pellet was dried at room temperature, dissolved in 4 M Urea, 1 mM DTT, 2% SDS and heated for 5 min at 95˚C. For subcellular fractionation, nuclear fraction was removed from cell lysates, obtained by mechanical disruption, upon centrifugation for 5 min at 500g and 4˚C. An aliquot of the supernatant was taken as total fraction. Next, the mitochondrial fraction was pelleted by centrifugation at 7000g and 4˚C for 10 min. Mitochondrial fraction was washed three times and sequentially resuspended in lysis buffer. The supernatant contained the ER/Golgi and cytosolic fraction. For murine tissue lysates, 20 mg of tissue was homogenized, in Precellys Soft Tissue homogenizing CK14

tubes, with 300 μL RIPA buffer in a Precellys 24 homogenizer at 5000 rpm for 10 sec. Further, solubilized proteins were separated from the tissue debris by centrifugation at 16,000 g for 10 min at 4˚C. Protein concentration was determined using Lowry method (Bio-Rad). SDS samples were prepared with Laemmli buffer and heated for 5 min at 95˚C. 10% or 15% SDS electrophoresis gels were used for running and separating protein samples. The proteins were blotted onto nitrocellulose membrane and detected using Ponceau S (Sigma Aldrich, P7170) following which the membrane was destained. Further, nitrocellulose membrane was blocked with 5% milk in 1x TBS-T and probed with the following primary antibodies overnight at 4˚C: MIC26 (#1: Sigma-Aldrich HPA003187, 1:500; #2: Invitrogen PA5-116197, 1:1000; #3: Invitrogen MA5-15493, 1:1000; #4: Pineda home-made, 1:100), MIC27 (Sigma-Aldrich HPA000612, 1:2000), myc-tag (Cell Signaling Technology 2276, 1:1000), ß-Tubulin (Abcam ab6046, 1:2000), Calreticulin (Cell Signaling Technology 2891, 1:1000), ANT2 (Sigma-Aldrich HPA046835, 1:1000) and GFP (Sigma-Aldrich 11814460001, 1:2000). Goat IgG anti-Mouse IgG (Abcam ab97023, 1:10000) and Goat IgG anti-Rabbit IgG (Dianova SBA-4050-05, 1:10000) conjugated to HRP were used as secondary antibodies. The chemiluminescent signals were obtained using Signal Fire ECL reagent (Cell Signaling Technology) and VILBER LOURMAT Fusion SL equipment (Peqlab).

RNA isolation and quantification

Total RNA was extracted from murine liver tissue using RNeasy Mini Kit (Qiagen) according to the manufacturer's protocol. RNA quality and quantity were assessed using BioSpectrometer (Eppendorf). cDNA synthesis from 1 μg RNA was performed using the GoScript™ Reverse Transcriptase Kit (Promega). Next, quantitative real-time PCR was performed in Rotor Gene 6000 (Corbett Research) using GoTagR qPCR Master Mix (Promega) according to manufacturer's instructions with the following primers:

1. HPRT1 (Housekeeping gene) forward:
   5'- CTGGTGAAAAGGACCTCTCGAAG -3'
2. HPRT1 (Housekeeping gene) reverse:
   5'- CCAGTTTCACTAATGACACAAACG -3'
3. MIC26 forward:
   5'- AGCACCCAAAAAGGACTCGCCT -3'
4. MIC26 reverse:
   5'- GGCTCACAATGATGTCGGAGTTG -3'
5. MIC27 forward:
   5'- GTCTATCTGAAGAATCCTCCGCA -3'
6. MIC27 reverse:
   5'- CAAACAGTCGCTCCTAATGTGGC -3'

C_t values were normalized to housekeeping gene *HPRT1* followed by normalization of ΔC_t values to average ΔC_t of db/+ control group.

Mass spectrometry

Coomassie stained SDS-PAGE cut-outs of the ≈ 47 to 63 kDa band were processed as described before [56] with minor changes: In brief, slices were destained and washed (alternating cycles of 10 mM Ammonium bicarbonate (ABC) and 100 mM ABC/50% Acetonitrile (ACN); 3 repeats). Proteins were reduced and alkylated in-gel (10 mM DTT followed by 55

mM IAA),washed again as before and dried. Digestion was performed for 16 h, 37˚C with 0.1 μg trypsin in 100 mM NH_4HCO_3. Peptides were extracted twice, using a 1:1 mixture of ACN/0.1% TFA (v/v), combined extracts were dried again and resuspended in 0.1% (v/v) TFA.

Half of each sample was used for LC-MS analysis (Ultimate 3000 rapid separation liquid chromatography system, coupled to a QExactive plus, both Thermo Fisher scientific) using the following parameters: Samples were separated on PepMap (Thermo Fisher scientific) C18 loading and separating columns, using a 2h gradient (going from 4% Buffer B to 40% in 64 minutes, followed by 95%B and 4%B equilibration respectively; Buffer A: 0,1% FA, Buffer B: 84% ACN, 0,1% FA). Data was collected using a resolution of 140k, AGC target of 3e6, maximum injection times of 50ms for MS1 and a scan range of 200-2000m/z, data dependent MS2 spectra were recorded using a resolution of 17,5k, AGC target 1e5, maximum It 50ms, NCE 30 in a TopN [20] experiment using dynamic exclusion for 10 seconds after selection.

Data Processing was performed using MaxQuant 1.6.17.0 [57], using standard parameters if not stated otherwise. Searches were performed against a database containing 79038 human proteins (UP000005640, downloaded 01/2022 from uniport.org). The following modifications were considered: fixed: Carbamidomethylation (C); variable: Oxidation (M); Acetyl (Protein N-term). Potential contaminant IDs were removed and annotation of IDs was performed using Perseus [58], due to the nature of the search, no additional filtering was applied, but results were colour coded, based on the number of peptides assigned to the respective protein IDs in each sample: red: 0 or 1 peptide, green >3 peptides.

Mouse tissues

Tissues from 12-week-old male control and db/db.BKS mice (#000642, Jackson Laboratories, USA) were used for this study. Animal procedures were approved by the Department for Environment and Consumer Protection of North Rhine-Westphalia, Germany (LANUV; #81–02.04.2019.A321) and the DDZ Institutional Animal Welfare Committee.

Results

The presumed 55 kDa glycosylated protein is not decreased in cells depleted for *MIC26* and *MIC27*

Previous studies have either focused on the role of $MIC26_{55kDa}$ glycosylated protein in the context of diabetes and fatty acid metabolism [43,44,47,51,52,54] or $MIC26_{22kDa}$ protein in mitochondrial function [31,46,48,59]. Mitochondrial function and diabetes are intricately connected [60]. Therefore, in order to understand their relationship, we investigated the functional link between $MIC26_{22kDa}$ mitochondrial and $MIC26_{55kDa}$ glycosylated protein. For this, we first focussed on the downregulation of *MIC26* in HEK293 cells (Fig 1A). Western Blots (WBs) consistently revealed a marked reduction of $MIC26_{22kDa}$ protein upon downregulating *MIC26* with three different siRNA, targeting different exons, resulting in negligible amounts of protein levels compared to control siRNA demonstrating the expected sensitivity of $MIC26_{22kDa}$ protein to *MIC26* downregulation. On the contrary, we found no differences in the levels of the $MIC26_{55kDa}$ protein (Fig 1A, uppermost panel) indicating that the $MIC26_{55kDa}$ protein is not affected upon downregulation of *MIC26*. Upon revisiting previous literature, we found two reports showing similar unresponsive nature of the $MIC26_{55kDa}$ glycosylated protein upon downregulation of *MIC26* using multiple siRNA in HeLa cells and shRNA in 143B cells [40,59]. However, this was not further explored. Overall, only the mitochondrial $MIC26_{22kDa}$ protein was responsive while the $MIC26_{55kDa}$ was resistant to *MIC26* downregulation leading us to question the specificity of the $MIC26_{55kDa}$ glycosylated protein.

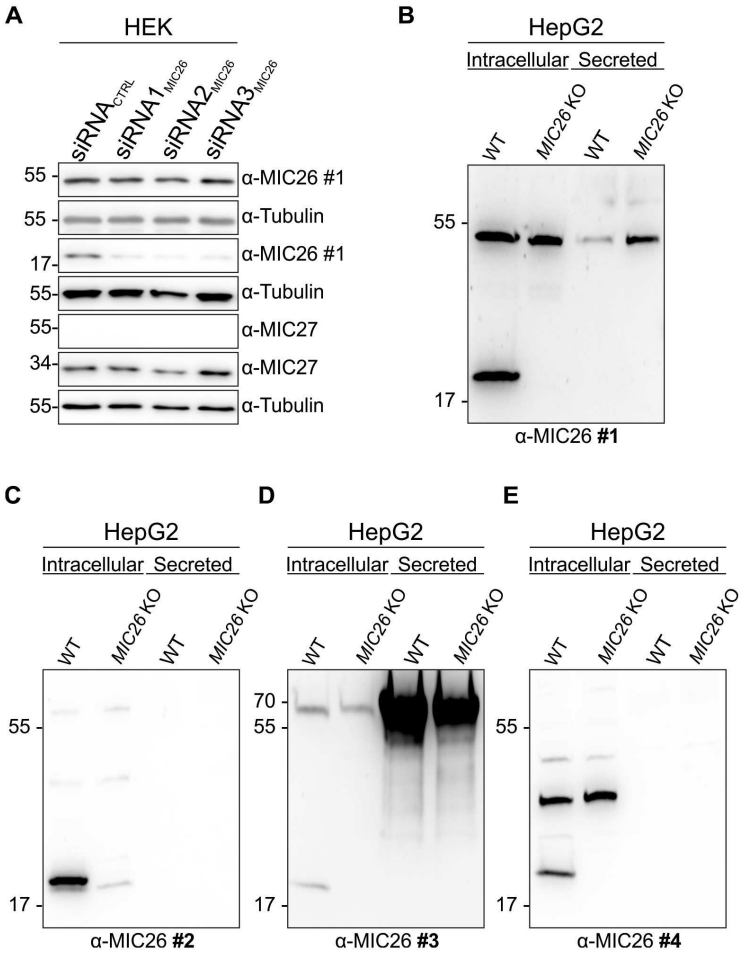

Fig 1. The MIC26$_{55kDa}$ form is neither sensitive to knockdown nor knockout of *MIC26*. A) Western blot (WB) analysis of HEK293 cells knocked down for *MIC26* reveal the loss of mitochondrial MIC26$_{22kDa}$ but not MIC26$_{55kDa}$. In order to downregulate *MIC26*, three siRNAs were used. B)–E) WB analysis of cell lysates and secreted proteins, using WT and *MIC26* KO HepG2 cells, were done using four anti-MIC26 antibodies. All four WBs show the presence of intracellular mitochondrial MIC26$_{22kDa}$ form in WT cells but not in *MIC26* KO cells as expected. However, unexpected and inconsistent results were obtained w.r.t the 55 kDa protein. (B) Antibody #1 detects an intra- and extracellular 55 kDa band in WT as well as *MIC26* KOs. (C) Antibody #2 detects only an intracellular protein band around 70 kDa. (D) Antibody #3 identifies an intracellular and secreted protein (in culture medium) at ≈ 70 kDa in both WT and *MIC26* KO HepG2 cells. The considerable increase in ≈ 70 kDa protein correlates to the production and secretion of albumin by human HepG2 cells, which is nonspecifically recognized by this antibody. (E) Antibody #4 is not recognizing a 55 kDa band in WT and *MIC26* KO HepG2 cells.

https://doi.org/10.1371/journal.pone.0286756.g001

The previous reports on $MIC26_{55kDa}$ glycosylation had not employed any *MIC26* KO cell line [43,44,47]. One of our studies used *MIC26* and *MIC27* KOs in HAP1 cells but rather focussed on mitochondrial $MIC26_{22kDa}$ and the relationship between mitochondrial ultrastructure and functioning [31]. In order to further explore the unresponsive nature of the $MIC26_{55kDa}$ protein to *MIC26* downregulation, we generated *MIC26* KO in HepG2 cells, using the CRISPR/Cas system, which have appreciable secretory properties and where the $MIC26_{55kDa}$ was described to be secreted [43]. Using WBs, we examined the cell lysates as well as culture media containing the secretory proteins of WT and *MIC26* KO HepG2 cells (Fig 1B) to check for the presence of both the intracellular and secreted $MIC26_{55kDa}$, respectively. Further, in order to corroborate our previous results, we used a set of four anti-MIC26 antibodies available to us. For clarity, we compiled the details of various anti-MIC26 antibodies used in this study and other studies (S1A Fig). The antigens used to elicit antibody response are also shown with different colour-codes from various studies (S1B Fig). All four antibodies consistently detected the human mitochondrial $MIC26_{22kDa}$ in WT HepG2 cell lysates while $MIC26_{22kDa}$ was not observed in *MIC26* KOs as expected (Fig 1B–1E). We observed the putative $MIC26_{55kDa}$ secreted protein in culture media of WT as well as *MIC26* KO HepG2 cells when antibody #1 was used (Fig 1B). Moreover, antibody #1 recognised the presumed intracellular 55 kDa protein (Fig 1B) while a protein band having a molecular weight larger than 55 kDa was detected when antibodies #2 and #3 were used (Fig 1C and 1D). Antibody #2 did not reveal any secreted proteins around 55 kDa while the nearest intracellular protein detected had a molecular weight well above 55 kDa (Fig 1C). Using antibody #4, neither an intracellular nor secreted protein was found in the 55 kDa region (Fig 1E). Thus, the inconsistent detection of proteins of varied molecular weight around 55 kDa, in accordance with no loss of the 55 kDa protein in HepG2 *MIC26* KOs, with different anti-MIC26 antibodies indicates that $MIC26_{55kDa}$ protein is of nonspecific nature and that MIC26 most likely exists in the mitochondria as a 22 kDa protein across many cell types.

In order to check the mitochondrial localisation of MIC26 using all four antibodies, we isolated mitochondria from HEK293 cell lysates and performed immunoblotting (S2 Fig). As expected, we consistently found that MIC26 was only present in the mitochondrial fraction using all antibodies #1–4 (S2A–S2D Fig). ANT2, a mitochondrial protein was only found in the mitochondrial fraction as expected. We also loaded the fraction which contain the endoplasmic reticulum (ER), Golgi and the rest of cytosolic fraction. While calreticulin, an ER protein, was detected in this fraction as expected, mitochondrial MIC26 was not observed showing that mitochondrial MIC26 is not present in the secretory fraction (S2A–S2D Fig).

A nonspecific 55 kDa band is still recognised in knockouts of *MIC26* and *MIC27* in various human cell lines

In order to ascertain if the 55 kDa protein belongs to either MIC26 and/or MIC27 and to overcome cell-type specific effects, we employed KOs of *MIC26* and *MIC27* in various cell lines. During the course of this study, we generated corresponding single KOs of *MIC26* and *MIC27* in HEK293, HeLa and HepG2 cells using the CRISPR/Cas system. Additionally, we used *MIC26* and *MIC27* KO HAP1 cells along with WT cells already available from our previous study [31]. Altogether, we used KOs of *MIC26* and *MIC27* belonging to four different human cell lines (Fig 2A–2D). Since the 55 kDa MIC26 protein was consistently detected in mammalian cell lysates and cell culture medium using only one antibody (#1) out of four anti-MIC26 antibodies available (Fig 1B–1E), we performed subsequent experiments with WT, *MIC26* and *MIC27* KOs using antibody #1 (Fig 2A–2D). WBs, using lysates from HEK293 (Fig 2A), HepG2 (Fig 2B), HeLa (Fig 2C) and HAP1 (Fig 2D) cells, revealed that the respective MIC26

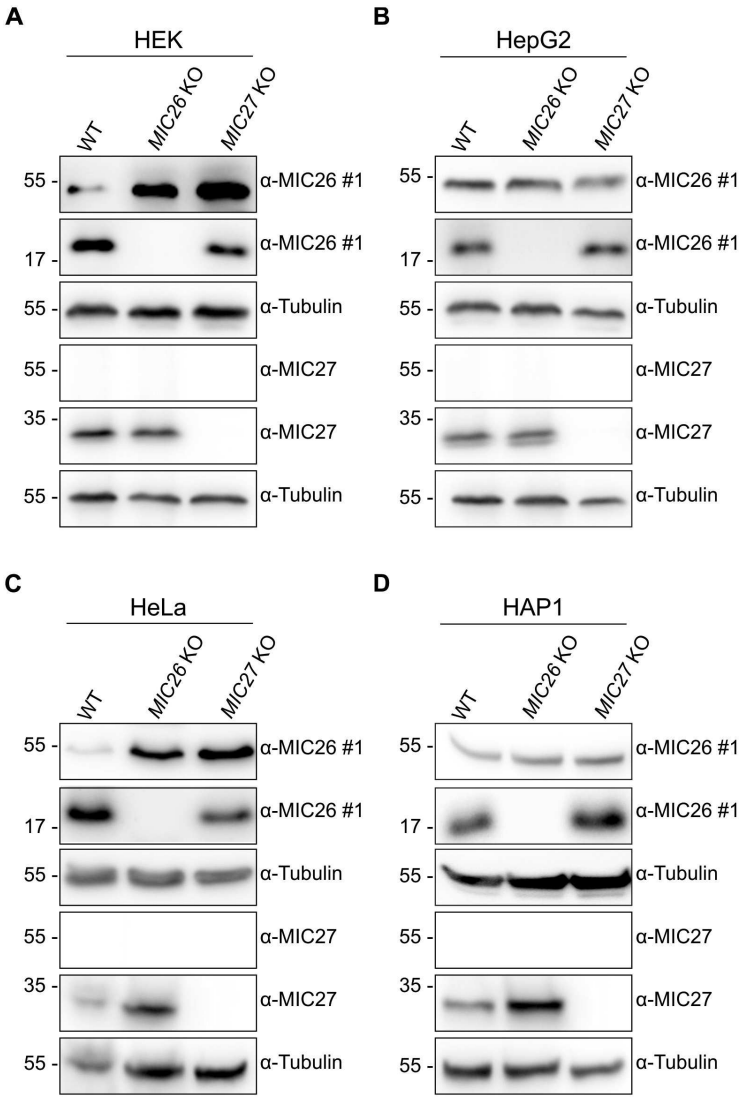

Fig 2. *MIC26* KOs reveal the nonspecific nature of the 55 kDa band in various human cell lines. WB analysis of WT, *MIC26* and *MIC27* KO cell lysates, obtained from HEK293, HepG2, HeLa and HAP1 cells are shown. *MIC26* KOs reveal a loss of mitochondrial $MIC26_{22kDa}$ but not the 55 kDa band. There is no protein band detected in WT and *MIC27* KOs at 55 kDa region when anti-MIC27 antibody was used. A) In *MIC26* KOs of HEK293 cells, a loss of $MIC26_{22kDa}$ is observed contrary to an increased amount of 55 kDa protein in WT. B) The KO of *MIC26* in HepG2 cells leads to the loss of the 22kDa form but unchanged expression of the 55 kDa band. C) HeLa cells show similar results to HEK293 cells w.r.t loss of the 22 kDa form and an increased expression of the 55 kDa band. D) In HAP1 cells, the *MIC26* KO leads to a loss of the mitochondrial $MIC26_{22kDa}$ protein contrary to unaltered expression of the 55 kDa protein in WT cells.

https://doi.org/10.1371/journal.pone.0286756.g002

and MIC27 proteins were absent when the corresponding genes were knocked out as expected when compared to respective control cells. On the contrary, no loss of 55 kDa protein was observed when using an antibody directed against MIC26 (Fig 2A–2D, topmost panels). Similarly, immunoblotting using an anti-MIC27 antibody does not show a protein in the 55 kDa region in WT cells as well as when cells were knocked out for *MIC27* (Fig 2A–2D and S3A–S3D Fig). In conclusion, the 55 kDa protein belongs neither to MIC26 nor MIC27 confirming that MIC26 and MIC27 only exist as *bona fide* mitochondrial proteins.

Mutation of various predicted glycosylation sites leads to no change in the level of 55 kDa protein

The experiments involving downregulation (Fig 1A) and KOs of *MIC26* and *MIC27* in multiple human cell lines (Fig 2) using antibody #1 showed that the 55 kDa protein is nonspecific. Further, in order to rule out the possibility that the glycosylation of MIC26 is a possible reason why all four antibodies employed against MIC26 do not recognise the $MIC26_{55kDa}$ protein, we used WT HEK293 cells exogenously expressing MIC26-GFP and probed with an anti-GFP antibody which must recognise GFP of the $MIC26_{55kDa}$-GFP fusion protein. If the $MIC26_{55kDa}$ protein exists, exogenous expression of MIC26-GFP in control HEK293 cells should lead to the formation of 82 kDa protein in addition to the untagged endogenous $MIC26_{55kDa}$ protein. When HEK293 cells expressing MIC26-GFP were probed with an anti-MIC26 (antibody #1) and anti-GFP antibody, a 47 kDa protein (Red asterisks) consistent with the size of mitochondrial MIC26-GFP was observed while no additional band at 82 kDa was detected (Fig 3A and 3B). This provides additional evidence that MIC26 exists only as a mitochondrial protein. In addition, we checked if the presumed $MIC26_{55kDa}$ was sensitive to the disruption of glycosylation pattern. Here, it was predicted *in silico* that three serine amino acid residues of MIC26 could be glycosylated at positions 34, 41 and 50 [46]. Thus, we separately mutated the three serine amino acid residues to alanine to render them incapable of glycosylation. Then, we expressed the theoretically predicted single mutant non-glycosylated versions of MIC26-GFP namely $MIC26^{S34A}$-GFP, $MIC26^{S41A}$-GFP and $MIC26^{S50A}$-GFP in control HEK293 cells and used an anti-MIC26 and anti-GFP antibody to check the size of MIC26-GFP (Fig 3A and 3B). While a 47 kDa protein comprising mitochondrial MIC26-GFP was detected (Fig 3A and 3B) (Red asterisks), a protein corresponding to 82 kDa (55 kDa protein tagged with GFP) was not found (Fig 3A and 3B). When HEK293 cells expressing either MIC26-GFP or the glycosylation defective mutants were further probed with another anti-MIC26 antibody #3, we neither detected a 55 kDa nor a 82 kDa protein (S4 Fig). However, exogenously expressed MIC26-GFP or variants of MIC26-GFP were detected as a 47 kDa protein. It was interesting to note that antibody #3 did not recognise the exogenously expressed $MIC26^{S41A}$-GFP in HEK293 cells showing that serine at position 41 is an important binding site for antibody #3 (S4 Fig). Taken together, we further corroborate that MIC26 only exists as a mitochondrial protein that is not apparently glycosylated.

Since the addition of a large GFP tag could probably disturb the glycosylation pattern of MIC26, we used *MIC26* KOs of HEK293 cells and expressed either an untagged or myc-tagged MIC26 on its C-terminus. WBs of *MIC26* KOs expressing MIC26-myc revealed a mitochondrial myc-specific form, when probed with an antibody against MIC26, that was running slightly above the untagged MIC26 protein (Fig 3C). Expression of MIC26-myc in *MIC26* KOs also revealed a myc-tagged MIC26 when an anti-myc antibody was used. However, we did not observe any increase of the 55 kDa protein while expressing either untagged or myc-tagged MIC26 in *MIC26* KOs. This was also in accordance with a previous report where HeLa cells expressing N-terminal myc-tagged MIC26 were used [46]. Although a mitochondrial

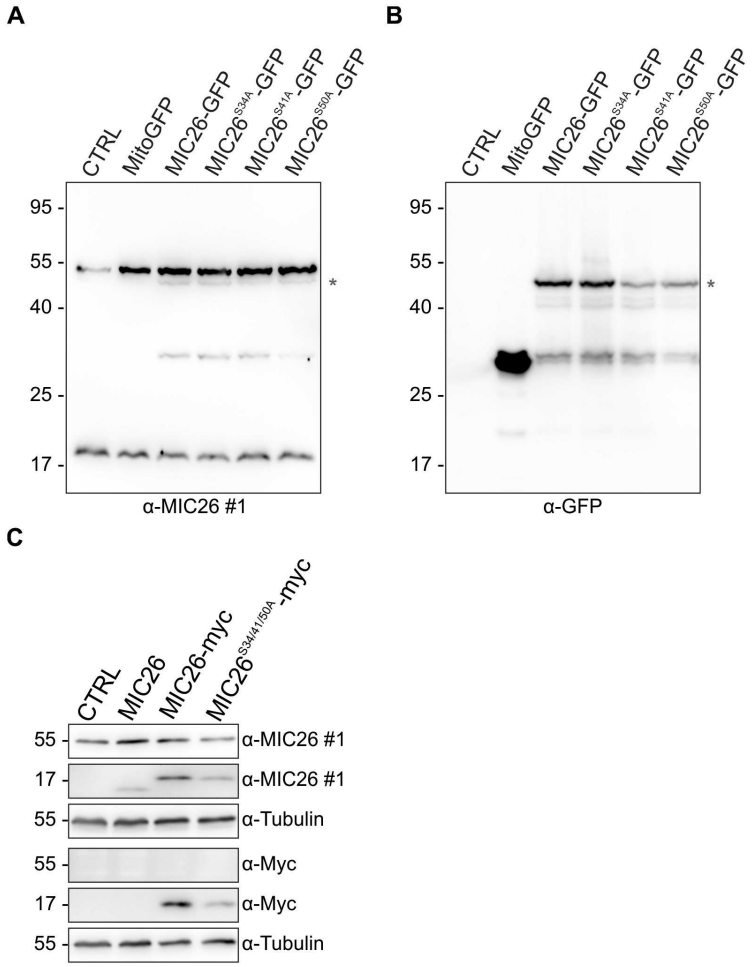

Fig 3. Exogenous expression of MIC26-GFP or MIC26-myc does not result in the formation of corresponding $MIC26_{55kDa}$-GFP or $MIC26_{55kDa}$-myc protein. WB analysis of HEK293 cells expressing MIC26-GFP or MIC26-myc along with various theoretically predicted glycosylation defective mutants. A) Overexpression of mitoGFP (control), MIC26-GFP and the single mutants of MIC26-GFP namely $MIC26^{S34A}$-GFP, $MIC26^{S41A}$-GFP and $MIC26^{S50A}$-GFP in HEK WT cells leads to detection of the endogenous $MIC26_{22kDa}$ protein, a $MIC26_{22kDa}$-GFP protein (≈ 50 kDa protein below the 55 kDa protein marked in red asterisks) and the endogenous 55 kDa band when antibody #1 was used. B) Immunoblotting with anti-GFP antibody shows a ≈ 50 kDa band detecting $MIC26_{22kDa}$-GFP. However, no band correlating to a $MIC26_{55kDa}$-GFP protein (≈ 80 kDa) could be observed. C) Exogenous expression of MIC26-myc in HEK293 *MIC26* KO leads to the formation of $MIC26_{22kDa}$-myc protein with an expected slight shift in molecular weight compared to the expression of untagged MIC26. However, $MIC26_{55kDa}$-myc protein was neither detected with anti-MIC26 nor anti-myc tag antibody. Expression of the glycosylation defective triple mutant, $MIC26^{S34A/S41A/S50A}$-myc, where the respective serine amino acids were mutated to alanine (S34A, S41A, S50A), showed unaltered 55 kDa protein levels.

https://doi.org/10.1371/journal.pone.0286756.g003

$MIC26_{22kDa}$-myc was detected with an anti-myc antibody, no protein was detected at 55 kDa. Further, we generated a C-terminal myc tag plasmid expressing a glycosylation defective triple mutant, S34A/S41A/S50A, in *MIC26* KOs where all three serine amino acids were mutated into alanine. Mutations of all three serine amino acid residues into alanine should lead to an abolished O-linked glycosylation and loss of the 55 kDa protein. However, despite mutating multiple serines into alanine, we neither observed a loss of the 55 kDa protein nor the expression of myc-tag protein in the 55 kDa region (Fig 3C). These observations show that the 55 kDa protein does not originate from MIC26.

The mitochondrial MIC26 is consistently detected in murine tissues, cells and human cells in contrast to the putative 55 kDa glycosylated version

We have performed *MIC26* downregulation with three different siRNAs in HEK293 cells, probed with four different anti-MIC26 antibodies using control and HepG2 *MIC26* KO cells and further tested *MIC26* KOs in three other human cell lines namely HEK293, HeLa and HAP1 cells (Fig 2), and exogenously expressed MIC26-GFP and MIC26-myc in HEK293 cells (Fig 3 and S4 Fig) which consistently validated that the 55 kDa protein of MIC26 does not exist. In addition, in order to corroborate our observations across species, we compared murine liver lysates from WT C57BL6/J mice with human HEK293 and HeLa cell lysates using multiple antibodies and tested for the presence of a 55 kDa protein. WBs consistently revealed the mitochondrial $MIC26_{22kDa}$ (Fig 4A and 4B, S5A and S5B Fig) reiterating that all four antibodies recognise the correct protein in human cell lines. In the respective WBs, we also loaded lysates of murine liver for comparing the immunoreactivity of anti-MIC26 antibody in human cells and murine tissue. In congruence with human cell line data, antibodies #1 and #2 detected the mitochondrial $MIC26_{22kDa}$ protein in murine liver (Fig 4A & 4B). Hence, antibody #1 and #2 could be used to detect the specific mitochondrial $MIC26_{22kDa}$ protein in human and murine samples. However, one must be cautious in interpreting a band with an apparent molecular weight around 55 kDa using antibody #1 (Fig 4A) as this is not specific to MIC26. Further, we used plasma from WT C57BL6/J mice and found that there is no detection of any protein of any size using anti-MIC26 antibodies #1 and #2 (Fig 4C and 4D) confirming that MIC26 is not secreted into murine plasma. In addition, in order to check whether $MIC26_{22kDa}$ is recognised by both these antibodies in cells having murine origin along with other murine tissues, we used murine lysates of white adipose tissue, muscle, liver and plasma along with C2C12 myoblast cell line and found that antibody #1 and #2 consistently recognise the mitochondrial $MIC26_{22kDa}$ (Fig 4E and 4F).

Further, we compared the WBs of HEK293 and HeLa cell lysates with murine liver lysates using two other antibodies (#3 and #4) against MIC26 (S5A and S5B Fig). As shown before (Fig 1D and 1E), antibodies #3 and #4 recognised the human cell lysates (S5A and S5B Fig). However, antibody #3 did not recognise the murine $MIC26_{22kDa}$ protein (S5A Fig) but recognised nonspecific proteins in murine liver lysates which includes a ≈ 25 kDa (Green asterisks) and a 55 kDa protein (S5A Fig). Since the antibody #3 was raised in mouse, the 25 and the 55 kDa proteins probably correspond to the IgG light and heavy chains which were only observed in murine plasma (S5C Fig), liver, muscle and white adipose tissue but not in C2C12 myoblast cell lysate (S5E Fig). We conclude that antibody #3 is not suitable for detecting MIC26 in murine samples. Next, in order to validate whether the 55 kDa protein is recognised in a non-specific manner in murine samples, we used our custom-made antibody #4 which was designed to immunoreact only to human $MIC26_{22kDa}$ and not murine $MIC26_{22kDa}$. The epitope used to elicit the anti-MIC26 antibody production in rabbit contained a total of 12 amino acids which perfectly match the human MIC26 but not mouse MIC26 as there was a four

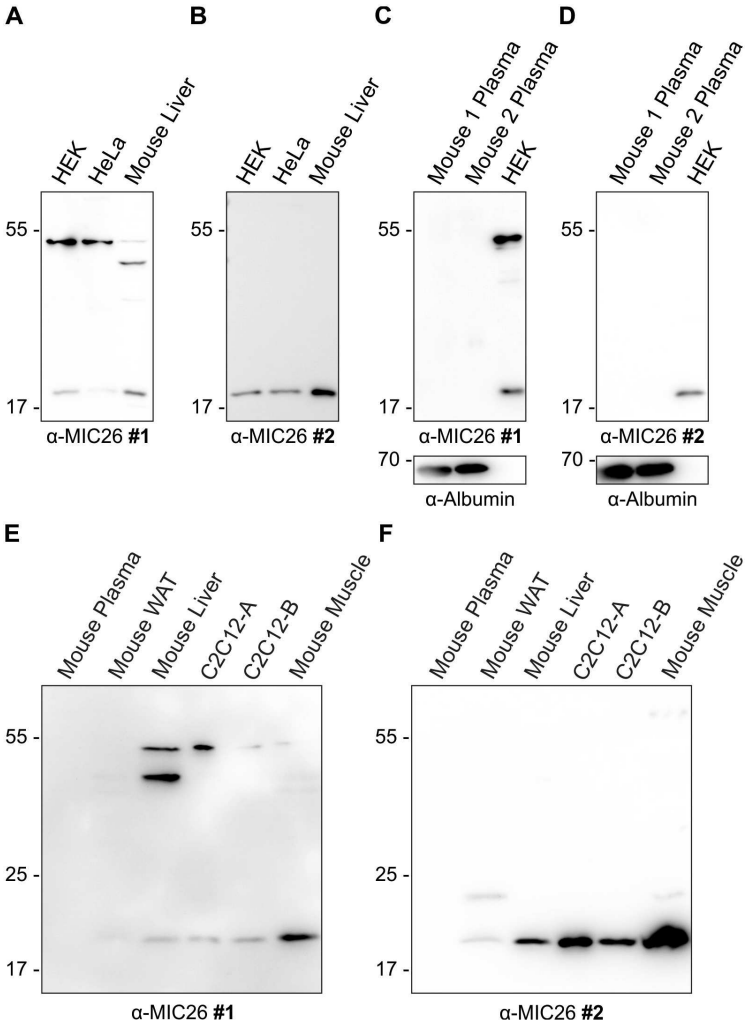

Fig 4. Unspecific nature of the 55 kDa band is neither cell line- or species-specific. WB analysis of human WT HEK293 and HeLa cell lysates along with murine liver tissue lysates and plasma comparing two different anti-MIC26 antibodies: A) Antibody #1 detects $MIC26_{22kDa}$ and an unspecific 55 kDa protein in HEK293 and HeLa as well as in murine liver. B) Antibody #2 exclusively detects the mitochondrial $MIC26_{22kDa}$, but no 55 kDa band. C) Antibody #1 does not recognize a mitochondrial $MIC26_{22kDa}$ and 55 kDa band in plasma samples from two mice. D) Antibody #2, like antibody #1, does not recognize any protein in murine plasma samples. E) Antibody #1 detects the $MIC26_{22kDa}$ as well as an unspecific 55 kDa band in C2C12 cell line along with different murine tissue lysates but not plasma. F) Antibody #2 detects $MIC26_{22kDa}$ in mouse cell lines and tissues but not the 55 kDa band. C2C12-A represents C2C12 cells lysed with RIPA buffer and C2C12-B represents C2C12 cells which were mechanically lysed.

https://doi.org/10.1371/journal.pone.0286756.g004

amino acid mis-alignment (S1C Fig). Accordingly, on one hand, in murine liver samples, we did not observe a mitochondrial $MIC26_{22kDa}$ band while observing a presumed nonspecific band at various sizes including a 55 kDa band (S5B Fig). On the other hand, in human HEK293 and HeLa cells, antibody #4 showed multiple bands including the $MIC26_{22kDa}$ and a protein at the 55 kDa region (S5B Fig). Therefore, antibody #4 specifically recognised human mitochondrial $MIC26_{22kDa}$ while multiple other nonspecific bands were detected on the WBs in murine liver, HEK293 and HeLa cell lysates including a 55 kDa protein (S5B Fig). Clearly, this inconsistent detection of the 55 kDa protein upon using different antibodies in mammalian HEK293, HeLa cell and murine liver lysates strongly argues further for its nonspecific nature. Thus, while all the four antibodies were recognising the mitochondrial $MIC26_{22kDa}$ version in human cell lysates, only two antibodies (#1 & #2) used in this study are suitable to recognise $MIC26_{22kDa}$ mitochondrial version in murine tissues and cells.

Mass spectrometry data of 55 kDa protein does not reveal MIC26-specific peptides

The experiments performed in this study conclude that the presumed 55 kDa protein recognised using anti-MIC26 antibodies is nonspecific. Finally, we tested for the presence of MIC26-specific peptides using mass spectrometry in WT, *MIC26* and *MIC27* KO HEK293 cells. For this, we ran the corresponding cell lysates on an SDS gel after which the protein bands at and around the 55 kDa region (≈ 47 to 63 kDa proteins) were excised and the samples were given for mass spectrometry (MS) analysis. We could detect a total of 1273 proteins in the excised gel pieces in all the three samples. In total 278 mitochondrial proteins were detected including e.g. Prohibitin-2, NADH dehydrogenase flavoprotein 1, TIM50, glycerol kinase 2. However, as expected, we did not find MIC26-specific peptides in the MS analysis in any of the three samples analysed which included WT, *MIC26* and *MIC27* KOs. The list of detected peptides is presented in the S1 Data file. Hence, all the experiments presented in this study including the MS results conclusively show that the 55 kDa protein is of nonspecific nature with respect to MIC26.

The levels of the $MIC26_{22kDa}$ mitochondrial protein are not altered in heart and livers of a db/db diabetic mouse model

MIC26 mRNA was previously found to be increased in hearts of people with diabetes mellitus [43]. *MIC26* was also elevated in the transcriptome of hearts of dogs fed with high-fat diet [50]. Therefore, we examined whether MIC26 levels were changed in a murine model of obesity-related diabetes. For this, we used db/db.BKS mice which during the first three months develop massive obesity and uncontrolled diabetes due to a mutation in the leptin receptor [61–63]. The lean db/+ mice are normoglycemic and served as controls. We obtained heart and liver tissues from three male diabetic (db/db) and control (db/+) mice at the age of 12 weeks (hence diabetic) [64] and performed WBs using antibody #2 which specifically recognised only the $MIC26_{22kDa}$ mitochondrial band in heart and liver of control and diabetic mice (Fig 5A and 5C). Quantification of the mitochondrial $MIC26_{22kDa}$ protein level (Fig 5B and 5D) revealed no change in heart and liver tissues between control and diabetic mice. Additionally, we checked *Mic26* and *Mic27* transcript levels in liver of db/db.BKS diabetic and control mice and found no differences (Fig 5E). Thus, we conclude that in this standard mouse model for obesity and diabetes, we do not observe differences of $MIC26_{22kDa}$ protein levels in the heart and liver tissues compared to control mice.

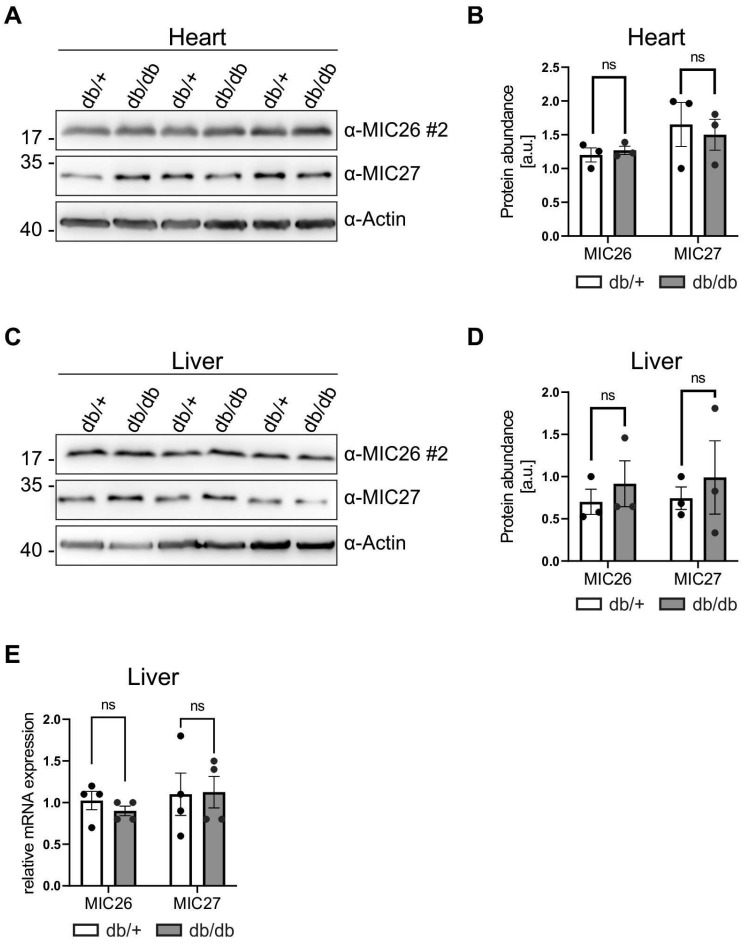

Fig 5. The diabetic db/db mouse model does not show different levels of the exclusively mitochondrially localized MIC26 and MIC27 proteins in heart and liver. WB analysis of lysates from heart (A) and liver (C) tissue, along with associated quantification showing protein levels of MIC26 and MIC27 (B and D) from control db/+ and diabetic db/db.BKS mice, reveal no significant differences in amounts of MIC26 and MIC27. E) *Mic26* and *Mic27* transcript levels are not changed in liver of control db/+ and db/db.BKS diabetic mice.

https://doi.org/10.1371/journal.pone.0286756.g005

Discussion

The MIC26 protein was first identified in 2006 where it was detected as a 55 kDa protein in the serum of human, mouse, dogs and in human heart and HepG2 cells despite the size of the recombinant protein being only 22 kDa [43]. Other studies convincingly showed $MIC26_{22kDa}$ was found to be localised to mitochondria which performs important roles in mitochondrial

ultrastructure and function in mammalian cell lines [31,46,48]. In fact, overexpression or downregulation of *MIC26* led to many defects in mitochondrial function [46,59]. During the course of experiments performed for this study, we found that downregulation of *MIC26* using three different siRNAs resulted in a drastic decrease of the mitochondrial $MIC26_{22kDa}$ but showed no effect on the $MIC26_{55kDa}$. In fact, the insensitivity of the $MIC26_{55kDa}$ to the downregulation of the *MIC26* was also observed in other publications but was not focussed upon [40,59]. Further, we employed the *MIC26* as well as *MIC27* KOs in HepG2, HeLa, HEK293 and HAP1 cells. The KO cell lines of *MIC26* did not show a decrease of the presumed 55 kDa protein of MIC26. This is the first report which focussed on the presence of 55 kDa in *MIC26* KO cell lines in combination with multiple validated antibodies. Next, when we expressed exogenous *MIC26-GFP* and *MIC26-myc* in WT and *MIC26* KOs of HEK293 cells respectively and probed with an antibody against MIC26 and GFP or MIC26 and myc, we were not able to detect the corresponding 55 kDa fusion protein of MIC26. However, the mitochondrial $MIC26_{22kDa}$ was consistently observed. A previous study overexpressing *Mic26* in H9C2 rat cardiac myoblast cells led to the formation of a protein which had the same size as recombinant mitochondrial 22 kDa MIC26 protein. Thus, we suppose that the detected protein was mitochondrial $MIC26_{22kDa}$ and not the 55 kDa protein as defined in a previous report [47]. In order to verify if the presumed 55 kDa MIC26 protein was detectable in other species, we studied plasma, tissue and cell lines of murine origin using four antibodies available. Two out of four antibodies are able to detect murine MIC26, while the other two antibodies exclusively showed human specific reactivity. Using an antibody which only showed species reactivity with human samples resulted in no detection of a MIC26 mitochondrial version in murine tissues as expected, while the presumed $MIC26_{55kDa}$ could still be detected. Different to the immunoreactivity of murine tissues, when we used cell lysates from HEK293 and HeLa cells, we consistently detected the $MIC26_{22kDa}$ band but not the $MIC26_{55kDa}$ band. Therefore, experiments involving RNAi, KO cell lines and overexpression of *MIC26* in combination with multiple antibodies demonstrate that the reported 55 kDa protein band does not represent MIC26. We were interested to check the $MIC26_{22kDa}$ in a well-established diabetic mouse model, db/db.BKS, since *MIC26* transcripts were found to be upregulated in the hearts of people with diabetes [43]. However, we were not able to detect differences on protein level in the heart and liver tissue lysates for MIC26 and MIC27. This discrepancy could arise from increased degradation of MIC26 in db/db mice compared to control mice which probably results in increased levels of MIC26 transcripts as a compensatory mechanism.

Previous studies showed that a $MIC26_{55kDa}$ was invariably observed [43,46,47,53,54,65] and several indications supported the wrong interpretation that this form is a glycosylated variant of MIC26. A cleavage of the presumed $MIC26_{55kDa}$ into an apparent 22 kDa form was observed after cABC treatment [43,46]. Similarly, treatment of cells with an inhibitor of glycosylation by using *p*-nitrophenyl-*β*-D-xyloside (PNPX) led to a partial increase of the $MIC26_{22kDa}$ band [43] which, however, was not very efficient. In addition, the secretion of MIC26 into the medium was decreased by using microsomal triglyceride transfer protein (MTP) inhibitors like Naringenin and CP-346086. However, even the secretion could only be inhibited to a maximum of 50%. Therefore, on one hand the authors of this manuscript stated that the $MIC26_{22kDa}$ is a result of cleaving the O-linked glycosylation of $MIC26_{55kDa}$, while on the other hand the inefficient cleavage of $MIC26_{55kDa}$ into $MIC26_{22kDa}$ was explained by $MIC26_{55kDa}$ possessing alternate glycosylation patterns. Further, while it is plausible that a protein could have multiple post-translational modifications including glycosylation, the specificity of the $MIC26_{55kDa}$ as a *bona fide* version of MIC26 protein was not validated through any depletion experiments in previous studies, which we have performed in multiple ways in this study, and which shed doubt over the nature of $MIC26_{55kDa}$ protein. In fact, when a transgenic

mouse overexpressing *Mic26* was used, the transcript levels of *Mic26* were roughly doubled as expected [47]. However, WBs showed a disproportionate increase in the $MIC26_{55kDa}$ band in this study. This could be explained by the fact that the antibody used to detect the 55 kDa band is promiscuously recognising another secreted protein which is affected due to the *MIC26* KOs. It is further possible that the unspecific protein being promiscuously recognised is also sensitive to partial cleavage by cABC which could explain previous data that glycosylation inhibitors like PNPX result in reduced amounts of the assumed 55 kDa glycosylated form of MIC26 or the apparent cleavage of the nonspecific 55 kDa protein after cABC treatment [43,46]. Still, we asked whether the 55 kDa protein of MIC26 really exists and is being secreted by checking the previous human secretome studies. 2641 proteins were predicted to be comprising the revised whole human secretome [65]. MIC26 despite being predicted to be secreted in the human blood was not empirically found in mass spectrometry analysis, antibody-based immunoassays and proximity extension assays [65]. Consistently, MIC26 was not found as a protein secreted by HepG2 cells [66,67]. Previously, it was found that oleic acid treatment of HepG2 cells increased the protein levels of the 55 kDa of MIC26 [52,54]. However, the secretome profile of HepG2 cells did not include MIC26 among the list of upregulated or downregulated proteins when cells were treated with oleic acid compared to untreated cells [66]. Accordingly, when we eluted proteins in the range of 47 to 63 kDa and analysed a list of 1273 proteins detected by MS, we were not able to detect MIC26-specific peptides in control cells as well as *MIC27* KOs. All the above observations provide evidence that the 55 kDa protein originally assigned as MIC26 is of nonspecific nature.

Various monoclonal and polyclonal antibodies respond differently with respect to the recognition of the presumed 55 kDa protein band of MIC26 in various studies (commercial or custom-made). In one of the initial studies, a mixture of two epitopes were used to generate an anti-MIC26 antibody where one epitope covered the N-terminus from amino acids 22 to 36 whereas another epitope covered the C-terminus covering amino acids 184–198. This antibody strongly detected the 55 kDa protein. Antibody #1 was made using an epitope of 66 amino acids covering C-terminus region from 133–198 of MIC26 whereas antibody #2 was made where the epitopes covered amino acids 9 to 38. While antibody #1 recognises a 55 kDa band, antibody #2 does not recognise it. Therefore, taken together it is possible that the nonspecificity of the 55 kDa form arises from the C-terminal region as antibodies made from exposure to N-terminal epitope do not recognise the 55 kDa region. Overall, this study demonstrates the importance of antibody validation using respective KO cell lines and gives valuable hints how to study the role of MIC26 in the future.

Supporting information

S1 Checklist. The ARRIVE guidelines 2.0: Author checklist.
(PDF)

S1 Fig. Overview and alignment of various anti-MIC26 antibodies. A) Summary of seven anti-MIC26 antibodies used in this study (#1-#4) and other (#1, #3, #5-#7) publications are described. The figure provides 1) the source of the antibody, 2) the host and region of the peptide used for antibody generation (amino acid numbers: aa), 3) the related color-code to (B), 4) publications describing the usage of the respective antibody, 5) if studies were performed regarding the 55 kDa form of MIC26 and if yes 6) which cell lines or tissues have been investigated. N/A is Not Applicable. B) Alignment of the human and mouse MIC26 amino acid sequence shows an identity of 83%. The epitopes used to generate different anti-MIC26 antibodies are highlighted by color-code and further described in the figure above. C) Alignment of the human and mouse MIC26 amino acid sequences, from position 61 to 110, with 12 amino-

acid epitope used to generate antibody #4 (Home-made, Pineda) which shows proper alignment of antibody #4 epitope to human MIC26, but not mouse MIC26 where four mismatches were detected. Red color shows eight amino acids which are matching out of 12 amino acids.
(TIF)

S2 Fig. MIC26 is exclusively present in mitochondrial fractions. A) WBs showing the total cellular fraction, mitochondrial fraction as well as a fraction containing combined ER, Golgi and remaining cytosol, when anti-MIC26 antibody #1 was used. Antibodies against ANT2 and calreticulin served as markers for the mitochondrial as well as the combined ER, Golgi and cytosolic fraction respectively. B-D) WBs showing different fractions mentioned above where anti-MIC26 antibodies #2–4 were used.
(TIF)

S3 Fig. A 55 kDa band is not detected by anti-MIC27 antibody. A-D) WB analysis of cell lysates from HEK293 (A), HepG2 (B), HeLa (C) and HAP1 (D) cells using anti-MIC27 antibody in WT, *MIC26* KO and *MIC27* KOs. Whole WBs are shown for clarity.
(TIF)

S4 Fig. Exogenous MIC26-GFP expression does not generate $MIC26_{55kDa}$-GFP. Antibody #3 detects the endogenous $MIC26_{22kDa}$ protein as well as $MIC26_{22kDa}$-GFP. However, no $MIC26_{22kDa}$-GFP protein was detected for the S41A mutant, leading to the assumption, that the antibody #3 has a strong binding affinity for serine in position 41. Furthermore, in accordance with anti-MIC26 antibody #1 and anti-GFP antibody (Fig 3), a ≈ 80 kDa $MIC26_{55kDa}$-GFP protein was not recognized.
(TIF)

S5 Fig. MIC26 antibody #3 and #4 recognize human but not murine $MIC26_{22kDa}$. A) Antibody #3 shows immunoreactivity against $MIC26_{22kDa}$ in human cell lines but not murine liver tissue lysates, providing evidence regarding the unspecific nature of the detected 25 kDa and 55 kDa proteins in liver lysates. Additionally, antibody #3 shows an unspecific binding of ≈ 70 kDa protein in human cell lines. B) Antibody #4, comparable to antibody #3, shows immunoreactivity against $MIC26_{22kDa}$ in human cell lines but not murine liver tissue lysate revealing the unspecific nature of several additional bands detected in murine liver. C) Antibody #3 non-specifically recognizes a 25 kDa and a 55 kDa protein in two different murine plasma samples, probably derived from light and heavy chain of IgG. D) Antibody #4 detects an unspecific band at approximately 70 kDa in murine plasma samples. E) Antibody #3 is not able to recognize $MIC26_{22kDa}$ protein in murine samples. However, it recognizes a 25 kDa and a 55 kDa band only in murine tissue samples but not in mouse cell lines indicating a nonspecific detection of the light and heavy chain of IgG. C2C12-A represents C2C12 cells lysed with RIPA buffer and C2C12-B represents C2C12 cells which were lysed mechanically.
(TIF)

S1 Data. Excel sheet of mass spectrometry analysis. The excel sheet depicts all identified peptides from mass spectrometry analysis of HEK293 WT, *MIC26* and *MIC27* KO cell lines, which were isolated from an SDS gel, having a molecular weight of ≈ 47–63 kDa. Sheet 1 contains all detected proteins, while sheet 2 is filtered only for mitochondrial proteins identified from Gene Ontology (GO) cellular compartments.
(XLSX)

S1 Raw images. Uncropped blots of all blots shown in the manuscript.
(PDF)

Acknowledgments

We thank Tanja Portugall for technical assistance in constructing the plasmids used in this study. Mass spectrometry experiments were performed at the proteomics facility, BMFZ, HHU, Düsseldorf. FACS cell sorting was performed at ITZ, UKD, HHU, Düsseldorf by Katharina Raba.

Author Contributions

Conceptualization: Arun Kumar Kondadi.

Formal analysis: Melissa Lubeck, Ritam Naha, Marc D. Driessen.

Funding acquisition: Ruchika Anand, Andreas S. Reichert, Arun Kumar Kondadi.

Investigation: Melissa Lubeck, Nick H. Derkum, Marc D. Driessen, Ruchika Anand.

Methodology: Melissa Lubeck, Arun Kumar Kondadi.

Project administration: Arun Kumar Kondadi.

Resources: Rebecca Strohm, Bengt-Frederik Belgardt, Michael Roden, Kai Stühler, Andreas S. Reichert.

Supervision: Andreas S. Reichert, Arun Kumar Kondadi.

Validation: Melissa Lubeck.

Visualization: Melissa Lubeck, Ritam Naha.

Writing – original draft: Arun Kumar Kondadi.

Writing – review & editing: Melissa Lubeck, Bengt-Frederik Belgardt, Michael Roden, Ruchika Anand, Andreas S. Reichert, Arun Kumar Kondadi.

References

1. Wurm CA, Jakobs S. Differential protein distributions define two sub-compartments of the mitochondrial inner membrane in yeast. FEBS letters. 2006; 580(24):5628–34. https://doi.org/10.1016/j.febslet.2006.09.012 PMID: 16997298
2. Vogel F, Bornhovd C, Neupert W, Reichert AS. Dynamic subcompartmentalization of the mitochondrial inner membrane. The Journal of cell biology. 2006; 175(2):237–47. https://doi.org/10.1083/jcb.200605138 PMID: 17043137
3. Kondadi AK, Anand R, Reichert AS. Cristae Membrane Dynamics—A Paradigm Change. Trends Cell Biol. 2020; 30(12):923–36. https://doi.org/10.1016/j.tcb.2020.08.008 PMID: 32978040
4. Zick M, Rabl R, Reichert AS. Cristae formation-linking ultrastructure and function of mitochondria. Biochimica et biophysica acta. 2009; 1793(1):5–19. https://doi.org/10.1016/j.bbamcr.2008.06.013 PMID: 18620004
5. Galloway CA, Yoon Y. Mitochondrial dynamics in diabetic cardiomyopathy. Antioxid Redox Signal. 2015; 22(17):1545–62. https://doi.org/10.1089/ars.2015.6293 PMID: 25738230
6. Baloyannis SJ. Mitochondrial alterations in Alzheimer's disease. Journal of Alzheimer's disease: JAD. 2006; 9(2):119–26. https://doi.org/10.3233/jad-2006-9204 PMID: 16873959
7. Vincent AE, Ng YS, White K, Davey T, Mannella C, Falkous G, et al. The Spectrum of Mitochondrial Ultrastructural Defects in Mitochondrial Myopathy. Sci Rep. 2016; 6:30610. https://doi.org/10.1038/srep30610 PMID: 27506553
8. Perkins G, Renken C, Martone ME, Young SJ, Ellisman M, Frey T. Electron tomography of neuronal mitochondria: three-dimensional structure and organization of cristae and membrane contacts. Journal of structural biology. 1997; 119(3):260–72. https://doi.org/10.1006/jsbi.1997.3885 PMID: 9245766
9. Perkins GA, Tjong J, Brown JM, Poquiz PH, Scott RT, Kolson DR, et al. The micro-architecture of mitochondria at active zones: electron tomography reveals novel anchoring scaffolds and cristae structured

for high-rate metabolism. The Journal of neuroscience: the official journal of the Society for Neuroscience. 2010; 30(3):1015–26. https://doi.org/10.1523/JNEUROSCI.1517-09.2010 PMID: 20089910

10. Frey TG, Renken CW, Perkins GA. Insight into mitochondrial structure and function from electron tomography. Biochimica et biophysica acta. 2002; 1555(1–3):196–203. https://doi.org/10.1016/s0005-2728(02)00278-5 PMID: 12206915
11. Mannella CA, Lederer WJ, Jafri MS. The connection between inner membrane topology and mitochondrial function. Journal of molecular and cellular cardiology. 2013; 62:51–7. https://doi.org/10.1016/j.yjmcc.2013.05.001 PMID: 23672826
12. Mannella CA, Marko M, Penczek P, Barnard D, Frank J. The internal compartmentation of rat-liver mitochondria: tomographic study using the high-voltage transmission electron microscope. Microscopy research and technique. 1994; 27(4):278–83. https://doi.org/10.1002/jemt.1070270403 PMID: 8186446
13. Mannella CA, Pfeiffer DR, Bradshaw PC, Moraru II, Slepchenko B, Loew LM, et al. Topology of the mitochondrial inner membrane: dynamics and bioenergetic implications. IUBMB life. 2001; 52(3–5):93–100. https://doi.org/10.1080/15216540152845885 PMID: 11798041
14. Wolf DM, Segawa M, Kondadi AK, Anand R, Bailey ST, Reichert AS, et al. Individual cristae within the same mitochondrion display different membrane potentials and are functionally independent. The EMBO journal. 2019; 38(22):e101056. https://doi.org/10.15252/embj.2018101056 PMID: 31609012
15. Harner M, Korner C, Walther D, Mokranjac D, Kaesmacher J, Welsch U, et al. The mitochondrial contact site complex, a determinant of mitochondrial architecture. The EMBO journal. 2011; 30(21):4356–70. https://doi.org/10.1038/emboj.2011.379 PMID: 22009199
16. Hoppins S, Collins SR, Cassidy-Stone A, Hummel E, Devay RM, Lackner LL, et al. A mitochondrial-focused genetic interaction map reveals a scaffold-like complex required for inner membrane organization in mitochondria. The Journal of cell biology. 2011; 195(2):323–40. https://doi.org/10.1083/jcb.201107053 PMID: 21987634
17. von der Malsburg K, Muller JM, Bohnert M, Oeljeklaus S, Kwiatkowska P, Becker T, et al. Dual role of mitofilin in mitochondrial membrane organization and protein biogenesis. Developmental cell. 2011; 21(4):694–707. https://doi.org/10.1016/j.devcel.2011.08.026 PMID: 21944719
18. Anand R, Strecker V, Urbach J, Wittig I, Reichert AS. Mic13 Is Essential for Formation of Crista Junctions in Mammalian Cells. PloS one. 2016; 11(8):e0160258. https://doi.org/10.1371/journal.pone.0160258 PMID: 27479602
19. Guarani V, McNeill EM, Paulo JA, Huttlin EL, Frohlich F, Gygi SP, et al. QIL1 is a novel mitochondrial protein required for MICOS complex stability and cristae morphology. eLife. 2015; 4. https://doi.org/10.7554/eLife.06265 PMID: 25997101
20. Urbach J, Kondadi AK, David C, Naha R, Deinert K, Reichert AS, et al. Conserved GxxxG and WN motifs of MIC13 are essential for bridging two MICOS subcomplexes. Biochim Biophys Acta Biomembr. 2021; 1863(12):183683. https://doi.org/10.1016/j.bbamem.2021.183683 PMID: 34271005
21. Ott C, Ross K, Straub S, Thiede B, Gotz M, Goosmann C, et al. Sam50 functions in mitochondrial intermembrane space bridging and biogenesis of respiratory complexes. Molecular and cellular biology. 2012; 32(6):1173–88. https://doi.org/10.1128/MCB.06388-11 PMID: 22252321
22. Tang J, Zhang K, Dong J, Yan C, Hu C, Ji H, et al. Sam50-Mic19-Mic60 axis determines mitochondrial cristae architecture by mediating mitochondrial outer and inner membrane contact. Cell death and differentiation. 2020; 27(1):146–60. https://doi.org/10.1038/s41418-019-0345-2 PMID: 31097788
23. Munoz-Gomez SA, Cadena LR, Gardiner AT, Leger MM, Sheikh S, Connell LB, et al. Intracytoplasmic-membrane development in alphaproteobacteria involves the homolog of the mitochondrial crista-developing protein Mic60. Current biology: CB. 2023.
24. Huynen MA, Muhlmeister M, Gotthardt K, Guerrero-Castillo S, Brandt U. Evolution and structural organization of the mitochondrial contact site (MICOS) complex and the mitochondrial intermembrane space bridging (MIB) complex. Biochimica et biophysica acta. 2016; 1863(1):91–101. https://doi.org/10.1016/j.bbamcr.2015.10.009 PMID: 26477565
25. Munoz-Gomez SA, Slamovits CH, Dacks JB, Baier KA, Spencer KD, Wideman JG. Ancient homology of the mitochondrial contact site and cristae organizing system points to an endosymbiotic origin of mitochondrial cristae. Current biology: CB. 2015; 25(11):1489–95. https://doi.org/10.1016/j.cub.2015.04.006 PMID: 26004762
26. Kaurov I, Vancova M, Schimanski B, Cadena LR, Heller J, Bily T, et al. The Diverged Trypanosome MICOS Complex as a Hub for Mitochondrial Cristae Shaping and Protein Import. Current biology: CB. 2018; 28(21):3393–407.e5. https://doi.org/10.1016/j.cub.2018.09.008 PMID: 30415698
27. Anand R, Reichert AS, Kondadi AK. Emerging Roles of the MICOS Complex in Cristae Dynamics and Biogenesis. Biology (Basel). 2021; 10(7). https://doi.org/10.3390/biology10070600 PMID: 34209580

28. Hessenberger M, Zerbes RM, Rampelt H, Kunz S, Xavier AH, Purfurst B, et al. Regulated membrane remodeling by Mic60 controls formation of mitochondrial crista junctions. Nature communications. 2017; 8:15258. https://doi.org/10.1038/ncomms15258 PMID: 28561061

29. Tarasenko D, Barbot M, Jans DC, Kroppen B, Sadowski B, Heim G, et al. The MICOS component Mic60 displays a conserved membrane-bending activity that is necessary for normal cristae morphology. The Journal of cell biology. 2017; 216(4):889–99. https://doi.org/10.1083/jcb.201609046 PMID: 28254827

30. Li H, Ruan Y, Zhang K, Jian F, Hu C, Miao L, et al. Mic60/Mitofilin determines MICOS assembly essential for mitochondrial dynamics and mtDNA nucleoid organization. Cell death and differentiation. 2016; 23(3):380–92. https://doi.org/10.1038/cdd.2015.102 PMID: 26250910

31. Anand R, Kondadi AK, Meisterknecht J, Golombek M, Nortmann O, Riedel J, et al. MIC26 and MIC27 cooperate to regulate cardiolipin levels and the landscape of OXPHOS complexes. Life Sci Alliance. 2020; 3(10):e202000711. https://doi.org/10.26508/lsa.202000711 PMID: 32788226

32. Kondadi AK, Anand R, Hansch S, Urbach J, Zobel T, Wolf DM, et al. Cristae undergo continuous cycles of membrane remodelling in a MICOS-dependent manner. EMBO Rep. 2020; 21(3):e49776. https://doi.org/10.15252/embr.201949776 PMID: 32067344

33. Michaud M, Gros V, Tardif M, Brugiere S, Ferro M, Prinz WA, et al. AtMic60 Is Involved in Plant Mitochondria Lipid Trafficking and Is Part of a Large Complex. Current biology: CB. 2016; 26(5):627–39. https://doi.org/10.1016/j.cub.2016.01.011 PMID: 26898467

34. Tsai PI, Papakyrikos AM, Hsieh CH, Wang X. Drosophila MIC60/mitofilin conducts dual roles in mitochondrial motility and crista structure. Molecular biology of the cell. 2017; 28(24):3471–9. https://doi.org/10.1091/mbc.E17-03-0177 PMID: 28904209

35. Zerbes RM, van der Klei IJ, Veenhuis M, Pfanner N, van der Laan M, Bohnert M. Mitofilin complexes: conserved organizers of mitochondrial membrane architecture. Biological chemistry. 2012; 393 (11):1247–61. https://doi.org/10.1515/hsz-2012-0239 PMID: 23109542

36. Eramo MJ, Lisnyak V, Formosa LE, Ryan MT. The 'mitochondrial contact site and cristae organising system' (MICOS) in health and human disease. J Biochem. 2020; 167(3):243–55. https://doi.org/10.1093/jb/mvz111 PMID: 31825482

37. Tsai PI, Lin CH, Hsieh CH, Papakyrikos AM, Kim MJ, Napolioni V, et al. PINK1 Phosphorylates MIC60/Mitofilin to Control Structural Plasticity of Mitochondrial Crista Junctions. Molecular cell. 2018; 69 (5):744–56.e6. https://doi.org/10.1016/j.molcel.2018.01.026 PMID: 29456190

38. Marco-Hernández AV, Tomás-Vila M, Montoya-Filardi A, Barranco-González H, Vilchez Padilla JJ, Azorín I, et al. Mitochondrial developmental encephalopathy with bilateral optic neuropathy related to homozygous variants in IMMT gene. Clin Genet. 2022; 101(2):233–41. https://doi.org/10.1111/cge.14093 PMID: 34842280

39. Guarani V, Jardel C, Chretien D, Lombes A, Benit P, Labasse C, et al. QIL1 mutation causes MICOS disassembly and early onset fatal mitochondrial encephalopathy with liver disease. eLife. 2016; 5. https://doi.org/10.7554/eLife.17163 PMID: 27623147

40. Beninca C, Zanette V, Brischigliaro M, Johnson M, Reyes A, Valle DAD, et al. Mutation in the MICOS subunit gene APOO (MIC26) associated with an X-linked recessive mitochondrial myopathy, lactic acidosis, cognitive impairment and autistic features. J Med Genet. 2021; 58(3):155–67. https://doi.org/10.1136/jmedgenet-2020-106861 PMID: 32439808

41. Baseler WA, Dabkowski ER, Williamson CL, Croston TL, Thapa D, Powell MJ, et al. Proteomic alterations of distinct mitochondrial subpopulations in the type 1 diabetic heart: contribution of protein import dysfunction. American journal of physiology Regulatory, integrative and comparative physiology. 2011; 300(2):R186–200. https://doi.org/10.1152/ajpregu.00423.2010 PMID: 21048079

42. Thapa D, Nichols CE, Lewis SE, Shepherd DL, Jagannathan R, Croston TL, et al. Transgenic overexpression of mitofilin attenuates diabetes mellitus-associated cardiac and mitochondria dysfunction. Journal of molecular and cellular cardiology. 2015; 79:212–23. https://doi.org/10.1016/j.yjmcc.2014.11.008 PMID: 25463274

43. Lamant M, Smih F, Harmancey R, Philip-Couderc P, Pathak A, Roncalli J, et al. ApoO, a novel apolipoprotein, is an original glycoprotein up-regulated by diabetes in human heart. The Journal of biological chemistry. 2006; 281(47):36289–302. https://doi.org/10.1074/jbc.M510861200 PMID: 16956892

44. Tian F, Wu CL, Yu BL, Liu L, Hu JR. Apolipoprotein O expression in mouse liver enhances hepatic lipid accumulation by impairing mitochondrial function. Biochemical and biophysical research communications. 2017; 491(1):8–14. https://doi.org/10.1016/j.bbrc.2017.06.128 PMID: 28647361

45. Weber TA, Koob S, Heide H, Wittig I, Head B, van der Bliek A, et al. APOOL is a cardiolipin-binding constituent of the Mitofilin/MINOS protein complex determining cristae morphology in mammalian mitochondria. PloS one. 2013; 8(5):e63683. https://doi.org/10.1371/journal.pone.0063683 PMID: 23704930

46. Koob S, Barrera M, Anand R, Reichert AS. The non-glycosylated isoform of MIC26 is a constituent of the mammalian MICOS complex and promotes formation of crista junctions. Biochimica et biophysica acta. 2015; 1853(7):1551–63. https://doi.org/10.1016/j.bbamcr.2015.03.004 PMID: 25764979

47. Turkieh A, Caubere C, Barutaut M, Desmoulin F, Harmancey R, Galinier M, et al. Apolipoprotein O is mitochondrial and promotes lipotoxicity in heart. The Journal of clinical investigation. 2014; 124 (5):2277–86. https://doi.org/10.1172/JCI74668 PMID: 24743151

48. Ott C, Dorsch E, Fraunholz M, Straub S, Kozjak-Pavlovic V. Detailed analysis of the human mitochondrial contact site complex indicate a hierarchy of subunits. PloS one. 2015; 10(3):e0120213. https://doi.org/10.1371/journal.pone.0120213 PMID: 25781180

49. Koob S, Reichert AS. Novel intracellular functions of apolipoproteins: the ApoO protein family as constituents of the Mitofilin/MINOS complex determines cristae morphology in mitochondria. Biological chemistry. 2014; 395(3):285–96. https://doi.org/10.1515/hsz-2013-0274 PMID: 24391192

50. Philip-Couderc P, Smih F, Pelat M, Vidal C, Verwaerde P, Pathak A, et al. Cardiac transcriptome analysis in obesity-related hypertension. Hypertension. 2003; 41(3):414–21. https://doi.org/10.1161/01.HYP.0000057573.32425.95 PMID: 12623937

51. Yu BL, Wu CL, Zhao SP. Plasma apolipoprotein O level increased in the patients with acute coronary syndrome. J Lipid Res. 2012; 53(9):1952–7. https://doi.org/10.1194/jlr.P023028 PMID: 22693255

52. Wu CL, Zhao SP, Yu BL. Microarray analysis provides new insights into the function of apolipoprotein O in HepG2 cell line. Lipids Health Dis. 2013; 12:186. https://doi.org/10.1186/1476-511X-12-186 PMID: 24341743

53. Schmidinger B, Weijler AM, Schneider WJ, Hermann M. Hepatosteatosis and estrogen increase apolipoprotein O production in the chicken. Biochimie. 2016; 127:37–43. https://doi.org/10.1016/j.biochi.2016.04.017 PMID: 27126072

54. Weijler AM, Schmidinger B, Kapiotis S, Laggner H, Hermann M. Oleic acid induces the novel apolipoprotein O and reduces mitochondrial membrane potential in chicken and human hepatoma cells. Biochimie. 2018; 147:136–42. https://doi.org/10.1016/j.biochi.2018.02.003 PMID: 29432786

55. Vaisar T, Pennathur S, Green PS, Gharib SA, Hoofnagle AN, Cheung MC, et al. Shotgun proteomics implicates protease inhibition and complement activation in the antiinflammatory properties of HDL. The Journal of clinical investigation. 2007; 117(3):746–56. https://doi.org/10.1172/JCI26206 PMID: 17332893

56. Brenig K, Grube L, Schwarzländer M, Köhrer K, Stühler K, Poschmann G. The Proteomic Landscape of Cysteine Oxidation That Underpins Retinoic Acid-Induced Neuronal Differentiation. Journal of proteome research. 2020; 19(5):1923–40. https://doi.org/10.1021/acs.jproteome.9b00752 PMID: 32202429

57. Tyanova S, Temu T, Cox J. The MaxQuant computational platform for mass spectrometry-based shotgun proteomics. Nature protocols. 2016; 11(12):2301–19. https://doi.org/10.1038/nprot.2016.136 PMID: 27809316

58. Tyanova S, Temu T, Sinitcyn P, Carlson A, Hein MY, Geiger T, et al. The Perseus computational platform for comprehensive analysis of (prote)omics data. Nature methods. 2016; 13(9):731–40. https://doi.org/10.1038/nmeth.3901 PMID: 27348712

59. Koob S, Barrera M, Anand R, Reichert AS. Data supporting the role of the non-glycosylated isoform of MIC26 in determining cristae morphology. Data in brief. 2015; 4:135–9. https://doi.org/10.1016/j.dib.2015.04.014 PMID: 26217777

60. Szendroedi J, Phielix E, Roden M. The role of mitochondria in insulin resistance and type 2 diabetes mellitus. Nat Rev Endocrinol. 2011; 8(2):92–103. https://doi.org/10.1038/nrendo.2011.138 PMID: 21912398

61. Hummel KP, Dickie MM, Coleman DL. Diabetes, a new mutation in the mouse. Science. 1966; 153 (3740):1127–8. https://doi.org/10.1126/science.153.3740.1127 PMID: 5918576

62. Coleman DL. Obese and diabetes: two mutant genes causing diabetes-obesity syndromes in mice. Diabetologia. 1978; 14(3):141–8. https://doi.org/10.1007/BF00429772 PMID: 350680

63. Chen H, Charlat O, Tartaglia LA, Woolf EA, Weng X, Ellis SJ, et al. Evidence that the diabetes gene encodes the leptin receptor: identification of a mutation in the leptin receptor gene in db/db mice. Cell. 1996; 84(3):491–5. https://doi.org/10.1016/s0092-8674(00)81294-5 PMID: 8608603

64. Belgardt BF, Ahmed K, Spranger M, Latreille M, Denzler R, Kondratiuk N, et al. The microRNA-200 family regulates pancreatic beta cell survival in type 2 diabetes. Nature medicine. 2015; 21(6):619–27. https://doi.org/10.1038/nm.3862 PMID: 25985365

65. Uhlen M, Karlsson MJ, Hober A, Svensson AS, Scheffel J, Kotol D, et al. The human secretome. Sci Signal. 2019; 12(609).

66. Park S, Park JH, Jung HJ, Jang JH, Ahn S, Kim Y, et al. A secretome profile indicative of oleate-induced proliferation of HepG2 hepatocellular carcinoma cells. Experimental & molecular medicine. 2018; 50 (8):1–14. https://doi.org/10.1038/s12276-018-0120-3 PMID: 30076294

67. Franko A, Hartwig S, Kotzka J, Ruoß M, Nüssler AK, Königsrainer A, et al. Identification of the Secreted Proteins Originated from Primary Human Hepatocytes and HepG2 Cells. Nutrients. 2019; 11(8). https://doi.org/10.3390/nu11081795 PMID: 31382615

5.2 A X-linked nonsense APOO/MIC26 variant causes a lethal mitochondrial disease with progeria-like phenotypes

Received: 13 June 2023 | Revised: 16 August 2023 | Accepted: 18 August 2023

DOI: 10.1111/cge.14420

ORIGINAL ARTICLE

CLINICAL GENETICS WILEY

A X-linked nonsense *APOO/MIC26* variant causes a lethal mitochondrial disease with progeria-like phenotypes

Leon Peifer-Weiß[1] | Mazen Kurban[2,3] | Céline David[1] | Melissa Lubeck[1] | Arun Kumar Kondadi[1] | Georges Nemer[4] | Andreas S. Reichert[1] | Ruchika Anand[1]

[1]Institute of Biochemistry and Molecular Biology I, Medical Faculty and University Hospital Düsseldorf, Heinrich Heine University Düsseldorf, Düsseldorf, Germany

[2]Department Biochemistry and Molecular Genetics, American University of Beirut, Beirut, Lebanon

[3]Department of Dermatology, American University of Beirut, Beirut, Lebanon

[4]College of Health and Life Sciences, Hamad Bin Khalifa University, Doha, Qatar

Correspondence
Georges Nemer, College of Health and Life Sciences, Hamad Bin Khalifa University, Education City, Doha, Qatar.
Email: gnemer@hbku.edu.qa

Ruchika Anand, Institute of Biochemistry and Molecular Biology I, Medical Faculty and University Hospital Düsseldorf, Heinrich Heine University Düsseldorf, Düsseldorf, Germany.
Email: anand@hhu.de

Present address
Leon Peifer-Weiß, Institute for Clinical Biochemistry and Pathobiochemistry, German Diabetes Center, Leibniz-Center for Diabetes Research at Heinrich Heine University, Düsseldorf, Germany.

Funding information
Deutsche Forschungsgemeinschaft, Grant/Award Numbers: AN 1440/3-1, AN 1440/4-1, KO 6519/1-1, GRK 2576 Vivid; Medizinische Fakultät, Heinrich-Heine-Universität Düsseldorf, Grant/Award Numbers: Foko-02/2015, FoKo-2020-71

Abstract

APOO/MIC26 is a subunit of the MICOS complex required for mitochondrial cristae morphology and function. Here, we report a novel variant of the *APOO/MIC26* gene that causes a severe mitochondrial disease with overall progeria-like phenotypes in two patients. Both patients developed partial agenesis of the corpus callosum, bilateral congenital cataract, hypothyroidism, and severe immune deficiencies. The patients died at an early age of 12 or 18 months. Exome sequencing revealed a mutation (NM_024122.5): c.532G>T (p.E178*) in the *APOO/MIC26* gene that causes a nonsense mutation leading to the loss of 20 C-terminal amino acids. This mutation resulted in a highly unstable and degradation prone MIC26 protein, yet the remaining minute amounts of mutant MIC26 correctly localized to mitochondria and interacted physically with other MICOS subunits. *MIC26* KO cells expressing MIC26 harboring the respective *APOO/MIC26* mutation showed mitochondria with perturbed cristae architecture and fragmented morphology resembling *MIC26* KO cells. We conclude that the novel mutation found in the *APOO/MIC26* gene is a loss-of-function mutation impairing mitochondrial morphology and cristae morphogenesis.

KEYWORDS
apolipoproteins, congenital disorder, mitochondria, mitochondrial disease, progeria

Leon Peifer-Weiß and Mazen Kurban shared first authors.

1 | INTRODUCTION

Mitochondria are vital cellular organelles as they perform many important cellular functions such as energy conversion, calcium homeostasis, programmed cell death, heme synthesis, cellular signaling, and metabolic processes. Endosymbiotic in origin, mitochondria contain their own genome (mtDNA) and encode few yet essential components required for oxidative phosphorylation and ATP production. All other mitochondrial proteins are encoded by the nuclear genome and therefore the functioning of many mitochondrial protein complexes including respiratory chain complexes (RCCs) rely on an intricate balance between assembly of the mtDNA-encoded and nuclear-encoded components. Genetic disorders in either nuclear-encoded or mtDNA genes can lead to set of diseases called mitochondrial diseases.[1] These are described as multisystemic diseases as many organs like brain, skeletal muscles, heart, liver, and kidney could be affected. No cure is available for mitochondrial diseases, which have a prevalence greater than 1.6 in 5000.[2]

The ultrastructure of the mitochondria is highly organized and contain two membranes, outer membrane (OM) and inner membrane (IM). Although the OM surrounds the mitochondria, the IM is located within and has many folds called cristae. The cristae membrane is compositionally distinct from the inner boundary membrane (IBM), a part of IM that runs parallel to OM.[3,4] RCCs are enriched in cristae and therefore cristae are the main energy producing spatial domains within mitochondria.[5] Cristae are connected to IBM by narrow openings called crista junctions (CJs).[6] CJs are highly conserved structures of very small diameter and thus limit the access of proteins and metabolites from the cristae lumen to the intermembrane space (IMS) or vice versa.[7] Recent advances in super-resolution imaging techniques show that cristae are dynamic entities,[8–12] that can constantly undergo cycles of putative fusion and fission.[13] The physiological benefits of these fast cristae dynamics on mitochondrial functions are not yet identified. A highly conserved protein complex called "mitochondrial contact site and cristae organizing system" (MICOS) is enriched at the CJs which maintains cristae structure and stabilizes CJs.[14–17] Mammalian MICOS complex contains seven bona fide subunits, IMMT/MIC60, CHCHD3/MIC19, CHCHD6/MIC25, MICOS10/MIC10, MICOS13/MIC13, APOO/MIC26, and APOOL/MIC27, which are organized into two smaller subcomplexes, MIC60-subcomplex (MIC60-19-25), and MIC10-subcomplex (MIC10-MIC13-MIC26-MIC27). MIC13 functions as a bridge between two subcomplexes[18,19] via its conserved GxxxG and WN motifs.[20] MIC60 and MIC10 are considered as the core subunits of MICOS complex because their deficiencies show severe cristae defects.[21] They both possess membrane bending activities.[22–24] Structural studies show that MIC60 forms bow-shaped tetrameric assemblies that are promoted by MIC19. This MIC60-MIC19 complex can transvers CJs and help in controlling CJ architecture.[25] The MIC60-subcomplex mainly interacts with OM proteins namely SAMM50 and Metaxins to form a larger "mitochondrial intermembrane space bridging" (MIB) complex that spans the IM and OM and helps in formation of contact sites between them.[26,27] Apart from their role in cristae organization, MICOS proteins participate in many other mitochondrial functions, including respiration, protein import, lipid transport, mtDNA organization, apoptosis, inflammation, and autophagy.[28–32]

APOO/MIC26 and APOOL/MIC27 belong to apolipoprotein family due to the presence of a conserved apolipoprotein domain. MIC26 was first identified at elevated levels in the cardiac transcriptome of high-fat diet fed dogs.[33] The protein levels of MIC26 were increased in plasma of patients with acute coronary syndrome.[34] *MIC26* deficiency in mouse adipocytes leads to aggravated brown adipose tissue whitening and diet-induced obesity indicating its role in regulating lipid metabolism.[35] Downregulation of *MIC26* shows differential expression of genes involved in fatty acid metabolism and inflammatory responses.[36] It was believed that MIC26 gets O-glycosylated and accumulates as a 55 KDa secreted protein. Later MIC26 was shown to be mitochondrially localized[37] and identified as a subunit of MICOS complex.[38] However, it was inconsistent that the recombinant MIC26 resulted in only 22 KDa band and there were discrepancies about the significance of the 55 KDa secreted form. We recently showed that MIC26 and MIC27 are exclusively mitochondrial localized as bona fide subunits of the MICOS complex and that MIC26 does not exist as a glycosylated form by using a combination of siRNAs and knockout (KO) of *MIC26* and *MIC27* in four different human cell lines and four anti-MIC26 antibodies. The 55 KDa band was present even in the KO of *MIC26* and mass spectrometry of 55 KDa protein did not contain any MIC26-specific peptides, showing that the 55 KDa band was non-specific.[39]

MIC26 and MIC27 show antagonistic regulation at the protein level where a decrease in the levels of one of them leads to an increase in protein levels of another and vice versa.[38] Although they are not considered as core components of MICOS complex, the double KO of *MIC26* and *MIC27* shows drastic loss of CJs. MIC26 and MIC27 cooperate to regulate the stability and integrity of the RCCs and the F_1F_O ATP synthase.[40] MIC27 binds cardiolipin[41] and both MIC26 and MIC27 cooperatively regulate the levels of cardiolipin in mitochondria.[40] In yeast, Mic26-Mic27 antagonism regulates the assembly of Mic10.[42] A mutation in transmembrane domain of *APOO/MIC26* was associated with mitochondrial myopathy, lactic acidosis, cognitive impairment, and autistic features.[43] Here, we report a novel variant of *MIC26* which was found in siblings from Lebanon. Unlike the other reported *MIC26* variant,[43] this variant is very severe and causes a lethal mitochondrial disease with progeria-like phenotypes.

2 | MATERIALS AND METHODS

2.1 | Patients recruitment and DNA samples

The recruitment of the family was conducted at the Genodermatoses' unit at the Department of Dermatology at the American University of Beirut Medical Center (AUBMC, Beirut, Lebanon). The clinical phenotypes were provided by the referring physician, and the project received approval from the Institutional Review Board at the American University of Beirut Medical Center. Written informed consent was obtained from the parents. Peripheral blood samples were collected from the participating individuals and stored at 4°C. Within 1 h of blood collection, DNA was extracted from the specimens and stored at 4°C.

2.2 | Whole exome sequencing

Whole Exome Sequencing (Huffmeier et al) was performed by Macrogen Laboratory in Seoul, South Korea. The sequencing was carried out using the Illumina NovaSeq6000 platform, generating 101 base pair (pair-ended) reads. The library preparation followed the manufacturer's protocol, involving random fragmentation of the DNA, adapter ligation, tagmentation, PCR amplification, gel purification, and loading the library into a flow cell. The fragments were captured on a lawn of surface-bound oligos for cluster generation, and each fragment was amplified using bridge amplification into distinctive, clonal clusters.

2.3 | Sequence analysis

The base calling of the captured raw images was performed using the RTA (Real Time Analysis) software. The BCL (base calls) binary data was converted into FASTQ (paired-end reads) using the Illumina package bcl2fastq. Quality control checks were conducted, ensuring a Phred score of approximately 33. The FASTQ files were then mapped to the Human GRCh37/hg19 reference assembly using CLC Genomics Workbench (version 20.0.4). Failed and broken reads were removed, and a minimum coverage of 10 reads and a minimum variant allele frequency of 35% were applied. The basic variant parameter ploidy was set at 2, and reference masking positions with coverage above 100,000 were ignored. CLC Genomics Workbench generated Binary Alignments Map (BAM) and Variant Call Format (VCF) files for each sample, including all the variants.

2.4 | Variant calling and annotation

The VCF files were uploaded to Illumina Variant Studio 3.0 for variant calling and annotation. The annotation was based on dbSNP, ClinVar, and the 1000 Genomes project. To identify mutations/variants potentially associated with the diseases, a stringent filter was applied using CLC Genomics and various in silico prediction tools. The criteria for filtering included: (1) novel/rare variants with minor allele frequency (MAF) <5% and read depth >20, conserved based on Genome Aggregation Database (gnomAD) ExAC, 1000 genomes, more than 300 Lebanese in-house exomes, and PhastCons and PhyloP-conservation scores; (2) functionality, pathogenicity, and protein effect predicted to be deleterious/pathogenic by PolyPhen/SIFT, American College of Medical Genetics and Genomics (ACMG) classification, mutation taster, and combined annotation dependent depletion (CADD) scores; (3) single nucleotide variants (SNVs), insertions, and deletions, including mutation types like nonsense, missense, frame shift, and splice; (4) genomic position; and (5) homozygous/heterozygous state determined by uploading BAM files to the integrative genomics viewer (IGV), a high-performance visualization tool for genomic annotations and correct calling.

The details of other materials and methods are included in Data S1.

3 | RESULTS

3.1 | Clinical presentation of patient 1

Patient 1 was first-born boy born in a non-consanguineous marriage of Lebanese parents (Figure 1A). Both the parents are healthy with no phenotypes in families on both sides. There was intrauterine growth retardation during delivery. Soon after birth, he showed phenotypes of suggestive cutis marmorata telangiectatica from the appearance of blood vessels. He had partial syndactyly of the 2nd and 3rd toes, wrinkled palm, and sole skin (Figure 1B). He developed bilateral congenital cataract, hypothyroidism, and partial agenesis of the corpus callosum. The peripheral blood immune profile showed a combined B and T cell immunodeficiencies (Table 1). There were recurrent episodes of bacterial and viral infections. In addition, he showed overall progeria phenotypes and failed to thrive. Patient 1 died at the age of 12 months because of recurrent infections.

3.2 | Clinical presentation of patient 2

Patient 2 was the second child from the same parents, sister of patient 1 (Figure 1A). She showed clinical features that were similar to her brother and included loose saggy skin and seborrheic dermatitis like features. She also had congenital hypothyroidism, bilateral congenital glaucoma and combined B and T cell immunodeficiency. She had similar overall progeria phenotypes along with recurrent bacterial and fungal infections which unfortunately led to her death at the age of 18 months.

3.3 | Identification of nonsense MIC26 variant

We performed whole exome sequencing in both the patients and their parents. There were no major changes except for a point mutation in *APOO/MIC26* (NM_024122.5):c.532G>T (p.E178*) which was inherited from the X chromosome of the mother who is heterozygous for the variant. This variant causes a nonsense mutation that replaces a glutamate with a premature stop codon leading to removal of the last 20 amino acids (Figure 1C). The variant has a minor allele frequency (null) in all the public available databases. We did not find it in any of the more than 200 exomes we analyzed so far on Lebanese patients or healthy individuals. Multiple sequence alignment of MIC26 in various species showed that E178 was conserved among numerous species, while the last 20 amino acids were not as conserved (Figure 1D).

3.4 | MIC26 variant is highly unstable, yet minute amounts of the remaining protein can localize to mitochondria and interact with other MICOS proteins

To determine how MIC26 mutant variant affects the localization and molecular function of MIC26, we generated a plasmid for expression

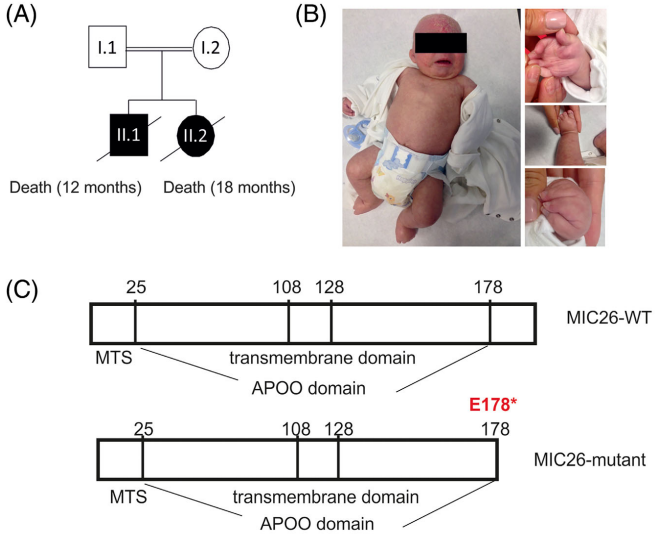

FIGURE 1 A novel missense mutation in *MIC26* causes severe mitochondrial disease with progeria-like symptoms. (A) Pedigree shows that two patients were born in a non-consanguineous marriage. (B) Images of Patient 1 showing symptoms of suggestive cutis marmorata telangiectatica from appearance of blood vessels. Partial syndactyly of the 2nd and 3rd toes, wrinkled palms are shown in insets. (C) Exome sequencing revealed a point mutation in *MIC26* gene which replaces a glutamate (E) at position 178 to a stop codon which causes immature termination and results in a truncated protein lacking last 20 amino acids. (D) Multiple sequence alignment of MIC26 shows that the C-terminal region is not as conserved, however the glutamate E178 is conserved among various species. [Colour figure can be viewed at wileyonlinelibrary.com]

of the human MIC26 mutant variant tagged with GFP, for easy visualization and detection, using site-directed mutagenesis along with WT human *MIC26* gene. MIC26^{WT}-GFP or MIC26^{MUT}-GFP were overexpressed in HeLa cells and visualized using fluorescence confocal microscopy. As expected, MIC26^{WT}-GFP was present in mitochondria shown by co-localization of GFP signal with mitochondrial

TABLE 1 Peripheral blood immune profile of patient 1 showed marked decrease in B-lymphocytes and T-lymphocytes.

Parameter	Percent	Value/absolute count
CD3+	57.39	1403.83
CD3 + CD8+	14.08	344.35
CD3 + CD4+	38.64	945.11
CD3 + CD4 + CD8+	0.19	4.61
CD16 + CD56+	20.00	489.16
CD19+	11.98	293.00
CD45+		2446.10
CD4/CD8 ratio		2.74

Note: Multiple gates on the peripheral blood using CD45 expression reveal a moderate decrease in total CD3 positive T-cell levels (moderate decrease in CD4 positive T-cells and marked decrease in CD8 positive T-cells with CD4/CD8 ratio of 2.74), associated with a marked decrease in total CD19 positive B-cells levels and adequate natural killer cells (CD16 + CD56+) levels.

matrix-targeted mCherry (Mito-mCherry). However, the GFP signal from MIC26^{MUT}-GFP was very low and barely visible (Figure 2A), still upon enhancing the contrast, MIC26^{MUT}-GFP was also found to be localized to mitochondria (Figure 2B). These results indicated that MIC26 variant is somehow unstable, yet small amounts of remaining MIC26 protein can localize to mitochondria. We further checked the steady-state expression levels of MIC26^{MUT}-GFP using western blot analysis and found that the levels of MIC26^{MUT}-GFP were very low compared to MIC26^{WT}-GFP (Figure 2C) implicating that the truncation of last 20 amino acids of MIC26 makes it highly unstable and prone to degradation. As the truncated MIC26 variant could localize to mitochondria, we asked whether it can still interact with other MICOS components and/or can incorporate in the MICOS complex. Co-immunoprecipitation experiments were performed by overexpressing MIC26^{WT}-GFP or MIC26^{MUT}-GFP in HAP1 *MIC26* KO cells using anti-GFP antibody. Large amounts of isolated mitochondria were used as an input in these experiments to overcome the problem of low levels of MIC26 mutant variant. Despite very low expression, we detect that most of the MICOS proteins could be eluted with MIC26 mutant variant indicating the ability of MIC26 variant to interact with MICOS components (Figure 2D). Overall, we conclude that the *MIC26* mutation reported here makes the protein very unstable in such a way that most of the mutant protein is either degraded or lost, however the remaining minute amounts of protein are able to localize to mitochondria and bind to other MICOS components.

3.5 | MIC26 variant shows "loss-of-function" phenotypes similar to *MIC26* knockout

In view of lack of material from the patients, we decided to generate a cell line that exclusively expresses the MIC26 mutant variant and can be used to assess the pathogenic effect of *MIC26* mutation on the cells. For this, we stably expressed untagged MIC26^{WT} or MIC26^{MUT} in the HAP1 *MIC26* KO cells, and named them as control-mimic or patient-mimic cell line respectively for convenience in this manuscript (Figure 3A). The HAP1 WT and *MIC26* KO cells expressing the empty vector (ev) were also generated for comparison as control cells. Western blot analysis shows that MIC26 patient-mimic cells lack the full-length MIC26 protein confirming our previous observation that the MIC26 mutant variant is unstable and mostly degraded (Figure 3A). The steady-state levels of other MICOS proteins remain unaltered except for MIC27 which show higher levels in patient-mimic cell lines as well as in the *MIC26* KO cells (Figure 3A) compared to control cell lines. This can be explained due to the antagonistic regulation between MIC26 and MIC27 as described earlier.[38,40] As MIC26 is virtually absent in patient-mimic cells, the MIC27 levels are increased concomitantly implying that the truncated MIC26 is either not fully functional or not in sufficient amount or both. We previously showed that MIC26 and MIC27 are dispensable for the incorporation of other MICOS subunits into the MICOS complex.[40] This means that the MICOS subcomplexes can be stabilized despite the absence or reduction of MIC26 in patient-mimic cells.

Next, we analyzed the effect of MIC26 mutant mitochondrial ultrastructure and cristae morphology using electron microscopy. Control-mimic cell expressing a wild type version of the MIC26 contained lamellar shaped cristae (Figure 3B). Patient-mimic cells showed highly aberrant cristae structures that were reminiscent of *MIC26* KO cells. These cristae were arranged as stacks as many of them lacked CJs (Figure 3B). Similar cristae structures were seen in *MIC26* KO cells. Usually, mitochondrial fragmentation within a cell is associated with mitochondrial dysfunction and acts as an indicator of mitochondrial stress. We analyzed the mitochondrial morphology in all the cell lines by overexpressing mitochondrially targeted GFP (Mito-GFP) to visualize mitochondria. Patient-mimic cells show highly fragmented mitochondria and the extent of fragmentation was similar to that found in *MIC26* KO cells, indicating that the patient-mimic cells show loss-of-function phenotypes (Figure 3C,D). The levels and assembly of RCCs complexes as analyzed by blue native gel electrophoresis were similar in all the cell lines, indicating no severe defects (Figure S1). Overall, we found that the phenotypes of patient-mimic cells were similar to *MIC26* KO w.r.t., mitochondrial as well as cristae morphology. We conclude that the *MIC26* mutation is a loss-of-function mutation.

4 | DISCUSSION

Here, we report a lethal mitochondrial disease due to a nonsense mutation in *APOO/MIC26* which showed an overall progeria-like phenotypes including suggestive cutis marmorata telangiectatica, wrinkled palms and sole skin. MIC26 is a nuclear-encoded mitochondrial protein involved in maintaining mitochondrial membrane architecture. MIC26 with its orthologous partner MIC27 is required for the formation of CJs, stability of respiratory chain (super) complexes, integrity of F_1F_O ATP synthase complexes and cellular respiration.[40] Aberrant cristae and fragmented mitochondria accumulated in patient-mimic cells,

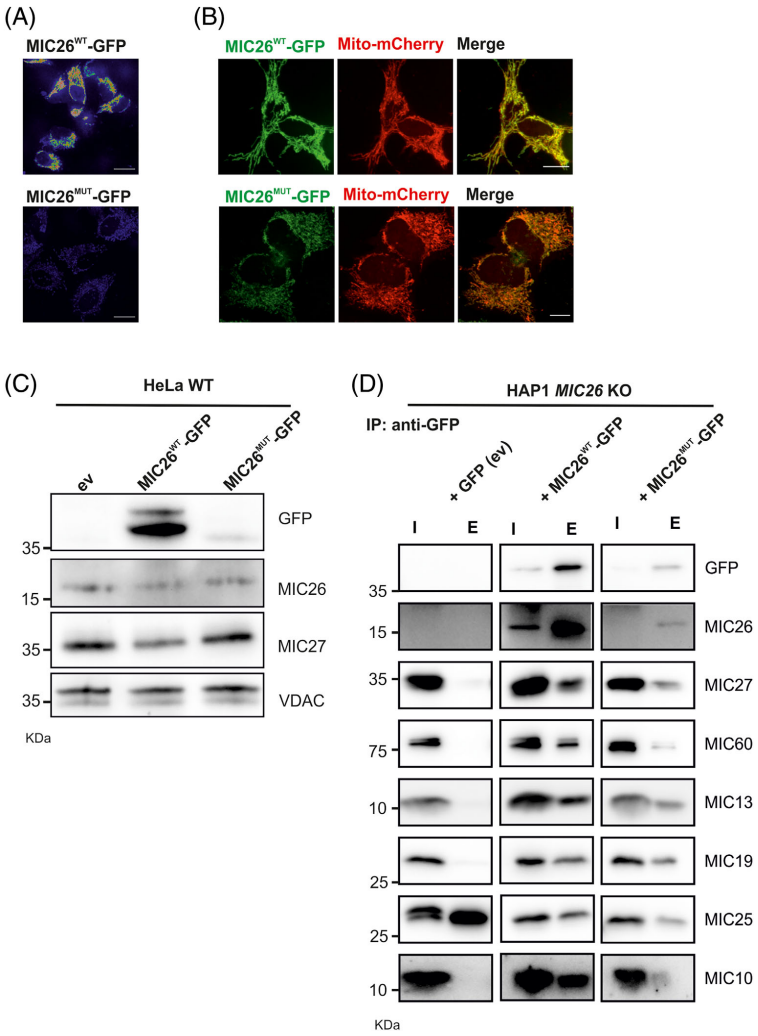

FIGURE 2 Mutant variant of MIC26 is highly unstable and prone to degradation. (A) The images of HeLa cells overexpressing MIC26^{WT}-GFP or MIC26^{MUT}-GFP represented in the rainbow LUT color coding where blue represents very low intensity and red represents high intensity pixels. It shows that the MIC26^{MUT}-GFP has very low expression compared to MIC26^{WT}-GFP. Scale bar 10 μm. (B) HeLa cells overexpressing MIC26^{WT}-GFP or MIC26^{MUT}-GFP were also transfected with mitochondrial-targeted mcherry (Mito-mCherry). MIC26^{WT}-GFP as well as the MIC26^{MUT}-GFP were localized to the mitochondria as shown by colocalization of GFP and mCherry signal. Note that MIC26^{MUT}-GFP was enhanced so that the signal is visible. Scale bar 5 μm. (C) Representative western blots of HeLa cells overexpressing MIC26^{WT}-GFP or MIC26^{MUT}-GFP show that MIC26^{MUT}-GFP was expressed in minute amounts or perhaps unstable. (D) MIC26^{WT}-GFP or MIC26^{MUT}-GFP was expressed in *MIC26* KO and a coimmunoprecipitation (co-IP) was performed using anti-GFP antibody. Huge amounts of mitochondrial samples were taken in these experiments to overcome the problem of very low initial amounts of MIC26^{MUT}-GFP. Despite the low amount of expression, MIC26^{MUT}-GFP could bind to other MICOS components ($N = 3$). [Colour figure can be viewed at wileyonlinelibrary.com]

providing a strong link between mitochondrial function and progression of the observed progeria-like lethal mitochondrial disease. Typical "Progeria" disease known as Hutchinson-Gilford syndrome (HGPA) occurs due to single gene mutation in nuclear gene Lamin A causing aberrant nuclear structure and cell division. Moreover, dysfunctional mitochondria with fragmented morphology, low membrane potential

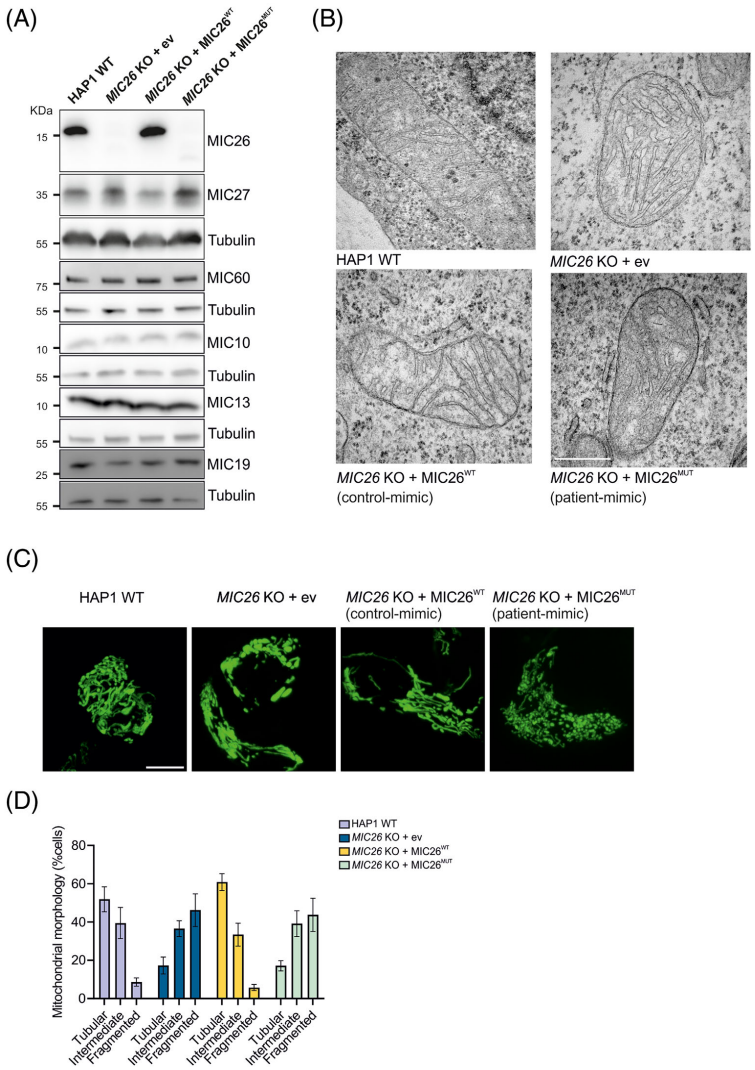

FIGURE 3 *MIC26* mutation behaves as a loss-of-function mutation. (A) Representative western blot for HAP1 WT, *MIC26* KO + ev, *MIC26* KO + MIC26^{WT} (control-mimic), *MIC26* KO + MIC26^{MUT} (patient-mimic) for MICOS proteins. MIC26 is lost in patient-mimic cell lines accompanied by increase in MIC27. This is similar to *MIC26* KO. (B) Representative electron microscopy images of four cell lines, HAP1 WT, *MIC26* KO + ev, *MIC26* KO + MIC26^{WT} (control-mimic), *MIC26* KO + MIC26^{MUT} (patient-mimic). While HAP1 WT and control-mimic cells show normal lamellar cristae structure, perturbed cristae with accumulation of cristae stacks in the mitochondria which lack crista junctions were present in *MIC26* KO + MIC26^{MUT} (patient-mimic) as well as *MIC26* KO cells. (C) Representative images of mitochondrial morphology in the following cells: HAP1 WT, *MIC26* KO + ev, *MIC26* KO + MIC26^{WT} (control-mimic), *MIC26* KO + MIC26^{MUT} (patient-mimic). HAP1 WT and control-mimic cells show normal tubular distribution, but both *MIC26* KO and patient-mimic cells display accumulation of fragmented mitochondria. (D) Bar graph showing the quantification of mitochondrial morphology from three independent experiment ($N = 3$) with each experiment having 40–75 cells from each cell line. [Colour figure can be viewed at wileyonlinelibrary.com]

and respiratory capacity, high ROS levels and low PGC1a levels also accumulated in Progeria.[44,45] Recently, null mutations in Metaxin-2 were found in progeroid disorder mandibuloacral dysplasia.[46] Metaxin-2 and MIC26 are part of a large protein complex called mitochondrial intermembrane space bridge complex (MIB) which help in shaping the mitochondrial cristae. Fibroblasts derived from patients harboring Metaxin-2 null-mutations showed altered nuclear morphology indicating a relationship between mitochondrial function and nuclear stability. This relationship is also reinforced in mutator mouse model which contains mtDNA mutations and shows similar nuclear genome instability as observed in progeric cells.[47]

Surprisingly, the female progeny despite the similar genetic background as her mother manifested a very severe phenotype, while the mother was only a carrier of the mutation. X-linked diseases manifest in males, but very rarely in females as they act as carrier of the variant. This occurs due to a phenomenon of X chromosome dosage compensation, called X inactivation where one of the X-chromosomes is silenced in a random manner to compensate for the differences in number of X chromosome in males and females. However, in very rare cases, a female can manifest a pathogenic variant if their X chromosome inactivation pattern is skewed such that the majority of their normal allele is not expressed. In fact, a study reporting the first *MIC26*

patient mutation also showed such skewed pattern of inheritance in females.[43]

MIC26 is transmembrane protein that resides in the inner membrane which contains a signal sequence, required for import into the mitochondria, and a conserved ApoO domain containing a hydrophobic domain.[38] The *MIC26* mutation occurs due to a single nucleotide mutation that causes the glutamate (E) residue to change to a stop codon leading to premature termination of translation and generation of a truncated protein lacking last 20 amino acids. No specific domain has been assigned to the last 20 amino acids of MIC26 (Figure 1D), however we show that the MIC26 mutant variant which lacks last 20 amino acids is highly unstable indicating faster degradation compared with the WT counterpart. Degradation could possibly take place after import into mitochondria or at the RNA level, however, the mechanism of degradation is not yet investigated. The minute amounts of the remaining MIC26 protein which escaped degradation could localize into mitochondria and also form a complex with other MICOS components. However, it was not sufficient to restore the MIC26 defects and the mutation behaved as a loss-of-function mutation. The previous described mutation in *MIC26* with the variant c.350T>C was shown to induce a missense mutation I117T in the predicted transmembrane domain of MIC26.[43] The mutation caused impaired processing of MIC26 during import and therefore reduced incorporation into the inner membrane. However, overall, the phenotypes of patients were mild with variable range of clinical presentation and severity among the patients that carry this mutation.

MIC26 KO cells as well as patient-mimic cells showed no drastic defect in the levels and assembly of the RCCs. In a previous publication as well, we showed normal RCCs assembly and respiration in *MIC26* KO.[40] Only upon deletion of both *MIC26* and *MIC27*, we found drastic defects in RCCs stability and respiration. Although the scenario could be different in the patient tissues, the general RCCs assembly patterns in cell culture conditions might not reflect the pleiotropic nature of mitochondrial diseases. Differences have been observed in mitochondrial function and activity depending on the kind of sample analyzed, for example, 50% of patients with RCCs defects in muscle biopsies show normal activities in skin fibroblast cultures.[48]

Since its discovery, the importance of MICOS components is growing as more and more pathologies are associated with it. Altered levels of MICOS proteins are associated with human diseases like epilepsy, Down's syndrome, Parkinson's disease, diabetes, and cardiomyopathy.[30] Mutations in *MICOS13/MIC13* cause severe form of mitochondrial encephalopathy with liver dysfunction.[49,50] *IMMT/MIC60* mutations were found in Parkinson's disease patients[51] and mitochondrial developmental encephalopathy with bilateral optic neuropathy.[52] What is surprising is that different proteins as well as different mutations of various MICOS proteins manifest into vastly different phenotypes and syndromes. This shows the importance of mitochondrial membrane structure for proper health and functionality.

AUTHOR CONTRIBUTIONS

Leon Peifer-Weiß: Investigation, methodology, formal analysis, visualization, writing—review and editing. **Mazen Kurban:** Investigation, methodology, data curation, formal analysis, visualization. **Céline David:** Investigation, methodology, formal analysis. **Melissa Lubeck:** Investigation, methodology, formal analysis. **Arun Kumar Kondadi:** Formal analysis, supervision, validation, writing—review and editing. **Georges Nemer:** Conceptualization, data curation, supervision, funding acquisition, investigation, project administration, writing—review and editing. **Andreas S. Reichert:** Conceptualization, supervision, funding acquisition, project administration, writing—review and editing. **Ruchika Anand:** Conceptualization, data curation, formal analysis, supervision, investigation, visualization, methodology, funding acquisition, project administration, writing—original draft, writing—review and editing.

ACKNOWLEDGMENTS

The authors would like to thank Andrea Borchardt and Tanja Portugall for their technical assistance in cloning, electron microscopy, and cell culture. Electron microscopy was performed at the Core facility for electron microscopy (CFEM) at the medical faculty of the Heinrich Heine University Düsseldorf. The research was supported by funding from Medical Faculty of Heinrich Heine University Düsseldorf, Foko-02/2015 (Ruchika Anand and Andreas S. Reichert) and FoKo-2020-71 (Ruchika Anand) and Deutsche Forschungsgemeinschaft (DFG) grants, AN 1440/3-1 (Ruchika Anand), AN 1440/4-1 (Ruchika Anand), KO 6519/1-1 (Arun Kumar Kondadi), and GRK 2576 Vivid (Andreas S. Reichert). Open Access funding enabled and organized by Projekt DEAL.

CONFLICT OF INTEREST STATEMENT

The authors declare no conflict of interest.

PEER REVIEW

The peer review history for this article is available at https://www.webofscience.com/api/gateway/wos/peer-review/10.1111/cge.14420.

DATA AVAILABILITY STATEMENT

The data that support the findings of this study are available from the corresponding author upon reasonable request.

ORCID

Leon Peifer-Weiß https://orcid.org/0000-0002-2391-1937
Mazen Kurban https://orcid.org/0000-0003-1011-0687
Melissa Lubeck https://orcid.org/0000-0002-3935-6552
Arun Kumar Kondadi https://orcid.org/0000-0002-5888-7834
Andreas S. Reichert https://orcid.org/0000-0001-9340-3113
Ruchika Anand https://orcid.org/0000-0001-7337-6007

REFERENCES

1. Vafai SB, Mootha VK. Mitochondrial disorders as windows into an ancient organelle. *Nature*. 2012;491(7424):374-383. doi:10.1038/nature11707
2. Stenton SL, Prokisch H. Genetics of mitochondrial diseases: identifying mutations to help diagnosis. *EBioMedicine*. 2020;56:102784. doi:10.1016/j.ebiom.2020.102784
3. Vogel F, Bornhovd C, Neupert W, Reichert AS. Dynamic subcompartmentalization of the mitochondrial inner membrane. *J Cell Biol*. 2006;175(2):237-247. doi:10.1083/jcb.200605138

4. Wurm CA, Jakobs S. Differential protein distributions define two sub-compartments of the mitochondrial inner membrane in yeast. Research support, non-U.S. Gov't. *FEBS Lett*. 2006;580(24):5628-5634. doi:10.1016/j.febslet.2006.09.012
5. Gilkerson RW, Selker JM, Capaldi RA. The cristal membrane of mitochondria is the principal site of oxidative phosphorylation. *FEBS Lett*. 2003;546(2–3):355-358. doi:10.1016/s0014-5793(03)00633-1
6. Perkins G, Renken C, Martone ME, Young SJ, Ellisman M, Frey T. Electron tomography of neuronal mitochondria: three-dimensional structure and organization of cristae and membrane contacts. *J Struct Biol*. 1997;119(3):260-272. doi:10.1006/jsbi.1997.3885
7. Mannella CA. Structure and dynamics of the mitochondrial inner membrane cristae. *Biochim Biophys Acta*. 2006;1763(5–6):542-548. doi:10.1016/j.bbamcr.2006.04.006
8. Kondadi AK, Anand R, Hansch S, et al. Cristae undergo continuous cycles of membrane remodelling in a MICOS-dependent manner. *EMBO Rep*. 2020;21(3):e49776. doi:10.15252/embr.201949776
9. Huang X, Fan J, Li L, et al. Fast, long-term, super-resolution imaging with hessian structured illumination microscopy. *Nat Biotechnol*. 2018;36:451-459. doi:10.1038/nbt.4115
10. Hu C, Shu L, Huang X, et al. OPA1 and MICOS regulate mitochondrial crista dynamics and formation. *Cell Death Dis*. 2020;11(10):940. doi:10.1038/s41419-020-03152-y
11. Stephan T, Roesch A, Riedel D, Jakobs S. Live-cell STED nanoscopy of mitochondrial cristae. *Sci Rep*. 2019;9(1):12419. doi:10.1038/s41598-019-48838-2
12. Wang C, Taki M, Sato Y, et al. A photostable fluorescent marker for the superresolution live imaging of the dynamic structure of the mitochondrial cristae. *Proc Natl Acad Sci U S A*. 2019;116(32):15817-15822. doi:10.1073/pnas.1905924116
13. Kondadi AK, Anand R, Reichert AS. Cristae membrane dynamics—a paradigm change. *Trends Cell Biol*. 2020;30(12):923-936. doi:10.1016/j.tcb.2020.08.008
14. Harner M, Korner C, Walther D, et al. The mitochondrial contact site complex, a determinant of mitochondrial architecture. Research support, non-U.S. Gov't. *EMBO J*. 2011;30(21):4356-4370. doi:10.1038/emboj.2011.379
15. Hoppins S, Collins SR, Cassidy-Stone A, et al. A mitochondrial-focused genetic interaction map reveals a scaffold-like complex required for inner membrane organization in mitochondria. Research support, N.I.H., extramural research support, non-U.S. Gov't. *J Cell Biol*. 2011;195(2):323-340. doi:10.1083/jcb.201107053
16. von der Malsburg K, Muller JM, Bohnert M, et al. Dual role of mitofilin in mitochondrial membrane organization and protein biogenesis. Research support, non-U.S. Gov't. *Dev Cell*. 2011;21(4):694-707. doi:10.1016/j.devcel.2011.08.026
17. Rabl R, Soubannier V, Scholz R, et al. Formation of cristae and crista junctions in mitochondria depends on antagonism between Fcj1 and Su e/g. *J Cell Biol*. 2009;185(6):1047-1063. doi:10.1083/jcb.200811099
18. Guarani V, McNeill EM, Paulo JA, et al. QIL1 is a novel mitochondrial protein required for MICOS complex stability and cristae morphology. *Elife*. 2015;4. doi:10.7554/eLife.06265
19. Anand R, Strecker V, Urbach J, Wittig I, Reichert AS. Mic13 is essential for formation of crista junctions in mammalian cells. *PloS One*. 2016;11(8):e0160258. doi:10.1371/journal.pone.0160258
20. Urbach J, Kondadi AK, David C, et al. Conserved GxxxG and WN motifs of MIC13 are essential for bridging two MICOS subcomplexes. *Biochim Biophys Acta Biomembr*. 2021;1863(12):183683. doi:10.1016/j.bbamem.2021.183683
21. Stephan T, Brüser C, Deckers M, et al. MICOS assembly controls mitochondrial inner membrane remodeling and crista junction redistribution to mediate cristae formation. *EMBO J*. 2020;39(14):e104105. doi:10.15252/embj.2019104105
22. Tarasenko D, Barbot M, Jans DC, et al. The MICOS component Mic60 displays a conserved membrane-bending activity that is necessary for normal cristae morphology. *J Cell Biol*. 2017;216(4):889-899. doi:10.1083/jcb.201609046
23. Barbot M, Jans DC, Schulz C, et al. Mic10 oligomerizes to bend mitochondrial inner membranes at cristae junctions. *Cell Metab*. 2015;21(5):756-763. doi:10.1016/j.cmet.2015.04.006
24. Hessenberger M, Zerbes RM, Rampelt H, et al. Regulated membrane remodeling by Mic60 controls formation of mitochondrial crista junctions. *Nat Commun*. 2017;8:15258. doi:10.1038/ncomms15258
25. Bock-Bierbaum T, Funck K, Wollweber F, et al. Structural insights into crista junction formation by the Mic60-Mic19 complex. *Sci Adv*. 2022;8(35):eabo4946. doi:10.1126/sciadv.abo4946
26. Ott C, Ross K, Straub S, et al. Sam50 functions in mitochondrial intermembrane space bridging and biogenesis of respiratory complexes. *Mol Cell Biol*. 2012;32(6):1173-1188. doi:10.1128/MCB.06388-11
27. Xie J, Marusich MF, Souda P, Whitelegge J, Capaldi RA. The mitochondrial inner membrane protein mitofilin exists as a complex with SAM50, metaxins 1 and 2, coiled-coil-helix coiled-coil-helix domain-containing protein 3 and 6 and DnaJC11. *FEBS Lett*. 2007;581(18):3545-3549. doi:10.1016/j.febslet.2007.06.052
28. Mukherjee I, Ghosh M, Meinecke M. MICOS and the mitochondrial inner membrane morphology—when things get out of shape. *FEBS Lett*. 2021;595(8):1159-1183. doi:10.1002/1873-3468.14089
29. Anand R, Reichert AS, Kondadi AK. Emerging roles of the MICOS complex in cristae dynamics and biogenesis. *Biology (Basel)*. 2021;10(7). doi:10.3390/biology10070600
30. Eramo MJ, Lisnyak V, Formosa LE, Ryan MT. The 'mitochondrial contact site and cristae organising system' (MICOS) in health and human disease. *J Biochem*. 2020;167(3):243-255. doi:10.1093/jb/mvz111
31. Colina-Tenorio L, Horten P, Pfanner N, Rampelt H. Shaping the mitochondrial inner membrane in health and disease. *J Intern Med*. 2020;287:645-664. doi:10.1111/joim.13031
32. Khosravi S, Harner ME. The MICOS complex, a structural element of mitochondria with versatile functions. *Biol Chem*. 2020;401(6–7):765-778. doi:10.1515/hsz-2020-0103
33. Philip-Couderc P, Smih F, Pelat M, et al. Cardiac transcriptome analysis in obesity-related hypertension. *Hypertension*. 2003;41(3):414-421. doi:10.1161/01.Hyp.0000057573.32425.95
34. Yu BL, Wu CL, Zhao SP. Plasma apolipoprotein O level increased in the patients with acute coronary syndrome. *J Lipid Res*. 2012;53(9):1952-1957. doi:10.1194/jlr.P023028
35. Guo X, Hu J, He G, et al. Loss of APOO (MIC26) aggravates obesity-related whitening of brown adipose tissue via PPARα-mediated functional interplay between mitochondria and peroxisomes. *Metabolism*. 2023;144:155564. doi:10.1016/j.metabol.2023.155564
36. Wu CL, Zhao SP, Yu BL. Microarray analysis provides new insights into the function of apolipoprotein O in HepG2 cell line. *Lipids Health Dis*. 2013;12:186. doi:10.1186/1476-511X-12-186
37. Turkieh A, Caubere C, Barutaut M, et al. Apolipoprotein O is mitochondrial and promotes lipotoxicity in heart. *J Clin Invest*. 2014;124(5):2277-2286. doi:10.1172/JCI74668
38. Koob S, Barrera M, Anand R, Reichert AS. The non-glycosylated isoform of MIC26 is a constituent of the mammalian MICOS complex and promotes formation of crista junctions. *Biochim Biophys Acta*. 2015;1853(7):1551-1563. doi:10.1016/j.bbamcr.2015.03.004
39. Lubeck M, Derkum NH, Naha R, et al. MIC26 and MIC27 are bona fide subunits of the MICOS complex in mitochondria and do not exist as glycosylated apolipoproteins. *PloS One*. 2023;18(6):e0286756. doi:10.1371/journal.pone.0286756
40. Anand R, Kondadi AK, Meisterknecht J, et al. MIC26 and MIC27 cooperate to regulate cardiolipin levels and the landscape of OXPHOS complexes. *Life Sci Alliance*. 2020;3(10):e202000711. doi:10.26508/lsa.202000711
41. Weber TA, Koob S, Heide H, et al. APOOL is a cardiolipin-binding constituent of the Mitofilin/MINOS protein complex determining

cristae morphology in mammalian mitochondria. *PloS One*. 2013;8(5):e63683. doi:10.1371/journal.pone.0063683
42. Rampelt H, Wollweber F, Gerke C, et al. Assembly of the mitochondrial cristae organizer Mic10 is regulated by Mic26-Mic27 antagonism and Cardiolipin. *J Mol Biol*. 2018;430(13):1883-1890. doi:10.1016/j.jmb.2018.04.037
43. Beninca C, Zanette V, Brischigliaro M, et al. Mutation in the MICOS subunit gene APOO (MIC26) associated with an X-linked recessive mitochondrial myopathy, lactic acidosis, cognitive impairment and autistic features. *J Med Genet*. 2021;58(3):155-167. doi:10.1136/jmedgenet-2020-106861
44. Xiong ZM, Choi JY, Wang K, et al. Methylene blue alleviates nuclear and mitochondrial abnormalities in progeria. *Aging Cell*. 2016;15(2):279-290. doi:10.1111/acel.12434
45. Monterrubio-Ledezma F, Navarro-Garcia F, Massieu L, et al. Rescue of mitochondrial function in Hutchinson-Gilford progeria syndrome by the pharmacological modulation of Exportin CRM1. *Cells*. 2023;12(2). doi:10.3390/cells12020275
46. Elouej S, Harhouri K, Le Mao M, et al. Loss of MTX2 causes mandibuloacral dysplasia and links mitochondrial dysfunction to altered nuclear morphology. *Nat Commun*. 2020;11(1):4589. doi:10.1038/s41467-020-18146-9
47. Hamalainen RH, Landoni JC, Ahlqvist KJ, et al. Defects in mtDNA replication challenge nuclear genome stability through nucleotide depletion and provide a unifying mechanism for mouse progerias. *Nat Metab*. 2019;1(10):958-965. doi:10.1038/s42255-019-0120-1
48. Thorburn DR. Practical problems in detecting abnormal mitochondrial function and genomes. *Hum Reprod*. 2000;15(suppl 2):57-67. doi:10.1093/humrep/15.suppl_2.57
49. Russell BE, Whaley KG, Bove KE, et al. Expanding and underscoring the hepato-encephalopathic phenotype of QIL1/MIC13. *Hepatology*. 2019;70(3):1066-1070. doi:10.1002/hep.30627
50. Zeharia A, Friedman JR, Tobar A, et al. Mitochondrial hepato-encephalopathy due to deficiency of QIL1/MIC13 (C19orf70), a MICOS complex subunit. *Eur J Hum Genet*. 2016;24(12):1778-1782. doi:10.1038/ejhg.2016.83
51. Tsai PI, Lin CH, Hsieh CH, et al. PINK1 phosphorylates MIC60/Mitofilin to control structural plasticity of mitochondrial crista junctions. *Mol Cell*. 2018;69(5):744-756. doi:10.1016/j.molcel.2018.01.026
52. Marco-Hernandez AV, Tomas-Vila M, Montoya-Filardi A, et al. Mitochondrial developmental encephalopathy with bilateral optic neuropathy related to homozygous variants in IMMT gene. *Clin Genet*. 2022;101(2):233-241. doi:10.1111/cge.14093

SUPPORTING INFORMATION

Additional supporting information can be found online in the Supporting Information section at the end of this article.

How to cite this article: Peifer-Weiß L, Kurban M, David C, et al. A X-linked nonsense *APOO/MIC26* variant causes a lethal mitochondrial disease with progeria-like phenotypes. *Clinical Genetics*. 2023;104(6):659-668. doi:10.1111/cge.14420

5.3 Mitochondrial Apolipoprotein MIC26 is a metabolic rheostat regulating central cellular fuel pathways

Mitochondrial Apolipoprotein MIC26 is a metabolic rheostat regulating central cellular fuel pathways

Melissa Lubeck[1], Ritam Naha[1], Yulia Schaumkessel[1], Philipp Westhoff[2,3], Anja Stefanski[4], Patrick Petzsch[5], Kai Stühler[4,6], Karl Köhrer[5], Andreas P. M. Weber[2,3], Ruchika Anand[1], Andreas S. Reichert[1], Arun Kumar Kondadi[1]*

[1]Institute of Biochemistry and Molecular Biology I, Medical Faculty and University Hospital Düsseldorf, Heinrich Heine University Düsseldorf, Düsseldorf, Germany

[2]Institute of Plant Biochemistry, Cluster of Excellence on Plant Sciences (CEPLAS), Heinrich Heine University Düsseldorf, Düsseldorf, Germany

[3]Plant Metabolism and Metabolomics Laboratory, Cluster of Excellence on Plant Sciences (CEPLAS), Heinrich Heine University, D-40225 Düsseldorf, Germany

[4]Molecular Proteomics Laboratory, Medical Faculty and University Hospital, Heinrich Heine University Düsseldorf, Düsseldorf, Germany

[5]Genomics & Transcriptomics Laboratory, BMFZ, Heinrich Heine University Düsseldorf, Düsseldorf, Germany

[6]Institute of Molecular Medicine, Protein Research, Medical Faculty and University Hospital, Heinrich Heine University Düsseldorf, Düsseldorf, Germany

Correspondence: kondadi@hhu.de

Summary

Mitochondria play central roles in metabolism and metabolic disorders such as type 2 diabetes. MIC26, a MICOS complex subunit, was linked to diabetes and modulation of lipid metabolism. Yet, the functional role of MIC26 in regulating metabolism under hyperglycemia is not understood. We employed a multi-omics approach combined with functional assays using WT and *MIC26* KO cells cultured in normoglycemia or hyperglycemia, mimicking altered nutrient availability. We show that MIC26 has an inhibitory role in glycolysis and cholesterol/lipid metabolism under normoglycemic conditions. Under hyperglycemia, this inhibitory role is reversed demonstrating that MIC26 is critical for metabolic adaptations. This is partially mediated by alterations of mitochondrial metabolite transporters. Furthermore, *MIC26* deletion led to a major metabolic rewiring of glutamine utilization as well as oxidative phosphorylation. We propose that MIC26 acts as a metabolic 'rheostat', that modulates mitochondrial metabolite exchange via regulating mitochondrial cristae, allowing cells to cope with nutrient overload.

Key words

Mitochondria, Apolipoproteins, MIC26, MICOS complex and Fatty acid metabolism

Introduction

The increasing prevalence of global obesity is a huge biological risk factor for development of a range of chronic diseases including cardiovascular diseases, musculoskeletal and metabolic disorders (Collaborators *et al*, 2017). At the cellular level, obesity is associated with DNA damage, inflammation, oxidative stress, lipid accumulation and mitochondrial dysfunction (Włodarczyk & Nowicka, 2019). Mitochondria play central roles in anabolic and catabolic pathways (Spinelli & Haigis, 2018) and as a consequence mitochondrial dysfunction is associated with a variety of metabolic diseases such as type 2 diabetes mellitus (T2DM) (Szendroedi *et al*, 2011). Mitochondrial dysfunction is often linked to abnormal mitochondrial ultrastructure (Eramo *et al*, 2020; Kondadi *et al*, 2020b; Zick *et al*, 2009) and abnormal mitochondrial ultrastructure was also associated with diabetes (Bugger *et al*, 2008; Xiang *et al*, 2020). Mitochondria harbour two membranes, the mitochondrial outer membrane (OM) and the inner membrane (IM). The part of the IM closely apposed to the OM is termed the inner boundary membrane (IBM) whereas the IM which invaginates towards the mitochondrial matrix is termed the cristae membrane (CM). Crista junctions (CJs) are pore-like structures around 12 to 25 nm in diameter, separating the IBM and CM, and are proposed to act as diffusion barriers for proteins and metabolites (Frey & Mannella, 2000; Mannella *et al*, 2013). Formation of CJs depends on Mic60 (Fcj1, Mitofilin, IMMT) which was shown to be located at CJs regulating cristae formation in concert with the F_1F_O ATP synthase (Rabl et al. 2009). Mic60 is a subunit of the 'mitochondrial contact site and cristae organising system' (MICOS) complex (Harner *et al*, 2011; Hoppins *et al*, 2011; von der Malsburg *et al*, 2011) which consists of seven proteins organised into two subcomplexes: MIC60/MIC19/MIC25 and MIC10/MIC26/MIC27 with MIC13 stabilizing the MIC10 subcomplex in mammals (Anand *et al*, 2016; Guarani *et al*, 2015; Urbach *et al*, 2021). MIC26/APOO harbours an apolipoprotein A1/A4/E family domain and therefore was classified as an apolipoprotein (Koob *et al*, 2015; Lamant *et al*, 2006). Traditionally, apolipoproteins mediate lipid and cholesterol metabolism by facilitating the formation of lipoproteins and regulating their distribution to different tissues via the blood stream (Mehta & Shapiro, 2022). Initially, MIC26 was identified as a protein of unknown function in cardiac transcriptome of dogs fed with high-fat diet (HFD) (Philip-Couderc *et al*, 2003) and was incorrectly assumed to exist as a 55 kDa O-linked glycosylated protein as it was immunopositive to a custom-generated MIC26 antibody in samples of human serum, heart tissue and HepG2 cell line (Lamant *et al.*, 2006). However, the recombinant protein was only observed at the expected size of 22 kDa (Lamant *et al.*, 2006) and it was later shown that this 22 kDa form is located to mitochondria (Koob *et al.*, 2015; Ott *et al*, 2015). Moreover, using several cellular *MIC26* deletion models and different antibodies, we showed recently that MIC26 is exclusively present as a 22 kDa mitochondrial protein and not as a 55 kDa protein (Lubeck *et al*, 2023). In light of these findings, the primary physiological function of MIC26 in

diabetes is linked to its role in the mitochondrial IM and not to an earlier proposed secreted form of MIC26.

Mutations in *MIC26* were reported to result in mitochondrial myopathy, lactic acidosis and cognition defects (Beninca *et al*, 2021) as well as a lethal progeria-like phenotype (Peifer-Weiß *et al*, 2023). Interestingly, there is an intricate connection between MIC26 and metabolic disorders. Patients with diabetes (Lamant *et al.*, 2006) and dogs fed with a HFD for 9 weeks (Philip-Couderc *et al.*, 2003) showed increased *Mic26* transcripts in the heart. Accordingly, adenovirus-mediated human *MIC26* overexpression in mice, administered through the tail vein, led to increased levels of triacylglycerides (TAG) in murine plasma, when fed with HFD, and TAG accumulation in the murine liver (Tian *et al*, 2017). In another study, MIC26 transgenic mice hearts displayed an increase of diacylglycerides (DAG) but not TAG (Turkieh *et al*, 2014) as in the previous described study (Tian *et al.*, 2017) suggesting modulatory roles of MIC26 in lipid metabolism. Recently, in mitochondria-rich brown adipose tissue (BAT), downregulation of *Mic26* mRNA and protein levels were reported in diet-induced or leptin-deficient obese (ob/ob) murine models compared to the respective controls. Mice with an adipose tissue specific deletion of *Mic26* which were fed with a HFD gained more total body weight and adipose tissue fat mass than control mice (Guo *et al*, 2023). Hence, we hypothesize that MIC26 has an unidentified regulatory role under nutrient-enriched conditions. Therefore, in order to understand the function of MIC26, we used WT and *MIC26* KO cells as a model system under standard glucose culture conditions as well as excessive glucose culture conditions termed normoglycemia and hyperglycemia, respectively. We employed a multi-omics approach encompassing transcriptomics, proteomics and targeted metabolomics to investigate the pathways regulated by MIC26. We found that the function of MIC26 is critical in various pathways regulating fatty acid synthesis, oxidation, cholesterol metabolism and glycolysis. Interestingly, we observed an entirely antagonistic effect of cellular *de novo* lipogenesis in *MIC26* KO cells compared to WT cells depending on the applied nutrient conditions. This showed that the response to high glucose conditions is strongly dependent on the presence of MIC26. In addition, we found that cells deleted for *MIC26* displayed alterations of mitochondrial glutamine usage and oxidative phosphorylation. Overall, we propose that MIC26 is a unique mitochondrial apolipoprotein functioning as a mitochondrial fuel sensor that regulates central metabolic pathways to meet mitochondrial and thus cellular energy demands.

Results

Mitochondrial apolipoprotein MIC26 is selectively increased in cells exposed to hyperglycemia

There is a strong link between metabolic abnormalities and pattern of *MIC26* expression. Increased levels of *MIC26* transcripts were observed in diabetic patients (Lamant *et al.*, 2006) and increased accumulation of lipids were found upon *Mic26* overexpression in the mouse (Tian *et al.*, 2017; Turkieh *et al.*, 2014). In order to understand the role of MIC26 in cellular metabolism, we used hepatocyte-derived HepG2 cells as the cellular model and generated *MIC26* KO cells using the CRISPR-Cas9 system. WT and *MIC26* KO cells were grown in standard (5.5 mM) and excessive concentrations of glucose (25 mM), defined as normoglycemic and hyperglycemic conditions respectively throughout the manuscript, for a prolonged period of three weeks to investigate long term effects of nutritional overload. Initially, we checked whether there is a difference in the amounts of various MICOS proteins in WT HepG2 cells grown in normoglycemia and hyperglycemia. Western blot (WB) analysis showed a significant increase of MIC26 and MIC27 along with MIC25 in cells grown in hyperglycemia compared to normoglycemia (**Fig 1A & B**). We did not observe any significant changes in the amounts of MIC19, MIC60, MIC10 and MIC13 in WT-Hyperglycemia (WT-H) compared to WT-Normoglycemia (WT-N) condition. This pointed to a specific role of the MICOS subunits, MIC26, MIC27 and MIC25 when cultured in hyperglycemia compared to normoglycemia. The significant increase of MIC27 and MIC25 observed in WT-H when compared to WT-N was abolished in *MIC26* KOs indicating a requirement of MIC26 in this response under nutrient-enriched conditions (**Fig 1A & B**).

The MICOS proteins regulate the IM remodelling by working in unison to maintain CJs and contact sites between IM and OM (Anand *et al*, 2021). Still, deficiency of different MICOS proteins shows variable effects on the extent of CJs loss and cristae ultrastructure (Anand *et al*, 2020; Kondadi *et al*, 2020a; Stephan *et al*, 2020; Weber *et al*, 2013). MIC10 and MIC60 have been considered as core regulators of IM remodelling displaying severe loss of CJs (Kondadi *et al.*, 2020a; Stephan *et al.*, 2020). The extent of mitochondrial ultrastructural abnormalities upon *MIC26* deletion varies among different cell lines tested (Anand *et al.*, 2020; Koob *et al.*, 2015; Stephan *et al.*, 2020). Therefore, we performed transmission electron microscopy (TEM) in WT and *MIC26* KO HepG2 cells which revealed a reduction of cristae content (cristae number per unit mitochondrial length per mitochondria) in *MIC26* KOs compared to WT cells in both nutrient conditions (**Fig 1C & E**). Thus, the loss of cristae was dependent on MIC26 and independent of the glucose concentration used in cell culture. In addition, there was a decrease in cristae number in WT cells grown in hyperglycemia compared to normoglycemia showing that higher glucose levels lead to decreased cristae

density, which is a common phenotype in diabetic mice models (Bugger *et al.*, 2008; Xiang *et al.*, 2020). As the number of cristae were already decreased in certain conditions, we analysed the number of CJs normalised to cristae number and found that a significant decrease of CJs was observed in *MIC26* KOs independent of the nutrient conditions (**Fig 1D & E**). Overall, the loss of MIC26 leads to mitochondrial ultrastructural abnormalities accompanied by reduced number of cristae as well as CJs compared to WT cells (**Fig 1C-E**).

Hyperglycemia confers antagonistic regulation of lipid and cholesterol pathways, in *MIC26* KO vs WT cells, compared to normoglycemia

In order to understand the role of MIC26 in an unbiased manner, we compared WT and *MIC26* KO cells cultured under respective nutrient conditions by employing quantitative transcriptomics and proteomics analyses. A total of 21,490 genes were obtained after the initial mapping of the RNA-Seq data, of which 2,933 were significantly altered in normoglycemic *MIC26* KO compared to WT cells (fold change of ±1.5 and Bonferroni correction $P \leq 0.05$), while in hyperglycemia, *MIC26* KO had 3,089 significantly differentially expressed genes (DEGs) as compared to WT-N cells. A clustering analysis of identified transcripts involving all four conditions along with respective replicates is depicted (**Fig S1A**). A Treemap representation shows comparison of significantly upregulated clustered pathways in *MIC26* KOs cultured in normoglycemia compared to WT (**Fig 2A**). Interestingly, the pathways relating to sterol, cholesterol biosynthetic processes and regulation of lipid metabolic processes were significantly upregulated in *MIC26* KO-N compared to WT-N. On the contrary, in *MIC26* KO-H compared to WT-H, pathways involved in sterol, secondary alcohol biosynthetic processes along with cholesterol biosynthesis and cellular amino acid catabolic processes including fatty acid oxidation (FAO) were mainly downregulated (**Fig 2B**). Thus, an antagonistic regulation is observed upon *MIC26* deletion when normoglycemia and hyperglycemia are compared. A detailed pathway enrichment analysis for significantly upregulated genes in *MIC26* KO vs WT cells grown in normoglycemia also revealed genes involved in cholesterol, steroid biosynthetic pathways, fatty acid synthesis and oxidation as well as glycolysis and gluconeogenesis (**Fig 2C**). The genes involved in cholesterol biosynthetic pathways, glycolysis and gluconeogenesis, FAO and fatty acid synthesis were significantly downregulated in *MIC26* KOs grown in hyperglycemia compared to WT cells (**Fig 2D**). The antagonistic behaviour of cholesterol metabolism observed using transcriptomics data (**Fig 2**) was also confirmed in the pathway enrichment analysis for proteomics (**Fig S1B & C**). Detailed analysis of the transcriptomics data in *MIC26* KO-N compared to WT-N showed that ≈80% of the genes regulating cholesterol biosynthesis were significantly upregulated upon normoglycemia (**Fig S2A**) while the opposite was true for hyperglycemia (**Fig S2B**). At the

proteome level, the effect of *MIC26* deletion was mainly observed in normoglycemic conditions where 8 out of 12 detected proteins involved in cholesterol biosynthesis showed a significant increase in peptide abundances, while this increase was diminished in *MIC26* KO-H compared to WT-H cells (**Fig S2C-N**). Thus, the loss of MIC26 strongly impacts cholesterol biosynthesis in a nutrient-dependent manner. In conclusion, under normoglycemic conditions, MIC26 acts as a repressor of cholesterol biosynthesis whereas under hyperglycemic conditions MIC26 rather drives this pathway. We further employed targeted metabolomics to decipher any altered cholesterol biosynthesis by quantifying the cholesterol amounts at steady state. In accordance with cholesterol synthesis promoting role of MIC26 in hyperglycemia, cholesterol levels were strongly reduced in *MIC26* KO-H compared to WT-H cells. Moreover, cholesterol levels were significantly increased in WT-H cells compared to WT-N which was not the case and even reversed in *MIC26* KO cells (**Fig S2O**). Thus, MIC26 is required to maintain cholesterol homeostasis and cellular cholesterol demand in a nutrient dependent manner and is of particular importance under hyperglycemia.

MIC26 maintains the glycolytic function

Besides an antagonistic regulation of the cholesterol biosynthetic pathway, we also observed an opposing trend of genes involved in lipid metabolism as well as glycolysis (**Fig 2C & D**). In order to gain further insights about the role of MIC26 regarding the differential regulation of glycolytic pathways in normoglycemia and hyperglycemia, we re-visited our transcriptomics (**Fig S3**) and proteomics (**Fig 3A-C and H-J**) datasets and investigated the genes regulating glycolysis upon *MIC26* deletion. On the one hand, in *MIC26* KO-N compared to WT-N, we found that the transcripts encoding hexokinase (*HK*) 1, phosphofructokinase 1 (*PFK1*) (**Fig S3A**) and aldolase (ALDOC) protein levels were significantly upregulated (**Fig 3A**), while glyceraldehyde-3-phosphate dehydrogenase (GAPDH) (**Fig 3B**) and enolase (ENO) were downregulated (**Fig S3A**). On the other hand, in *MIC26* KO-H compared to WT-H, we observed decreased GAPDH and glucose-6-phosphate isomerase (GPI) proteins and transcripts (**Fig 3B & C, Fig S3B**). This could indicate that in hyperglycemia, deletion of *MIC26* leads to deregulation of the glycolysis pathway resulting in increased accumulation of glucose (**Fig 3D**) and decreased glycolysis end products. Therefore, to evaluate the metabolic effect of differentially expressed genes (**Fig S3A & B**) and proteins involved in glucose uptake (**Fig 3 H-J**) and glycolysis (**Fig 3A-C**), we checked whether the glycolytic function is altered in *MIC26* KOs using a Seahorse Flux Analyzer with the glycolysis stress test (**Fig 3E & F**). Based on the extracellular acidification rate (ECAR), the ‘glycolytic reserve’ is an index of the ability to undergo a metabolic switch to glycolysis achieved by the cells upon inhibition of mitochondrial ATP generation whereas the ‘glycolytic capacity’ measures the maximum rates of glycolysis

which the cell is capable to undergo. Overall 'glycolytic function' is measured after cellular glucose deprivation for 1 h and subsequently by quantifying the ECAR primarily arising from cellular lactate formation after providing the cell with saturating glucose amounts. We observed that the glycolytic reserve was significantly increased only in cells cultured in normoglycemia and not in hyperglycemia upon deletion of *MIC26* (**Fig 3F**), while the glycolysis function as well as glycolytic capacity were not significantly increased in *MIC26* KO under both nutrient conditions (**Fig S3C & D**). Therefore, the ability of *MIC26* KO cells (compared to WT) to respond to energetic demand by boosting glycolysis is increased under normoglycemia, while *MIC26* KO cells primed to hyperglycemia were not able to increase glycolytic reserve indicating a clearly different regulation of glycolysis under normoglycemia versus hyperglycemia. In order to understand this better, we quantified the intracellular glucose levels, at steady state in WT and *MIC26* KO, which were significantly increased upon *MIC26* deletion only in hyperglycemia but not normoglycemia compared to the respective WT cells (**Fig 3D**). We further checked whether the increased glucose levels in cells cultured in hyperglycemia is due to increased glucose uptake. In normoglycemia, a glucose uptake assay showed a modest but significant increase of glucose uptake in *MIC26* KOs compared to WT cells (**Fig 3G**) which is consistent with a strong increase in GLUT3 amounts (**Fig 3H**) albeit accompanied by a downregulation of GLUT1 upon *MIC26* depletion (**Fig 3I**). GLUT2 levels remained unchanged in all conditions (**Fig 3J**). However, the observed increased glucose uptake in *MIC26* KO-N (compared to WT-N) was abolished in *MIC26* KO-H (compared to WT-H) and accordingly accompanied by no increase in GLUT3 levels showing that the high amounts of glucose in *MIC26* KO cells grown in hyperglycemia cannot be explained by an increased glucose uptake under these conditions (**Fig 3G**). In *MIC26* KO-N compared to WT-N, even though we observed an increase of glucose uptake, the amount of glycolysis end products, namely pyruvate (**Fig 3K**) and lactate (**Fig 3L**) were unchanged. In hyperglycemia, a significant reduction of pyruvate (**Fig 3K**) and lactate (**Fig 3L**) amounts were observed at steady-state despite increased glucose levels upon *MIC26* deletion. Overall, upon *MIC26* deletion pyruvate and lactate levels were decreased in hyperglycemia while no change was observed in normoglycemia. These results combined with the already discussed differentially regulated transcripts and proteins involved in glycolysis prompted us to check whether there is a difference of shuttling metabolic intermediates from glycolysis towards lipid anabolism. Glycerol-3-phosphate (G3P) is a precursor for lipid biosynthesis synthesized from dihydroxyacetone phosphate which is derived from glycolysis. We observed an increase in G3P levels upon *MIC26* deletion in normoglycemic conditions, while G3P levels were significantly reduced in *MIC26* KO-H cells, compared to the respective WT cells (**Fig 3M**). This opposing trend, together with the previously described antagonistic enrichment in fatty acid biosynthesis (**Fig 2C & D**), indicates that *MIC26* deletion rewires glycolytic function to drive lipogenesis in normoglycemia with an antagonistic effect in

hyperglycemia. Further, we checked the cellular effect of *MIC26* loss on lipid anabolism in normo- as well as hyperglycemia.

The loss of MIC26 leads to metabolic rewiring of cellular lipid metabolism via CPT1 and dysregulation of fatty acid synthesis

The respective increase and decrease of G3P (**Fig 3M**) in normoglycemia and hyperglycemia upon *MIC26* deletion when compared to WT as well as an opposing trend in fatty acid biosynthesis reflected in our transcriptomics data (**Fig 2C & D**) prompted us to explore the regulation of cellular lipid metabolism. Lipid droplets (LDs) play a key role in energy metabolism and membrane biology by acting as reservoirs to store TAG and sterol esters which are released to the relevant pathways according to cellular demand (Thiam *et al*, 2013). Using BODIPY staining, we checked the cellular LD content in unstimulated and palmitate-stimulated WT and *MIC26* KO cells grown in normoglycemia and hyperglycemia, respectively. The number of LDs and the respective fluorescence intensity of BODIPY are indicative of cellular lipid content (Chen *et al*, 2022). We observed a general increase of LD number in *MIC26* KOs irrespective of treatment conditions (**Fig 4A & B**). However, the increased intensity of BODIPY staining observed in normoglycemia was not evident in *MIC26* KO-H compared to respective WT cells (**Fig 4C & D**). Further, when we fed free fatty acids (FFAs) in the form of palmitate, there was again increased BODIPY intensity in *MIC26* Kos in normoglycemia even at a higher level. In contrast, under hyperglycemia *MIC26* KO cells showed lower LD intensity when compared to WT cells again demonstrating an antagonistic role of MIC26 when normoglycemia was compared to hyperglycemia (**Fig 4C & D**). These experiments allow us to conclude that the effect of *MIC26* deletion on LD accumulation depends on the nutrient condition which is enhanced under nutrient-rich (high-glucose/high-fat-like) conditions. Overall, MIC26 is essential to regulate the amount of cellular LD content in a nutrient-dependent manner (**Fig 4D**).

LD biogenesis is closely linked to increased cellular FFA levels (Zadoorian *et al*, 2023). Using targeted metabolomics, we investigated the steady state levels of long chain FFAs in WT and *MIC26* KO cell lines cultured in normoglycemia and hyperglycemia (**Fig 4E**). We identified that there was either no change or an increase of saturated FFAs including lauric (12:0), myristic (14:0), palmitic (16:0), stearic (18:0), arachidic (20:0) as well as behenic (22:0) acid in normoglycemia in *MIC26* KOs compared to WT cells (**Fig 4E, Fig S4**). In contrast, we consistently found a decrease in most of the above-mentioned saturated FFAs in *MIC26* KO-H compared to WT-H. This trend was also observed in unsaturated FFAs like oleic acid (18:1). Overall, we conclude that there is a consistent decrease of saturated FFAs in *MIC26* KO-H as opposed to *MIC26* KOs grown in normoglycemic conditions consistent to the observed trend

in LD formation. Increased level of FFAs and LDs can arise from increased FFAs biosynthesis as well as reduced FFA catabolism via mitochondrial β-oxidation (Afshinnia *et al*, 2018). Mitochondrial β-oxidation requires import of long chain FFAs using the carnitine shuttle comprised of carnitine palmitoyl transferase 1 (CPT1) and 2 (CPT2) and carnitine-acylcarnitine translocase (CACT), into the mitochondrial matrix. Depletion of CPT1A, which is the rate limiting step of FAO, coincides with lipid accumulation in the liver (Sun *et al*, 2021). Therefore, we determined the CPT1A amounts using WB analysis (**Fig 4F & G**) which were in line with transcriptomics and quantitative PCR data (**Fig S5A & B**). *MIC26* deletion revealed a reduction of CPT1A in normoglycemia compared to WT cells. In WT cells, hyperglycemia already triggered a reduction in CPT1A level and there was no further decrease of CPT1A in *MIC26* KOs grown in hyperglycemia (**Fig 4F & G**). In order to understand the functional significance of CPT1A reduction on mitochondrial function, we checked the FAO capacity of respective cell lines by feeding them with palmitate and analysing the induced basal respiration and spare respiratory capacity (SRC) of mitochondria compared to BSA control group (**Fig 4H and I, Fig S5C & D**). SRC is the difference between FCCP stimulated maximal respiration and basal oxygen consumption and therefore is the ability of the cell to respond to an increase in energy demand. We observed a significant reduction in palmitate-induced basal respiration as well as SRC in *MIC26* KO-N compared to WT-N determining decreased mitochondrial long chain fatty acid β-oxidation. It is important to note that we already observed a significant decrease in mitochondrial β-oxidation in WT-H condition which was not further affected in *MIC26* KO-H in agreement with the reduced CPT1A levels (**Fig 4F & G**). We further analysed the reduction of oxygen consumption rate (OCR) induced by etomoxir inhibition of CPT1A (**Fig 4J**). In *MIC26* KO-N compared to WT-N, palmitate-induced OCR was reduced moderately, yet this was not significant. For the respective hyperglycemic conditions, we did not observe a change which was again in line with the observed CPT1A levels. Thus, reduced β-oxidation in *MIC26* KO-N compared to WT-N is apparently contributing to increased FFA levels and LD content and could be mediated, at least in part, via the reduced levels of CPT1A resulting in reduced transport of FFAs into mitochondria.

We further checked whether FFA biosynthesis plays a role in the nutrition-dependent antagonistic regulation of lipid anabolism in *MIC26* KO cell line. FFA biosynthesis is initiated with the export of citrate generated in TCA cycle from mitochondria to the cytosol. The export is mediated by the citrate/malate exchanger SLC25A1 which is present in the mitochondrial IM. Proteomics and transcriptomics data showed that SLC25A1 was increased in normoglycemia in *MIC26*-KOs (compared to respective WT), but not in hyperglycemia (**Fig S5E & F**). We then checked for further changes in the transcriptome and proteome levels of key enzymes playing a role in FFA synthesis. We found that ATP citrate lyase (ACLY, **Fig**

S5G), acetyl-Co-A carboxylase (ACACA, **Fig S5H &I**) which converts acetyl-CoA into malonyl-CoA, fatty acid synthase (FASN, **Fig S5J & K**) and acetyl-CoA desaturase (SCD, **Fig S5L & M**) were increased in normoglycemia in *MIC26* KOs but mostly unchanged in hyperglycemia. In addition, hyperglycemia resulted in an increase of glycerol kinase (GK) in WT cells which was absent in *MIC26* KO cells (**Fig S5N**). Therefore, our data indicate that the FFA biosynthesis pathway is upregulated upon loss of *MIC26* KO in normoglycemia but not in hyperglycemia compared to respective WT conditions. An upregulation of FFA biosynthesis along with reduced mitochondrial β-oxidation partially mediated by reduced CPT1A amount in *MIC26* KO-N and a shift of glycolytic intermediates resulting in G3P accumulation show that loss of MIC26 leads to a cumulative metabolic rewiring towards increased cellular lipogenesis.

MIC26 deletion leads to hyperglycemia-induced decrease in TCA cycle intermediates

To synthesize FFA, citrate first needs to be generated by the TCA cycle in the mitochondrial matrix before it is exported to the cytosol. Using targeted metabolomics, we checked whether the TCA cycle metabolism is altered upon *MIC26* deletion at steady state in both nutrient conditions (**Fig 5A**). As previously described, glycolysis resulted in decreased pyruvate levels upon *MIC26* deletion in hyperglycemia, while no change was observed in normoglycemia (**Fig 3N**). Furthermore, most of the downstream metabolites including (iso-)citrate, succinate, fumarate and malate consistently showed a significant decrease in *MIC26* KO cells cultured in hyperglycemia, compared to WT condition, but not in normoglycemia following the previously observed trend in pyruvate levels. To elucidate a possible defect of mitochondrial pyruvate import, we checked mitochondrial pyruvate carrier 1 (MPC1) and MPC2 abundances (**Fig 5B & C**) as well as mitochondrial respiration after blocking mitochondrial pyruvate carrier (glucose / pyruvate dependency) using UK5099 inhibitor (**Fig 5D**). While we observed a downregulation of MPC1 in *MIC26* KO-N compared to WT-N, MPC1 abundances in *MIC26* KO-H compared to WT-H remained unchanged. Further we did not observe any changes in MPC2 level. Also, mitochondrial glucose/pyruvate dependency remained unchanged in the respective hyperglycemia combination while we observed a minor but significant decrease in *MIC26* KO-N compared to WT-N. In addition, elucidation of abundances of mitochondrial enzymes catalyzing TCA cycle metabolites (**Fig S6A-K**) as well as the respective cytosolic enzymes (**Fig S6L-N**) interestingly revealed an upregulation of citrate synthase (**Fig S6A**) and mitochondrial aconitase 2 (**Fig S6B**) in *MIC26* KO cells independent of nutrient conditions. Furthermore, the immediate downstream enzyme isocitrate dehydrogenase 2 which generates α-ketoglutarate (α-KG) was upregulated in *MIC26* KO condition (**Fig S6C**). In contrast to all previously described metabolites, the α-KG levels were increased in hyperglycemia in *MIC26* KO compared to WT. The accumulation of α-KG possibly arises from a significant

355 downregulation of α-KG dehydrogenase in *MIC26* KO independent of the nutrient condition
356 (**Fig S6E**). Following, an accumulation of α-KG by downregulation of α-KG dehydrogenase
357 would further explain the decreased formation of succinate in *MIC26* KO-H compared to WT-H.
358 Succinate dehydrogenases (**Fig S6G & H**) as well as fumarase (**Fig S6I**) did not show any
359 changes in abundances upon the respective *MIC26* KO to WT comparison reflecting the
360 uniform metabolite trend in succinate, fumarate and malate. Overall, we observed a general
361 decrease in several TCA cycle metabolites in *MIC26* KO-H compared to WT-H. Therefore, we
362 propose that a downregulation of FFA biosynthesis in *MIC26* KO-H compared to WT-H results
363 from a limited formation of citrate via the mitochondrial TCA cycle presumably arising from
364 reduced utilization of glucose.

365

366 **Aberrant glutamine metabolism is observed in *MIC26* KOs independent of nutritional**
367 **status**

368 Glutaminolysis feeds α-KG in the TCA cycle. To check whether the increase in α-KG could be
369 (apart from downregulation of α-KG dehydrogenase amounts) derived from glutaminolysis, we
370 also checked glutamine (**Fig 6A**) and glutamate levels (**Fig 5A**). The amounts of glutamine at
371 steady-state were uniformly increased in *MIC26* KOs irrespective of nutrient conditions (**Fig**
372 **6A**). Glutamate was decreased in *MIC26* KO-N compared to WT-N (**Fig 5A**). Mitochondria
373 mainly oxidise three types of cellular fuels namely pyruvate (from glycolysis), glutamate (from
374 glutaminolysis) and FFAs. We used a 'mito-fuel-flex-test' for determining the contribution of
375 glutamine as a cellular fuel. The contribution of glutamine as cellular fuel could be determined
376 using BPTES, an allosteric inhibitor of glutaminase (GLS1), which converts glutamine to
377 glutamate. The extent of reduction of mitochondrial oxygen consumption upon BPTES
378 inhibition is used as a measure for determining the glutamine dependency while the capacity
379 is the ability of mitochondria to oxidise glutamine when glycolysis and FFA oxidation are
380 inhibited. Intriguingly, we observed that the *MIC26* KOs do not depend on glutamine as a fuel
381 (**Fig 6B**, left histogram). However, they still can use glutamine when the other two pathways
382 were inhibited (**Fig 6B**, right histogram). The glutamine oxidation capacity of *MIC26* KO cells
383 cultured in normoglycemia as well as hyperglycemia appears slightly decreased compared to
384 WT but this decrease is not statistically significant. Overall, we observe a remarkable metabolic
385 rewiring of *MIC26* KOs to bypass glutaminolysis. In order to understand whether the
386 independency on glutamine as fuel arises due to the possibility of aberrant transport of
387 glutamine into the mitochondria, we analysed transcripts and proteins that were not only
388 significantly downregulated but also present in the mitochondria IM and interacted with MIC26.
389 For this, we investigated putative MIC26 interactors by compiling a list using BioGRID,
390 NeXtProt and IntAct databases. SLC25A12, an antiporter of cytoplasmic glutamate and

mitochondrial aspartate, was significantly downregulated (**Fig S7A**) while showing up in the interactome of MIC26 (**Fig S7E**). Accordingly, WB analysis reveal a reduction of SLC25A12 in *MIC26* KOs compared to WT HepG2 cells in both normoglycemia and hyperglycemia (**Fig 6C & D**). Further, it is known that a variant of SLC1A5 transcribed from an alternative transcription start site and present in the mitochondrial IM is responsible for transporting glutamine into mitochondria (Yoo *et al*, 2020a). Transcriptomics data revealed a reduction of SLC1A5 in *MIC26* KOs while proteomics revealed a significant reduction in normoglycemia and non-significant reduction in hyperglycemia in *MIC26* KOs compared to WT (**Fig S7B & C**). An increase of cellular glutamine levels in *MIC26* KOs (**Fig 6A**) along with reduced levels of SLC1A5 and reduced mitochondrial glutamine dependency (**Fig 6B**) indicate a reduced transport of glutamine destined for glutaminolysis into mitochondria.

In order to delineate whether the increased glutamine levels at steady-state are due to decreased glutamine utilisation or increased flux, we performed a metabolic tracing experiment where WT and *MIC26* KO cells, cultured in normoglycemia and hyperglycemia, were fed with labelled glutamine [U-$^{13}C_5$, $^{15}N_2$] for 0.5 h and 6 h (**Fig 6E-O**). Glutamine is converted to glutamate by glutaminase (GLS) in the mitochondria. The GLS amounts were not altered in *MIC26* KO cells when compared to respective WT cells grown in normoglycemia and hyperglycemia (**Fig S7D**). In line, label enriched glutamate species (m+1 - m+4) did not show major differences in all four conditions at both timepoints (**Fig 6E**). Following this, we hypothesize that accumulation of glutamine in *MIC26* KO cells arises from other cellular pathways utilising glutamine being impaired, for example synthesis of purine, pyrimidine or amino acids. However, labelled α-KG (m+1 - m+5) was increased upon *MIC26* deletion with a pronounced effect in cells cultured in hyperglycemia similar to the detected steady-state amounts of α-KG (**Fig 6F**). To check the conversion rates of different metabolite reactions, we determined the enzyme conversion rates by calculating the ratio of the highest labelled species from the end-metabolite compared to the starting-metabolite. In accordance to the observed level of α-KG, the conversion ratio from glutamate to α-KG was significantly increased in *MIC26* KO cells (**Fig 6K**). We further checked the flux of TCA metabolites downstream to α-KG namely succinate, fumarate and malate. Despite the increased α-KG levels, the labelled succinate species (m+1 - m+4) was decreased in *MIC26* KO cells (**Fig 6H**). In line, the conversion rate from α-KG to succinate was significantly downregulated in *MIC26* KO cells independent of glucose concentrations and timepoints (**Fig 6M**). However, the conversion ratio from succinate to fumarate catalysed by mitochondrial complex II subunits, succinate dehydrogenases A-D, was increased in *MIC26* KO cell lines at the 6 h timepoint compared to WT in both normoglycemia and hyperglycemia (**Fig 6N**). Despite the increase in fumarate conversion, the labelled fumarate and malate were decreased in *MIC26* KO compared to WT in normoglycemia but not in hyperglycemia (**Fig 6I & J**) while there were minor differences at

0.5 h. The conversion ratio from α-KG to malate was decreased upon *MIC26* deletion in both nutrient conditions at 0.5 h and 6 h of glutamine labelling. Thus, despite increased conversion of succinate to fumarate as well as increased flux from glutamate to α-KG (in hyperglycemia) upon loss of MIC26, cellular glutaminolysis does not function optimally. We also checked the labelled citrate levels which showed minor changes after 0.5 h treatment but a major change in all labelled species (m+1 - m+5) after 6 h (**Fig 6G**). Correspondingly, the levels of citrate in WT-N cells were highly increased compared to all three other conditions. Conversion rates from α-KG (m+5) to citrate (m+5) were significantly reduced in *MIC26* KO cell lines compared to the respective WT cells (**Fig 6L**). Overall, the flux of glutamine through the TCA cycle is accompanied by decreased conversion of TCA cycle intermediates. Therefore, we conclude that aberrant glutaminolysis is observed upon loss of MIC26.

MIC26 regulates mitochondrial bioenergetics by restricting the ETC activity and OXPHOS (super-)complex formation

We have shown that the loss of *MIC26* leads to dysregulation of various central fuel pathways. In order to understand the effect of *MIC26* deletion on cellular bioenergetics, we checked the mitochondrial membrane potential ($\Delta\Psi_m$) of WT and *MIC26* KO cells in both nutrient conditions by employing TMRM dye (**Fig 7A & B**). Loss of MIC26 leads to decreased $\Delta\Psi_m$ compared to control cells in both normoglycemia and hyperglycemia. It is well known that mitochondrial loss of membrane potential is connected to mitochondrial dynamics (Giacomello *et al*, 2020). Thus, we checked the mitochondrial morphology and observed that loss of MIC26 consistently leads to a significant increase of mitochondrial fragmentation compared to WT-N (**Fig 7C & D**). In addition, WT cells grown in hyperglycemia despite maintaining the $\Delta\Psi_m$ exhibited fragmented mitochondria. We also checked the levels of major mitochondrial dynamic regulators: MFN1, MFN2, DRP1 as well as OPA1 processing into short forms. WB analysis showed that MFN1 levels were significantly decreased upon *MIC26* deletion in both normoglycemia and hyperglycemia compared to respective WT cells (**Fig S8A & B**) which could account for increased fragmentation. There was no major effect on the amounts of other factors which could account for mitochondrial fragmentation. Thus, *MIC26* deletion is characterized by reduced $\Delta\Psi_m$ and fragmentation of mitochondria which indicate altered mitochondrial bioenergetics. To determine this, we checked the mitochondrial function in WT and *MIC26* KO cells by using a mitochondrial oxygen consumption assay (**Fig 7E**). We observed an increased basal respiration in *MIC26* KOs in both normoglycemia and hyperglycemia compared to the respective WT (**Fig 7F**). The ATP production was increased in *MIC26* KO cells in hyperglycemia compared to WT-H (**Fig S8C**). In addition, decreased SRC was observed in *MIC26* KO-N when compared to WT-N condition (**Fig S8D**). Overall, *MIC26* KOs demonstrate

higher basal respiration in both nutrient conditions. In order to elucidate the increased basal respiration, we performed blue native PAGE to understand the assembly of OXPHOS complexes along with in-gel activity assays (**Fig 7G**). *MIC26* deletion consistently led to an increase in the levels of OXPHOS complexes I, III, IV and dimeric and oligomeric complex V (shown in green arrows) (**Fig 7G**, left blots respectively for each complex). The increased assembly of OXPHOS complexes was also accompanied by respective increase of in-gel activity (shown in blue arrows) (**Fig 7G**, right blots respectively for each complex). This is consistent with the previously observed increased basal respiration (**Fig 7F**) and the succinate to fumarate conversion representing an increased complex II activity (**Fig 6N**). Altogether, we conclude that formation and stability of OXPHOS (super-) complexes as well as their activity is dependent on MIC26.

Discussion

Our study identifies MIC26 as a critical regulator at the crossroads of several major metabolic pathways. Based on detailed multi-omics analyses, we deciphered an intricate interplay between MIC26, a mitochondrial IM protein, and global cellular metabolic adaptations. To understand these metabolic changes and their dependency on mitochondrial ultrastructure and function is of high medical relevance as nutrient-overload is known to cause obesity and T2DM in humans. In fact, *MIC26* mutations are also associated with mitochondrial myopathy, lactic acidosis (Beninca *et al.*, 2021) as well as lethality and progeria-like phenotypes (Peifer-Weiß *et al.*, 2023). We showed that cellular fatty acid synthesis, cholesterol biosynthesis and LD formation is promoted by MIC26 under high glucose conditions but that these pathways are conversely inhibited by MIC26 under normal glucose concentrations (**Fig 7H**). The important role of MIC26 in channelling nutrient excess from glucose into lipids underscores its reported links to obesity (Tian *et al.*, 2017) and diabetes (Lamant *et al.*, 2006) as it known that ectopic lipid accumulation is a common feature of the development of metabolic diseases including NAFLD and insulin resistance. Moreover, metabolism of glutamine via glutaminolysis is strongly impaired in the absence of MIC26. First, we discuss, how and why MIC26 promotes lipid anabolism in hyperglycemia and what is known from earlier studies in this context. Previously in mammalian cells, we characterised the role of MIC26, which contained a conserved apolipoprotein A1/A4/E family domain, in regulating mitochondrial ultrastructure and function (Koob *et al.*, 2015). We showed that both an increase and decrease of MIC26 was detrimental to mitochondrial function indicating that optimal MIC26 amounts are essential for cellular homeostasis. Despite the demonstration of an increase of mitochondrial structural proteins, like MIC60, SAMM50 and MIC19, connected with upregulation of key metabolic pathways in mice fed with HFD compared to normal diet (Guo *et al*, 2013), the interplay of

MICOS proteins, including MIC26, and metabolism is not clear. Since, classically apolipoproteins bind to lipids and mediate their transport in the bloodstream (Mehta & Shapiro, 2022), the presence of MIC26 in a non-classical environment like the IM raises various questions about its function. Interestingly, a previous report revealed a connection between increased levels of *MIC26* transcripts and nutrient conditions mimicked by oleic acid treatment (Wu *et al*, 2013). How does the loss of MIC26 alter central metabolic pathways including lipid metabolism in hyperglycemia? In this study, we found an increase of MIC26 in WT cells cultured in hyperglycemia. Concomitant to MIC26 increase, we found that MIC26 stimulates the formation of LDs when glucose is in excess. We demonstrate that MIC26 is essential for glucose utilisation and channelling glycolytic intermediates towards lipid anabolism regulating the accumulation of the LD content. This is supported by several findings including the determined levels of pyruvate and TCA cycle intermediates indicating that by boosting pyruvate levels, MIC26 further increases the amounts of the TCA cycle metabolites including citrate levels which serve as a precursor for cholesterol as well as FFA synthesis. This connection between lipid synthesis and MIC26 is further strengthened by earlier reports in the context of diabetes or obese models. Dogs fed with a HFD for 9 weeks (Philip-Couderc *et al.*, 2003) and diabetic patients (Lamant *et al.*, 2006) showed increased *Mic26* transcripts in the heart. Increased TAG and DAG were found upon *MIC26* overexpression in murine liver (Tian *et al.*, 2017) and hearts (Turkieh *et al.*, 2014) respectively showing modulatory roles of MIC26 in lipid metabolism. Our data reveals a major MIC26-dependent alteration of metabolite transporters of the mitochondrial IM and also metabolite levels. Thus, loss of MIC26 either alters the level, the activity, or the submitochondrial distribution of various metabolite transporters. In line with our data, the export of citrate from the mitochondrial matrix to the cytosol is presumably of particular importance. MIC26 could regulate metabolite exchange mechanistically either via protein-protein interactions of MIC26 to distinct metabolite transporters such as SLC25A12, by altering the accessibility of metabolites to various transporters due to altered cristae morphology. Overall, we propose that MIC26 regulates metabolite exchange between the cytosol and mitochondria and vice versa in a nutrient-dependent manner which is critical for adaptations to excess of glucose.

Under balanced nutrient conditions, MIC26 plays a different role compared to nutrient excess conditions. MIC26 decreases the key enzymes regulating the upper half of glycolytic pathway involved in ATP consumption phase. MIC26 prevents an increase of FFAs and G3P culminating in uncontrolled accumulation of LD content. In line with this, it was recently shown that the loss of MIC26 in BAT led to upregulation of glycolysis and fatty acid synthesis pathways (Guo *et al.*, 2023). This was accompanied by impaired thermogenic activity of BAT, mitochondrial ultrastructure and function which reiterates the role of MIC26 in metabolic reprogramming. In normoglycemia, we found that the presence of MIC26 leads to a decrease

of majority of the transcripts enzymes participating in cholesterol biosynthesis, including the sterol regulatory element binding transcription factor 2 (SREBP2) (**Fig S9C**) which is a master regulator of genes involved in sterol and fatty acid synthesis (Madison, 2016). However, we observed equal amounts of cholesterol in *MIC26* KO and WT cells under normoglycemia. Thus, MIC26 in normoglycemia facilitates equal metabolite distribution to either cholesterol biosynthesis or lipogenesis. This MIC26-mediated metabolic switch based on the amount/type of cellular fuel is essential for maintaining key metabolic pathways. A balanced amount of MIC26 is essential for how much glucose is channelled into lipid synthesis. In congruence with our observations, key lipid metabolism genes were altered upon *Mic26* overexpression with an interesting antagonistic regulation of *de novo* lipid synthesis genes depending on nutritional conditions (Tian *et al.*, 2017). This study demonstrated an increase of important transcripts regulating lipid synthesis like ACACA, FASN and SCD in mice, overexpressing *Mic26*, fed with normal diet and a decrease when fed with HFD, compared to respective control mice. We further observed a decrease in CPT1A level and activity in *MIC26* KO cell lines as well as WT-H. CPT1A activity is known to be regulated either on a transcriptional level via peroxisome proliferator activated receptor α (PPARα) and peroxisome proliferator-activated receptor gamma coactivator 1 alpha (PGC-1α) or by allosteric inhibition through malonyl-CoA (López-Viñas *et al*, 2007; Song *et al*, 2010). A recent study demonstrated the downregulation of PPARα protein level in BAT in adipose tissue-specific *MIC26* KO mice (Guo *et al.*, 2023). Further, we observed a high upregulation of ACACA enzyme, which converts acetyl-CoA to malonyl-CoA during *de novo* lipogenesis. Accordingly, it is possible that *MIC26* deletion in normoglycemia could on one hand reduce the expression of PPARα leading to decreased CPT1A expression and on the other hand increase malonyl-CoA formation leading to decreased CPT1A activity. Taken together, we used a multi-omics approach as well as a variety of functional assays to decipher that loss of MIC26 leads to an antagonistic regulation of glycolysis, lipid as well as cholesterol synthesis dependent on cellular nutritional stimulation.

Besides the antagonistic regulation mediated by MIC26 in different nutrient conditions, there are general roles of MIC26 in metabolic pathways which are independent of nutrient conditions. Among the MICOS proteins, proteins like MIC60 are considered as core components as *MIC60* deletion leads to a consistent loss of CJs (Kondadi *et al.*, 2020a; Stephan *et al.*, 2020) while the effect of *MIC26* deletion on loss of CJs varies with the cell line. Loss of CJs was observed in 143B (Koob *et al.*, 2015) and HAP1 cells (Anand *et al.*, 2020) in contrast to HeLa cells (Stephan *et al.*, 2020). *MIC26* deletion in HepG2 cells in this study revealed a significant reduction of CJs when normalised to the cristae number, highlighting a possible major role of MIC26 in liver-derived cell lines. Concomitant to the reduction of CJs, we also observed alterations of vital transporters in the mitochondrial IM and OM. It was recently described that deletion of stomatin-like protein 2 (*SLP2*) leads to a drastic MIC26 degradation mediated by

the YME1L protease (Naha *et al*, 2023). SLP2 was proposed as a membrane scaffold for PARL and YME1L named as the SPY complex (Wai *et al*, 2016). It is therefore conceivable that MIC26 could be concentrated in lipid-enriched nanodomains of the IM justifying its apolipoprotein nomenclature. When we checked the mitochondrial function upon *MIC26* deletion in HepG2 cells, we found that RCCs have enhanced respiratory capacity which was due to: a) increase in the levels of native RCCs as well as supercomplexes and b) increase in the activity of RCCs corresponding to increased RCC amounts. Thus, MIC26 could perform structural as well as functional roles which may or may not be mutually exclusive to the MICOS complex. A reduction of SLC25A12, an antiporter of cytoplasmic glutamate and mitochondrial aspartate, which is present in the IM was observed upon *MIC26* deletion independent of the nutritional status. We also found that SLC25A12 could be an interactor of MIC26 upon using standard interaction databases available online. Presumably, the interaction of SLC25A12 with MIC26 is important for the stability of the former. Such an intricate relationship between MIC26 and metabolite transporters in the IM makes it tempting to speculate that mitochondrial membrane remodelling is linked to its metabolic function. In fact, a closer look at the mitochondrial carrier family (SLC25) transcriptomics and proteomics data sets revealed that a majority of the SLC25 transporters were differentially regulated upon *MIC26* deletion in normoglycemia as well as hyperglycemia (**Fig S9A & B**). A prominent example is the reduction of SLC1A5 in *MIC26* KO when compared to WT in hyperglycemia as well as normoglycemia. A recent study showed that a variant of SLC1A5 present in the mitochondrial IM is responsible for transporting glutamine into the mitochondria (Yoo *et al.*, 2020a). *MIC26* deletion leading to reduced total amounts of SLC1A5 also indicates reduced transport of glutamine into mitochondria. This was in line with an accumulation of glutamine upon loss of MIC26 at steady state. However, using glutamine tracing experiments we did not observe a decrease in labelled glutamate species but we observed an accumulation of α-KG. This could be due to the observed decrease in α-KG dehydrogenase resulting in reduced conversion of α-KG to other metabolites of the TCA cycle in particular under high glucose conditions. On the other hand, besides mitochondrial glutamine usage to fuel the TCA cycle, glutamine is known to be an essential source for nucleotide biosynthesis (Yoo *et al*, 2020b). *MIC26* KO cells showed a decreased growth rate (**Fig S9D-F**). Hence, glutamine accumulation and with that reduced conversion to nucleotides is a possible mechanism leading to growth deficiencies of *MIC26* KO cells. We found that the transcripts as well as protein levels of NUBPL were prominently downregulated upon *MIC26* deletion independent of the glucose concentrations of the cell culture media (**Fig S9G & H**). NUBPL was demonstrated to function as an assembly factor for complex I (Sheftel *et al*, 2009). Despite the prominent reduction of NUBPL, we did not find any discrepancy in complex I assembly or its activity most likely due to increased RCC amounts. We also found that the transcripts and protein levels of DHRS2 were significantly reduced in

MIC26 KO (**Fig S9I & J**). DHRS2 is implicated in reprogramming of lipid metabolism (Li *et al*, 2021) and was found to be downregulated in T2DM (De Silva K 2022).

We further found that hyperglycemia as well as *MIC26* deletion resulted in a fragmented mitochondrial morphology compared to WT-N. Mitochondrial dynamics and cellular metabolism including nutritional demands are closely interlinked (Mishra & Chan, 2016). Nutritional overload was associated with increased mitochondrial fragmentation (Yu *et al*, 2006) while starvation led to formation of a tubular mitochondrial network (Gomes *et al*, 2011). Further, mice lacking the ability to undergo mitochondrial fission by liver specific deletion of *Drp1* were protected from lipid accumulation in the liver as well as insulin resistance upon HFD feeding (Wang *et al*, 2015). Obesity is associated with increased mitochondrial fragmentation in multiple studies. A recent study showed that mitochondrial fragmentation is positively correlated to mitochondrial long chain FFA oxidation capacity via an increased activity of CPT1A (Ngo *et al*, 2023). A stronger membrane curvature resulting from mitochondrial fragmentation induces a conformational change leading to a decreased inhibitory binding ability of malonyl-CoA on CPT1 activity. Even though we observed mitochondrial fragmentation upon *MIC26* deletion, we did not observe increased FAO. This discrepancy could be explained by a reduction of CPT1A amount on one hand and likely increased production of malonyl-CoA on the other hand due to increased amounts of SLC25A1 and ACACA participating in fatty acid synthesis. Hence, deletion of MIC26, leading to mitochondrial fragmentation, contributes to ectopic cellular lipid accumulation but not FAO.

In sum, under balanced nutrient availability, we provide evidence that MIC26 is important to allow efficient metabolite channelling, mainly via glycolysis, thereby preventing unwanted channelling into lipogenesis. In addition, MIC26 is important to promote exactly the latter when glucose is in excess. This is important for cells to adapt to nutrient overload and explains earlier reports linking MIC26 to diabetes. We propose that MIC26 acts as a sensor and valve that opens towards lipid synthesis only when glucose is in excess. Future studies will have to decipher how changes in IM structure directly affect metabolite exchange and how this is regulated dynamically.

Acknowledgments

A.K.K received Deutsche Forschungsgemeinschaft (DFG, German Research Foundation) Grant KO 6519/1-1. A.S.R received grants from DFG Graduiertenkolleg VIVID RTG 2576 and DFG SFB 1208, project B12 (ID 267205415). R.A received DFG Grant AN 1440/3-1. We thank Gisela Pansegrau and Andrea Borchardt for technical assistance in western blot and electron microscopy experiments, respectively. We are thankful for excellent technical support by Maria

Graf, Elisabeth Klemp, and Katrin Weber (CMML). RNA-sequencing was performed at the Genomics & Transcriptomics facility, Biological and Medical Research Center (BMFZ), Medical Faculty, Heinrich-Heine-University Düsseldorf. Computational infrastructure and support were provided by the Centre for Information and Media Technology at Heinrich Heine University Düsseldorf. Proteome experiments were performed at the proteomics facility, BMFZ, HHU, Düsseldorf. Metabolite analyses were supported by the CEPLAS Plant Metabolism and Metabolomics Laboratory, which is funded by the DFG under Germany´s Excellence Strategy – EXC-2048/1 – project ID 390686111.

Author Contributions

A.K.K. and A.S.R. conceptualized the research goals and the experiments of the study. M.L. planned, performed and analysed the results from majority of the experiments. R.N analysed and visualized proteomics and transcriptomics data. Y.S. planned, performed and analysed BN-PAGE and CN-PAGE. P.W. and A.P.M.W. performed and analysed metabolomics data. A.S. and K.S. performed and analysed proteomics data. P.P. and K.K. performed and analysed transcriptomics data. R.A. contributed with scientific and critical inputs to the study. A.K.K. and M.L. wrote the manuscript with input from all authors. A.K.K. supervised the study.

Declaration of interests

The authors declare no competing interests

Figure legends

Figure 1. Mitochondrial apolipoprotein MIC26 is selectively increased in cells exposed to hyperglycemia

(A and B) Western blot analysis of all MICOS subunits from HepG2 WT and *MIC26* KO cells cultured in normo- and hyperglycemia (N = 3-5). Chronic hyperglycemia treatment leads to increased levels of MIC27, MIC26 and MIC25 in WT cells. Loss of MIC26 is accompanied by decreased MIC10 in normoglycemia.

(C, D and E) Electron microscopy data including quantification of cristae number per unit length (µm) per mitochondrial section (C) as well as crista junctions per cristae per mitochondrial section (D), along with representative images (E) from HepG2 WT and *MIC26* KO cells cultured in normo- and hyperglycemia (N = 2). Loss of MIC26 led to decreased cristae number and crista junctions independent of normo- and hyperglycemia. Red arrows in lower row indicate outer membrane (OM) or cristae. Scale bar represents 500 nm.

Data are represented as mean ± SEM (B, C and D). Statistical analysis was performed using one-way ANOVA with **P* < 0.05, ***P* < 0.01, ****P* < 0.001, *****P* < 0.0001. N represents the number of biological replicates.

Figure 2. Hyperglycemia confers antagonistic regulation of lipid and cholesterol pathways, in *MIC26* KO vs WT cells, compared to normoglycemia

(A and B) Hierarchical Treemap clustering of significant gene ontology (GO) enriched terms of biological processes upregulated in normoglycemic *MIC26* KO (A) and downregulated in hyperglycemic *MIC26* KO (B) compared to respective WT. Each rectangle represents one BioProcess pathway. Every colour represents clustering of different sub-pathways to pathway families. The rectangle sizes indicate the *P*-value of the respective GO term.

(C and D) WikiPathway enrichment using EnrichR analysis of differentially expressed genes (C) upregulated in normoglycemic *MIC26* KO and (D) downregulated in hyperglycemic *MIC26* KO cells compared to respective WT. Arrows indicate antagonistically regulated metabolic pathways including glycolysis, cholesterol biosynthesis, fatty acid synthesis and oxidation.

Differentially expressed genes were considered statistically significant with a cut-off fold change of ±1.5 and Bonferroni correction $P \leq 0.05$. Treemap representation of GO enrichment was plotted with statistically significant pathways with cut-off $P \leq 0.05$.

Figure 3. MIC26 maintains the glycolytic function

(A – C) Peptide abundances of enzymes involved in glycolysis pathway curated from proteomics data (N = 5).

(D) Steady state metabolomics (GC-MS) data reveals increased cellular glucose accumulation upon *MIC26* deletion in hyperglycemia (N = 3-4).

(E and F) Representative glycolysis stress test seahorse assay analysis, with sequential injection of glucose, oligomycin and 2-deoxyglucose, reveals a tendency towards increased glycolysis upon *MIC26* deletion (E) (n = 23). Quantification from various biological replicates shows a significant increase of cellular glycolytic reserve in normoglycemic, but not in hyperglycemic conditions (F) (N = 3).

(G) Cellular glucose uptake was measured using Glucose uptake Glo assay normalized to WT-N. *MIC26* deletion leads to an increased glucose uptake upon normoglycemia (N = 3).

(H – J) Peptide abundances of transporters involved in glucose uptake namely GLUT3 (H), GLUT1 (I) and GLUT2 (J) curated from proteomics data (N = 5).

(K and L) Steady state metabolomics (GC-MS) shows unaltered cellular pyruvate (K) and lactate (L) levels in *MIC26* KO cell lines in normoglycemia but decreased levels upon *MIC26* deletion in hyperglycemia (N = 3-4).

(M) *MIC26* deletion increases glycerol-3-phosphate amount in normoglycemia with an antagonistic effect in hyperglycemia compared to the respective WT (N = 3-4).

Data are represented as mean ± SEM (A-M). Statistical analysis was performed using one-way ANOVA with $*P < 0.05$, $**P < 0.01$, $***P < 0.001$, $****P < 0.0001$. N represents the number of biological replicates and n the number of technical replicates.

Figure 4. The loss of MIC26 leads to metabolic rewiring of cellular lipid metabolism via CPT1A and dysregulation of fatty acid synthesis

(A – D) Analysis of lipid droplet formation in WT and *MIC26* KO cells cultured in normo- and hyperglycemia either in standard growth condition (CTRL) or upon palmitate stimulation (100 µM, 24 h). Representative confocal images of lipid droplets stained using BODIPY 493/503 are shown (A). Quantification shows number of lipid droplets normalized to the total cell area [μm^2] (B) and mean fluorescence intensity per cell normalized to mean intensity of WT-N in all biological replicates (C). *MIC26* deletion leads to a nutritional-independent increase in lipid droplet number. However, an opposing effect, leading to increase or decrease of mean fluorescence intensity of lipid droplets, upon comparison of *MIC26* KO to WT was

729 observed in normo- and hyperglycemia respectively, with a pronounced effect upon feeding
730 palmitate (N = 3). Scale bar represents 5 µm.

731 (E) Heat map representing the abundance of steady state FFA species in WT and *MIC26* KO
732 cells cultured in normo- and hyperglycemia. 11 out of 19 of the FFA species represent an
733 antagonistic behavior upon comparing *MIC26* KO to WT in normo- (increase) and
734 hyperglycemia (decrease) (N = 3-4).

735 (F and G) Western blot analysis (F), along with respective quantification (G) of WT and
736 *MIC26* KO cells cultured in normo- and hyperglycemia, show a reduction of CPT1A in WT-H,
737 *MIC26* KO-N and *MIC26* KO-H compared to WT-N (N = 3).

738 (H – J) Mitochondrial fatty acid oxidation analyzed using Seahorse XF analyzer shows a
739 decreased palmitate-induced basal respiration (H) and spare respiratory capacity (I) and a
740 nonsignificant reduction of etomoxir-sensitive OCR decrease upon comparing *MIC26* KO to
741 WT in normoglycemia (N = 3).

742 Data are represented as mean ± SEM (B-C and G-J). Statistical analysis was performed using
743 one-way ANOVA with **P* < 0.05, ***P* < 0.01, ****P* < 0.001, *****P* < 0.0001. N represents the
744 number of biological replicates.

745 **Figure 5. *MIC26* deletion leads to hyperglycemia-induced decrease in TCA cycle**
746 **intermediates**

747 (A) Representation of the relative amounts (GC-MS) of TCA cycle metabolites and associated
748 precursors at steady state in WT and *MIC26* KO cells cultured in normo- and hyperglycemia.
749 All the TCA cycle metabolites with the exception of α-ketoglutarate showed a decreasing trend
750 upon *MIC26* KO when compared to WT in hyperglycemia (N = 3-4).

751 (B and C) Mitochondrial pyruvate carrier 1 (MPC1) (B), but not MPC2 (C), is significantly
752 decreased in *MIC26* KO-N compared to WT-N, as revealed by peptide abundances from
753 proteomics data (N = 5).

754 (D) Mitochondrial glucose / pyruvate dependency analysis, using Seahorse XF analyzer mito
755 fuel flex test assay, reveals a decreased mitochondrial respiratory dependency of *MIC26* KO
756 on glucose / pyruvate in normoglycemia (N = 3).

757 Data are represented as mean ± SEM (A-C). Statistical analysis was performed using one-
758 way ANOVA with **P* < 0.05, ***P* < 0.01, ****P* < 0.001, *****P* < 0.0001. N represents the number
759 of biological replicates.

Figure 6. Aberrant glutamine metabolism is observed in *MIC26* KOs independent of nutritional status

(A) Metabolomics analysis (GC-MS) shows that glutamine levels were strongly increased in *MIC26* KO cells cultured in both normo- and hyperglycemia at steady state compared to respective WT (N = 3-4).

(B) Quantification of mitochondrial glutamine dependency and capacity analysis, using Seahorse XF analyzer mito fuel flex test assay, shows a diminished mitochondrial respiratory dependency on glutamine. A nonsignificant mitochondrial respiratory decreased capacity of *MIC26* KO cells was observed compared to respective WT conditions (N = 3).

(C and D) Western Blot analysis (C) along with respective quantification (D) show reduced amounts of the glutamate aspartate antiporter SLC25A12 (ARALAR / AGC1), present in mitochondria, in *MIC26* KO cell lines compared to respective WT cells (N = 3).

(E – J) Representation of labeled (m+1 - m+6) and unlabeled (m+0) species of glutamate (GC-MS) (E), and TCA cycle metabolites (AEC-MS) α-KG (F), citrate (G), succinate (H), fumarate (I) and malate (J), from glutamine tracing experiments after labelling for 0.5 h and 6 h (N = 4).

(K – O) Conversion rates from different TCA cycle reactions calculated using the ratio of highest labeled species abundances for the conversions of glutamate to α-KG (K), α-KG to citrate (L), α-KG to succinate (M), succinate to fumarate (N) and α-KG to malate (N = 4).

Data are represented as mean ± SEM (A-B and D-O). Statistical analysis was performed using one-way ANOVA with $*P < 0.05$, $**P < 0.01$, $***P < 0.001$, $****P < 0.0001$. N represents the number of biological replicates.

Figure 7. MIC26 regulates mitochondrial bioenergetics by restricting the ETC activity and OXPHOS (super-)complex formation

(A and B) Representative pseudocolour rainbow LUT intensities from confocal images of WT and *MIC26* KO HepG2 cells stained with TMRM show a reduction in $\Delta\Psi_m$ upon *MIC26* deletion in both normoglycemia and hyperglycemia when compared to respective WT cells (A). Quantification represents mean TMRM fluorescence intensity per cell normalized to mean intensity of WT-N in all biological replicates (B) (N = 3). Scale bar represents 5 µm.

(C and D) Representative confocal images of mitochondrial morphology, visualized by MitoTracker green staining (C), show that loss of MIC26 shifts mitochondrial morphology from tubular mitochondrial network in WT normoglycemic conditions to fragmented phenotype irrespective of supplemented glucose amount (D) (N = 3). Scale bar represents 5 µm.

(E and F) Representative mitochondrial stress test with Seahorse XF analyzer, with sequential injection of oligomycin, FCCP and rotenone/antimycin (E) (n = 19-23). Quantification from various biological replicates shows a significant increase of basal respiration in *MIC26* KOs cultured in both normo- and hyperglycemia (F) (N = 3).

(G) Blue native (respective left panel) and clear native (respective right panel) PAGE analysis reveals an overall increase of OXPHOS complex formation (for CI, CIII, CIV and CV, green arrows) as well as corresponding increased in-gel activity of supercomplexes, and complex III_2IV (blue arrows) upon *MIC26* deletion. CV shows no in-gel activity alterations while a decreased in-gel activity of F_1 occurs upon loss of MIC26. Native PAGEs were performed in three biological replicates and representative gels are shown.

(H) Model representing the antagonistic regulation of metabolic pathways encompassing glucose usage, lipid droplet formation, cholesterol synthesis, as well as decrease in TCA cycle metabolites in MIC26 deficient HepG2 cells dependent on nutritional conditions compared to respective WT cells. An increase of glutamine levels as well as assembly of various OXPHOS complexes is observed in *MIC26* KOs independent of the nutritional status. Arrows indicate respective up (red) or downregulated (blue) protein/metabolite or activity levels, respectively. In the model, left panel indicates normoglycemic while the right panel represents the hyperglycemic conditions.

Data are represented as mean ± SEM (B and D-F). Statistical analysis was performed using one-way ANOVA with $*P < 0.05$, $**P < 0.01$, $***P < 0.001$, $****P < 0.0001$. N represents the number of biological replicates and n the number of technical replicates.

Supplementary Information

S1 Figure. MIC26 loss leads to an opposing regulation of cholesterol biosynthesis pathway upon nutritional stimulation

(A) Overview of transcriptomics clustering analysis showing upregulated (red) and downregulated (blue) transcripts (without fold change or significance cut-offs). All sample replicates are represented (N = 4).

(B and C) Proteomics data represented by WikPathway enrichment using EnrichR analysis comparing pathways upregulated in normoglycemia (B) and downregulated in hyperglycemia (C) upon *MIC26* deletion compared to respective WT (N = 5). Arrows indicate increased levels of proteins participating in cholesterol synthesis and glycolysis pathways similar to those observed with transcriptomics data (Fig 2C and D). Differentially expressed proteins were considered statistically significant with a cut-off value of fold change of ±1.5 and Bonferroni correction $P \leq 0.05$.

S2 Figure. Loss of MIC26 leads to an opposing regulation of cholesterol biosynthesis pathway in normoglycemia and hyperglycemia

(A and B) The transcripts of various enzymes regulating cholesterol synthesis are represented using Cytoscape software comparing log2FC data of *MIC26* KO and WT cell lines in normo- (A) and hyperglycemia (B) (N = 4). In *MIC26* KO cell lines, normoglycemia strongly increases transcripts of enzymes participating in cholesterol biosynthesis while an opposing effect is observed in hyperglycemia.

(C – N) Peptide abundances of various enzymes participating in cholesterol biosynthesis curated from proteomics data (N = 5).

(O) Metabolomics data reveals that cholesterol levels are exclusively decreased in *MIC26* KO at steady state in hyperglycemia compared to WT but not in normoglycemia (N = 3-4).

Data are represented as mean ± SEM (C-O). Statistical analysis was performed using one-way ANOVA with $*P < 0.05$, $**P < 0.01$, $***P < 0.001$, $****P < 0.0001$. N represents the number of biological replicates.

S3 Figure. *MIC26* deletion causes opposing transcriptional regulation of genes involved in glycolysis

(A and B) The transcripts of various enzymes participating in glycolysis are represented using Cytoscape software comparing log2FC data of *MIC26* KO and WT cell lines in normo- (A) and hyperglycemia (B) (N = 4).

(C and D) Glycolysis stress test Seahorse assay reveals a nonsignificant tendency towards increased glycolysis and glycolytic capacity upon *MIC26* KO in normoglycemic, but not in hyperglycemic conditions (N = 3).

Data are represented as mean ± SEM (C and D). Statistical analysis was performed using one-way ANOVA with **P* < 0.05, ***P* < 0.01, ****P* < 0.001, *****P* < 0.0001. N represents the number of biological replicates.

S4 Figure. Majority of free fatty acid species are antagonistically regulated upon *MIC26* deletion in normoglycemia and hyperglycemia when compared to respective to WT cells

Detailed representation of abundances of various free fatty acid species in WT and *MIC26* KO cell lines cultured in normo- and hyperglycemia (N = 3-4).

Data are represented as mean ± SEM. Statistical analysis was performed using one-way ANOVA with **P* < 0.05, ***P* < 0.01, ****P* < 0.001, *****P* < 0.0001. N represents the number of biological replicates.

S5 Figure. *MIC26* deletion leads to alteration of key enzymes regulating lipid metabolism

(A and B) The transcripts of mitochondrial long-chain fatty acid importer CPT1A are strongly decreased in WT-H and *MIC26* KO conditions, compared to WT-N, as shown from transcriptomics data (A) (N = 4) and quantitative PCR (B) (N = 3) analysis.

(C and D) Representative fatty acid oxidation assay analyzed using oxygen consumption rates of WT and *MIC26* KO HepG2 cells cultured in normoglycemia (C) and hyperglycemia (D) upon feeding either with BSA or palmitate (n = 8-12).

(E and F) Mitochondrial citrate malate exchanger (SLC25A1) is significantly increased upon *MIC26* deletion in normoglycemia compared to WT as detected using proteomics (E) (N = 5) and transcriptomics (F) (N = 4) data.

(G – M) Transcripts and available peptide abundances of key genes involved in lipid metabolism curated from transcriptomics (N = 4) and proteomics data (N = 5). Under normoglycemic conditions, loss of MIC26 increases the expression of ATP citrate lyase (G), acetyl-CoA carboxylase 1 (H and I), fatty acid synthase (J and K) and acetyl-CoA desaturase (L and M).

(N) Peptide abundances of glycerol kinase is increased in WT-H compared to WT-N but similar in *MIC26* KO-N and *MIC26* KO-H (N = 5).

Data are represented as mean ± SEM (A-N). Statistical analysis was performed using one-way ANOVA with **P* < 0.05, ***P* < 0.01, ****P* < 0.001, *****P* < 0.0001. N represents the number of biological replicates and n the number of technical replicates.

878 **S6 Figure. TCA cycle enzymes are altered upon *MIC26* knockout**

879 (A – K) Representation of peptide abundances of various mitochondrial TCA cycle enzymes
880 curated from proteomics data (N = 5).

881 (L – N) Peptide abundances of cytosolic enzymes involved in metabolite conversion (N = 5).

882 Data are represented as mean ± SEM (A-N). Statistical analysis was performed using one-
883 way ANOVA with **P* < 0.05, ***P* < 0.01, ****P* < 0.001, *****P* < 0.0001. N represents the number
884 of biological replicates.

885 **S7 Figure. Mitochondrial glutamine and glutamate carriers are downregulated upon loss**
886 **of MIC26**

887 (A) Transcripts of mitochondrial glutamate aspartate antiporter *SLC25A12* (A) are decreased
888 upon *MIC26* deletion in normo- and hyperglycemia (N = 4).

889 (B and C) Transcripts (B) (N = 4) and peptide abundances (C) (N = 5) of cellular and
890 mitochondrial glutamine importer SLC1A5 are significantly decreased upon *MIC26* deletion in
891 both normo- and hyperglycemia in relation to respective WT cells.

892 (D) Peptide abundances of glutaminase (GLS) are unaltered upon loss of MIC26 compared to
893 respective WT conditions.

894 (E) MIC26 interactome, based cumulatively on BioGRID, NeXtProt and IntAct databases,
895 generated with Cytoscape software. From this study, downregulated transcripts comparing
896 *MIC26* KO and WT in normoglycemic condition are highlighted in blue while upregulated
897 transcripts are highlighted in red.

898 Data are represented as mean ± SEM (A-D). Statistical analysis was performed using one-
899 way ANOVA with **P* < 0.05, ***P* < 0.01, ****P* < 0.001, *****P* < 0.0001. N represents the number
900 of biological replicates.

901 **S8 Figure. MIC26 maintains mitochondrial morphology and bioenergetics**

902 (A and B) Western Blots (A) and quantification (B) show a decrease of key mitochondrial fusion
903 mediator MFN1 in *MIC26* KO cells while MFN2 was unchanged. Mitochondrial fission mediator
904 DRP1 is decreased in *MIC26* KO-H compared to WT-H. OPA1 processing shows no significant
905 changes upon *MIC26* deletion and nutritional status (N = 3-4).

906 (C and D) ATP production (C) and spare respiratory capacity (D) determined by mito stress
907 test using Seahorse XF analyzer. Deletion of *MIC26* caused increased ATP production and
908 decreased metabolic flexibility (indicated by SRC) in normoglycemia (N = 3).

Data are represented as mean ± SEM (B-D). Statistical analysis was performed using one-way ANOVA with **P* < 0.05, ***P* < 0.01, ****P* < 0.001, *****P* < 0.0001. N represents the number of biological replicates.

S9 Figure. *MIC26* deletion induces alterations of SLC25 mitochondrial carrier protein family expression and induces growth defects

(A and B) Heat map overview from mean z-score of transcripts (A) (N = 4) and peptide abundances (B) (N = 5) of mitochondrial transporters belonging to SLC25 family.

(C) Transcript abundances of *SREBP2* (C) of WT and *MIC26* KO cells grown in normo- and hyperglycemia (N = 4).

(D – F) Proliferation of respective cell lines after 24 h (C), 48 h (D) and 72 h (E) determined using SRB assay normalized to WT-N (N = 4).

(G – J) Transcripts (N = 4) and peptide abundances (N = 5) of NUBPL (G and H) and DHRS2 (I and J) are respectively shown.

Data are represented as mean ± SEM (C-J). Statistical analysis was performed using one-way ANOVA with **P* < 0.05, ***P* < 0.01, ****P* < 0.001, *****P* < 0.0001. N represents the number of biological replicates.

Supplementary Tables

Supplementary Table S1

Raw data of targeted metabolomics at steady state including polar metabolites (sheet 1) and free fatty acids (FFAs) (sheet 2) indicating corresponding cell line, group, replicate, cell number, multiplication factor, measured compound name, internal standard (ISTD) name, measured total compound response, ISTD response, ratio of total compound response to ISTD response, relative response and technical procedure data. Relative response is calculated from compound response normalized to ISTD response and cell number multiplied by multiplication factor and used for data representation.

Supplementary Table S2

Raw data of targeted metabolomics from tracing experiments including AEC-MS (sheet 1) and GC-MS (sheet 2) data including cell line group analysed, compound isotopologue species, corrected ratio to naturally occurring isotopologues timepoint and technical information.

Supplementary Table S3

Proteomics raw data analysis including gene description, mean abundance ratio, adjusted *P*-value, mean abundances per group, total measured abundances of all replicate samples and technical data are represented in sheet 1. Filtered significantly (adj. *P*-value ≤ 0.05) altered peptide abundances with log2FC > ±1.5 for *MIC26* KO-N vs WT-N or *MIC26* KO-H and WT-H are represented in sheet 2 and 3 respectively. Detected peptides with less than three out of five hits in both of the compared groups were not considered.

Supplementary Table S4

Transcriptomics raw data analysis with sheet 1 representing raw data for all sample replicates, including gene description. Calculated log2FC, FC, *P*-Value, FDR adjusted *P*-Value and Bonferroni correction, as well as raw data from total reads, RPKM, TPM and CPM. DEGs filtered by Bonferroni correction ≤ 0.05 and log2FC > ±1.5 for *MIC26* KO-N vs WT-N and *MIC26* KO-H vs WT-H are represented in sheet 2 and 3 respectively. Sheet 4 is showing an overview of number of differentially expressed genes including respective cut-offs.

952 ## Materials and Methods

953 ### Key resources table

954

REAGENT or RESOURCE	SOURCE	IDENTIFIER
Antibodies		
MIC26	Invitrogen	Cat# PA5-116197 RRID: AB_2900831
MIC27	Sigma-Aldrich	Cat# HPA000612 RRID: AB_1078594
MIC10	Abcam	Cat# ab84969 RRID: AB_1924831
MIC13	Pineda	custom made
MIC25	Protein tech	Cat# 20639-1-AP RRID: AB_1069767
MIC60	Abcam	Cat# ab110329 RRID: AB_10859613
MIC19	Protein tech	Cat# 25625-1-AP RRID: AB_2687533
MFN1	Santa Cruz Biotechnologies	Cat# sc-50330 RRID: AB_2250540
MFN2	Abcam	Cat# ab50838 RRID: AB_881507
OPA1	Pineda	custom made
DRP1	Cell Signaling Technologies	Cat# 5391 RRID: AB_11178938
β-Actin	Invitrogen	Cat# MA1-744 RRID: AB_2223496
HSP60	Sigma Aldrich	Cat# SAB4501464 RRID: AB_10746162
CPT1A	Proteintech	Cat# 15184-1-AP RRID: AB_2084676
Goat IgG anti-Mouse IgG	Abcam	Cat# ab97023 RRID: AB_10679675
Goat IgG anti-Rabbit IgG	Dianova	Cat# SBA-4050-05 RRID: AB_2795955
NDUFB4	Abcam	Cat# ab110243 RRID: AB_10890994
UQCRC2	Abcam	Cat# ab14745 RRID: AB_2213640
COXIV	Abcam	Cat# ab16056 RRID: AB_443304
ATP5A	Abcam	Cat# ab14748 RRID: AB_301447
SLC25A12	Santa Cruz Biotechnologies	Cat# sc-271056 RRID: AB10608837
Bacterial and virus strains		
N/A		
Biological samples		
N/A		
Chemicals, peptides, and recombinant proteins		
Etomoxir	Sigma Aldrich	Cat# E1905; CAS: 828934-41-4
3,3'-diaminobenzidine tetrahydrochloride	Sigma Aldrich	Cat# 32750; CAS: 868272-85-9

horse heart cytochrome c	Thermo Scientific	Cat# 147530010; CAS: 9007-43-6
NADH	Biomol	Cat# 16132.1 CAS: 606-68-8
Nitroblue tetrazolium chloride	Biomol	Cat# 06428.1 CAS: 298-83-9
Adenosine 5' triphosphate (ATP)	Sigma Aldrich	Cat# A7699 CAS: 34369-07-8
Lead (II) nitrate / $Pb(NO_3)_2$	Sigma Aldrich	Cat# 1073980100 CAS: 10099-74-8
MitoTracker Green	Invitrogen	Cat# M7514 CAS: 201860-17-5
TMRM	Invitrogen	Cat# T668
BODIPY 493/503	Cayman Chemicals	Cat# Cay25892-5 CAS: 121207-31-6
Poly-D-lysine	Sigma Aldrich	Cat# P7886 CAS: 2796-99-4
Stable Glutamine	PAN-Biotech	Cat# P04-82100
PenStrep	PAN-Biotech	Cat# P06-07100
BSA	Biomol	Cat#Cay29556
Palmitate-BSA	Biomol	Cat#Cay29558
L-Carnitine	Sigma Aldrich	Cat#C0283 CAS: 645-46-1
Ribitol	Sigma Aldrich	Cat# A5502
L-Glutamine-13C5-15N2	Sigma Aldrich	Cat# 607983 CAS: 607983
Critical commercial assays		
Glycolysis Stress Test	Agilent Technologies	Cat# 103020-100
Mito Stress Test	Agilent Technologies	Cat# 103015-100
Mito Fuel Flex Test	Agilent Technologies	Cat# 103260-100
Glucose Uptake Glo	Promega	Cat# J1241
GoScript Reverse Transcription Mix, Oligo(dT)	Promega	Cat# A2791
GoTaq qPCR Master Mix	Promega	Cat# A6002
RNeasy Mini Kit	Qiagen	Cat# 74106
Deposited data		
MIC26 interactome	N/A	Nextprot, Intact BioGrid
Experimental models: Cell lines		
HepG2	Sigma Aldrich	Cat# 85011430 RRID: CVCL_0027
Experimental models: Organisms/strains		
N/A		
Oligonucleotides		
Primer CPT1A Forward GATCCTGGACAATACCTCGGAG	This paper	N/A
Primer CPT1A Reverse CTCCACAGCATCAAGAGACTGC	This paper	N/A
Primer HPRT1 Forward 5'-CATTATGCTGAGGATTTGGAAAGG-3'	This paper	N/A
Primer HPRT1 Reverse 5'-CTTGAGCACACAGAGGGCTACA-3'	This paper	N/A
Recombinant DNA		
Double Nickase Plasmid MIC26 KO	Santa Cruz Biotechnology	Cat# sc-413137-NIC
Software and algorithms		

Prism	GraphPad	RRID: SCR_002798
Seahorse Wave	Agilent Technologies	RRID: SCR_014526
R Studio	Posit PBC	RRID: SCR_000432
Cytoscape	Cytoscape Consortium	RRID: SCR_003032
Volocity 3D Image Analysis Software	Perkin Elmer	RRID: SCR_002668
MassHunter Qualitative	Agilent Technologies	RRID: SCR_015040
BCL Convert Tool	Illumina	N/A
CLC Genomics Workbench	Qiagen	RRID: SCR_017396
CLC Gene Set Enrichment Test	Qiagen	RRID: SCR_003199
Proteome Discoverer	Thermo Fischer Scientific	RRID: SCR_014477
Other		
DMEM 1 g/L glucose	PAN-Biotech	Cat# P04-01500
DMEM 4.5 g/L glucose	PAN-Biotech	Cat# P04-82100
FBS	Capricorn Scientific	Cat# FBS-11A

Cell culture and treatment conditions

HepG2 cells were cultured in 1 g/L glucose DMEM (PAN-Biotech) supplemented with 10% FBS (Capricorn Scientific), 2 mM stable glutamine (PAN-Biotech) and penstrep (PAN-Biotech, penicillin 100 U/mL and 100 µg/mL streptomycin). Cells were grown at 37°C supplied with 5% CO_2. *MIC26* HepG2 KO cells were generated using the double nickase method as described before (Lubeck *et al.*, 2023). Cells cultured in standard growth media were divided equally into two cell culture flasks and grown in either 1 g/L glucose DMEM (normoglycemia) or 4.5 g/L glucose DMEM (hyperglycemia) (PAN-Biotech) supplemented with above-mentioned reagents. Cells were cultured in normoglycemia and hyperglycemia for a prolonged duration of three weeks. During the three weeks, cell splitting was carried out twice a week with the corresponding media.

SDS gel electrophoresis and Western Blotting

After three washes with 2 mL DPBS (PAN-Biotech), the cells were harvested by scraping and resuspending in an appropriate volume of RIPA buffer (150 mM NaCl, 0.1 % SDS, 0.05 % Sodium deoxycholate, 1 % Triton-X-100, 1 mM EDTA, 1mM Tris, pH 7.4, 1x protease inhibitor (Sigma-Aldrich), PhosSTOP (Roche). Protein concentration was determined using DC™ protein assay Kit (BIO-RAD, 5000116). SDS samples were prepared with Laemmli buffer and heated for 5 min at 95°C. Depending on the proteins investigated, a variety of SDS electrophoresis gels (8%, 10%, 12% or 15%) were used for running and separating protein samples. Subsequently, proteins were transferred onto nitrocellulose membranes and stained using Ponceau S (Sigma Aldrich). After destaining, nitrocellulose membranes were blocked with 5 % milk in 1x TBS-T for 1 h, washed three times with TBS-T and probed at 4°C overnight with the following primary antibodies: MIC26 (Invitrogen, 1:1000), MIC27 (Sigma-Aldrich, 1:2000), MIC10 (Abcam, 1:1000), MIC13 (Pineda custom-made, 1:1000), MIC25 (Proteintech, 1:1000), MIC60 (Abcam, 1:1000), MIC19 (Proteintech, 1:1000), MFN1 (Santa Cruz

Biotechnologies, 1:1000), MFN2 (Abcam, 1:1000), OPA1 (Pineda custom-made, 1:1000), DRP1 (Cell Signaling Technology, 1:1000), β-Actin (Invitrogen, 1:2000), HSP60 (Sigma-Aldrich, 1:2000) and CPT1A (Proteintech, 1:1000). Goat IgG anti-Mouse IgG (Abcam, 1:10000) and Goat IgG anti-Rabbit IgG (Dianova, 1:10000) conjugated to HRP were used as secondary antibodies. The chemiluminescent signals were obtained using Signal Fire ECL reagent (Cell Signaling Technology) and VILBER LOURMAT Fusion SL equipment (Peqlab).

Blue Native and Clear Native PAGE

5 x 10^6 HepG2 cells were seeded onto 15 cm dishes and cell culture medium was replaced every two days until 80 % confluency was reached. Cells were washed three times with cold PBS, scraped and pelleted at 900 g, 4°C for 5 min. Cell pellets were resuspended in 1 mL lysis buffer (210 mM mannitol, 70 mM sucrose, 1 mM EDTA, 20 mM HEPES, 0,1 % BSA, 1x protease inhibitor) and incubated on ice for 10 min. Mitochondria were isolated by repetitive strokes of mechanical disruption using a 20G canula and sequential centrifugation steps at 1000 x g, 4°C for 10 min to remove cell debris and 10,000 x g, 4°C for 15 min to pellet mitochondria. Mitochondrial pellet was resuspended in BSA-free lysis buffer and protein concentration was determined using DC Protein Assay Kit.

For blue native page, 100 µg of mitochondria was solubilized for 1 h on ice using 2.5 g/g of digitonin to protein ratio. The samples were centrifuged for 20 min at 20,000 x g and 4°C to pellet insolubilized material. The supernatants were supplemented with loading buffer (50% glycerol, 8 g/g Coomassie to detergent ratio) and immediately loaded onto 3-13% gradient gel. Complexes were separated at 150 V, 15 mA for 16 h. Thereafter, protein complexes were transferred onto PVDF membrane and blocked overnight with 5 % milk in TBS-T at 4°C. For identification of relevant protein complexes, the membranes were decorated with the following antibodies: NDUFB4 (Abcam, 1:1000), UQCRC2 (Abcam, 1:1000), COXIV (Abcam, 1:1000) ATP5A (Abcam, 1:1000) Goat IgG anti-Mouse IgG (Abcam, 1:10000) and Goat IgG anti-Rabbit IgG (Dianova, 1:10000) conjugated to HRP. The chemiluminescent signals were obtained using Pierce™ SuperSignal™ West Pico PLUS chemiluminescent substrate reagent (Thermo Scientific) and VILBER LOURMAT Fusion SL equipment (Peqlab).
For clear native gels, 300 µg mitochondria was solubilized on ice for 1 h with 2.5 g/g digitonin to protein ratio. The samples were centrifuged for 20 min at 20,000 x g and 4°C to pellet insolubilized material. The supernatants were supplemented with loading buffer (50% glycerol, 0.01 % Ponceau S) and immediately loaded onto 3-13% gradient gels. Complexes were separated at 150 V, 15 mA for 16 h. To assess complex in-gel activity, the gel slices were incubated in respective buffer solutions for several hours at room temperature. For complex I activity, the gel was incubated in 5 mM Tris-HCl (pH 7.4), 0.1 mg/mL NADH and 2.5 mg/mL nitro blue tetrazolium chloride (NBT). For complex III, the gel was incubated in 50 mM sodium

phosphate buffer (pH 7.2), 0.1 % 3,3'-diaminobenzidine tetrahydrochloride (DAB). To assess complex IV activity, the gel was incubated in 50 mM sodium phosphate buffer (pH 7.2), 0.05 % DAB and 50 µM horse heart cytochrome *c* and for complex V, the gel was incubated in 35 mM Tris-base, 270 mM glycine, 14 mM $MgSO_4$, 0.2 % (w/v) $Pb(NO_3)_2$ and 8 mM ATP.

RNA isolation and quantification

Total RNA was extracted from cell pellets using RNeasy Mini Kit (Qiagen) according to the manufacturer's protocol. RNA quality and quantity were assessed using BioSpectrometer (Eppendorf). cDNA synthesis from 5 µg RNA was performed using the GoScript™ Reverse Transcriptase Kit (Promega). Next, quantitative real-time PCR was performed in Rotor Gene 6000 (Corbett Research) using GoTagR qPCR Master Mix (Promega) according to manufacturer's instructions with the following primers:

1. *CPT1A*:
   Forward: 5'- GATCCTGGACAATACCTCGGAGC-3'
   Reverse: 5'- CTCCACAGCATCAAGAGACTGC-3'
2. *HPRT1* (Housekeeping gene):
   Forward: 5'-CATTATGCTGAGGATTTGGAAAGG-3'
   Reverse: 5'-CTTGAGCACACAGAGGGCTACA-3'

C_t values were normalized to housekeeping gene *HPRT1* followed by normalization of ΔC_t values to average ΔC_t of WT-N control group.

Transcriptomics

Cells were seeded in quadruplicates onto 10 cm dishes in corresponding cell culture media and medium was replaced every two days until 80 % cell confluency was obtained. For preparation of RNA, cells were washed three times with cold PBS and subsequently scraped and pelleted. RNA isolation from cell pellets was performed using RNeasy Mini Kit (Qiagen) including DNase digestion according to the manufacturer's protocol. Sample concentration was determined and 1 µg RNA was aliquoted for transcriptomics analysis. Total RNA samples were quantified (Qubit RNA HS Assay, Thermo Fisher Scientific, MA, USA) and quality measured by capillary electrophoresis using the Fragment Analyzer and the 'Total RNA Standard Sensitivity Assay' (Agilent Technologies, Inc. Santa Clara, CA, USA). All samples in this study showed RNA Quality Numbers (RQN) with a mean of 10.0. The library preparation was performed according to the manufacturer's protocol using the 'VAHTS™ Stranded mRNA-Seq Library Prep Kit' for Illumina®. Briefly, 700 ng total RNA were used as input for mRNA capturing, fragmentation, the synthesis of cDNA, adapter ligation and library amplification. Bead purified libraries were normalized and finally sequenced on the NextSeq2000 system (Illumina Inc. San Diego, CA, USA) with a read setup of 1x100 bp. The BCL Convert Tool

(version 3.8.4) was used to convert the bcl files to fastq files as well for adapter trimming and demultiplexing.

Data analyses on fastq files were conducted with CLC Genomics Workbench (version 22.0.2, Qiagen, Venlo, Netherlands). The reads of all probes were adapter trimmed (Illumina TruSeq) and quality trimmed (using the default parameters: bases below Q13 were trimmed from the end of the reads, ambiguous nucleotides maximal 2). Mapping was done against the *Homo sapiens* (hg38; GRCh38.107) (July 20, 2022) genome sequence. After grouping of samples (four biological replicates) according to their respective experimental conditions, the statistical differential expression was determined using the CLC differential expression for RNA-Seq tool (version 2.6, Qiagen, Venlo, Netherlands). The resulting *P* values were corrected for multiple testing by FDR and Bonferroni-correction. A *P* value of ≤0.05 was considered significant. The CLC gene set enrichment test (version 1.2, Qiagen, Venlo, Netherlands) was done with default parameters and based on the GO term 'biological process' (*H. sapiens*; May 01, 2021).

The data discussed in this publication have been deposited in NCBI's Gene Expression Omnibus (Edgar *et al*, 2002) and are accessible through GEO Series accession number GSE248848.

Proteomics

Cells were seeded in quintuplicates onto 10 cm dishes in corresponding cell culture media and medium was replaced every two days until 80 % cell confluency was obtained. Cells were washed four times with PBS, scraped and pelleted in a pre-weighed Eppendorf tube. After complete removal of PBS, cells were immediately frozen in liquid nitrogen and sample weight was determined for normalization. Proteins were extracted from frozen cell pellets as described elsewhere (Poschmann *et al*, 2014). Briefly, cells were lysed and homogenized in urea buffer with a TissueLyser (Qiagen) and supernatants were collected after centrifugation for 15 min at 14,000 x g and 4°C. Protein concentration was determined by means of Pierce 660 nm protein assay (Thermo Fischer Scientific). For LC-MS analysis, a modified magnetic bead-based sample preparation protocol according to Hughes and colleagues was applied (Hughes *et al*, 2019). Briefly, 20 µg total protein per sample was reduced by adding 10 µL 100 mM DTT (dithiothreitol) and shaking for 20 min at 56°C and 1000 rpm, followed by alkylation with the addition of 13 µL 300 mM IAA and incubation for 15 min in the dark. A 20 µg/µL bead stock of 1:1 Sera-Mag SpeedBeads was freshly prepared and 10 µL was added to each sample. Afterwards, 84 µL ethanol was added and incubated for 15 min at 24°C. After three rinsing steps with 80% EtOH and one rinsing step with 100% ACN, beads were resuspended in 50 mM TEAB buffer and digested with final 1:50 trypsin at 37°C and 1,000 rpm overnight. Extra-digestion was carried out by adding trypsin (final 1:50) and shaking at 37°C and 1000 rpm for

4 h. The supernatants were collected and 500 ng of each sample digest was subjected to LC-MS.

For the LC-MS acquisition, an Orbitrap Fusion Lumos Tribrid Mass Spectrometer (Thermo Fisher Scientific) coupled to an Ultimate 3000 Rapid Separation liquid chromatography system (Thermo Fisher Scientific) equipped with an Acclaim PepMap 100 C18 column (75 µm inner diameter, 25 cm length, 2 µm particle size from Thermo Fisher Scientific) as separation column and an Acclaim PepMap 100 C18 column (75 µm inner diameter, 2 cm length, 3 µm particle size from Thermo Fisher Scientific) as trap column was used. A LC-gradient of 180 min was applied. Survey scans were carried out over a mass range from 200-2,000 m/z at a resolution of 120,000. The target value for the automatic gain control was 250,000 and the maximum fill time 60 ms. Within a cycle time of 2 s, the most intense peptide ions (excluding singly charged ions) were selected for fragmentation. Peptide fragments were analysed in the ion trap using a maximal fill time of 50 ms and automatic gain control target value of 10,000 operating in rapid mode. Already fragmented ions were excluded for fragmentation for 60 seconds.

Data analysis was performed with Proteome Discoverer (version 2.4.1.15, Thermo Fisher Scientific). All RAW files were searched against the human Swissprot database (Download: 23.01.2020) and the Maxquant Contaminant database (Download: 20.02.2021), applying a precursor mass tolerance of 10 ppm and a mass tolerance of 0.6 Da for fragment spectra. Methionine oxidation, N-terminal acetylation, N-terminal methionine loss and N-terminal methionine loss combined with acetylation were considered as variable modifications, carbamidomethylation as static modification as well as tryptic cleavage specificity with a maximum of two missed cleavage sites. Label-free quantification was performed using standard parameters within the predefined workflow. Post processing, proteins were filtered to 1% FDR and a minimum of 2 identified peptides per protein. The mass spectrometry proteomics data have been deposited to the ProteomeXchange Consortium via the PRIDE (Perez-Riverol *et al*, 2022) partner repository with the dataset identifier PXD047246.

Metabolomics

Metabolites were analyzed by gas chromatography (GC) and anion exchange chromatography (AEC) coupled to mass spectrometry (MS). 1.5 x 10^6 cells were seeded in quadruplicates onto 6 cm dishes and cultured in the corresponding media overnight. For glutamine tracing experiments, medium was replaced with corresponding growth media containing 2 mM labeled glutamine [U-$^{13}C_5$, $^{15}N_2$] (Sigma-Aldrich) either for 30 min or 6 h prior to cell harvesting. For metabolite extraction, cells were washed five times with ice-cold isotonic NaCl solution (0.9 %), followed by scraping of cells in 1 mL ice-cold MeOH. Cells were transferred to a 15 mL tube and diluted with 1 mL MilliQ water. Cell suspension was immediately frozen in liquid nitrogen.

After thawing on ice, 0.5 mL MilliQ water was added supplemented with 10 µM internal standard ribitol (Sigma Aldrich) for polar metabolite analysis. After that 1.5 mL MTBE was added containing 5.4 µL heptadecanoic acid (1mg/ml) as internal standard for free fatty acid analysis. After repetitive mixing, samples were incubated on ice for 10 min. Subsequently, polar and nonpolar phases were separated by centrifugation at 4000 x g for 10 min at 4°C. The apolar phase was collected, frozen at -80°C and used for free fatty acid analysis. The aqueous phase was diluted with MilliQ water to decrease the organic proportion below 15 %. The sample was then frozen at -80°C, dried by lyophilization reconstituted in 500 µL MilliQ water and filtered prior to analysis.

For GC-MS, 100 µL was dried by vacuum filtration. Metabolite analysis was conducted using a 7890B gas chromatography system connected to a 7200 QTOF mass spectrometer (Agilent Technologies) as described previously (Shim *et al*, 2019). In brief, methoxyamine hydrochloride and N-methyl-N-(trimethylsilyl)trifluoroacetamide were subsequently added to the dried sample to derivatize functional groups of polar compounds. With an injection volume of 1 µL, samples were introduced into the GC-MS system and compounds were separated on a HP-5MS column (30m length, 0.25mm internal diameter and 0.25µm film thickness). The software MassHunter Qualitative (v b08, Agilent Technologies) was used for compound identification by comparing mass spectra to an in-house library of authentic standards and to the NIST14 Mass Spectral Library (https://www.nist.gov/srd/nist-standard-reference-database-1a-v14). Peak areas were integrated using MassHunter Quantitative (v b08, Agilent Technologies) and normalized to the internal standard ribitol and cell number. To determine the ^{13}C and ^{15}N incorporation, isotopologues for individual fragments were analyzed according to the number of possible incorporation sites. The normalized peak areas were corrected for the natural abundance using the R package IsoCorrectoR (Heinrich *et al*, 2018).

For the analysis of anionic compounds by AEC-MS, samples were diluted with MilliQ water (1:2 v/v). Measurements were performed using combination of a Dionex ICS-6000 HPIC and a high field Thermo Scientific Q Exactive Plus quadrupole-Orbitrap mass spectrometer (both Thermo Fisher Scientific) as described earlier with minor modifications (Curien *et al*, 2021). 10 µL of sample was injected via a Dionex AS-AP autosampler in push partial mode. Anion exchange chromatography was conducted on a Dionex IonPac AS11-HC column (2 mm X 250 mm, 4 µm particle size, Thermo Scientific) equipped with a Dionex IonPac AG11-HC guard column (2 mm X 50 mm, 4 µm, Thermo Scientific) at 30°C. The mobile phase was established using an eluent generator with a potassium hydroxide cartridge to produce a potassium hydroxide gradient. The column flow rate was set to 380 µL min^{-1} with a starting KOH concentration of 5 mM for one minute. The concentration was increased to 85 mM within 35 min and held for 5 min. The concentration was immediately reduced to 5 mM and the system

equilibrated for 10 min. Spray stability was achieved with a makeup consisting of methanol with 10 mM acetic acid delivered with 150 µL min^{-1} by an AXP Pump. The electro spray was achieved in the ESI source using the following parameters: sheath gas 30, auxiliary gas 15, sweep gas 0, spray voltage - 2.8 kV, capillary temperature 300°C, S-Lens RF level 45, and auxiliary gas heater 380°C. For the untargeted approach, the mass spectrometer operated in a combination of full mass scan and a data-dependent Top5 MS2 (ddMS2) experiment. The full scan (60-800 m/z) was conducted with a resolution of 140,000 and an automatic gain control (AGC) target of 10^6 ions with a maximum injection time of 500 ms. The Top5 ddMS2 experiment was carried out with a resolution of 17,500 and an AGC target of 10^5 and a maximum IT of 50 ms. The stepped collision energy was used with the steps (15, 25, 35) to create an average of NCE 25. Data analysis was conducted using Compound Discoverer (version 3.1, Thermo Scientific) using the "untargeted Metabolomics workflow" for steady state analysis. Compound identification was achieved on the level of mass accuracy (MS1 level), fragment mass spectra matching (MS2 level) and retention time comparison with authentic standards. For the enrichment analysis with stable heavy isotopes, the standard workflow for "stable isotope labelling" was chosen with the default settings 5 ppm mass tolerance, 30 % intensity tolerance and 0.1 % intensity threshold for isotope pattern matching and a maximum exchange rate was of 95%.

For free fatty acid analysis via GC-MS, lipids were hydrolysed and free fatty acids were methylated to fatty acid methyl esters (FAMEs). To do so, the organic phase was transferred into a glass vial and dried under a stream of nitrogen gas. The dried sample was resuspended in 1 mL of methanolic hydrochloride (MeOH/3 N HCl) and incubated at 90°C for 1 h. One mL of hexane and 1 mL of NaCl solution (1%) were added before centrifugation at 2000 *g* for 5 min. The FAME-containing organic phase (top layer) was collected in a clean glass vial and stored at −20°C until measurement as described recently (Vasilopoulos *et al*, 2023).

Quantification of mitochondrial morphology, membrane potential ($\Delta\Psi_m$) and cellular lipid droplets

HepG2 cells (0.25 x 10^6 cells) were seeded onto 35 mm Poly-D-Lysine-coated (50 µg/ml) live-imaging dishes (MATTEK P35G-1.5-14-C) and incubated for 24 h at 37°C, 5 % CO_2 in the corresponding normoglycemic or hyperglycemic media. The assessment of mitochondrial morphology, $\Delta\Psi_m$ and cellular lipid droplets was performed by addition of MitoTracker Green (Invitrogen, 200 nM), TMRM (Invitrogen, 50 nM), BODIPY 493/503 (Cayman Chemicals, 10 µM) respectively for 30 min at 37°C, followed by washing thrice. Live-cell microscopy was performed using a spinning disc confocal microscope (PerkinElmer) equipped with a 60x oil-immersion objective (N.A = 1.49) and a Hamamatsu C9100 camera (1000 X 1000 pixel). The

cells were maintained at 37°C in DMEM supplemented with 10 mM HEPES for the imaging duration. MitoTracker Green and BODIPY 493/503 were excited with a 488 nm laser while TMRM was excited with a 561 nm laser. The images were obtained at emission wavelength of 527 nm (W55) and 615 nm (W70) for 488 nm and 561 nm excitation respectively. The cell population was classified into tubular, intermediate and fragmented mitochondrial morphology based on the majority of mitochondria belonging to the respective class. Cells classified as tubular and fragmented contained mostly long tubular and short fragments respectively whereas cells classified as intermediate had a mixture of mostly short pieces, few long tubes as well as fragmented mitochondria. Volocity image analysis software was used for the quantification regarding $\Delta\Psi_m$ and lipid droplets. The total fluorescence intensities of TMRM and BODIPY were obtained per cell after respective background subtraction. Each cell was manually demarcated by drawing a ROI. Lipid droplet number within a ROI was obtained automatically using find spots by setting threshold of brightest spot within a radius of 0.5 µm and compartmentalization to ROI.

Glucose Uptake Assay

3 x10^4 HepG2 cells were seeded in triplicates onto a dark 96-well plate overnight and in parallel onto a clear-96 well plate for cell normalization. Cellular glucose uptake was measured using Glucose Uptake-Glo™ Assay kit (Promega), according to the manufacturer's protocol. Luminescence was measured by microplate reader (CLARIOstar Plus, BMG LABTECH) with 1 s integration after 1 h of incubation. Normalization was performed using Hoechst staining and mean of signal intensity was used for normalizing luminescence intensities. Luciferase signals were normalized to WT-N measurement.

Mitochondrial respirometry

A variety of respirometry experiments were performed using Seahorse XFe96 Analyzer (Agilent). HepG2 cells were seeded onto Poly-D-Lysine-coated (50 µg/ml) Seahorse XF96 cell culture plate (Agilent) at a density of 3.0 x 10^4 cells per well. For mitochondrial stress test, mitochondrial fuel flexibility test and glycolysis stress test, cells were incubated overnight in standard growth media. For fatty acid oxidation (FAO) test, standard growth medium was replaced by serum-deprived growth medium (DMEM without glucose, pyruvate and glutamine), containing 1 % FBS, 0.5 mM glucose, 0.5 mM L-Carnitine (Sigma Aldrich) and 1.0 mM glutamine 10 h after cell seeding and incubated overnight.

Prior to performing the assay, old medium was removed and cells were washed twice after which cells were supplemented with the corresponding assay media followed by 45 min CO_2-free incubation. Mitochondrial stress test was performed using Seahorse assay media (Agilent) supplemented with 10 mM glucose, 2 mM stable glutamine and 1 mM sodium pyruvate.

Mitochondrial oxygen consumption was measured after sequential addition of oligomycin (1 µM), FCCP (0.25 µM) and rotenone/antimycin (0.5 µM) according to the manufacturer's protocol. Mitochondrial fuel flexibility test was performed using Seahorse assay media containing 10 mM glucose, 2 mM stable glutamine and 1 mM sodium pyruvate. After initial acquisition of basal respiration, glucose, glutamine and FAO dependency and capacity was assessed according to manufacturer's protocol by sequential incubation with UK5099 (2 µM) and Etomoxir (4 µM) / BPTES (3 µM), BPTES (3 µM) and Etomoxir (4 µM) / UK5099 (2 µM) or Etomoxir (4 µM) and UK5099 (2 µM) / BPTES (3 µM) respectively. Glycolysis stress test was performed in Seahorse assay media supplemented with 2 mM glutamine. After 15 min of basal ECAR determination, glycolysis was induced by addition of glucose (10 mM), followed by oligomycin (1 µM) and lastly 2-DG (50 mM). For assessment of FAO, cells were pretreated with Seahorse assay media containing BSA (Biomol, 200 µM) or Palmitate (Biomol, 200 µM). FAO was measured by sequential addition of etomoxir (Sigma Aldrich, 4 µM) or media and mitochondrial stress test kit chemicals oligomycin (1.5 µM), FCCP (1 µM), rotenone/antimycin A (0.5 µM). Cell numbers were normalized using Hoechst (10 ug/mL) staining intensity assessed by microplate reader (Tecan M200 pro). Data were analyzed using wave software (Agilent) and Microsoft Excel.

Electron Microscopy

4 x 10^6 HepG2 cells were grown overnight in 10 cm petri dishes at 37°C with 5% CO_2 in the corresponding treatment media. Cells were fixed using 3 % glutaraldehyde, 0.1 M sodium cacodylate buffer at pH 7.2 and subsequently pelleted. Cell pellets were washed in fresh 0.1 M sodium cacodylate buffer at pH 7.2 and embedded in 3 % low melting agarose. Cells were stained using 1% osmium tetroxide for 50 min, washed twice with 0.1 M sodium cacodylate buffer and once using 70% ethanol for 10 min each. Thereafter, cells were stained using 1% uranyl acetate/1% phosphotungstic acid in 70% ethanol for 1 h. Stained samples were embedded in spur epoxy resin for polymerization at 70°C for 24 hours. Ultrathin sections were prepared using a microtome and imaged on a transmission electron microscope (Hitachi, H600) at 75 V equipped with Bioscan 792 camera (Gatan). Image analysis was performed using ImageJ software.

Sulforhodamine B (SRB) assay

Cell viability was assessed by SRB colorimetry assay. 2.5 x 10^4 HepG2 cells were seeded in 24 well plates and incubated for 24 h, 48 h or 72 h. Subsequently, cells were washed with PBS and fixed with 10% (w/v) cold trichloroacetic acid solution (500 µL/well) for 1 h at 4°C. After washing five times with MilliQ water, cells were dried at RT overnight. Fixed cells were stained with SRB solution (0.4% (w/v) in 1% acetic acid, 300 µl/well) for 15 min at RT, washed five times with 1% acetic acid and dried at RT for 1 h. SRB extraction was performed by addition

of 400 µL TRIS-Base (10 mmol/l) per well. The absorbance was measured, after 5 min of shaking, at 492 nm and 620 nm using a microplate reader (Tecan M200 pro). Total intensity was calculated from signal intensity at 492 nm after background subtraction of 620 nm intensity. Proliferation was normalized to WT-N.

Statistics and data representation

Data are represented as mean ± standard error mean (SEM). Statistical significance was determined by one-way ANOVA followed by Šídák's test for multiple comparisons of selected pairs with **P*-value ≤ 0.05, ***P*-value ≤ 0.01, ****P*-value ≤ 0.001, *****P*-value ≤ 0.0001. Data analysis was performed using Microsoft Excel. Data representation and statistical analysis was performed using GraphPad Prism.

References

Afshinnia F, Rajendiran TM, Soni T, Byun J, Wernisch S, Sas KM, Hawkins J, Bellovich K, Gipson D, Michailidis G *et al* (2018) Impaired β-Oxidation and Altered Complex Lipid Fatty Acid Partitioning with Advancing CKD. *J Am Soc Nephrol* 29: 295-306

Anand R, Kondadi AK, Meisterknecht J, Golombek M, Nortmann O, Riedel J, Peifer-Weiss L, Brocke-Ahmadinejad N, Schlutermann D, Stork B *et al* (2020) MIC26 and MIC27 cooperate to regulate cardiolipin levels and the landscape of OXPHOS complexes. *Life Sci Alliance* 3: e202000711

Anand R, Reichert AS, Kondadi AK (2021) Emerging Roles of the MICOS Complex in Cristae Dynamics and Biogenesis. *Biology (Basel)* 10

Anand R, Strecker V, Urbach J, Wittig I, Reichert AS (2016) Mic13 Is Essential for Formation of Crista Junctions in Mammalian Cells. *PloS one* 11: e0160258

Beninca C, Zanette V, Brischigliaro M, Johnson M, Reyes A, Valle DAD, A JR, Degiorgi A, Yeates A, Telles BA *et al* (2021) Mutation in the MICOS subunit gene APOO (MIC26) associated with an X-linked recessive mitochondrial myopathy, lactic acidosis, cognitive impairment and autistic features. *J Med Genet* 58: 155-167

Bugger H, Boudina S, Hu XX, Tuinei J, Zaha VG, Theobald HA, Yun UJ, McQueen AP, Wayment B, Litwin SE *et al* (2008) Type 1 diabetic akita mouse hearts are insulin sensitive but manifest structurally abnormal mitochondria that remain coupled despite increased uncoupling protein 3. *Diabetes* 57: 2924-2932

Chen J, Yue F, Kuang S (2022) Labeling and analyzing lipid droplets in mouse muscle stem cells. *STAR Protoc* 3: 101849

Collaborators GBDO, Afshin A, Forouzanfar MH, Reitsma MB, Sur P, Estep K, Lee A, Marczak L, Mokdad AH, Moradi-Lakeh M *et al* (2017) Health Effects of Overweight and Obesity in 195 Countries over 25 Years. *N Engl J Med* 377: 13-27

Curien G, Lyska D, Guglielmino E, Westhoff P, Janetzko J, Tardif M, Hallopeau C, Brugière S, Dal Bo D, Decelle J *et al* (2021) Mixotrophic growth of the extremophile Galdieria sulphuraria reveals the flexibility of its carbon assimilation metabolism. *New Phytol* 231: 326-338

Edgar R, Domrachev M, Lash AE (2002) Gene Expression Omnibus: NCBI gene expression and hybridization array data repository. *Nucleic Acids Res* 30: 207-210

Eramo MJ, Lisnyak V, Formosa LE, Ryan MT (2020) The 'mitochondrial contact site and cristae organising system' (MICOS) in health and human disease. *J Biochem* 167: 243-255

Frey TG, Mannella CA (2000) The internal structure of mitochondria. *Trends in biochemical sciences* 25: 319-324

Giacomello M, Pyakurel A, Glytsou C, Scorrano L (2020) The cell biology of mitochondrial membrane dynamics. *Nat Rev Mol Cell Biol*

Gomes LC, Di Benedetto G, Scorrano L (2011) During autophagy mitochondria elongate, are spared from degradation and sustain cell viability. *Nat Cell Biol* 13: 589-598

Guarani V, McNeill EM, Paulo JA, Huttlin EL, Frohlich F, Gygi SP, Van Vactor D, Harper JW (2015) QIL1 is a novel mitochondrial protein required for MICOS complex stability and cristae morphology. *eLife* 4

1315 Guo X, Hu J, He G, Chen J, Yang Y, Qin D, Li C, Huang Z, Hu D, Wei C *et al* (2023) Loss of
1316 APOO (MIC26) aggravates obesity-related whitening of brown adipose tissue via PPARα-
1317 mediated functional interplay between mitochondria and peroxisomes. *Metabolism* 144:
1318 155564

1319 Guo Y, Darshi M, Ma Y, Perkins GA, Shen Z, Haushalter KJ, Saito R, Chen A, Lee YS, Patel
1320 HH *et al* (2013) Quantitative proteomic and functional analysis of liver mitochondria from high
1321 fat diet (HFD) diabetic mice. *Molecular & cellular proteomics : MCP* 12: 3744-3758

1322 Harner M, Korner C, Walther D, Mokranjac D, Kaesmacher J, Welsch U, Griffith J, Mann M,
1323 Reggiori F, Neupert W (2011) The mitochondrial contact site complex, a determinant of
1324 mitochondrial architecture. *The EMBO journal* 30: 4356-4370

1325 Heinrich P, Kohler C, Ellmann L, Kuerner P, Spang R, Oefner PJ, Dettmer K (2018) Correcting
1326 for natural isotope abundance and tracer impurity in MS-, MS/MS- and high-resolution-
1327 multiple-tracer-data from stable isotope labeling experiments with IsoCorrectoR. *Sci Rep* 8:
1328 17910

1329 Hoppins S, Collins SR, Cassidy-Stone A, Hummel E, Devay RM, Lackner LL, Westermann B,
1330 Schuldiner M, Weissman JS, Nunnari J (2011) A mitochondrial-focused genetic interaction
1331 map reveals a scaffold-like complex required for inner membrane organization in mitochondria.
1332 *The Journal of cell biology* 195: 323-340

1333 Hughes CS, Moggridge S, Müller T, Sorensen PH, Morin GB, Krijgsveld J (2019) Single-pot,
1334 solid-phase-enhanced sample preparation for proteomics experiments. *Nat Protoc* 14: 68-85

1335 Kondadi AK, Anand R, Hansch S, Urbach J, Zobel T, Wolf DM, Segawa M, Liesa M, Shirihai
1336 OS, Weidtkamp-Peters S *et al* (2020a) Cristae undergo continuous cycles of membrane
1337 remodelling in a MICOS-dependent manner. *EMBO Rep* 21: e49776

1338 Kondadi AK, Anand R, Reichert AS (2020b) Cristae Membrane Dynamics - A Paradigm
1339 Change. *Trends Cell Biol* 30: 923-936

1340 Koob S, Barrera M, Anand R, Reichert AS (2015) The non-glycosylated isoform of MIC26 is a
1341 constituent of the mammalian MICOS complex and promotes formation of crista junctions.
1342 *Biochimica et biophysica acta* 1853: 1551-1563

1343 Lamant M, Smih F, Harmancey R, Philip-Couderc P, Pathak A, Roncalli J, Galinier M, Collet
1344 X, Massabuau P, Senard JM *et al* (2006) ApoO, a novel apolipoprotein, is an original
1345 glycoprotein up-regulated by diabetes in human heart. *J Biol Chem* 281: 36289-36302

1346 Li Z, Liu H, Bode A, Luo X (2021) Emerging roles of dehydrogenase/reductase member 2
1347 (DHRS2) in the pathology of disease. *Eur J Pharmacol* 898: 173972

1348 López-Viñas E, Bentebibel A, Gurunathan C, Morillas M, de Arriaga D, Serra D, Asins G,
1349 Hegardt FG, Gómez-Puertas P (2007) Definition by functional and structural analysis of two
1350 malonyl-CoA sites in carnitine palmitoyltransferase 1A. *J Biol Chem* 282: 18212-18224

1351 Lubeck M, Derkum NH, Naha R, Strohm R, Driessen MD, Belgardt BF, Roden M, Stühler K,
1352 Anand R, Reichert AS *et al* (2023) MIC26 and MIC27 are bona fide subunits of the MICOS
1353 complex in mitochondria and do not exist as glycosylated apolipoproteins. *PloS one* 18:
1354 e0286756

1355 Madison BB (2016) Srebp2: A master regulator of sterol and fatty acid synthesis. *J Lipid Res*
1356 57: 333-335

1357 Mannella CA, Lederer WJ, Jafri MS (2013) The connection between inner membrane topology
1358 and mitochondrial function. *Journal of molecular and cellular cardiology* 62: 51-57

1359 Mehta A, Shapiro MD (2022) Apolipoproteins in vascular biology and atherosclerotic disease.
1360 *Nat Rev Cardiol* 19: 168-179

1361 Mishra P, Chan DC (2016) Metabolic regulation of mitochondrial dynamics. *The Journal of cell*
1362 *biology*

1363 Naha R, Strohm R, Urbach J, Wittig I, Reichert AS, Kondadi AK, Anand R (2023) MIC13 and
1364 SLP2 seed the assembly of MIC60-subcomplex to facilitate crista junction formation. *bioRxiv*:
1365 2023.2009.2004.556207

1366 Ngo J, Choi DW, Stanley IA, Stiles L, Molina AJA, Chen PH, Lako A, Sung ICH, Goswami R,
1367 Kim MY *et al* (2023) Mitochondrial morphology controls fatty acid utilization by changing CPT1
1368 sensitivity to malonyl-CoA. *The EMBO journal*: e111901

1369 Ott C, Dorsch E, Fraunholz M, Straub S, Kozjak-Pavlovic V (2015) Detailed analysis of the
1370 human mitochondrial contact site complex indicate a hierarchy of subunits. *PloS one* 10:
1371 e0120213

1372 Peifer-Weiß L, Kurban M, David C, Lubeck M, Kondadi AK, Nemer G, Reichert AS, Anand R
1373 (2023) A X-linked nonsense APOO/MIC26 variant causes a lethal mitochondrial disease with
1374 progeria-like phenotypes. *Clin Genet*

1375 Perez-Riverol Y, Bai J, Bandla C, García-Seisdedos D, Hewapathirana S, Kamatchinathan S,
1376 Kundu DJ, Prakash A, Frericks-Zipper A, Eisenacher M *et al* (2022) The PRIDE database
1377 resources in 2022: a hub for mass spectrometry-based proteomics evidences. *Nucleic Acids*
1378 *Res* 50: D543-d552

1379 Philip-Couderc P, Smih F, Pelat M, Vidal C, Verwaerde P, Pathak A, Buys S, Galinier M,
1380 Senard JM, Rouet P (2003) Cardiac transcriptome analysis in obesity-related hypertension.
1381 *Hypertension* 41: 414-421

1382 Poschmann G, Seyfarth K, Besong Agbo D, Klafki HW, Rozman J, Wurst W, Wiltfang J, Meyer
1383 HE, Klingenspor M, Stuhler K (2014) High-fat diet induced isoform changes of the Parkinson's
1384 disease protein DJ-1. *J Proteome Res* 13: 2339-2351

1385 Sheftel AD, Stehling O, Pierik AJ, Netz DJ, Kerscher S, Elsässer HP, Wittig I, Balk J, Brandt
1386 U, Lill R (2009) Human ind1, an iron-sulfur cluster assembly factor for respiratory complex I.
1387 *Mol Cell Biol* 29: 6059-6073

1388 Shim SH, Lee SK, Lee DW, Brilhaus D, Wu G, Ko S, Lee CH, Weber APM, Jeon JS (2019)
1389 Loss of Function of Rice Plastidic Glycolate/Glycerate Translocator 1 Impairs Photorespiration
1390 and Plant Growth. *Front Plant Sci* 10: 1726

1391 Song S, Attia RR, Connaughton S, Niesen MI, Ness GC, Elam MB, Hori RT, Cook GA, Park
1392 EA (2010) Peroxisome proliferator activated receptor alpha (PPARalpha) and PPAR gamma
1393 coactivator (PGC-1alpha) induce carnitine palmitoyltransferase IA (CPT-1A) via independent
1394 gene elements. *Mol Cell Endocrinol* 325: 54-63

1395 Spinelli JB, Haigis MC (2018) The multifaceted contributions of mitochondria to cellular
1396 metabolism. *Nat Cell Biol* 20: 745-754

1397 Stephan T, Bruser C, Deckers M, Steyer AM, Balzarotti F, Barbot M, Behr TS, Heim G, Hubner
1398 W, Ilgen P *et al* (2020) MICOS assembly controls mitochondrial inner membrane remodeling
1399 and crista junction redistribution to mediate cristae formation. *The EMBO journal* 39: e104105

1400 Sun W, Nie T, Li K, Wu W, Long Q, Feng T, Mao L, Gao Y, Liu Q, Gao X *et al* (2021) Hepatic
1401 CPT1A Facilitates Liver-Adipose Cross-Talk via Induction of FGF21 in Mice. *Diabetes*

1402 Szendroedi J, Phielix E, Roden M (2011) The role of mitochondria in insulin resistance and
1403 type 2 diabetes mellitus. *Nat Rev Endocrinol* 8: 92-103

1404 Thiam AR, Farese RV, Jr., Walther TC (2013) The biophysics and cell biology of lipid droplets.
1405 *Nat Rev Mol Cell Biol* 14: 775-786

1406 Tian F, Wu CL, Yu BL, Liu L, Hu JR (2017) Apolipoprotein O expression in mouse liver
1407 enhances hepatic lipid accumulation by impairing mitochondrial function. *Biochem Biophys*
1408 *Res Commun* 491: 8-14

1409 Turkieh A, Caubere C, Barutaut M, Desmoulin F, Harmancey R, Galinier M, Berry M, Dambrin
1410 C, Polidori C, Casteilla L *et al* (2014) Apolipoprotein O is mitochondrial and promotes
1411 lipotoxicity in heart. *J Clin Invest* 124: 2277-2286

1412 Urbach J, Kondadi AK, David C, Naha R, Deinert K, Reichert AS, Anand R (2021) Conserved
1413 GxxxG and WN motifs of MIC13 are essential for bridging two MICOS subcomplexes. *Biochim*
1414 *Biophys Acta Biomembr* 1863: 183683

1415 Vasilopoulos G, Heflik L, Czolkoss S, Heinrichs F, Kleetz J, Yesilyurt C, Tischler D, Westhoff
1416 P, Exterkate M, Aktas M *et al* (2023) Characterization of multiple lysophosphatidic acid
1417 acyltransferases in the plant pathogen Xanthomonas campestris. *Febs j*

1418 von der Malsburg K, Muller JM, Bohnert M, Oeljeklaus S, Kwiatkowska P, Becker T,
1419 Loniewska-Lwowska A, Wiese S, Rao S, Milenkovic D *et al* (2011) Dual role of mitofilin in
1420 mitochondrial membrane organization and protein biogenesis. *Developmental cell* 21: 694-707

1421 Wai T, Saita S, Nolte H, Müller S, König T, Richter-Dennerlein R, Sprenger HG, Madrenas J,
1422 Mühlmeister M, Brandt U *et al* (2016) The membrane scaffold SLP2 anchors a proteolytic hub
1423 in mitochondria containing PARL and the i-AAA protease YME1L. *EMBO Rep* 17: 1844-1856

1424 Wang L, Ishihara T, Ibayashi Y, Tatsushima K, Setoyama D, Hanada Y, Takeichi Y, Sakamoto
1425 S, Yokota S, Mihara K *et al* (2015) Disruption of mitochondrial fission in the liver protects mice
1426 from diet-induced obesity and metabolic deterioration. *Diabetologia* 58: 2371-2380

1427 Weber TA, Koob S, Heide H, Wittig I, Head B, van der Bliek A, Brandt U, Mittelbronn M,
1428 Reichert AS (2013) APOOL is a cardiolipin-binding constituent of the Mitofilin/MINOS protein
1429 complex determining cristae morphology in mammalian mitochondria. *PloS one* 8: e63683

1430 Włodarczyk M, Nowicka G (2019) Obesity, DNA Damage, and Development of Obesity-
1431 Related Diseases. *Int J Mol Sci* 20

1432 Wu CL, Zhao SP, Yu BL (2013) Microarray analysis provides new insights into the function of
1433 apolipoprotein O in HepG2 cell line. *Lipids Health Dis* 12: 186

1434 Xiang RL, Huang Y, Zhang Y, Cong X, Zhang ZJ, Wu LL, Yu GY (2020) Type 2 diabetes-
1435 induced hyposalivation of the submandibular gland through PINK1/Parkin-mediated
1436 mitophagy. *J Cell Physiol* 235: 232-244

1437 Yoo HC, Park SJ, Nam M, Kang J, Kim K, Yeo JH, Kim JK, Heo Y, Lee HS, Lee MY *et al*
1438 (2020a) A Variant of SLC1A5 Is a Mitochondrial Glutamine Transporter for Metabolic
1439 Reprogramming in Cancer Cells. *Cell Metab* 31: 267-283.e212

1440 Yoo HC, Yu YC, Sung Y, Han JM (2020b) Glutamine reliance in cell metabolism. *Exp Mol Med*
1441 52: 1496-1516

1442 Yu T, Robotham JL, Yoon Y (2006) Increased production of reactive oxygen species in
1443 hyperglycemic conditions requires dynamic change of mitochondrial morphology. *Proc Natl*
1444 *Acad Sci U S A* 103: 2653-2658

1445 Zadoorian A, Du X, Yang H (2023) Lipid droplet biogenesis and functions in health and
1446 disease. *Nat Rev Endocrinol* 19: 443-459

1447 Zick M, Rabl R, Reichert AS (2009) Cristae formation-linking ultrastructure and function of
1448 mitochondria. *Biochimica et biophysica acta* 1793: 5-19

Figure 1

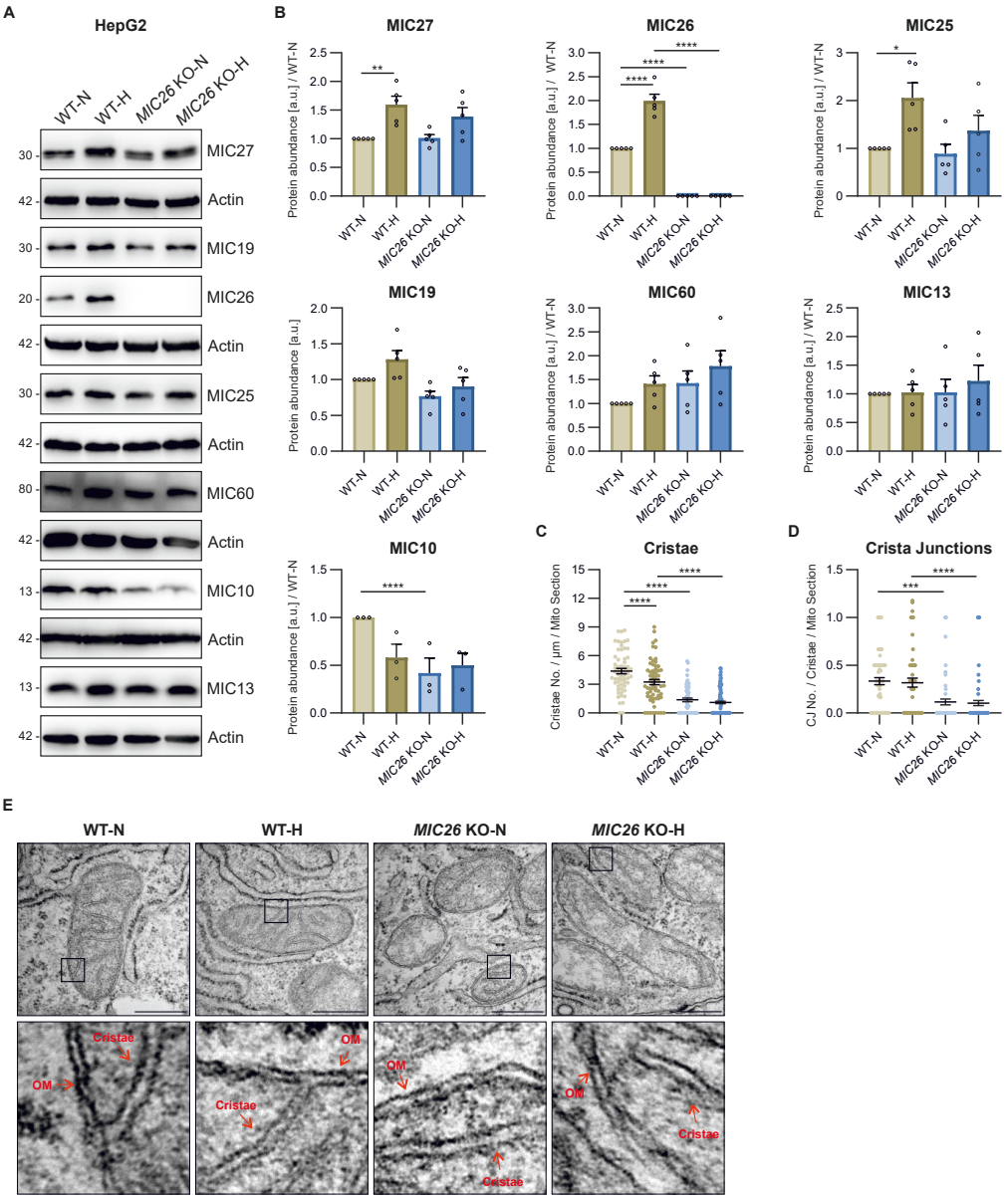

Figure 1. Mitochondrial apolipoprotein MIC26 is selectively increased in cells exposed to hyperglycemia

(A and B) Western blot analysis of all MICOS subunits from HepG2 WT and *MIC26* KO cells cultured in normo- and hyperglycemia (N = 3-5). Chronic hyperglycemia treatment leads to increased levels of MIC27, MIC26 and MIC25 in WT cells. Loss of MIC26 is accompanied by decreased MIC10 in normoglycemia.

(C, D and E) Electron microscopy data including quantification of cristae number per unit length (µm) per mitochondrial section (C) as well as crista junctions per cristae per mitochondrial section (D), along with representative images (E) from HepG2 WT and *MIC26* KO cells cultured in normo- and hyperglycemia (N = 2). Loss of MIC26 led to decreased cristae number and crista junctions independent of normo- and hyperglycemia. Red arrows in lower row indicate outer membrane (OM) or cristae. Scale bar represents 500 nm.

Data are represented as mean ± SEM (B, C and D). Statistical analysis was performed using one-way ANOVA with $*P < 0.05$, $**P < 0.01$, $***P < 0.001$, $****P < 0.0001$. N represents the number of biological replicates.

Figure 2

Figure 2. Hyperglycemia confers antagonistic regulation of lipid and cholesterol pathways, in *MIC26* KO vs WT cells, compared to normoglycemia

(A and B) Hierarchical Treemap clustering of significant gene ontology (GO) enriched terms of biological processes upregulated in normoglycemic *MIC26* KO (A) and downregulated in hyperglycemic *MIC26* KO (B) compared to respective WT. Each rectangle represents one BioProcess pathway. Every colour represents clustering of different sub-pathways to pathway families. The rectangle sizes indicate the *P*-value of the respective GO term.

(C and D) WikiPathway enrichment using EnrichR analysis of differentially expressed genes (C) upregulated in normoglycemic *MIC26* KO and (D) downregulated in hyperglycemic *MIC26* KO cells compared to respective WT. Arrows indicate antagonistically regulated metabolic pathways including glycolysis, cholesterol biosynthesis, fatty acid synthesis and oxidation.

Differentially expressed genes were considered statistically significant with a cut-off fold change of ±1.5 and Bonferroni correction $P \leq 0.05$. Treemap representation of GO enrichment was plotted with statistically significant pathways with cut-off $P \leq 0.05$.

Figure 3

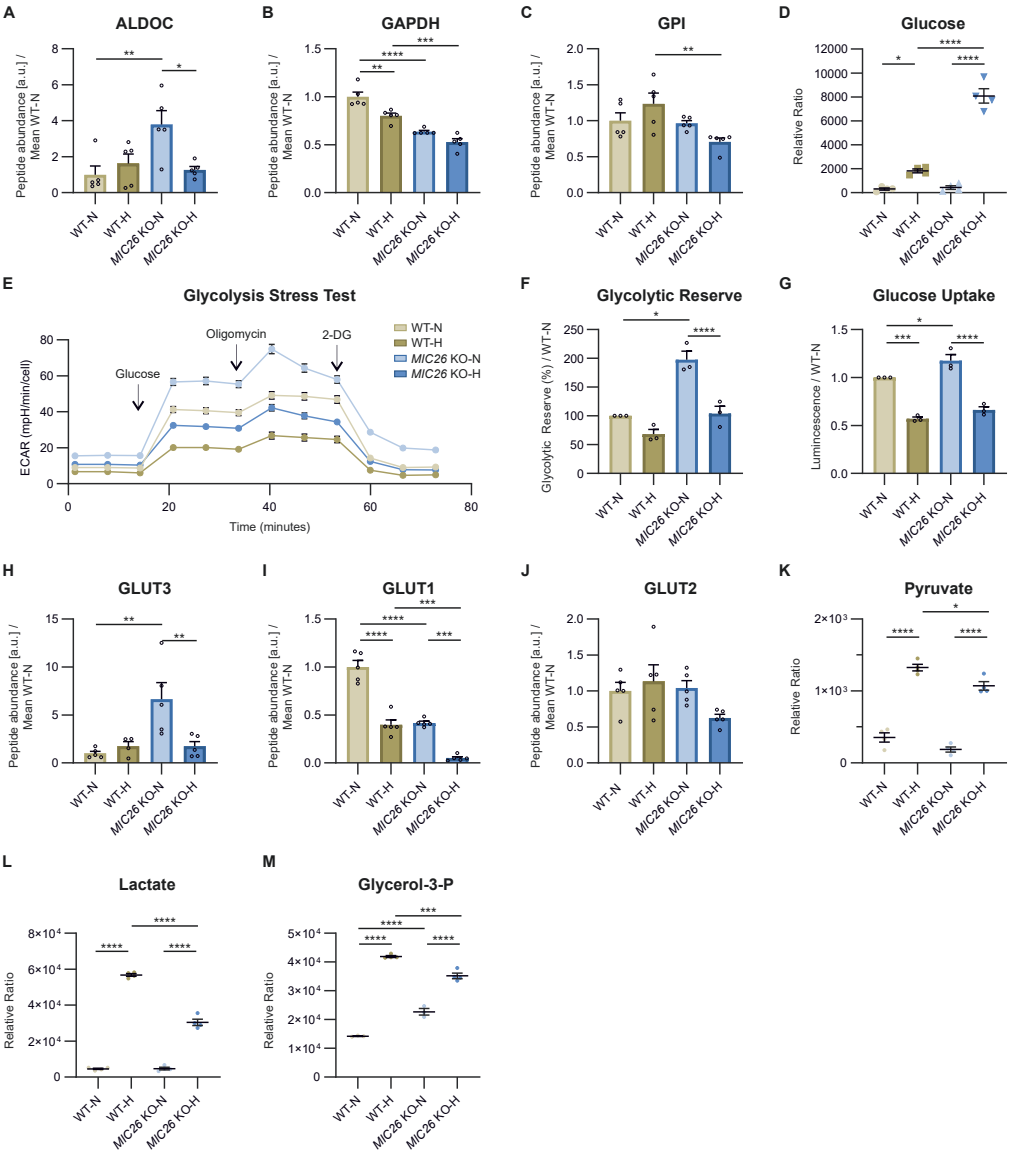

Figure 3. MIC26 maintains the glycolytic function

(A – C) Peptide abundances of enzymes involved in glycolysis pathway curated from proteomics data (N = 5).

(D) Steady state metabolomics (GC-MS) data reveals increased cellular glucose accumulation upon *MIC26* deletion in hyperglycemia (N = 3-4).

(E and F) Representative glycolysis stress test seahorse assay analysis, with sequential injection of glucose, oligomycin and 2-deoxyglucose, reveals a tendency towards increased glycolysis upon *MIC26* deletion (E) (n = 23). Quantification from various biological replicates shows a significant increase of cellular glycolytic reserve in normoglycemic, but not in hyperglycemic conditions (F) (N = 3).

(G) Cellular glucose uptake was measured using Glucose uptake Glo assay normalized to WT-N. *MIC26* deletion leads to an increased glucose uptake upon normoglycemia (N = 3).

(H – J) Peptide abundances of transporters involved in glucose uptake namely GLUT3 (H), GLUT1 (I) and GLUT2 (J) curated from proteomics data (N = 5).

(K and L) Steady state metabolomics (GC-MS) shows unaltered cellular pyruvate (K) and lactate (L) levels in *MIC26* KO cell lines in normoglycemia but decreased levels upon *MIC26* deletion in hyperglycemia (N = 3-4).

(M) *MIC26* deletion increases glycerol-3-phosphate amount in normoglycemia with an antagonistic effect in hyperglycemia compared to the respective WT (N = 3-4).

Data are represented as mean ± SEM (A-M). Statistical analysis was performed using one-way ANOVA with $*P < 0.05$, $**P < 0.01$, $***P < 0.001$, $****P < 0.0001$. N represents the number of biological replicates and n the number of technical replicates.

Figure 4

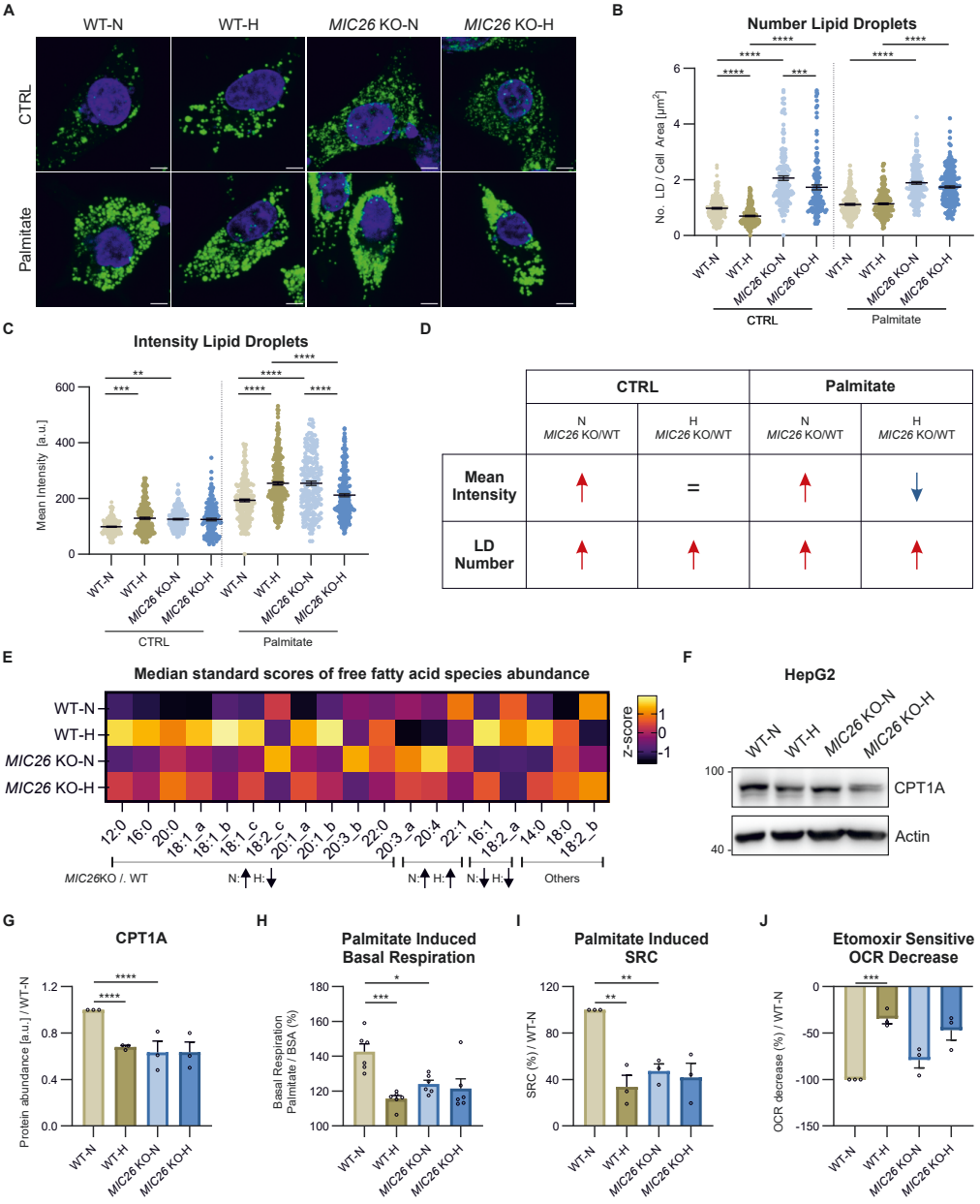

Figure 4. The loss of MIC26 leads to metabolic rewiring of cellular lipid metabolism via CPT1A and dysregulation of fatty acid synthesis

(A – D) Analysis of lipid droplet formation in WT and *MIC26* KO cells cultured in normo- and hyperglycemia either in standard growth condition (CTRL) or upon palmitate stimulation (100 µM, 24 h). Representative confocal images of lipid droplets stained using BODIPY 493/503 are shown (A). Quantification shows number of lipid droplets normalized to the total cell area [µm^2] (B) and mean fluorescence intensity per cell normalized to mean intensity of WT-N in all biological replicates (C). *MIC26* deletion leads to a nutritional-independent increase in lipid droplet number. However, an opposing effect, leading to increase or decrease of mean fluorescence intensity of lipid droplets, upon comparison of *MIC26* KO to WT was observed in normo- and hyperglycemia respectively, with a pronounced effect upon feeding palmitate (N = 3). Scale bar represents 5 µm.

(E) Heat map representing the abundance of steady state FFA species in WT and *MIC26* KO cells cultured in normo- and hyperglycemia. 11 out of 19 of the FFA species represent an antagonistic behavior upon comparing *MIC26* KO to WT in normo- (increase) and hyperglycemia (decrease) (N = 3-4).

(F and G) Western blot analysis (F), along with respective quantification (G) of WT and *MIC26* KO cells cultured in normo- and hyperglycemia, show a reduction of CPT1A in WT-H, *MIC26* KO-N and *MIC26* KO-H compared to WT-N (N = 3).

(H – J) Mitochondrial fatty acid oxidation analyzed using Seahorse XF analyzer shows a decreased palmitate-induced basal respiration (H) and spare respiratory capacity (I) and a nonsignificant reduction of etomoxir-sensitive OCR decrease upon comparing *MIC26* KO to WT in normoglycemia (N = 3).

Data are represented as mean ± SEM (B-C and G-J). Statistical analysis was performed using one-way ANOVA with *P < 0.05, **P < 0.01, ***P < 0.001, ****P < 0.0001. N represents the number of biological replicates.

Figure 5

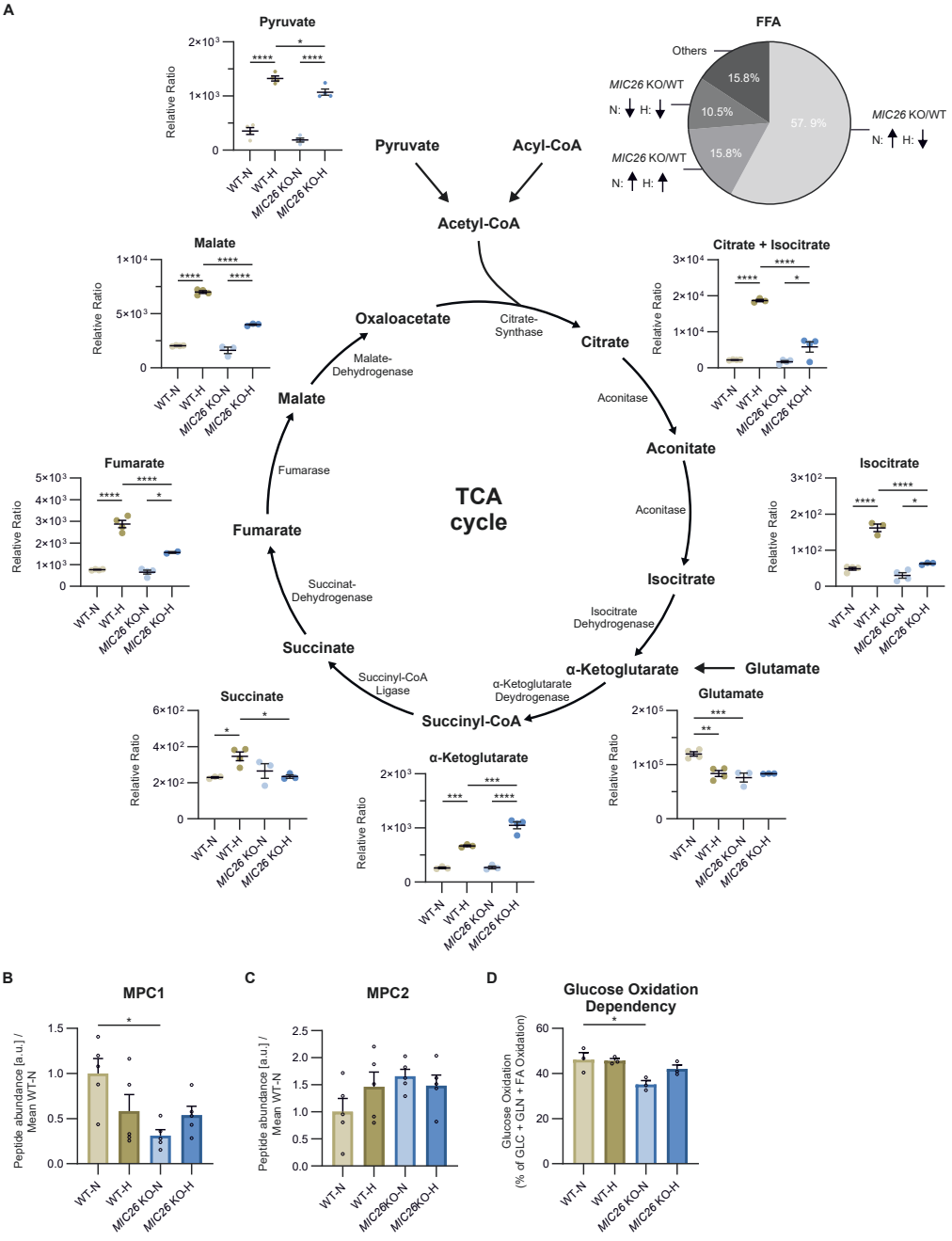

Figure 5. *MIC26* deletion leads to hyperglycemia-induced decrease in TCA cycle intermediates

(A) Representation of the relative amounts (GC-MS) of TCA cycle metabolites and associated precursors at steady state in WT and *MIC26* KO cells cultured in normo- and hyperglycemia. All the TCA cycle metabolites with the exception of α-ketoglutarate showed a decreasing trend upon *MIC26* KO when compared to WT in hyperglycemia (N = 3-4).

(B and C) Mitochondrial pyruvate carrier 1 (MPC1) (B), but not MPC2 (C), is significantly decreased in *MIC26* KO-N compared to WT-N, as revealed by peptide abundances from proteomics data (N = 5).

(D) Mitochondrial glucose / pyruvate dependency analysis, using Seahorse XF analyzer mito fuel flex test assay, reveals a decreased mitochondrial respiratory dependency of *MIC26* KO on glucose / pyruvate in normoglycemia (N = 3).

Data are represented as mean ± SEM (A-C). Statistical analysis was performed using one-way ANOVA with **P* < 0.05, ***P* < 0.01, ****P* < 0.001, *****P* < 0.0001. N represents the number of biological replicates.

Figure 6

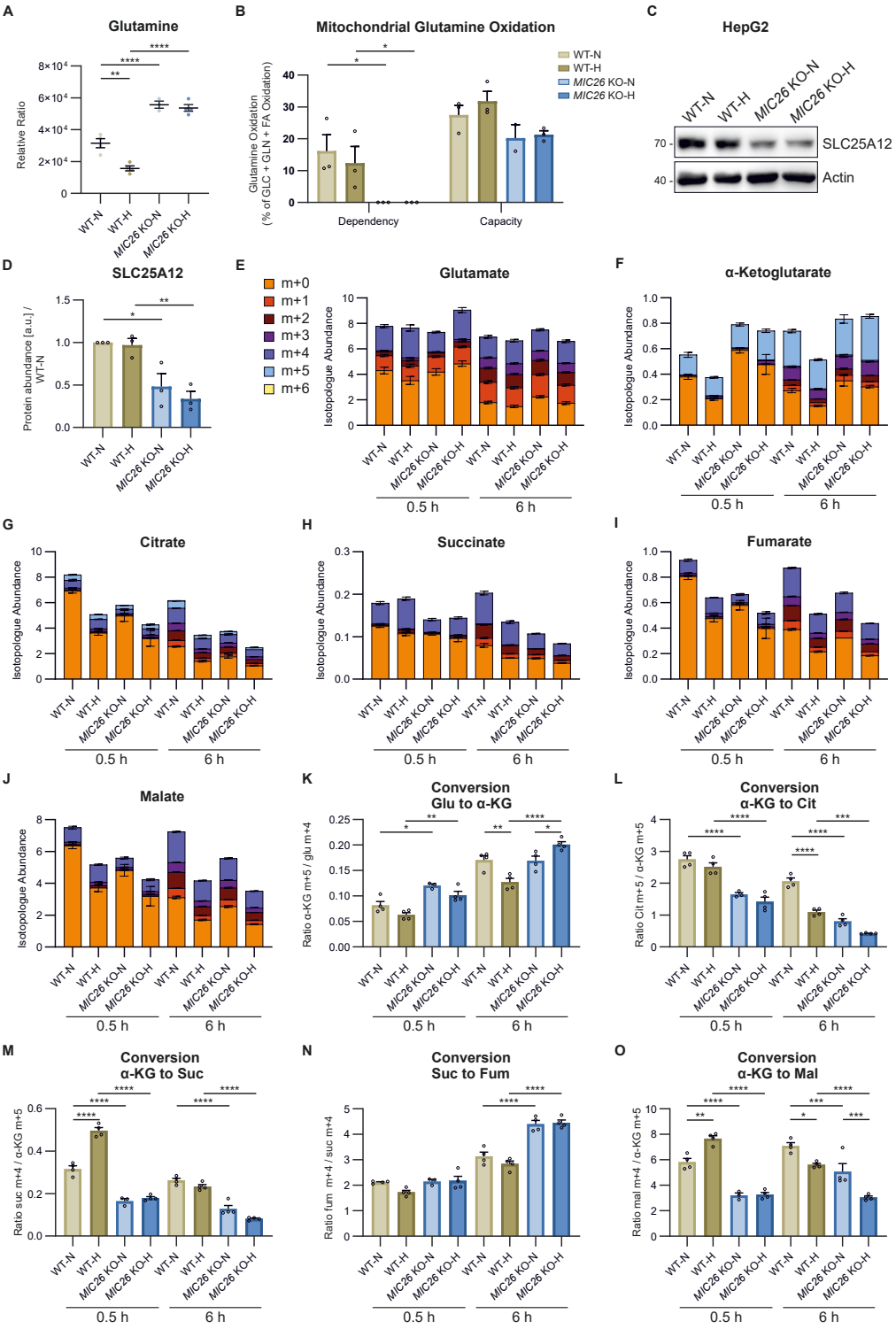

Figure 6. Aberrant glutamine metabolism is observed in *MIC26* KOs independent of nutritional status

(A) Metabolomics analysis (GC-MS) shows that glutamine levels were strongly increased in *MIC26* KO cells cultured in both normo- and hyperglycemia at steady state compared to respective WT (N = 3-4).

(B) Quantification of mitochondrial glutamine dependency and capacity analysis, using Seahorse XF analyzer mito fuel flex test assay, shows a diminished mitochondrial respiratory dependency on glutamine. A nonsignificant mitochondrial respiratory decreased capacity of *MIC26* KO cells was observed compared to respective WT conditions (N = 3).

(C and D) Western Blot analysis (C) along with respective quantification (D) show reduced amounts of the glutamate aspartate antiporter SLC25A12 (ARALAR / AGC1), present in mitochondria, in *MIC26* KO cell lines compared to respective WT cells (N = 3).

(E – J) Representation of labeled (m+1 - m+6) and unlabeled (m+0) species of glutamate (GC-MS) (E), and TCA cycle metabolites (AEC-MS) α-KG (F), citrate (G), succinate (H), fumarate (I) and malate (J), from glutamine tracing experiments after labelling for 0.5 h and 6 h (N = 4).

(K – O) Conversion rates from different TCA cycle reactions calculated using the ratio of highest labeled species abundances for the conversions of glutamate to α-KG (K), α-KG to citrate (L), α-KG to succinate (M), succinate to fumarate (N) and α-KG to malate (N = 4).

Data are represented as mean ± SEM (A-B and D-O). Statistical analysis was performed using one-way ANOVA with $*P < 0.05$, $**P < 0.01$, $***P < 0.001$, $****P < 0.0001$. N represents the number of biological replicates.

Figure 7

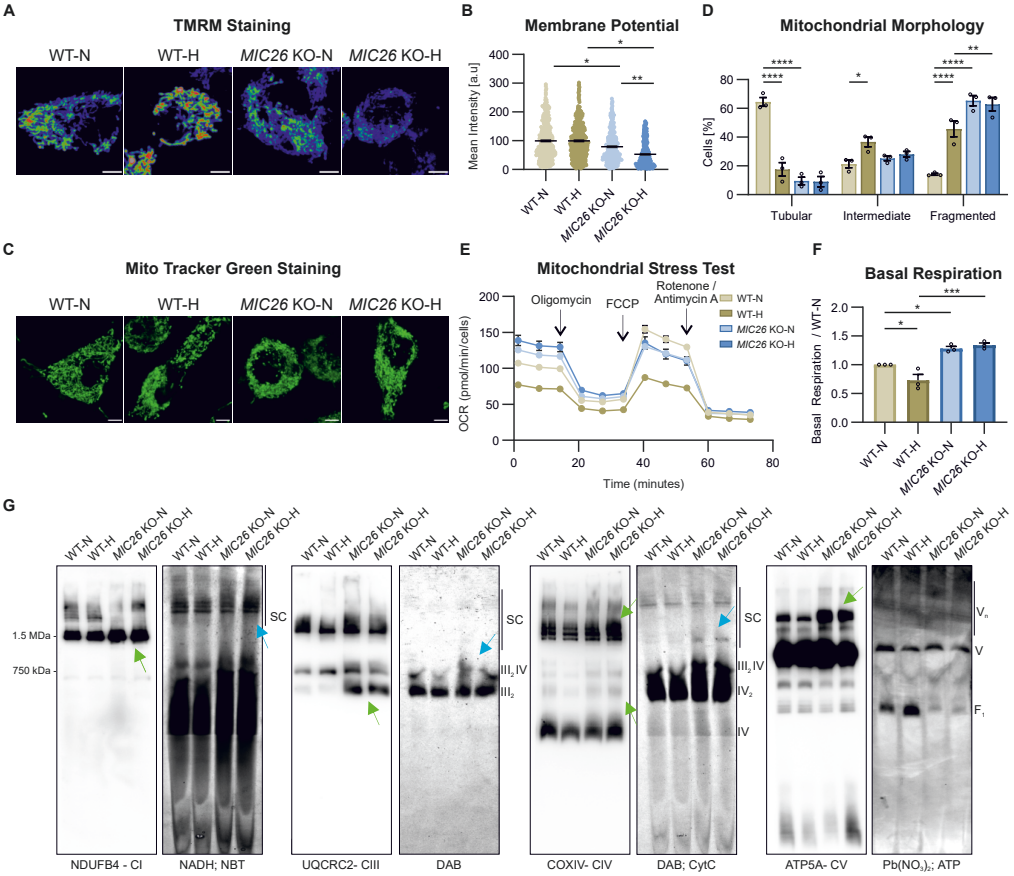

Figure 7. MIC26 regulates mitochondrial bioenergetics by restricting the ETC activity and OXPHOS (super-)complex formation

(A and B) Representative pseudocolour rainbow LUT intensities from confocal images of WT and *MIC26* KO HepG2 cells stained with TMRM show a reduction in $\Delta\Psi_m$ upon *MIC26* deletion in both normoglycemia and hyperglycemia when compared to respective WT cells (A). Quantification represents mean TMRM fluorescence intensity per cell normalized to mean intensity of WT-N in all biological replicates (B) (N = 3). Scale bar represents 5 µm.

(C and D) Representative confocal images of mitochondrial morphology, visualized by MitoTracker green staining (C), show that loss of MIC26 shifts mitochondrial morphology from tubular mitochondrial network in WT normoglycemic conditions to fragmented phenotype irrespective of supplemented glucose amount (D) (N = 3). Scale bar represents 5 µm.

(E and F) Representative mitochondrial stress test with Seahorse XF analyzer, with sequential injection of oligomycin, FCCP and rotenone/antimycin (E) (n = 19-23). Quantification from various biological replicates shows a significant increase of basal respiration in *MIC26* KOs cultured in both normo- and hyperglycemia (F) (N = 3).

(G) Blue native (respective left panel) and clear native (respective right panel) PAGE analysis reveals an overall increase of OXPHOS complex formation (for CI, CIII, CIV and CV, green arrows) as well as corresponding increased in-gel activity of supercomplexes, and complex III_2IV (blue arrows) upon *MIC26* deletion. CV shows no in-gel activity alterations while a decreased in-gel activity of F_1 occurs upon loss of MIC26. Native PAGEs were performed in three biological replicates and representative gels are shown.

(H) Model representing the antagonistic regulation of metabolic pathways encompassing glucose usage, lipid droplet formation, cholesterol synthesis, as well as decrease in TCA cycle metabolites in MIC26 deficient HepG2 cells dependent on nutritional conditions compared to respective WT cells. An increase of glutamine levels as well as assembly of various OXPHOS complexes is observed in *MIC26* KOs independent of the nutritional status. Arrows indicate respective up (red) or downregulated (blue) protein/metabolite or activity levels, respectively. In the model, left panel indicates normoglycemic while the right panel represents the hyperglycemic conditions.

Data are represented as mean ± SEM (B and D-F). Statistical analysis was performed using one-way ANOVA with $*P < 0.05$, $**P < 0.01$, $***P < 0.001$, $****P < 0.0001$. N represents the number of biological replicates and n the number of technical replicates.

S1 Figure

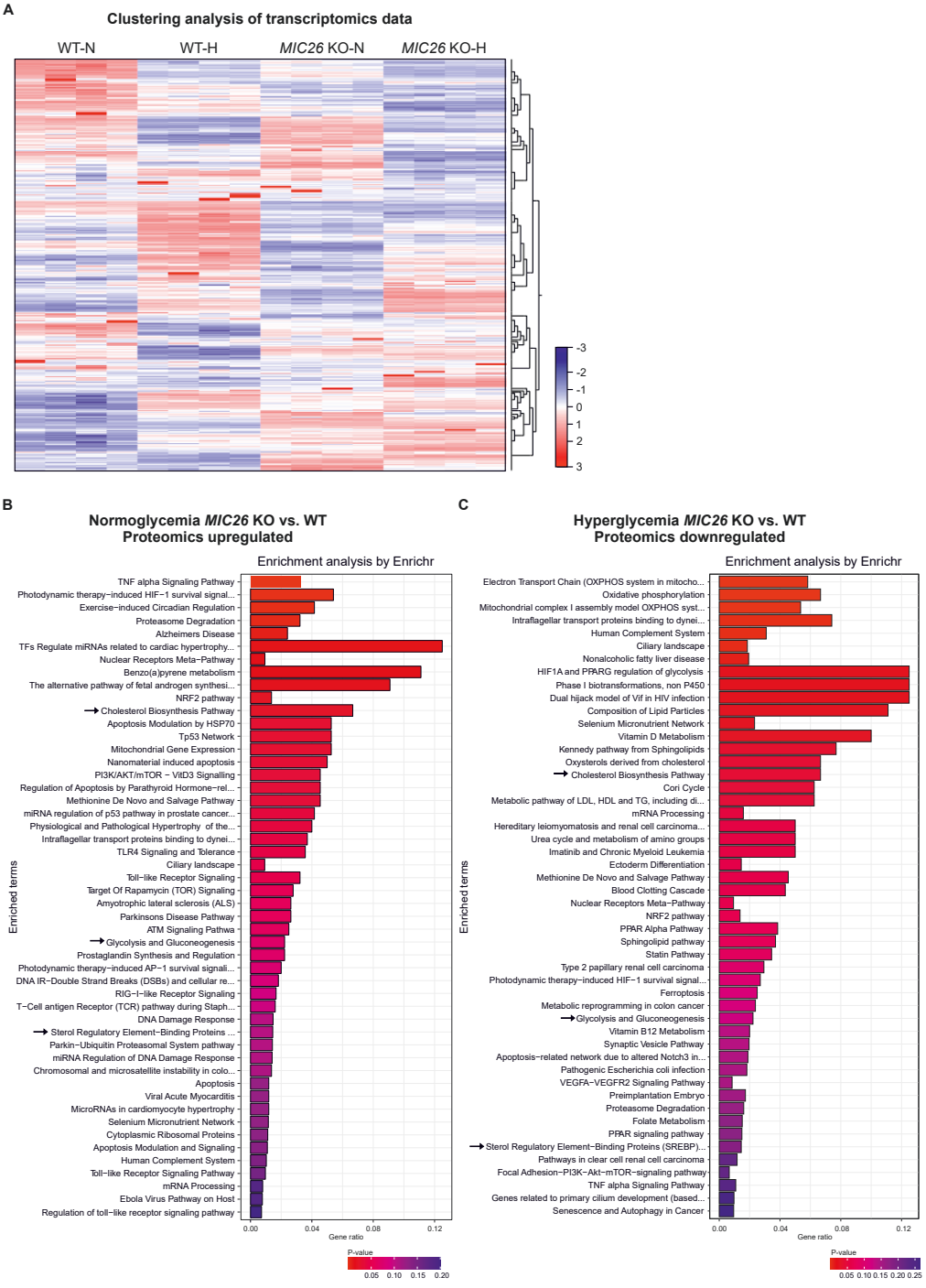
A
Clustering analysis of transcriptomics data
WT-N
WT-H
MIC26 KO-N
MIC26 KO-H
-3
-2
-1
0
1
2
3
B
Normoglycemia MIC26 KO vs. WT
Proteomics upregulated
Enrichment analysis by Enrichr
TNF alpha Signaling Pathway
Photodynamic therapy−induced HIF−1 survival signal...
Exercise−induced Circadian Regulation
Proteasome Degradation
Alzheimers Disease
TFs Regulate miRNAs related to cardiac hypertrophy...
Nuclear Receptors Meta−Pathway
Benzo(a)pyrene metabolism
The alternative pathway of fetal androgen synthesi...
NRF2 pathway
→ Cholesterol Biosynthesis Pathway
Apoptosis Modulation by HSP70
Tp53 Network
Mitochondrial Gene Expression
Nanomaterial induced apoptosis
PI3K/AKT/mTOR − VitD3 Signalling
Regulation of Apoptosis by Parathyroid Hormone−rel...
Methionine De Novo and Salvage Pathway
miRNA regulation of p53 pathway in prostate cancer...
Physiological and Pathological Hypertrophy of the...
Intraflagellar transport proteins binding to dynei...
TLR4 Signaling and Tolerance
Ciliary landscape
Toll−like Receptor Signaling
Target Of Rapamycin (TOR) Signaling
Amyotrophic lateral sclerosis (ALS)
Parkinsons Disease Pathway
ATM Signaling Pathwa
→ Glycolysis and Gluconeogenesis
Prostaglandin Synthesis and Regulation
Photodynamic therapy−induced AP−1 survival signali...
DNA IR−Double Strand Breaks (DSBs) and cellular re...
RIG−I−like Receptor Signaling
T−Cell antigen Receptor (TCR) pathway during Staph...
DNA Damage Response
→ Sterol Regulatory Element−Binding Proteins ...
Parkin−Ubiquitin Proteasomal System pathway
miRNA Regulation of DNA Damage Response
Chromosomal and microsatellite instability in colo...
Apoptosis
Viral Acute Myocarditis
MicroRNAs in cardiomyocyte hypertrophy
Selenium Micronutrient Network
Cytoplasmic Ribosomal Proteins
Apoptosis Modulation and Signaling
Human Complement System
Toll−like Receptor Signaling Pathway
mRNA Processing
Ebola Virus Pathway on Host
Regulation of toll−like receptor signaling pathway
Enriched terms
0.00
0.04
0.08
0.12
Gene ratio
P-value
0.05
0.10
0.15
0.20
C
Hyperglycemia MIC26 KO vs. WT
Proteomics downregulated
Enrichment analysis by Enrichr
Electron Transport Chain (OXPHOS system in mitocho...
Oxidative phosphorylation
Mitochondrial complex I assembly model OXPHOS syst...
Intraflagellar transport proteins binding to dynei...
Human Complement System
Ciliary landscape
Nonalcoholic fatty liver disease
HIF1A and PPARG regulation of glycolysis
Phase I biotransformations, non P450
Dual hijack model of Vif in HIV infection
Composition of Lipid Particles
Selenium Micronutrient Network
Vitamin D Metabolism
Kennedy pathway from Sphingolipids
Oxysterols derived from cholesterol
→ Cholesterol Biosynthesis Pathway
Cori Cycle
Metabolic pathway of LDL, HDL and TG, including di...
mRNA Processing
Hereditary leiomyomatosis and renal cell carcinoma...
Urea cycle and metabolism of amino groups
Imatinib and Chronic Myeloid Leukemia
Ectoderm Differentiation
Methionine De Novo and Salvage Pathway
Blood Clotting Cascade
Nuclear Receptors Meta−Pathway
NRF2 pathway
PPAR Alpha Pathway
Sphingolipid pathway
Statin Pathway
Type 2 papillary renal cell carcinoma
Photodynamic therapy−induced HIF−1 survival signal...
Ferroptosis
Metabolic reprogramming in colon cancer
→ Glycolysis and Gluconeogenesis
Vitamin B12 Metabolism
Synaptic Vesicle Pathway
Apoptosis−related network due to altered Notch3 in...
Pathogenic Escherichia coli infection
VEGFA−VEGFR2 Signaling Pathway
Preimplantation Embryo
Proteasome Degradation
Folate Metabolism
PPAR signaling pathway
→ Sterol Regulatory Element−Binding Proteins (SREBP)...
Pathways in clear cell renal cell carcinoma
Focal Adhesion−PI3K−Akt−mTOR−signaling pathway
TNF alpha Signaling Pathway
Genes related to primary cilium development (based...
Senescence and Autophagy in Cancer
Enriched terms
0.00
0.04
0.08
0.12
Gene ratio
P-value
0.05
0.10
0.15
0.20
0.25

S2 Figure

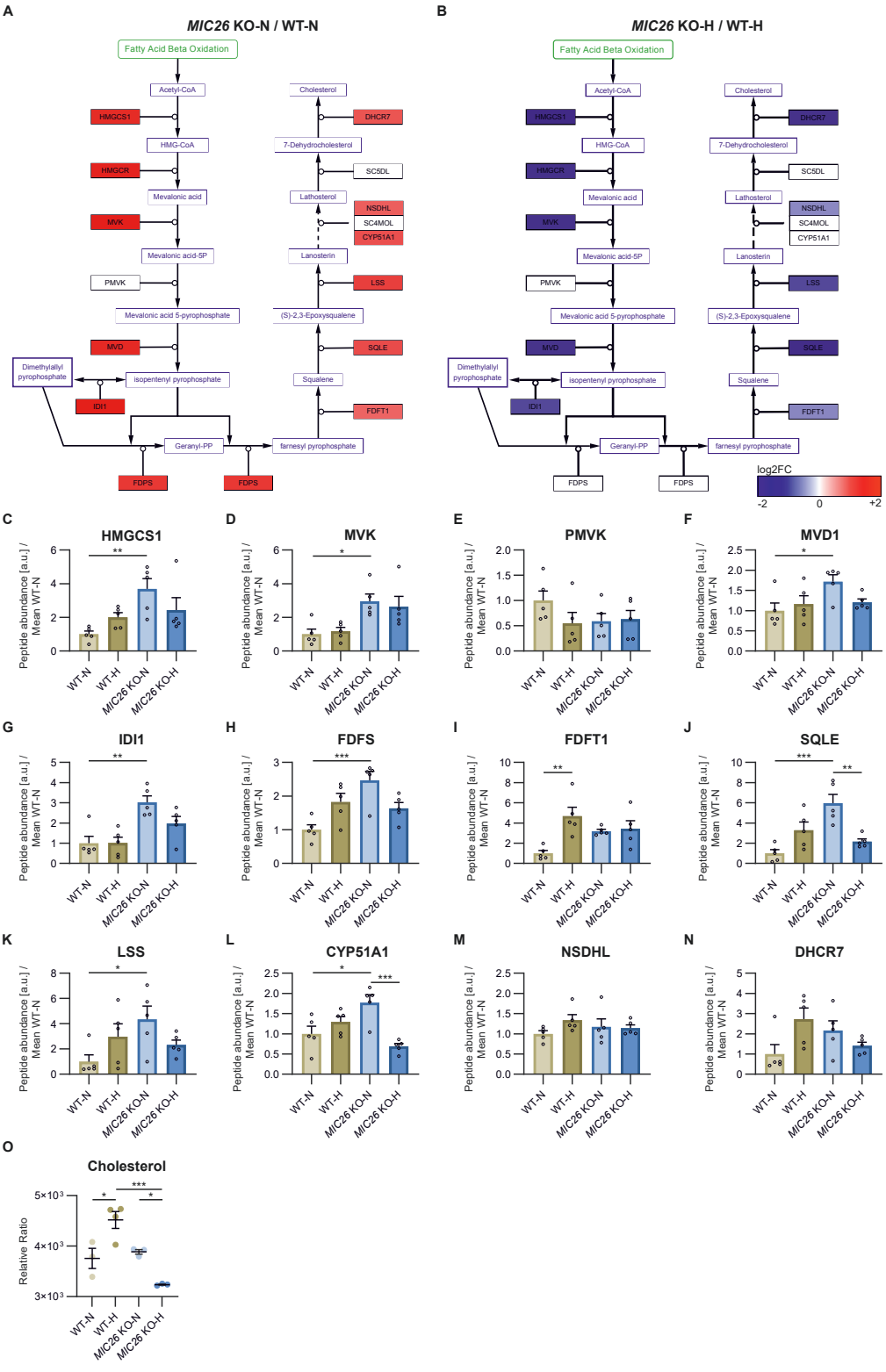
A
MIC26 KO-N / WT-N
B
MIC26 KO-H / WT-H
Fatty Acid Beta Oxidation
Acetyl-CoA
HMGCS1
HMG-CoA
HMGCR
Mevalonic acid
MVK
Mevalonic acid-5P
PMVK
Mevalonic acid 5-pyrophosphate
MVD
Dimethylallyl pyrophosphate
isopentenyl pyrophosphate
IDI1
Geranyl-PP
farnesyl pyrophosphate
FDPS
Cholesterol
DHCR7
7-Dehydrocholesterol
SC5DL
Lathosterol
NSDHL
SC4MOL
CYP51A1
Lanosterin
LSS
(S)-2,3-Epoxysqualene
SQLE
Squalene
FDFT1
log2FC
-2
0
+2
C
HMGCS1
D
MVK
E
PMVK
F
MVD1
G
IDI1
H
FDFS
I
FDFT1
J
SQLE
K
LSS
L
CYP51A1
M
NSDHL
N
DHCR7
Peptide abundance [a.u.] / Mean WT-N
WT-N
WT-H
MIC26 KO-N
MIC26 KO-H
O
Cholesterol
Relative Ratio

S3 Figure

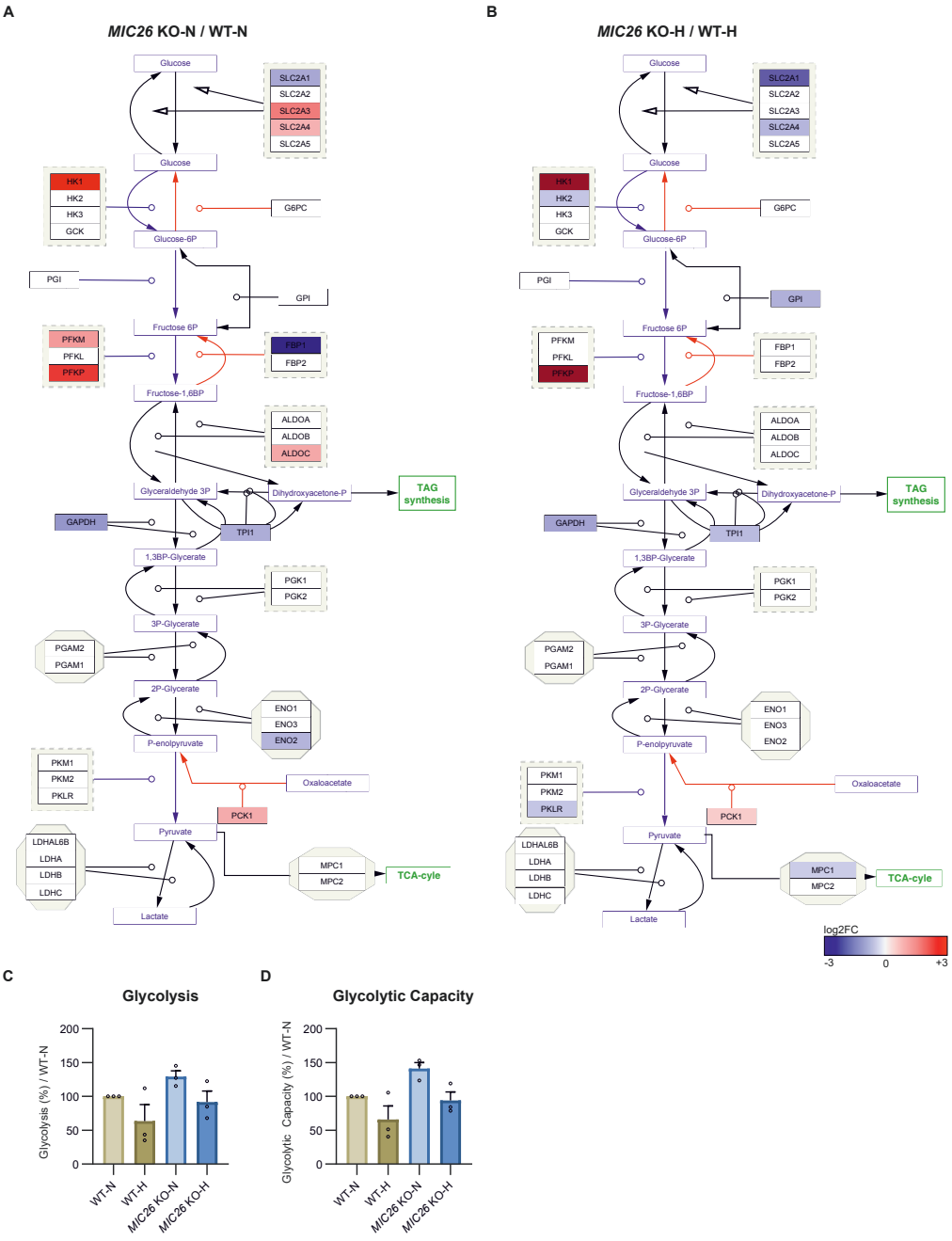
A
MIC26 KO-N / WT-N
B
MIC26 KO-H / WT-H
Glucose
SLC2A1
SLC2A2
SLC2A3
SLC2A4
SLC2A5
HK1
HK2
HK3
GCK
G6PC
Glucose-6P
PGI
GPI
Fructose 6P
PFKM
PFKL
PFKP
FBP1
FBP2
Fructose-1,6BP
ALDOA
ALDOB
ALDOC
Glyceraldehyde 3P
Dihydroxyacetone-P
TAG synthesis
GAPDH
TPI1
1,3BP-Glycerate
PGK1
PGK2
3P-Glycerate
PGAM2
PGAM1
2P-Glycerate
ENO1
ENO3
ENO2
P-enolpyruvate
PKM1
PKM2
PKLR
Oxaloacetate
PCK1
Pyruvate
LDHAL6B
LDHA
LDHB
LDHC
MPC1
MPC2
TCA-cyle
Lactate
log2FC
-3
0
+3
C
Glycolysis
Glycolysis (%) / WT-N
200
150
100
50
0
WT-N
WT-H
MIC26 KO-N
MIC26 KO-H
D
Glycolytic Capacity
Glycolytic Capacity (%) / WT-N
200
150
100
50
0
WT-N
WT-H
MIC26 KO-N
MIC26 KO-H

S4 Figure

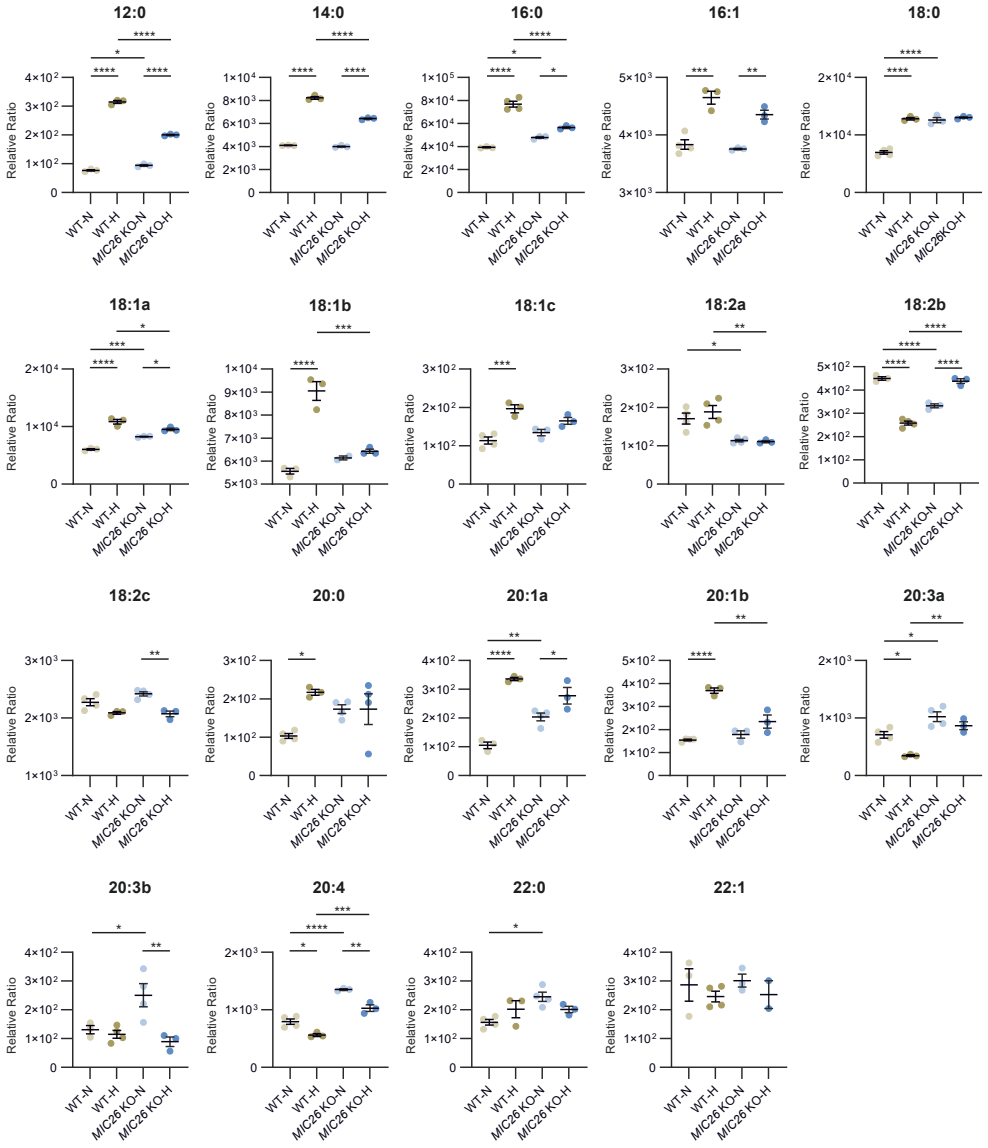
12:0
14:0
16:0
16:1
18:0
18:1a
18:1b
18:1c
18:2a
18:2b
18:2c
20:0
20:1a
20:1b
20:3a
20:3b
20:4
22:0
22:1
Relative Ratio
WT-N
WT-H
MIC26 KO-N
MIC26 KO-H

S5 Figure

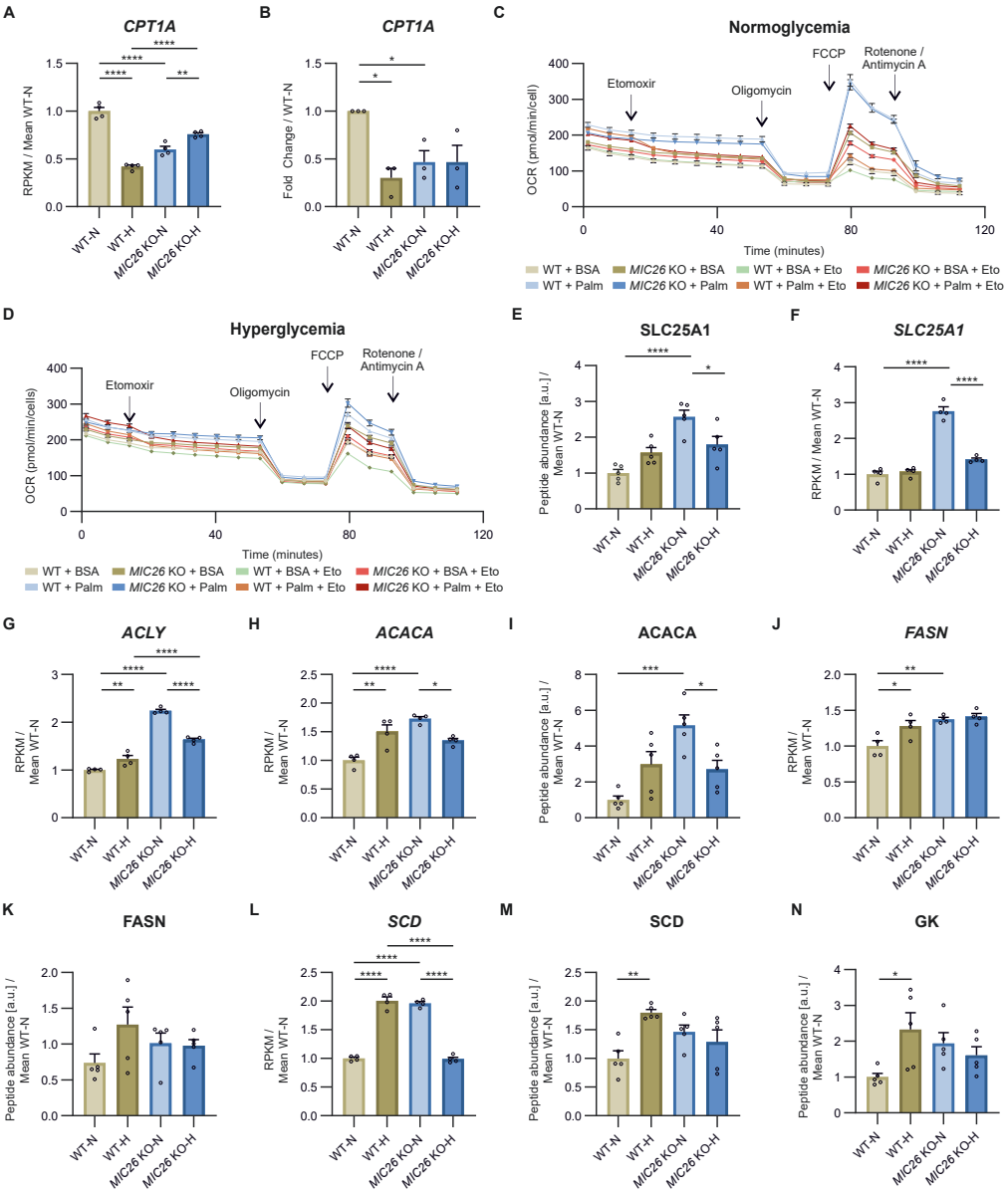
A
CPT1A
RPKM / Mean WT-N
B
CPT1A
Fold Change / WT-N
C
Normoglycemia
OCR (pmol/min/cell)
Etomoxir
Oligomycin
FCCP
Rotenone / Antimycin A
Time (minutes)
WT + BSA
MIC26 KO + BSA
WT + BSA + Eto
MIC26 KO + BSA + Eto
WT + Palm
MIC26 KO + Palm
WT + Palm + Eto
MIC26 KO + Palm + Eto
D
Hyperglycemia
E
SLC25A1
Peptide abundance [a.u.] / Mean WT-N
F
SLC25A1
RPKM / Mean WT-N
G
ACLY
H
ACACA
I
ACACA
J
FASN
K
FASN
L
SCD
M
SCD
N
GK
WT-N
WT-H
MIC26 KO-N
MIC26 KO-H

S6 Figure

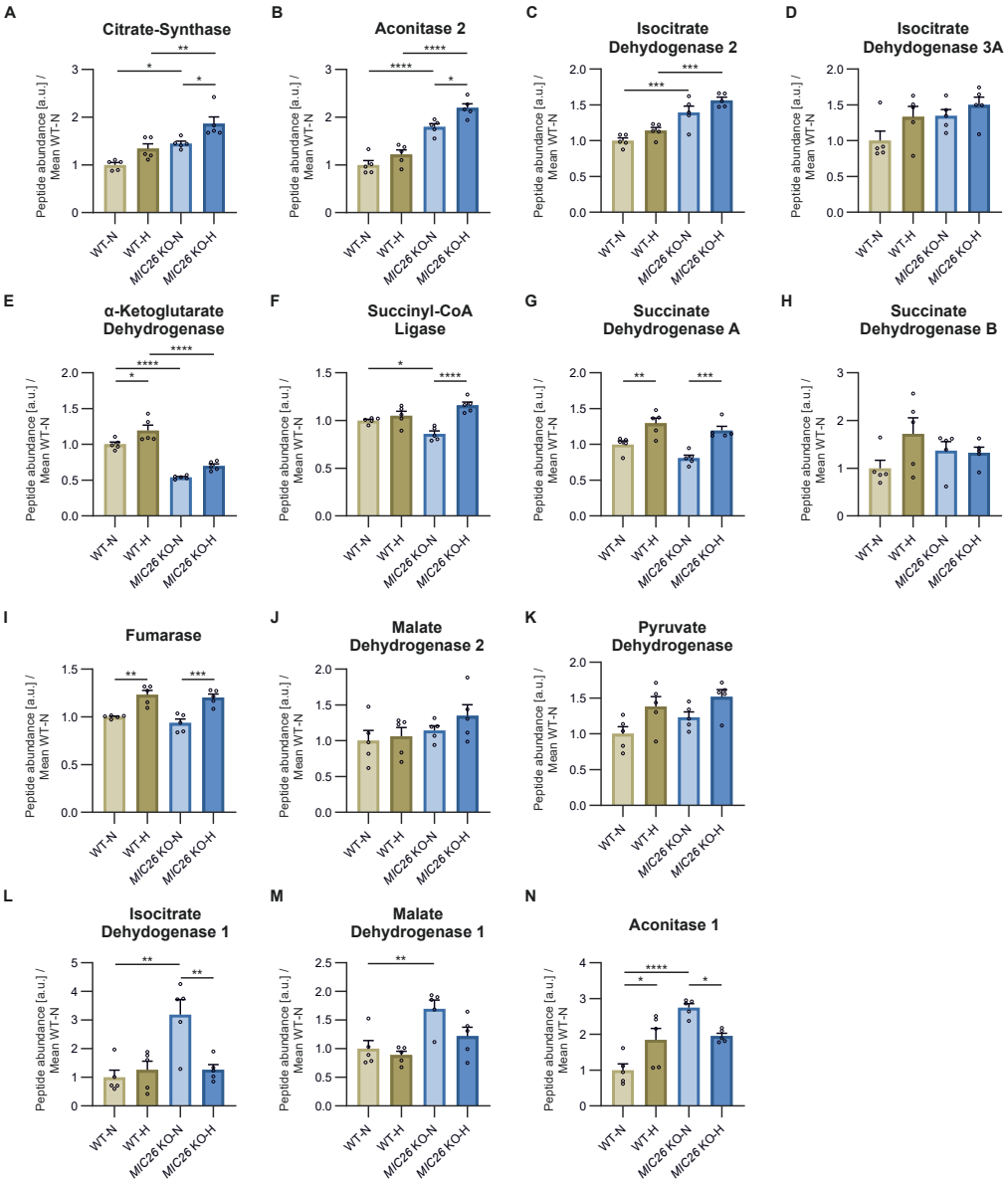
A
Citrate-Synthase
B
Aconitase 2
C
Isocitrate Dehydrogenase 2
D
Isocitrate Dehydrogenase 3A
E
α-Ketoglutarate Dehydrogenase
F
Succinyl-CoA Ligase
G
Succinate Dehydrogenase A
H
Succinate Dehydrogenase B
I
Fumarase
J
Malate Dehydrogenase 2
K
Pyruvate Dehydrogenase
L
Isocitrate Dehydrogenase 1
M
Malate Dehydrogenase 1
N
Aconitase 1
Peptide abundance [a.u.] / Mean WT-N
WT-N
WT-H
MIC26 KO-N
MIC26 KO-H

S7 Figure

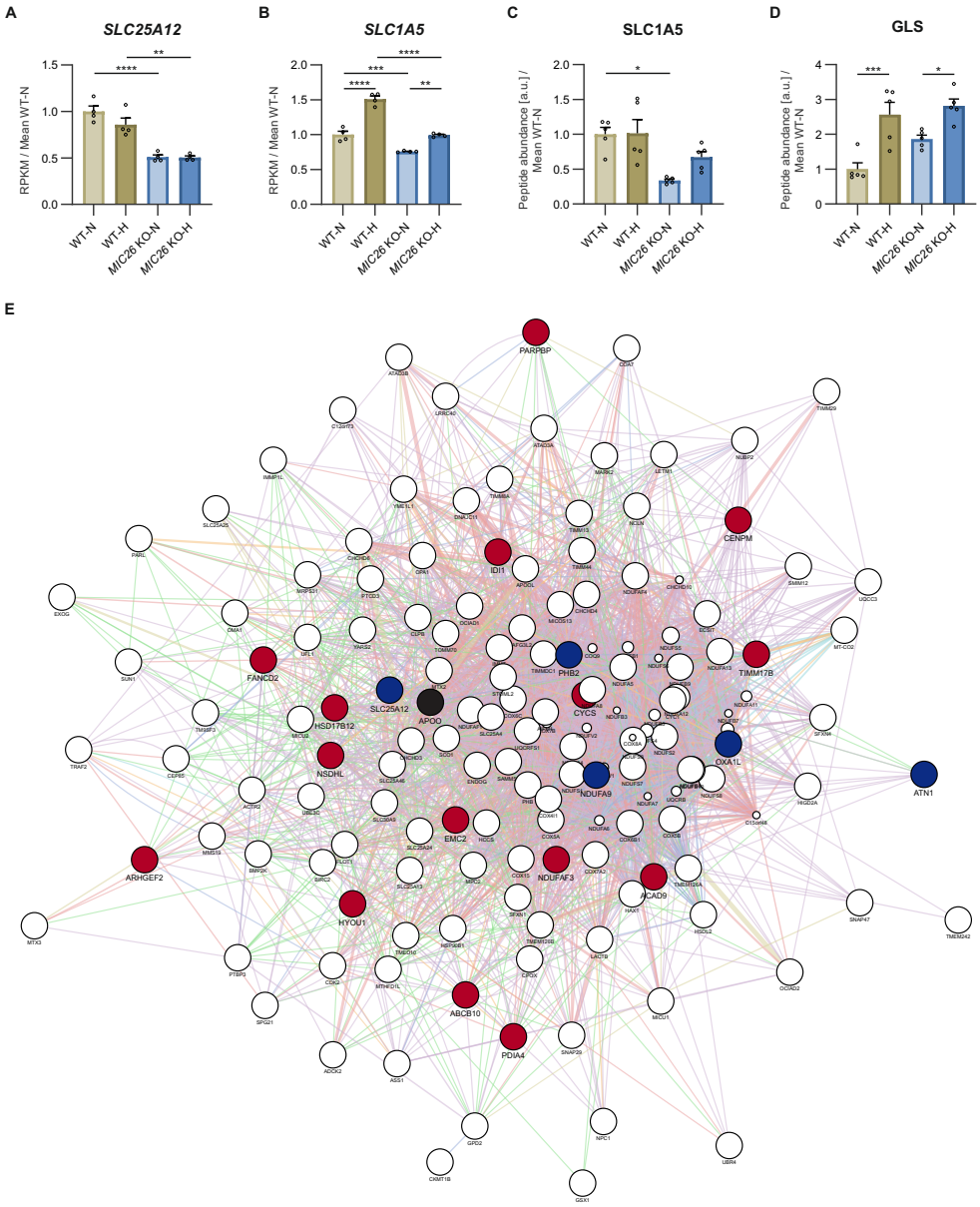
A
SLC25A12
RPKM / Mean WT-N
WT-N
WT-H
MIC26 KO-N
MIC26 KO-H
B
SLC1A5
RPKM / Mean WT-N
C
SLC1A5
Peptide abundance [a.u.] / Mean WT-N
D
GLS
Peptide abundance [a.u.] / Mean WT-N
E
PARPBP
CENPM
IDI1
FANCD2
PHB2
TIMM17B
SLC25A12
APOO
CYCS
HSD17B12
NSDHL
NDUFA9
OXA1L
ATN1
EMC2
ARHGEF2
NDUFAF3
ACAD9
HYOU1
ABCB10
PDIA4

S8 Figure

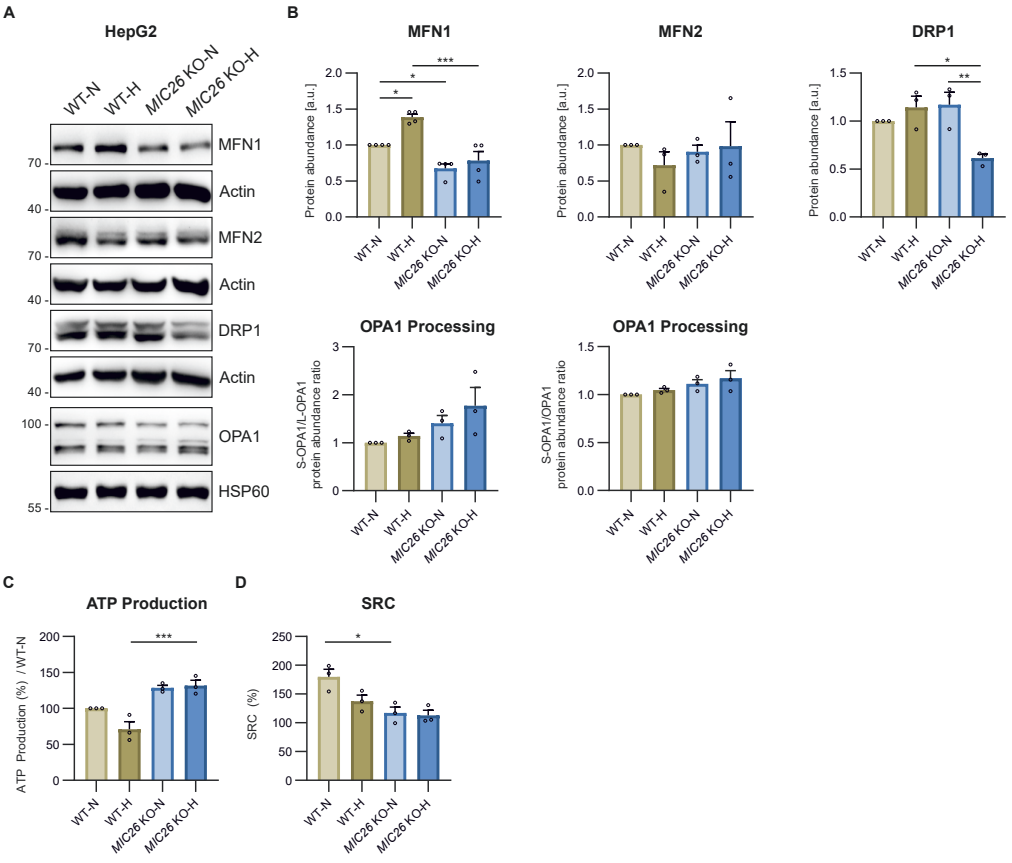
A
HepG2
WT-N
WT-H
MIC26 KO-N
MIC26 KO-H
MFN1
Actin
MFN2
Actin
DRP1
Actin
OPA1
HSP60
70
40
70
40
70
40
100
55
B
MFN1
MFN2
DRP1
Protein abundance [a.u.]
OPA1 Processing
S-OPA1/L-OPA1 protein abundance ratio
S-OPA1/OPA1 protein abundance ratio
C
ATP Production
ATP Production (%) / WT-N
D
SRC
SRC (%)

S9 Figure

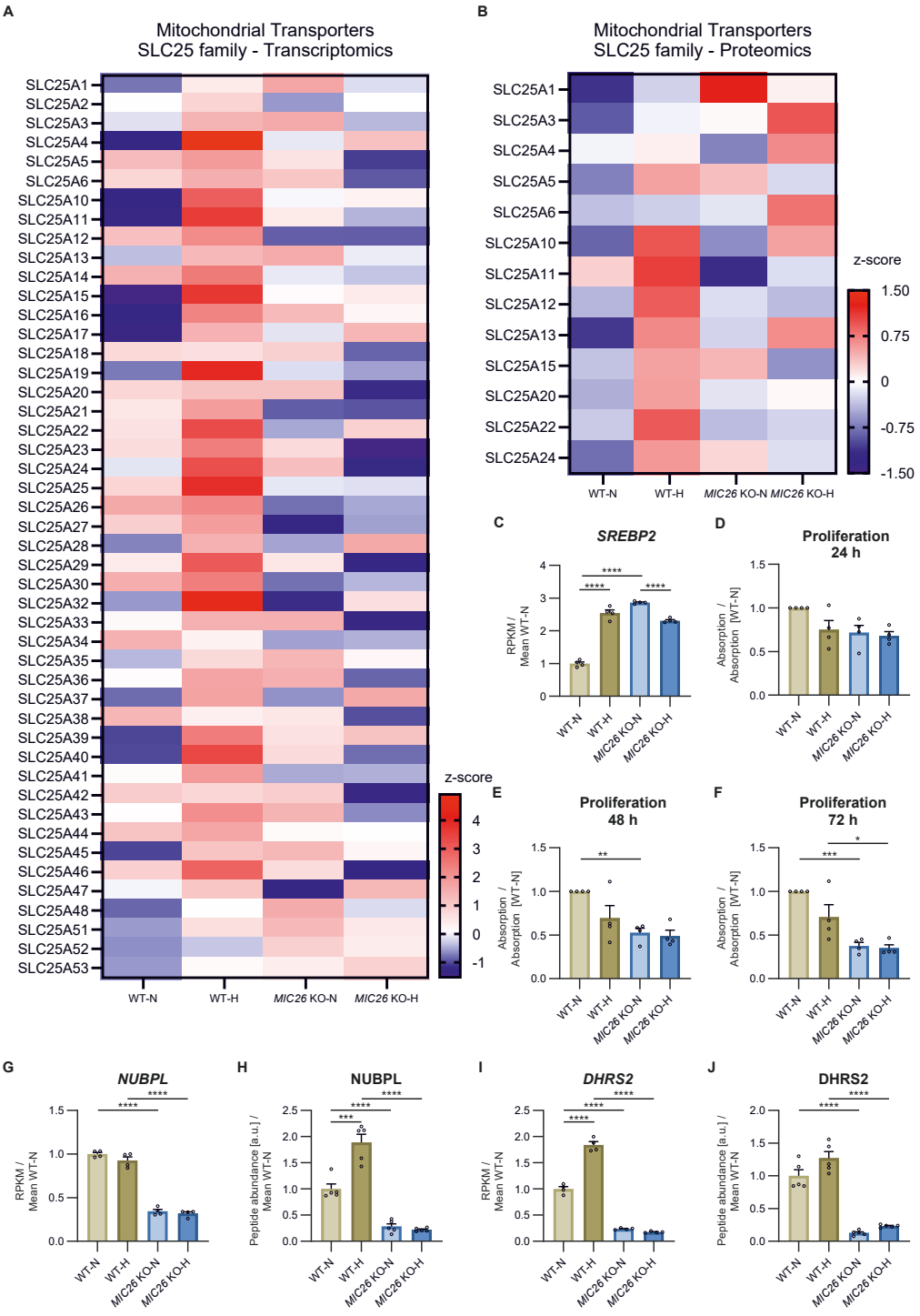
A
Mitochondrial Transporters
SLC25 family - Transcriptomics
SLC25A1
SLC25A2
SLC25A3
SLC25A4
SLC25A5
SLC25A6
SLC25A10
SLC25A11
SLC25A12
SLC25A13
SLC25A14
SLC25A15
SLC25A16
SLC25A17
SLC25A18
SLC25A19
SLC25A20
SLC25A21
SLC25A22
SLC25A23
SLC25A24
SLC25A25
SLC25A26
SLC25A27
SLC25A28
SLC25A29
SLC25A30
SLC25A32
SLC25A33
SLC25A34
SLC25A35
SLC25A36
SLC25A37
SLC25A38
SLC25A39
SLC25A40
SLC25A41
SLC25A42
SLC25A43
SLC25A44
SLC25A45
SLC25A46
SLC25A47
SLC25A48
SLC25A51
SLC25A52
SLC25A53
WT-N
WT-H
MIC26 KO-N
MIC26 KO-H
z-score
4
3
2
1
0
-1
B
Mitochondrial Transporters
SLC25 family - Proteomics
SLC25A1
SLC25A3
SLC25A4
SLC25A5
SLC25A6
SLC25A10
SLC25A11
SLC25A12
SLC25A13
SLC25A15
SLC25A20
SLC25A22
SLC25A24
WT-N
WT-H
MIC26 KO-N
MIC26 KO-H
z-score
1.50
0.75
0
-0.75
-1.50
C
SREBP2
RPKM / Mean WT-N
D
Proliferation 24 h
Absorption / Absorption [WT-N]
E
Proliferation 48 h
F
Proliferation 72 h
G
NUBPL
RPKM / Mean WT-N
H
NUBPL
Peptide abundance [a.u.] / Mean WT-N
I
DHRS2
RPKM / Mean WT-N
J
DHRS2
Peptide abundance [a.u.] / Mean WT-N

6 Discussion

The aim of this dissertation was to better understand the roles and functions of the MIC26 forms in regulating cellular metabolic processes and, to further understand resulting phenotypes from abnormalities in MIC26 protein level. Abnormalities in MIC26 expression have been described in the context of different nutritional circumstances, gene mutations or as a consequence of loss of other MICOS subunits, e.g. MIC19, MIC60, MIC13 and MIC10. In summary, the above described results contribute to a clarification of the MIC26 conundrum of two different modified MIC26 forms and showed that MIC26 is exclusively present as a 22 kDa protein in the mitochondria. Furthermore, we showed that not only overexpression but also loss of function of MIC26 is detrimental for human health and causes early-onset lethality. To gain insights into the regulatory function of MIC26, that can cause lipotoxicity and disease development in a possibly nutritional dependent manner we performed a multi-omics study revealing MIC26 to act as a metabolic rheostat, regulating mitochondrial function as well as central metabolic pathways like glycolysis, lipid and sterol metabolism in a glucose-dependent manner, and OXPHOS and glutaminolysis in a glucose-independent manner.

6.1 MIC26 regulates key cellular metabolic pathways

Balanced amounts of MIC26 have been shown throughout different model systems, including cell lines, transgenic or KO mice, dogs, and humans, to be an essential regulator of healthy life maintenance. The status of nutritional availability modulates MIC26 mRNA and protein levels. For example, feeding dogs a HFD for 9 weeks, elevated MIC26 levels in the cardiac transcriptome (Philip-Couderc et al., 2003). Diabetic patients known to be hyperglycemic showed an increased MIC26 mRNA level in the heart (Lamant et al., 2006). MIC26 mRNA was also stimulated in liver HepG2 and LMH cells by treatment with high concentrations of oleic acid (OA) (Chen-Lu Wu, 2013; Schmidinger et al., 2016). Feeding a diet enriched in oil and cholesterol for 6 weeks increased MIC26 mRNA expression in chicken liver (Schmidinger et al., 2016). In contrast, BAT from 18 weeks HFD fed mice and 8 weeks old ob/ob mice showed decreased MIC26 mRNA and protein levels (Guo et al., 2023). These opposing findings highlight the importance of classifying the type of fuel altering MIC26 levels and to considering tissue specific regulation.

MIC26 harbors an apolipoprotein signature domain but does not fulfill classical apolipoprotein functions. Classical apolipoproteins, like the most commonly described apolipoproteins ApoAI, ApoCII-III, ApoB100, or ApoE, regulate lipoprotein metabolism by stimulating their formation, stabilizing their structure, and mediating their distribution throughout the body via the bloodstream. Lipoproteins are lipid-protein particles that are rich in TAG and cholesterol, serving as energy reservoirs that mediate whole-body fuel metabolism by distributing TAG and

cholesterol between tissues (Dominiczak & Caslake, 2011; Mehta & Shapiro, 2022). The liver is the primary organ secreting endogenously formed TAG via very low-density lipoprotein (VLDL) particles. Here, the liver either uses FFA from the bloodstream or FFA/TAG generated via *de novo* lipogenesis. Thus, VLDL generation is highly sensitive to nutritional availability (Heeren & Scheja, 2021). Based on the relevance of apolipoproteins in hepatocytes, the association with lipid metabolism regulation, and the sensitivity to nutrient supplementation, we performed an unbiased multi-omics study in the hepatocyte derived cell line HepG2 using *MIC26* KO and WT control cells stimulated with either normoglycemic or hyperglycemic conditions to gain insights into the metabolic function of MIC26.
Deletion of MIC26 induces cellular metabolic rewiring with nutrition-dependent antagonistic regulation of the cholesterol biosynthesis pathway, lipid anabolism, and glycolysis, and nutrition-independent changes in glutaminolysis and OXPHOS.

6.2 Loss of MIC26 reduces cellular glutamine usage

Pyruvate, FFA and glutamine are the three major fuels consumed by mitochondria to generate energy and required cellular metabolites. By investigating the mitochondrial fuel preferences, comparing *MIC26* KO and WT cell lines, we found an independence of glutamine usage in the *MIC26* KO cell lines irrespective of the nutrient condition, while the WT had a mean 15 % dependency on glutamine. However, *MIC26* KO cells still had the capacity to oxidize glutamine as a fuel when pyruvate and FFA usage were blocked. Additionally, we observed an accumulation of glutamine at the steady state level in the *MIC26* KO cell line. Using tracing experiments, we observed that glutamine ended up in a minor reduction of glutamate (m+4) amounts in *MIC26* KO-N compared to WT-N after 0.5 h, which however equilibrated after 6h. Decreased glutamate levels after 0.5 h could derive from decreased glutamine transporter SLC1A5 levels, which have a dual localization, once in the plasma membrane and once in the mitochondrial IM (Yoo et al., 2020), and were significantly downregulated in *MIC26* KO cell lines. However, no major impairment in glutamine conversion to glutamate was observed. Following, glutamine accumulation at the steady state level could derive from other cellular pathways using glutamine, e.g. nucleotide biosynthesis. Cell proliferation requires high rates of nucleotide biosynthesis (Lane & Fan, 2015). Proliferation in *MIC26* KO cells was highly impaired, highlighting an effect of decreased glutamine usage in nucleotide biosynthesis and thus growth defects. Furthermore, in contrast to the majority of determined TCA cycle enzymes we observed an accumulation of α-KG in *MIC26* KO-H cell lines at the steady state level and also in labeled α-KG (m+5) species. We observed downregulated α-KG dehydrogenase protein levels in *MIC26* KO cell lines as well as an increased conversion from glutamate to α-KG and decreased conversion from α-KG to succinate as well as citrate. Thus, the accumulation of α-KG could promote a reverse conversion of α-KG towards glutamine. This

could explain that *MIC26* KO cells appeared to be glutamine independent, based on compensatory usage of accumulated α-KG levels for mitochondrial respiration. Furthermore, a possible interaction of MIC26 with the glutamate importer SLC25A12 (AGC1/ARALAR) was reported on BioGRID. Decreased mitochondrial glutamate import could promote cytosolic glutamate accumulation and stimulate the reconversion to glutamine. A recent study also reported MIC60 to interact with several mitochondrial IM transporters including the 2-oxoglutarate/malate carrier SLC25A11 and the glutamate/H+ symporter SLC25A22 (Feng et al., 2023). SLC25A11 protein level were also highly downregulated in *MIC26* KO cell lines while SLC25A22 protein level were exclusively reduced upon the hyperglycemia *MIC26* KO to WT comparison, reflecting that IM presence of MIC26 influences the transporter protein presence. MIC60 and MIC26, both subunits of the MICOS complex, are located in close proximity to each other. Interactions with several SLC25 proteins involved in metabolite transport suggest a crucial role of the MICOS complex in mitochondrial fuel and metabolite regulations.

Overall, we demonstrated that MIC26 is involved in cellular glutamine usage, and the loss of *MIC26* leads to an independence of glutamine as a fuel. Further, we observed a dysregulation of α-KG usage. Interestingly, MIC26 presumably interacts with the glutamate aspartate transporter SLC25A12/A13 and downregulates SLC25A12 and SLC1A5 protein levels, which could lead to alterations of mitochondrial glutamine and glutamate import.

6.3 MIC26 mediates the glycolytic switch

We demonstrated that under normoglycemia, the loss of MIC26 increases cellular glucose uptake, presumably through the upregulation of GLUT3 protein levels. However, this did not result in an increase in the steady-state levels of glucose, pyruvate, or lactate. Investigation of glycolytic function showed a non-significant increase in glycolysis under basal conditions, consistent with equal steady-state lactate and pyruvate metabolites. Forced glycolytic ATP generation, via the inhibition of mitochondrial energy production, revealed an elevated glycolytic reserve in *MIC26* KO cells.

Peptide abundances of glycolytic enzymes represented an upregulation of aldolase (ALDOC), while glycerol-aldehyde dehydrogenase (GAPDH) was downregulated. This antagonistic effect prompted us to check further glycolysis derived metabolites except for glycolysis end products. Glycerol-3-phosphate (G3P) was significantly upregulated in *MIC26* KO cells. Along with increased glucose uptake, that did not accumulate in glucose or glycolysis end products, we hypothesized a channeling of glycolysis intermediates towards lipid anabolism. In hyperglycemia, the loss of MIC26 led to an enormous accumulation of glucose. Functional characterization of glucose uptake, glycolysis, and glycolytic reserve did not reveal any significant alterations compared to the respective WT group. However, glycerol-6-phosphate

isomerase (GPI) and GAPDH were significantly downregulated. Furthermore, pyruvate, lactate, and G3P levels were significantly decreased in *MIC26* KO-H.

The glycolytic switch, describing the shift from OXPHOS to glycolysis, is a well described phenomenon upon mitochondrial dysfunction. However, mitochondrial dysfunction is a broad term describing several mitochondrial abnormalities. Impaired OXPHOS (Rafikov et al., 2015), increased mitochondrial fragmentation (Guido et al., 2012) and abnormalities in mitochondrial ultrastructure, which are mostly interconnected occurring phenotypes were reported to induce an increased glycolytic switch (Scrimieri et al., 2023). Loss of MIC26 promoted mitochondrial fragmentation and loss of mitochondrial cristae and CJs independent of the respective nutritional condition. However, we observed increased CI, III-V assembly, increased CI, CIII-IV in gel activity, maintained CV in gel activity, and increased basal mitochondrial respiration and slightly increased ATP production in MIC26 deleted cells compared to the respective WT cells. Furthermore, tracing experiments revealed an increased conversion rate of succinate to fumarate within the TCA cycle mediated by CII. Together we concluded that under basal conditions, *MIC26* KO leads to an upregulation and increased activity of the OXPHOS machinery. The upregulation of OXPHOS assembly and activity could either derive from altered membrane structure and composition or could serve as a compensatory mechanism to increase the reduced mitochondrial membrane potential. Thus, under basal and normoglycemic conditions, OXPHOS ATP generation is increased upon MIC26 deletion. Following, cells do not require increased glycolytic function for energy generation and redirect glycolysis intermediates towards increased energy storage via lipid anabolism. Nutritional overload, here mimicked via hyperglycemia treatment, is known to cause increased energy storage, and in line, we observed an increase in all metabolites, including glucose, lactate, pyruvate, and G3P compared to normoglycemic conditions. However, the comparison of *MIC26* KO-H to WT-H reveals an accumulation of glucose which is not channeled into increased pyruvate, lactate, or G3P. ATP levels are known to fulfill feedback inhibition of glycolytic function, regulating phosphofructokinase (PFK) activity (Locasale, 2018). Basal respiration, complex activity as well as calculated ATP production were significantly increased in *MIC26* KO-H cells while WT-H showed an enormous impairment in basal respiration and supercomplex and CV_n formation, and decreased ATP levels. Thus, we conclude that the loss of *MIC26* under hyperglycemia is unable to deal with glucose overload and leads to decreased energy storage in the form of LD channeling while WT-H cells increase glycolysis to accompany decreased OXPHOS.

In conclusion, this highlights an essential role of MIC26 in mediating cellular glycolytic function. Here, we showed that MIC26 has a nutritional dependent role in handling glucose availability by mediating proper utilization under normoglycemic conditions and storing energy under hyperglycemic conditions. These findings explain the observed upregulation of MIC26 levels

in nutrient stimulated WT-H cells as well as in other previously described studies (Chen-Lu Wu, 2013; Lamant et al., 2006), to induce an adaptive cellular mechanism to deal with increased nutrient availability.

6.4 MIC26 induces nutrient dependent rewiring of lipid and cholesterol biosynthesis

Even though MIC26 is not performing classical apolipoprotein functions in term of undergoing secretion within binding to lipoprotein particles, domain homology with the apolipoproteins A1/A4/E, however, suggest a possible role of MIC26 in lipoprotein metabolism. Lipoproteins are responsible for maintaining whole body lipid and cholesterol metabolism. Mitochondria are known to perform steroidogenesis (Bassi et al., 2021), using cholesterol e.g. delivered via lipoprotein particles, but also mediate cellular lipid metabolism (Aon et al., 2014).
Transcriptomics analysis from whole cell HepG2 mitochondria revealed differential regulation of FAO and cholesterol biosynthesis in a nutrient dependent manner after *MIC26* deletion. Along with an antagonistic regulation of G3P levels we were prompted to explore lipid metabolism. Overall loss of *MIC26* induced an increase in the number of LDs. However, LD intensity was increased in normoglycemic conditions and decreased in hyperglycemic conditions stimulated with palmitate. This aligns with an antagonistic regulation showing a similar trend for the majority of investigated FFA. We showed that increased lipid accumulation in *MIC26* KO-N compared to WT-N derived from increased *de novo* lipid synthesis, via an upregulation of a range of essential enzymes regulating this pathway, and a downregulation of FAO partially mediated via decreased levels and activity of CPT1A.
In hyperglycemia, comparing *MIC26* KO and WT cell lines, FAO, CPT1A levels and activity, as well as protein levels of *de novo* lipogenesis enzymes, showed no alteration. However, *de novo* lipid synthesis requires the starting metabolites G3P, which was downregulated as previously described, as well as citrate. Citrate is mainly synthesized via the mitochondrial TCA cycle. Investigations of the TCA cycle metabolites showed, except for α-KG, a constant and high decrease in *MIC26* KO compared to respective WT cell lines. Hence, we hypothesize that the previously described accumulation in glucose levels causes a deficiency in pyruvate and subsequent TCA cycle metabolites, including citrate, leading to decreased lipogenesis resulting from a lack of starting material comparing *MIC26* KO-H and WT-H cell lines. Mitochondrial fuel dependent adaptation in light of altered fusion fission processes have been frequently observed (Liesa & Shirihai, 2013). Cellular fuel overload increases mitochondrial fragmentation while starvation promotes mitochondrial elongation (Gomes et al., 2011). Overall high glucose levels are known to reduce FAO with a pronounced effect of chronic hyperglycemia (Aas et al., 2011). Further increased LD accumulation upon high glucose treatment was shown with cellular 3D ultrastructural analysis (Scrimieri et al., 2023). A key mediator of this effect is decreased activity of CPT1A (Visiedo et al., 2013). Accordingly, with

these reported effects, cells supplemented with high glucose amounts for a prolonged time period compared to cells treated with low glucose amounts showed a fragmented mitochondrial morphology, which was in line with cell type independent overall decreased FAO accompanied by reduced CPT1A protein levels and overall increased LD accumulation. FAO and CTP1A levels showed no differences between both cell types. Hence, altered FAO does not grossly contribute to the observed metabolic phenotype in *MIC26* KO hyperglycemia. Comparable to the effect of elevated LD accumulation, decreased FAO and CPT1A expression caused by hyperglycemia, the absence of *MIC26* KO cells maintained in normoglycemia exhibited a similar lipid metabolism phenotype. Here, even though there was no increased nutrient availability, *MIC26* KO-N cells also showed a shift to a fragmented mitochondrial morphology. The key driver of this effect was a decreased level of MFN1, while MFN2, OPA1, and DRP1 protein levels were maintained. Recently, it was reported that mitochondrial fragmentation stimulates mitochondrial FAO oxidation by increased activity of CPT1A. Increased activity of CPT1A was accomplished by decreased accessibility of the inhibitory malonyl-CoA binding pocket. However, these processes were mainly investigated upon short time excess of FFA. We observed reduced CPT1A level, presumably based on genetic mitochondrial modifications in *MIC26* KO-N. CPT1A activity undergoes regulation through two primary mechanisms: transcriptional control mediated by PPARα and peroxisome proliferator-activated receptor gamma coactivator 1 alpha (PGC-1α), and allosteric inhibition via malonyl-CoA (Lopez-Vinas et al., 2007; Song et al., 2010). A recent investigation showed a reduction in PPARα protein levels within brown adipose tissue (BAT) of adipose tissue-specific *MIC26* KO mice (Guo et al., 2023). Following, even though we had a fragmented mitochondrial phenotype that increases membrane curvature and promotes CPT1A activity, this was not able to compensate for the loss of CPT1A protein levels. Moreover, a notable elevation in the activity of ACACA enzyme, responsible for converting acetyl-CoA to malonyl-CoA during de novo lipogenesis, was observed. Malonyl-CoA levels induce feedback inhibition of CPT1A, which can further stimulate reduced CPT1A activity and thus FAO. Overall inhibition of CPT1A led to a decrease in OCR, which was not significant. However, the effect on palmitate induced basal respiration and SRC was more pronounced. Except for reduction in CPT1A, deletion of *MIC26* altered the transcript and protein levels of a range of IM transporters. Citrate is generated in the mitochondrial TCA cycle and exported via the citrate malate antiporter CIC (SLC25A1). CIC is highly expressed in adipose as well as liver tissue, and high levels were reported to correlate with human nonalcoholic steatohepatitis (NASH) disease as well as in mice fed a HFD. Inhibition of CIC in mice resulted in decreased cholesterol and TAG levels and protected from steatosis as well as liver injury (Tan et al., 2020). CIC protein levels were highly elevated in the *MIC26* KO cell line under normoglycemic conditions. Hence, loss of *MIC26* leads to an increased citrate metabolite channeling from mitochondria to the cytosol

promoting cholesterol biosynthesis as well as *de novo* lipid synthesis. A significant impaired expression of mRNA levels from the mitochondrial transporter SLC25A47 (*MIC26* KO-N vs. WT-N log2FC = -1.53) was furthermore observed. Recent publications characterized the role of the liver specific transporter SLC25A47, which was correlated to cellular lipid content and cholesterol levels as well as NAD^+ transport (Bresciani et al., 2022; Cheng et al., 2023). *Slc25a47* KO mice showed a strong upregulation of *de novo* lipogenesis enzyme and cholesterol biosynthesis enzyme transcript levels, which were correlated to decreased AMP kinase α (AMPKα) phosphorylation as well as SREBP1 and majorly SREBP2 upregulation. These mice gained increased liver weight and DAG, TAG, FFA, and CL levels. Furthermore, deletion caused decreased NAD^+ uptake into mitochondria. Loss of *MIC26* reduces the expression of SLC25A47 in normoglycemia, and slightly, but not significantly, increased the expression in hyperglycemia. Till today, no direct protein-protein interactions between MIC26 and SLC25A47 have been demonstrated. However, the observed phenotype shows high similarities to the observed MIC26 phenotype regarding cholesterol and lipid metabolism and is also in line with an observed antagonistic regulation comparing normo- and hyperglycemia. This suggests that MIC26 might regulate cholesterol and lipid metabolism together with or via SLC25A47. Employing the interactome of MIC26 and comparing it to the significantly altered transcripts in *MIC26* KO cell lines we found an upregulation of acyl-CoA dehydrogenase 9 (ACAD9). ACAD9 was reported to fulfill two distinct functions, first, upon binding of FAD in the catalytic pocket of ACAD9, it acts in the first step of FAO, converting acyl-CoA into enoyl-CoA, and second upon the release of FAD, it promotes CI assembly (Giachin et al., 2021; Nouws et al., 2014). Loss of *MIC26* promoted the expression of ACAD9 as well as CI assembly, while FAO was reduced. Possible protein-protein interactions of MIC26 and ACAD9 (Antonicka et al., 2020) suggest a role of MIC26 in regulating the function of ACAD9 promoting FAO.

Besides effects of MIC26 on lipid metabolism, also MICOS subunit MIC19 was reported to influence cellular lipid metabolism. A recent study investigated *MIC19* liver specific KO mice and reported abnormal fatty acid metabolism, with increased FFA and TAG level (Dong et al., 2024). Interestingly they also reported reductions of CPT1A, CPT2 and ACAD9 mRNA level in fasted but not fed mice. Important to mention is, that MIC19 loss led to a strong decrease in MIC10 protein level in these mice, which in turn is reported to strongly reduce MIC26 protein level (Stephan et al., 2020). Effects on the FAO enzymes CPT1A, CPT2 and ACAD9 in a nutrient dependent manner further strengthens the hypothesis of a nutrient dependent sensing of the MICOS complex or MIC26 alone.

Additionally, they reported MIC19 to interact with SLC25A46 and that loss of MIC19 reduces besides MIC10, MIC60 and MIC13 also SLC25A46 protein level (Dong et al., 2024). The OM protein SLC25A46 interacts with the EMC ER membrane complex and facilitates ER-

mitochondrial lipid transfer (Janer et al., 2016). Together these data suggest that the integrity of the MICOS complex is crucial to maintain mitochondrial and cellular lipid metabolism.
It has been shown, that a particular cellular population of mitochondria build up direct contacts with LDs, termed peridroplet mitochondria (PDM), while the population not associated with mitochondria is termed cytoplasmic mitochondria (CM) (Benador et al., 2018). In the context of PDM, controversial results showed on the one hand that they either promote FAO (Talari et al., 2023) or support TAG synthesis and LD expansion (Benador et al., 2018). These opposing results can either derive from the different used target tissues, liver and BAT respectively, or from different nutritional circumstances. MIC26 is located at the neck of cristae as part of the MICOS complex. With this central mitochondrial location, MIC26 can possibly serve as an interaction module with several mitochondrial compartments, including the cristae lumen, the IMS as well as the mitochondrial matrix. This central location could allow MIC26 to function as a sensor for mitochondrial lipid environment and energy requirements. Therefore, MIC26 would serve as an interesting candidate to investigate protein function in terms of mediating a nutrient dependent switch of PDM supporting TAG synthesis and LD expansion or favoring energy generation via promotion of FAO. This hypothesis is supported by MIC26 sensitive expression to different nutritional stimuli, as well as the development of lipid metabolism abnormalities, when MIC26 is overexpressed, or downregulated.
In summary, this also points towards a possible role of MICOS in the context of PDM association. Importantly, MIC26 is not inducing loss of further MICOS subunit protein level, while in turn deletion of several other MICOS subunits, including MIC60, MIC19, MIC10 and MIC13 causes defects in MIC26 protein level. The effect of MICOS on lipid metabolism alterations following has to be considered as an influence via the MIC26 axis, when interpreting data on lipid metabolism of the other above mentioned MICOS subunits.
Overall, we observed that MIC26 regulates cellular cholesterol and lipid metabolism, including *de novo* lipogenesis and FAO, by preventing ectopic lipid accumulation upon normoglycemic conditions and thus preventing possible disease development, including NAFLD or IR. In hyperglycemia, MIC26 is essential to mediate the switch to increased glucose utilization and energy storage in the form of LD.

6.5 MIC26 abnormalities are detrimental for human health

MIC26 has been described, on the one hand, to correlate with nutritional overload, cardiomyopathy, NAFLD, and diabetes-like phenotypes (Lamant et al., 2006; Tian et al., 2017; Turkieh et al., 2014). On the other hand, it has been reported to cause a pathogenic phenotype, including lactic acidosis, cognitive impairment with autistic features, and X-linked recessive mitochondrial myopathy in the case of a MIC26^{I117T} mutation (Beninca et al., 2021; Turkieh et

al., 2014). The National Library of Medicine records various clinical variants of MIC26/ApoO. including the mutations V35M, V45F, T75K, I117T, G163A, and L166V. However, most of them have not been further investigated. Recently, we reported the *APOO/MIC26* (NM_024122.5):c.532G>T (p.E178*) variant, which caused a mitochondrial disease with progeria-like phenotypes, resulting in lethality for two infants at the ages of 12 or 18 months (Peifer-Weiss et al., 2023). Both patients exhibited combined B and T cell immunodeficiencies, recurrent bacterial and fungal infections, and an overall progeria-like phenotype with failure to thrive.

Progeria, also termed Hutchinson-Gilford Progeria Syndrome (HGPS), is mostly induced via a single nucleotide substitution in the LMNA gene, leading to a 50 AA truncated Lamin^{G608G} protein variant termed progerin (Eriksson et al., 2003). Progerin, in contrast to Lamin, lacks the ability to properly integrate into the inner nuclear membrane, resulting in abnormal nuclear morphology and severely perturbed nucleus functions related to gene expression and epigenetic regulation (Constantinescu et al., 2010; Goldman et al., 2002; Liu et al., 2006). These dysfunctions induce a faster aging phenotype (McClintock et al., 2007), accompanied by increased inflammation, DNA damage, and general metabolic dysfunction (Kreienkamp & Gonzalo, 2020). Investigations of patient derived fibroblast and progeria mouse models revealed mitochondrial dysfunction, including impaired OXPHOS machinery, reduced ATP production, and an upregulation of glycolytic enzymes (Lopez-Mejia et al., 2014; Rivera-Torres et al., 2013; Villa-Bellosta et al., 2013). Furthermore, mitochondrial dysfunction has been described to induce excessive vascular calcification and the loss of vascular smooth muscle cells (VSMC), which is one of the main characteristics of HGPS (Villa-Bellosta et al., 2013).

In line with the reported mitochondrial dysfunctions in HGPS disease, the clinically occurring MIC26^{E178} mutant also exhibited abnormal mitochondrial ultrastructure with previously reported impaired mitochondrial respiration and a change in glycolytic function (Guo et al., 2023; Koob et al., 2015b). However, it remains to be investigated whether mitochondrial dysfunction induced by the MIC26 loss of function mutation can lead to abnormal nuclear morphology and function. An example of a mitochondrial protein investigated in this regard is MTX2, located in the IMS and crucial for the formation of the MIB complex. A recessive mutation in MTX2, similar to MIC26^{E178}, was reported to lead to a disease with clinical features resembling HGPS. Patient derived fibroblast showed mitochondrial fragmentation and impaired OXPHOS protein levels, hinting towards reduced ATP production. Interestingly, MTX2 deficiency induced nuclear defects in fibroblast and *C. elegans*, similar to the progerin induced phenotype in HGPS (Elouej et al., 2020). This suggests a possible primary role of mitochondrial dysfunction in retrograde signaling and the induction of nuclear defects, promoting HGPS-like disease progression. Mitochondrial retrograde signaling includes mitochondrial membrane potential, ROS signaling, and changes in TCA cycle metabolites, which are essential for several metabolic functions,

including nuclear functions (Butow & Avadhani, 2004). Similar to the observed MIC26^{E178} mutant phenotypes, early onset clinical abnormalities, including neurodegenerative abnormalities, hypotonia, lactic acidosis, and failure to thrive were reported in cases of α-KG dehydrogenase deficiency, further linking mitochondrial retrograde signaling via TCA cycle metabolite impairments to metabolic disease progression (Bonnefont et al., 1992; Rustin et al., 1997). In context of the before described results of a decreased conversion rate of α-KG via the α-KG dehydrogenase, which in turn showed decreased protein level in the HepG2 *MIC26* KO cell line, abnormalities of MIC26 might lead to an impaired mitochondrial retrograde signaling. Further, we could also observe a major growth deficiency in HepG2 *MIC26* KO cells which in turn could derive from decreased cellular glutamine usage, which is an essential source for generation of purine, pyrimidine and AA synthesis and thus might reflect the outcome of failure to thrive.

In light of the first study investigating a patient loss of function mutation of MIC26, we can conclude that alterations of MIC26 protein levels either upregulated (Tian et al., 2017; Turkieh et al., 2014) or depleted (Peifer-Weiss et al., 2023) lead to severe disease outcomes in vivo. MIC27 protein levels have been reported to be antagonistically regulated, when MIC26 is overexpressed (Koob et al., 2015b) or deleted (Anand et al., 2020). As MIC26 and MIC27 share a high sequence homology this phenome raises the question if MIC27 is able to fulfill similar functions as MIC26, to safeguard inconsistencies in MIC26 protein level. However, the antagonistic regulation of MIC26 and MIC27 protein levels seem to be a cell line dependent effect, which we observed majorly in HAP1 and HeLa cells, but not in HEK and HepG2 cells.

Worth mentioning is that elevated expression of MIC27 in patient mimetic cells can not compensate for MIC26 loss in terms of human health and is thus not able to rescue the MIC26 loss of function phenotypes. Following, it is important to consider both proteins to fulfill distinct mitochondrial functions, rather than overlapping functions. The patient phenotypes of lactic acidosis and failure to thrive strengths the hypothesis of MIC26 as a mitochondrial regulator of cellular metabolism and the availability of metabolites.

By mediating cellular lipid metabolism, MIC26 is an interesting candidate to study the development of NAFLD, IR, and diabetes. Studies showed that dysfunctional mitochondria in terms of insufficient oxidation of FFA serves as an source of DAG accumulation and thus can induce insulin resistance (Aon et al., 2014). Overexpression of MIC26 was also reported to induce DAG level and lipotoxicity (Turkieh et al., 2014) and could thus lead to a development of IR under abnormal regulation of MIC26 protein level. In our study we also observed an ectopic accumulation of FFA and LDs even under standard cultivation conditions upon the loss of MIC26. Accumulation of lipids in non-adipose tissues, e.g. the liver, can cause NAFLD or non-alcoholic steatohepatitis (Bence & Birnbaum, 2021; Sheka et al., 2020). Investigations of DAG and ceramide level as well as the cellular insulin signaling cascade would contribute to

understand a possible role of MIC26 in IR development. When we investigated mRNA and protein level in the db/db mouse model we could not observe alterations in MIC26 and MIC27 expression compared to db/+ mice. This could however be a model dependent effect, due to that in patients with diabetes MIC26 mRNA level have been increased. Following, it might be possible that other factors, like high fat and high sucrose diet, mediate MIC26 expression, which then in turn could lead to disease development. Besides a correlation between MIC26 and diabetes, also MIC60 and MIC19 were reported in this context. A reduction in MIC60 protein levels has been reported in the context of STZ induced diabetes in interfibrillar mitochondria (Baseler et al., 2011). Overexpression of MIC60 in STZ induces diabetes rescued ETC activities, mitochondrial ultrastructure, defective lipid peroxidation and attenuated diabetes associated cardiac and mitochondrial dysfunction (Thapa et al., 2015).
Ectopic expression of MIC19 in the liver was demonstrated to protect against obesity and T2D by an increase in energy expenditure (Sohn et al., 2023).
Important to mention is that MIC26 protein level are highly decreased by deletion of MIC60 and MIC19 proteins, which raises the possibility of the MICOS complex as a unit being a lipid metabolism regulator via the MIC26 axis and thus playing a crucial role for mitochondrial function and in the development of metabolic diseases like diabetes and NAFLD.

6.6 Conclusion and outlook

This dissertation aimed to investigate the role of the two earlier postulated MIC26 forms in the cellular lipid metabolism and mitochondrial functioning, to lay the ground for further understanding of the role of MIC26 in the reported disease development of diabetes, cardiomyopathy, hepatic steatosis and others (Beninca et al., 2021; Lamant et al., 2006; Peifer-Weiss et al., 2023; Tian et al., 2017; Turkieh et al., 2014). Initially, we showed that MIC26 is not present in two different forms within a variety of human and murine samples. Following, we concluded that all reported MIC26 effects can be attributed to the mitochondrial MICOS subunit MIC26. Nevertheless, sequence homology of MIC26 with the apolipoprotein A1/A4/E family members as well as reported effects on lipid metabolism suggest MIC26 to have an impact on lipoprotein metabolism as a non-classical apolipoprotein. Sequence analysis shows an overlap of AA 51-74 of MIC26 with the AA 252-275 sequence of ApoE, which has been identified as the lipid-binding domain of ApoE (Mahley et al., 2009). Using a trypsin protease protection assay, it was shown that the N-terminal domain of MIC26, including the conserved apolipoprotein lipid-binding domain, faces the mitochondrial matrix (Koob et al., 2015b). A matrix localized lipid-binding domain of MIC26 suggests an essential role of MIC26 in binding matrix located lipids. Besides a correlation between MIC26 and lipids, MIC26 shows nutrient dependent alteration of its mRNA and protein level (Chen-Lu Wu, 2013) (Guo et al., 2023). Studying two patients carrying a loss of function mutation of MIC26 showed that loss of MIC26 activities is detrimental for human health. Further, we could show that even though the integrity

of the other MICOS complex subunits remained, mitochondria showed strong ultrastructure and dynamics abnormalities, suggesting MIC26 to partially act in a MICOS independent manner. Patient failure to thrive further supports the hypothesis of MIC26 as an essential metabolic regulator. To gain insights into metabolic abnormalities caused by loss of MIC26 and to understand a possible nutritional impact on MIC26 function we performed a multi-omics study including extensive biochemical evaluations. On the one hand, we explored a regulatory role of MIC26 in mitochondrial FAO. ACAD9, involved in the first step of FAO, was reported to interact with MIC26. Thus, MIC26 could be involved in FAO by binding Acyl-CoA released by CPT2 in the mitochondrial IM and mediating the activity of ACAD9, promoting FAO. Furthermore, the loss of MIC26 was reported to reduce cellular CL levels in HAP1 cells (Anand et al., 2020). MIC26 is a MICOS complex subunit with a major localization to the CJs. Here, MIC26 could be an essential regulator of distributing CL between cristae and IBM. A change in CL composition or distribution throughout the mitochondrial IM compartments could be a possible explanation for several observed alterations in IM localized mitochondrial transporters, including SLC25A1, SLC25A12, or SLC1A5. Furthermore, our data suggest MIC26 in the integrity of the MICOS complex to interact with several metabolite transporters and alter their protein levels and activities in a nutrient dependent manner. By this MIC26 acts as a metabolic rheostat, regulating mitochondrial function as well as central metabolic pathways like glycolysis, lipid and sterol metabolism in a nutrition-dependent manner, and OXPHOS and glutaminolysis in a nutrition-independent manner. By stabilizing proper mitochondrial ultrastructure, interacting with different SLC25A family members, and possessing a matrix faced lipid binding domain, it directly or indirectly allows efficient metabolic channeling required for the metabolic adaptations in the context of cellular energy metabolism. To further understand the role of MIC26 in vivo studies employing the alterations of whole-body loss of MIC26 have to be studied. Here, an interesting target is to employ the differences of loss of MIC26 in PDM in comparison to CM. Furthermore, cell type specific effects of MIC26 have been described. This dissertation mainly focused on the effects of MIC26 in a liver derived cell line. An impact of MIC26 on lipid metabolism also suggest adipose tissue like mitochondria rich BAT as an interesting target to study. Furthermore, our study described an impact on glucose metabolism including glucose uptake and glycolysis. The SkM is known to be the organ consuming up to 80% of the nutrient delivered glucose (Merz & Thurmond, 2020). Employing effects on SkM metabolism is thus an interesting field of study. Based on that as well as reported correlation with lipotoxicity and diabetes make employing in vivo glucose homeostasis to a crucial target for further understanding the role of MIC26. Especially investigating direct interaction partners e.g. from SLC25A family will help understand the molecular mechanism, how MIC26 acts. Here a focus must lie on the investigation of different nutritional circumstances.

7 References

Aas, V., Hessvik, N. P., Wettergreen, M., Hvammen, A. W., Hallen, S., Thoresen, G. H., & Rustan, A. C. (2011). Chronic hyperglycemia reduces substrate oxidation and impairs metabolic switching of human myotubes. *Biochim Biophys Acta*, *1812*(1), 94-105. https://doi.org/10.1016/j.bbadis.2010.09.014

Acehan, D., Xu, Y., Stokes, D. L., & Schlame, M. (2007). Comparison of lymphoblast mitochondria from normal subjects and patients with Barth syndrome using electron microscopic tomography. *Lab Invest*, *87*(1), 40-48. https://doi.org/10.1038/labinvest.3700480

Adeva-Andany, M. M., Carneiro-Freire, N., Seco-Filgueira, M., Fernandez-Fernandez, C., & Mourino-Bayolo, D. (2019). Mitochondrial beta-oxidation of saturated fatty acids in humans. *Mitochondrion*, *46*, 73-90. https://doi.org/10.1016/j.mito.2018.02.009

Aguirre, V., Uchida, T., Yenush, L., Davis, R., & White, M. F. (2000). The c-Jun NH(2)-terminal kinase promotes insulin resistance during association with insulin receptor substrate-1 and phosphorylation of Ser(307). *J Biol Chem*, *275*(12), 9047-9054. https://doi.org/10.1074/jbc.275.12.9047

Alabduladhem, T. O., & Bordoni, B. (2023). Physiology, Krebs Cycle. In *StatPearls*. https://www.ncbi.nlm.nih.gov/pubmed/32310492

Alrbyawi, H., Poudel, I., Dash, R. P., Srinivas, N. R., Tiwari, A. K., Arnold, R. D., & Babu, R. J. (2019). Role of Ceramides in Drug Delivery. *AAPS PharmSciTech*, *20*(7), 287. https://doi.org/10.1208/s12249-019-1497-6

An, J., Muoio, D. M., Shiota, M., Fujimoto, Y., Cline, G. W., Shulman, G. I., Koves, T. R., Stevens, R., Millington, D., & Newgard, C. B. (2004). Hepatic expression of malonyl-CoA decarboxylase reverses muscle, liver and whole-animal insulin resistance. *Nat Med*, *10*(3), 268-274. https://doi.org/10.1038/nm995

Anand, R., Kondadi, A. K., Meisterknecht, J., Golombek, M., Nortmann, O., Riedel, J., Peifer-Weiss, L., Brocke-Ahmadinejad, N., Schlutermann, D., Stork, B., Eichmann, T. O., Wittig, I., & Reichert, A. S. (2020). MIC26 and MIC27 cooperate to regulate cardiolipin levels and the landscape of OXPHOS complexes. *Life Sci Alliance*, *3*(10). https://doi.org/10.26508/lsa.202000711

Anand, R., Reichert, A. S., & Kondadi, A. K. (2021). Emerging Roles of the MICOS Complex in Cristae Dynamics and Biogenesis. *Biology (Basel)*, *10*(7). https://doi.org/10.3390/biology10070600

Anand, R., Strecker, V., Urbach, J., Wittig, I., & Reichert, A. S. (2016). Mic13 Is Essential for Formation of Crista Junctions in Mammalian Cells. *PLoS One*, *11*(8), e0160258. https://doi.org/10.1371/journal.pone.0160258

Anand, R., Wai, T., Baker, M. J., Kladt, N., Schauss, A. C., Rugarli, E., & Langer, T. (2014). The i-AAA protease YME1L and OMA1 cleave OPA1 to balance mitochondrial fusion and fission. *J Cell Biol*, *204*(6), 919-929. https://doi.org/10.1083/jcb.201308006

Anderson, E. J., Lustig, M. E., Boyle, K. E., Woodlief, T. L., Kane, D. A., Lin, C. T., Price, J. W., 3rd, Kang, L., Rabinovitch, P. S., Szeto, H. H., Houmard, J. A., Cortright, R. N., Wasserman, D. H., & Neufer, P. D. (2009). Mitochondrial H2O2 emission and cellular redox state link excess fat intake to insulin resistance in both rodents and humans. *J Clin Invest*, *119*(3), 573-581. https://doi.org/10.1172/JCI37048

Antonicka, H., Lin, Z. Y., Janer, A., Aaltonen, M. J., Weraarpachai, W., Gingras, A. C., & Shoubridge, E. A. (2020). A High-Density Human Mitochondrial Proximity Interaction Network. *Cell Metab*, *32*(3), 479-497 e479. https://doi.org/10.1016/j.cmet.2020.07.017

Aon, M. A., Bhatt, N., & Cortassa, S. C. (2014). Mitochondrial and cellular mechanisms for managing lipid excess. *Front Physiol*, *5*, 282. https://doi.org/10.3389/fphys.2014.00282

Arnold, P. K., & Finley, L. W. S. (2023). Regulation and function of the mammalian tricarboxylic acid cycle. *J Biol Chem*, *299*(2), 102838. https://doi.org/10.1016/j.jbc.2022.102838

Bach, D., Naon, D., Pich, S., Soriano, F. X., Vega, N., Rieusset, J., Laville, M., Guillet, C., Boirie, Y., Wallberg-Henriksson, H., Manco, M., Calvani, M., Castagneto, M., Palacin, M., Mingrone, G., Zierath, J. R., Vidal, H., & Zorzano, A. (2005). Expression of Mfn2, the Charcot-Marie-Tooth neuropathy type 2A gene, in human skeletal muscle: effects of type 2 diabetes, obesity, weight loss, and the regulatory role of tumor necrosis factor alpha and interleukin-6. *Diabetes*, *54*(9), 2685-2693. https://doi.org/10.2337/diabetes.54.9.2685

Bach, D., Pich, S., Soriano, F. X., Vega, N., Baumgartner, B., Oriola, J., Daugaard, J. R., Lloberas, J., Camps, M., Zierath, J. R., Rabasa-Lhoret, R., Wallberg-Henriksson, H., Laville, M., Palacin, M., Vidal, H., Rivera, F., Brand, M., & Zorzano, A. (2003). Mitofusin-2 determines mitochondrial network architecture and mitochondrial metabolism. A novel regulatory mechanism altered in obesity. *J Biol Chem*, *278*(19), 17190-17197. https://doi.org/10.1074/jbc.M212754200

Baradaran, R., Berrisford, J. M., Minhas, G. S., & Sazanov, L. A. (2013). Crystal structure of the entire respiratory complex I. *Nature*, *494*(7438), 443-448. https://doi.org/10.1038/nature11871

Barsoum, M. J., Yuan, H., Gerencser, A. A., Liot, G., Kushnareva, Y., Graber, S., Kovacs, I., Lee, W. D., Waggoner, J., Cui, J., White, A. D., Bossy, B., Martinou, J. C., Youle, R. J., Lipton, S. A., Ellisman, M. H., Perkins, G. A., & Bossy-Wetzel, E. (2006). Nitric oxide-induced mitochondrial fission is regulated by dynamin-related GTPases in neurons. *EMBO J*, *25*(16), 3900-3911. https://doi.org/10.1038/sj.emboj.7601253

Baseler, W. A., Dabkowski, E. R., Williamson, C. L., Croston, T. L., Thapa, D., Powell, M. J., Razunguzwa, T. T., & Hollander, J. M. (2011). Proteomic alterations of distinct mitochondrial subpopulations in the type 1 diabetic heart: contribution of protein import dysfunction. *Am J Physiol Regul Integr Comp Physiol*, *300*(2), R186-200. https://doi.org/10.1152/ajpregu.00423.2010

Bassi, G., Sidhu, S. K., & Mishra, S. (2021). The Expanding Role of Mitochondria, Autophagy and Lipophagy in Steroidogenesis. *Cells*, *10*(8). https://doi.org/10.3390/cells10081851

Basu, K., Lajoie, D., Aumentado-Armstrong, T., Chen, J., Koning, R. I., Bossy, B., Bostina, M., Sik, A., Bossy-Wetzel, E., & Rouiller, I. (2017). Molecular mechanism of DRP1 assembly studied in vitro by cryo-electron microscopy. *PLoS One*, *12*(6), e0179397. https://doi.org/10.1371/journal.pone.0179397

Belgardt, B. F., Ahmed, K., Spranger, M., Latreille, M., Denzler, R., Kondratiuk, N., von Meyenn, F., Villena, F. N., Herrmanns, K., Bosco, D., Kerr-Conte, J., Pattou, F., Rulicke, T., & Stoffel, M. (2015). The microRNA-200 family regulates pancreatic beta cell survival in type 2 diabetes. *Nat Med*, *21*(6), 619-627. https://doi.org/10.1038/nm.3862

Benador, I. Y., Veliova, M., Mahdaviani, K., Petcherski, A., Wikstrom, J. D., Assali, E. A., Acin-Perez, R., Shum, M., Oliveira, M. F., Cinti, S., Sztalryd, C., Barshop, W. D., Wohlschlegel, J. A., Corkey, B. E., Liesa, M., & Shirihai, O. S. (2018). Mitochondria Bound to Lipid Droplets Have Unique Bioenergetics, Composition, and Dynamics that Support Lipid Droplet Expansion. *Cell Metab*, *27*(4), 869-885 e866. https://doi.org/10.1016/j.cmet.2018.03.003

Bence, K. K., & Birnbaum, M. J. (2021). Metabolic drivers of non-alcoholic fatty liver disease. *Mol Metab*, *50*, 101143. https://doi.org/10.1016/j.molmet.2020.101143

Beninca, C., Zanette, V., Brischigliaro, M., Johnson, M., Reyes, A., Valle, D. A. D., A, J. R., Degiorgi, A., Yeates, A., Telles, B. A., Prudent, J., Baruffini, E., ML, S. F. S., RL, R. d. S., Fernandez-Vizarra, E., Whitworth, A. J., & Zeviani, M. (2021). Mutation in the MICOS subunit gene APOO (MIC26) associated with an X-linked recessive mitochondrial myopathy, lactic acidosis, cognitive impairment and autistic features. *J Med Genet*, *58*(3), 155-167. https://doi.org/10.1136/jmedgenet-2020-106861

Bharath, L. P., Ruan, T., Li, Y., Ravindran, A., Wan, X., Nhan, J. K., Walker, M. L., Deeter, L., Goodrich, R., Johnson, E., Munday, D., Mueller, R., Kunz, D., Jones, D., Reese, V., Summers, S. A., Babu, P. V., Holland, W. L., Zhang, Q. J., . . . Symons, J. D. (2015). Ceramide-Initiated Protein Phosphatase 2A Activation Contributes to Arterial Dysfunction In Vivo. *Diabetes*, *64*(11), 3914-3926. https://doi.org/10.2337/db15-0244

Bonnard, C., Durand, A., Peyrol, S., Chanseaume, E., Chauvin, M. A., Morio, B., Vidal, H., & Rieusset, J. (2008). Mitochondrial dysfunction results from oxidative stress in the skeletal muscle of diet-induced insulin-resistant mice. *J Clin Invest*, *118*(2), 789-800. https://doi.org/10.1172/JCI32601

Bonnefont, J. P., Chretien, D., Rustin, P., Robinson, B., Vassault, A., Aupetit, J., Charpentier, C., Rabier, D., Saudubray, J. M., & Munnich, A. (1992). Alpha-ketoglutarate dehydrogenase deficiency presenting as congenital lactic acidosis. *J Pediatr*, *121*(2), 255-258. https://doi.org/10.1016/s0022-3476(05)81199-0

Bouzakri, K., Austin, R., Rune, A., Lassman, M. E., Garcia-Roves, P. M., Berger, J. P., Krook, A., Chibalin, A. V., Zhang, B. B., & Zierath, J. R. (2008). Malonyl CoenzymeA decarboxylase regulates lipid and glucose metabolism in human skeletal muscle. *Diabetes*, *57*(6), 1508-1516. https://doi.org/10.2337/db07-0583

Braathen, G. J., Sand, J. C., Lobato, A., Hoyer, H., & Russell, M. B. (2010). MFN2 point mutations occur in 3.4% of Charcot-Marie-Tooth families. An investigation of 232 Norwegian CMT families. *BMC Med Genet*, *11*, 48. https://doi.org/10.1186/1471-2350-11-48

Brandt, T., Mourier, A., Tain, L. S., Partridge, L., Larsson, N. G., & Kuhlbrandt, W. (2017). Changes of mitochondrial ultrastructure and function during ageing in mice and Drosophila. *Elife*, *6*. https://doi.org/10.7554/eLife.24662

Bresciani, N., Demagny, H., Lemos, V., Pontanari, F., Li, X., Sun, Y., Li, H., Perino, A., Auwerx, J., & Schoonjans, K. (2022). The Slc25a47 locus is a novel determinant of hepatic mitochondrial function implicated in liver fibrosis. *J Hepatol*, *77*(4), 1071-1082. https://doi.org/10.1016/j.jhep.2022.05.040

Bruce, C. R., Hoy, A. J., Turner, N., Watt, M. J., Allen, T. L., Carpenter, K., Cooney, G. J., Febbraio, M. A., & Kraegen, E. W. (2009). Overexpression of carnitine palmitoyltransferase-1 in skeletal muscle is sufficient to enhance fatty acid oxidation and improve high-fat diet-induced insulin resistance. *Diabetes*, *58*(3), 550-558. https://doi.org/10.2337/db08-1078

Buchanan, J., Mazumder, P. K., Hu, P., Chakrabarti, G., Roberts, M. W., Yun, U. J., Cooksey, R. C., Litwin, S. E., & Abel, E. D. (2005). Reduced cardiac efficiency and altered substrate metabolism precedes the onset of hyperglycemia and contractile dysfunction in two mouse models of insulin resistance and obesity. *Endocrinology*, *146*(12), 5341-5349. https://doi.org/10.1210/en.2005-0938

Bugger, H., Schwarzer, M., Chen, D., Schrepper, A., Amorim, P. A., Schoepe, M., Nguyen, T. D., Mohr, F. W., Khalimonchuk, O., Weimer, B. C., & Doenst, T. (2010). Proteomic remodelling of mitochondrial oxidative pathways in pressure overload-induced heart failure. *Cardiovasc Res*, *85*(2), 376-384. https://doi.org/10.1093/cvr/cvp344

Butow, R. A., & Avadhani, N. G. (2004). Mitochondrial signaling: the retrograde response. *Mol Cell*, *14*(1), 1-15. https://doi.org/10.1016/s1097-2765(04)00179-0

Cai, D., Yuan, M., Frantz, D. F., Melendez, P. A., Hansen, L., Lee, J., & Shoelson, S. E. (2005). Local and systemic insulin resistance resulting from hepatic activation of IKK-beta and NF-kappaB. *Nat Med*, *11*(2), 183-190. https://doi.org/10.1038/nm1166

Carvalho, F., Spier, A., Chaze, T., Matondo, M., Cossart, P., & Stavru, F. (2020). Listeria monocytogenes Exploits Mitochondrial Contact Site and Cristae Organizing System Complex Subunit Mic10 To Promote Mitochondrial Fragmentation and Cellular Infection. *mBio*, *11*(1). https://doi.org/10.1128/mBio.03171-19

Chan, D. C. (2020). Mitochondrial Dynamics and Its Involvement in Disease. *Annu Rev Pathol*, *15*, 235-259. https://doi.org/10.1146/annurev-pathmechdis-012419-032711

Chathoth, S., Ismail, M. H., Alghamdi, H. M., Zakaria, H. M., Hassan, K. A., Alshomimi, S., Vatte, C., Cyrus, C., Alsaif, H. S., Mostafa, A., Shaaban, H., & Al Ali, A. (2022). Insulin resistance induced by de novo pathway-generated C16-ceramide is associated with type 2 diabetes in an obese population. *Lipids Health Dis*, *21*(1), 24. https://doi.org/10.1186/s12944-022-01634-w

Chatzispyrou, I. A., Guerrero-Castillo, S., Held, N. M., Ruiter, J. P. N., Denis, S. W., L, I. J., Wanders, R. J., van Weeghel, M., Ferdinandusse, S., Vaz, F. M., Brandt, U., & Houtkooper, R. H. (2018). Barth syndrome cells display widespread remodeling of mitochondrial complexes without affecting metabolic flux distribution. *Biochim Biophys Acta Mol Basis Dis*, *1864*(11), 3650-3658. https://doi.org/10.1016/j.bbadis.2018.08.041

Chen, H., Detmer, S. A., Ewald, A. J., Griffin, E. E., Fraser, S. E., & Chan, D. C. (2003). Mitofusins Mfn1 and Mfn2 coordinately regulate mitochondrial fusion and are essential for embryonic development. *J Cell Biol*, *160*(2), 189-200. https://doi.org/10.1083/jcb.200211046

Chen, W., Zhao, H., & Li, Y. (2023). Mitochondrial dynamics in health and disease: mechanisms and potential targets. *Signal Transduct Target Ther*, *8*(1), 333. https://doi.org/10.1038/s41392-023-01547-9

Chen-Lu Wu, S.-P. Z. a. B.-L. Y. (2013). Microarray analysis provides new insights into the function of apolipoprotein O in HepG2 cell line. *Lipids in Health and Disease*.

Cheng, L., Deepak, R., Wang, G., Meng, Z., Tao, L., Xie, M., Chi, W., Zhang, Y., Yang, M., Liao, Y., Chen, R., Liang, Y., Zhang, J., Huang, Y., Wang, W., Guo, Z., Wang, Y., Lin, J. D., Fan, H., & Chen, L. (2023). Hepatic mitochondrial NAD + transporter SLC25A47 activates AMPKalpha mediating lipid metabolism and tumorigenesis. *Hepatology*, *78*(6), 1828-1842. https://doi.org/10.1097/HEP.0000000000000314

Chew, N. W. S., Ng, C. H., Tan, D. J. H., Kong, G., Lin, C., Chin, Y. H., Lim, W. H., Huang, D. Q., Quek, J., Fu, C. E., Xiao, J., Syn, N., Foo, R., Khoo, C. M., Wang, J. W., Dimitriadis, G. K., Young, D. Y., Siddiqui, M. S., Lam, C. S. P., . . . Muthiah, M. D. (2023). The global burden of metabolic disease: Data from 2000 to 2019. *Cell Metab*, *35*(3), 414-428 e413. https://doi.org/10.1016/j.cmet.2023.02.003

Cho, D. H., Nakamura, T., Fang, J., Cieplak, P., Godzik, A., Gu, Z., & Lipton, S. A. (2009). S-nitrosylation of Drp1 mediates beta-amyloid-related mitochondrial fission and neuronal injury. *Science*, *324*(5923), 102-105. https://doi.org/10.1126/science.1171091

Choo, H. J., Kim, J. H., Kwon, O. B., Lee, C. S., Mun, J. Y., Han, S. S., Yoon, Y. S., Yoon, G., Choi, K. M., & Ko, Y. G. (2006). Mitochondria are impaired in the adipocytes of type 2 diabetic mice. *Diabetologia*, *49*(4), 784-791. https://doi.org/10.1007/s00125-006-0170-2

Constantinescu, D., Csoka, A. B., Navara, C. S., & Schatten, G. P. (2010). Defective DSB repair correlates with abnormal nuclear morphology and is improved with FTI treatment in Hutchinson-Gilford progeria syndrome fibroblasts. *Exp Cell Res*, *316*(17), 2747-2759. https://doi.org/10.1016/j.yexcr.2010.05.015

Cross, D. A., Watt, P. W., Shaw, M., van der Kaay, J., Downes, C. P., Holder, J. C., & Cohen, P. (1997). Insulin activates protein kinase B, inhibits glycogen synthase kinase-3 and activates glycogen synthase by rapamycin-insensitive pathways in skeletal muscle and adipose tissue. *FEBS Lett*, *406*(1-2), 211-215. https://doi.org/10.1016/s0014-5793(97)00240-8

da Silva Rosa, S. C., Nayak, N., Caymo, A. M., & Gordon, J. W. (2020). Mechanisms of muscle insulin resistance and the cross-talk with liver and adipose tissue. *Physiol Rep*, *8*(19), e14607. https://doi.org/10.14814/phy2.14607

DeBerardinis, R. J., Mancuso, A., Daikhin, E., Nissim, I., Yudkoff, M., Wehrli, S., & Thompson, C. B. (2007). Beyond aerobic glycolysis: transformed cells can engage in glutamine metabolism that

exceeds the requirement for protein and nucleotide synthesis. *Proc Natl Acad Sci U S A*, *104*(49), 19345-19350. https://doi.org/10.1073/pnas.0709747104

Deng, R., Wang, W., Xu, X., Ding, J., Wang, J., Yang, S., Li, H., Shen, H., Li, X., & Chen, G. (2021). Loss of MIC60 Aggravates Neuronal Death by Inducing Mitochondrial Dysfunction in a Rat Model of Intracerebral Hemorrhage. *Mol Neurobiol*, *58*(10), 4999-5013. https://doi.org/10.1007/s12035-021-02468-w

Dikov, D., & Reichert, A. S. (2011). How to split up: lessons from mitochondria. *EMBO J*, *30*(14), 2751-2753. https://doi.org/10.1038/emboj.2011.219

DiPilato, L. M., Ahmad, F., Harms, M., Seale, P., Manganiello, V., & Birnbaum, M. J. (2015). The Role of PDE3B Phosphorylation in the Inhibition of Lipolysis by Insulin. *Mol Cell Biol*, *35*(16), 2752-2760. https://doi.org/10.1128/MCB.00422-15

Dobbins, R. L., Szczepaniak, L. S., Bentley, B., Esser, V., Myhill, J., & McGarry, J. D. (2001). Prolonged inhibition of muscle carnitine palmitoyltransferase-1 promotes intramyocellular lipid accumulation and insulin resistance in rats. *Diabetes*, *50*(1), 123-130. https://doi.org/10.2337/diabetes.50.1.123

Dobrowsky, R. T., Kamibayashi, C., Mumby, M. C., & Hannun, Y. A. (1993). Ceramide activates heterotrimeric protein phosphatase 2A. *J Biol Chem*, *268*(21), 15523-15530. https://www.ncbi.nlm.nih.gov/pubmed/8393446

Dominiczak, M. H., & Caslake, M. J. (2011). Apolipoproteins: metabolic role and clinical biochemistry applications. *Ann Clin Biochem*, *48*(Pt 6), 498-515. https://doi.org/10.1258/acb.2011.011111

Dong, J., Chen, L., Ye, F., Tang, J., Liu, B., Lin, J., Zhou, P. H., Lu, B., Wu, M., Lu, J. H., He, J. J., Engelender, S., Meng, Q., Song, Z., & He, H. (2024). Mic19 depletion impairs endoplasmic reticulum-mitochondrial contacts and mitochondrial lipid metabolism and triggers liver disease. *Nat Commun*, *15*(1), 168. https://doi.org/10.1038/s41467-023-44057-6

Dong, T., Zhang, Z. Q., Sun, L. H., Zhang, W., Zhu, Z., Lin, L., Yang, L., Lv, A., Liu, C., Li, Q., Yang, R. F., Zhang, X., Niu, Y., Chen, H. Z., Liu, D. P., & Tong, W. M. (2023). Mic60 is essential to maintain mitochondrial integrity and to prevent encephalomyopathy. *Brain Pathol*, *33*(4), e13157. https://doi.org/10.1111/bpa.13157

Dong, X. C., Copps, K. D., Guo, S., Li, Y., Kollipara, R., DePinho, R. A., & White, M. F. (2008). Inactivation of hepatic Foxo1 by insulin signaling is required for adaptive nutrient homeostasis and endocrine growth regulation. *Cell Metab*, *8*(1), 65-76. https://doi.org/10.1016/j.cmet.2008.06.006

Du, Z., Zhou, X., Lai, Y., Xu, J., Zhang, Y., Zhou, S., Feng, Z., Yu, L., Tang, Y., Wang, W., Yu, L., Tian, C., Ran, T., Chen, H., Guddat, L. W., Liu, F., Gao, Y., Rao, Z., & Gong, H. (2023). Structure of the human respiratory complex II. *Proc Natl Acad Sci U S A*, *120*(18), e2216713120. https://doi.org/10.1073/pnas.2216713120

Duvezin-Caubet, S., Koppen, M., Wagener, J., Zick, M., Israel, L., Bernacchia, A., Jagasia, R., Rugarli, E. I., Imhof, A., Neupert, W., Langer, T., & Reichert, A. S. (2007). OPA1 processing reconstituted in yeast depends on the subunit composition of the m-AAA protease in mitochondria. *Mol Biol Cell*, *18*(9), 3582-3590. https://doi.org/10.1091/mbc.e07-02-0164

Elouej, S., Harhouri, K., Le Mao, M., Baujat, G., Nampoothiri, S., Kayserili, H., Menabawy, N. A., Selim, L., Paneque, A. L., Kubisch, C., Lessel, D., Rubinsztajn, R., Charar, C., Bartoli, C., Airault, C., Deleuze, J. F., Rotig, A., Bauer, P., Pereira, C., . . . De Sandre-Giovannoli, A. (2020). Loss of MTX2 causes mandibuloacral dysplasia and links mitochondrial dysfunction to altered nuclear morphology. *Nat Commun*, *11*(1), 4589. https://doi.org/10.1038/s41467-020-18146-9

Eriksson, M., Brown, W. T., Gordon, L. B., Glynn, M. W., Singer, J., Scott, L., Erdos, M. R., Robbins, C. M., Moses, T. Y., Berglund, P., Dutra, A., Pak, E., Durkin, S., Csoka, A. B., Boehnke, M., Glover, T. W., & Collins, F. S. (2003). Recurrent de novo point mutations in lamin A cause Hutchinson-Gilford progeria syndrome. *Nature*, *423*(6937), 293-298. https://doi.org/10.1038/nature01629

Essig, M. (2020). Toxic and Metabolic Disorders: Metabolic Diseases. In J. Hodler, R. A. Kubik-Huch, & G. K. von Schulthess (Eds.), *Diseases of the Brain, Head and Neck, Spine 2020-2023: Diagnostic Imaging* (pp. 105-109). https://doi.org/10.1007/978-3-030-38490-6_9

Eura, Y., Ishihara, N., Yokota, S., & Mihara, K. (2003). Two mitofusin proteins, mammalian homologues of FZO, with distinct functions are both required for mitochondrial fusion. *J Biochem*, *134*(3), 333-344. https://doi.org/10.1093/jb/mvg150

Fahed, G., Aoun, L., Bou Zerdan, M., Allam, S., Bou Zerdan, M., Bouferraa, Y., & Assi, H. I. (2022). Metabolic Syndrome: Updates on Pathophysiology and Management in 2021. *Int J Mol Sci*, *23*(2). https://doi.org/10.3390/ijms23020786

Fan, J., Kamphorst, J. J., Mathew, R., Chung, M. K., White, E., Shlomi, T., & Rabinowitz, J. D. (2013). Glutamine-driven oxidative phosphorylation is a major ATP source in transformed mammalian cells in both normoxia and hypoxia. *Mol Syst Biol*, *9*, 712. https://doi.org/10.1038/msb.2013.65

Feng, S. T., Wang, Z. Z., Yuan, Y. H., Wang, X. L., Guo, Z. Y., Hu, J. H., Yan, X., Chen, N. H., & Zhang, Y. (2021). Inhibition of dynamin-related protein 1 ameliorates the mitochondrial ultrastructure via PINK1 and Parkin in the mice model of Parkinson's disease. *Eur J Pharmacol*, *907*, 174262. https://doi.org/10.1016/j.ejphar.2021.174262

Feng, Y., Imam Aliagan, A., Tombo, N., & Bopassa, J. C. (2023). Mitofilin Heterozygote Mice Display an Increase in Myocardial Injury and Inflammation after Ischemia/Reperfusion. *Antioxidants (Basel)*, *12*(4). https://doi.org/10.3390/antiox12040921

Ferreira-da-Silva, A., Valacca, C., Rios, E., Populo, H., Soares, P., Sobrinho-Simoes, M., Scorrano, L., Maximo, V., & Campello, S. (2015). Mitochondrial dynamics protein Drp1 is overexpressed in oncocytic thyroid tumors and regulates cancer cell migration. *PLoS One*, *10*(3), e0122308. https://doi.org/10.1371/journal.pone.0122308

Frazier, A. E., Thorburn, D. R., & Compton, A. G. (2019). Mitochondrial energy generation disorders: genes, mechanisms, and clues to pathology. *J Biol Chem*, *294*(14), 5386-5395. https://doi.org/10.1074/jbc.R117.809194

Frey, T. G., & Mannella, C. A. (2000). The internal structure of mitochondria. *Trends Biochem Sci*, *25*(7), 319-324. https://doi.org/10.1016/s0968-0004(00)01609-1

Frey, T. G., Renken, C. W., & Perkins, G. A. (2002). Insight into mitochondrial structure and function from electron tomography. *Biochim Biophys Acta*, *1555*(1-3), 196-203. https://doi.org/10.1016/s0005-2728(02)00278-5

Galkin, A. S., Grivennikova, V. G., & Vinogradov, A. D. (1999). -->H+/2e- stoichiometry in NADH-quinone reductase reactions catalyzed by bovine heart submitochondrial particles. *FEBS Lett*, *451*(2), 157-161. https://doi.org/10.1016/s0014-5793(99)00575-x

Galloway, C. A., Lee, H., Brookes, P. S., & Yoon, Y. (2014). Decreasing mitochondrial fission alleviates hepatic steatosis in a murine model of nonalcoholic fatty liver disease. *Am J Physiol Gastrointest Liver Physiol*, *307*(6), G632-641. https://doi.org/10.1152/ajpgi.00182.2014

Galloway, C. A., Lee, H., Nejjar, S., Jhun, B. S., Yu, T., Hsu, W., & Yoon, Y. (2012). Transgenic control of mitochondrial fission induces mitochondrial uncoupling and relieves diabetic oxidative stress. *Diabetes*, *61*(8), 2093-2104. https://doi.org/10.2337/db11-1640

Gan, K. X., Wang, C., Chen, J. H., Zhu, C. J., & Song, G. Y. (2013). Mitofusin-2 ameliorates high-fat diet-induced insulin resistance in liver of rats. *World J Gastroenterol*, *19*(10), 1572-1581. https://doi.org/10.3748/wjg.v19.i10.1572

Gao, C. L., Zhu, C., Zhao, Y. P., Chen, X. H., Ji, C. B., Zhang, C. M., Zhu, J. G., Xia, Z. K., Tong, M. L., & Guo, X. R. (2010). Mitochondrial dysfunction is induced by high levels of glucose and free fatty acids in 3T3-L1 adipocytes. *Mol Cell Endocrinol*, *320*(1-2), 25-33. https://doi.org/10.1016/j.mce.2010.01.039

Giachin, G., Jessop, M., Bouverot, R., Acajjaoui, S., Saidi, M., Chretien, A., Bacia-Verloop, M., Signor, L., Mas, P. J., Favier, A., Borel Meneroud, E., Hons, M., Hart, D. J., Kandiah, E., Boeri Erba, E., Buisson, A., Leonard, G., Gutsche, I., & Soler-Lopez, M. (2021). Assembly of The Mitochondrial Complex I Assembly Complex Suggests a Regulatory Role for Deflavination. *Angew Chem Int Ed Engl*, *60*(9), 4689-4697. https://doi.org/10.1002/anie.202011548

Goldman, R. D., Gruenbaum, Y., Moir, R. D., Shumaker, D. K., & Spann, T. P. (2002). Nuclear lamins: building blocks of nuclear architecture. *Genes Dev*, *16*(5), 533-547. https://doi.org/10.1101/gad.960502

Golombek, M., Tsigaras, T., Schaumkessel, Y., Hansch, S., Weidtkamp-Peters, S., Anand, R., Reichert, A. S., & Kondadi, A. K. (2024). Cristae dynamics is modulated in bioenergetically compromised mitochondria. *Life Sci Alliance*, *7*(2). https://doi.org/10.26508/lsa.202302386

Gomes, L. C., Di Benedetto, G., & Scorrano, L. (2011). During autophagy mitochondria elongate, are spared from degradation and sustain cell viability. *Nat Cell Biol*, *13*(5), 589-598. https://doi.org/10.1038/ncb2220

Guarani, V., Jardel, C., Chretien, D., Lombes, A., Benit, P., Labasse, C., Lacene, E., Bourillon, A., Imbard, A., Benoist, J. F., Dorboz, I., Gilleron, M., Goetzman, E. S., Gaignard, P., Slama, A., Elmaleh-Berges, M., Romero, N. B., Rustin, P., Ogier de Baulny, H., . . . Schiff, M. (2016). QIL1 mutation causes MICOS disassembly and early onset fatal mitochondrial encephalopathy with liver disease. *Elife*, *5*. https://doi.org/10.7554/eLife.17163

Guerrero-Castillo, S., Baertling, F., Kownatzki, D., Wessels, H. J., Arnold, S., Brandt, U., & Nijtmans, L. (2017). The Assembly Pathway of Mitochondrial Respiratory Chain Complex I. *Cell Metab*, *25*(1), 128-139. https://doi.org/10.1016/j.cmet.2016.09.002

Guido, C., Whitaker-Menezes, D., Lin, Z., Pestell, R. G., Howell, A., Zimmers, T. A., Casimiro, M. C., Aquila, S., Ando, S., Martinez-Outschoorn, U. E., Sotgia, F., & Lisanti, M. P. (2012). Mitochondrial fission induces glycolytic reprogramming in cancer-associated myofibroblasts, driving stromal lactate production, and early tumor growth. *Oncotarget*, *3*(8), 798-810. https://doi.org/10.18632/oncotarget.574

Guo, C., Sun, L., Chen, X., & Zhang, D. (2013). Oxidative stress, mitochondrial damage and neurodegenerative diseases. *Neural Regen Res*, *8*(21), 2003-2014. https://doi.org/10.3969/j.issn.1673-5374.2013.21.009

Guo, X., Hu, J., He, G., Chen, J., Yang, Y., Qin, D., Li, C., Huang, Z., Hu, D., Wei, C., Wang, F., & Yu, B. (2023). Loss of APOO (MIC26) aggravates obesity-related whitening of brown adipose tissue via PPARalpha-mediated functional interplay between mitochondria and peroxisomes. *Metabolism*, *144*, 155564. https://doi.org/10.1016/j.metabol.2023.155564

Habersetzer, J., Larrieu, I., Priault, M., Salin, B., Rossignol, R., Brethes, D., & Paumard, P. (2013). Human F1F0 ATP synthase, mitochondrial ultrastructure and OXPHOS impairment: a (super-)complex matter? *PLoS One*, *8*(10), e75429. https://doi.org/10.1371/journal.pone.0075429

Han, C. Y. (2016). Roles of Reactive Oxygen Species on Insulin Resistance in Adipose Tissue. *Diabetes Metab J*, *40*(4), 272-279. https://doi.org/10.4093/dmj.2016.40.4.272

Harner, M., Korner, C., Walther, D., Mokranjac, D., Kaesmacher, J., Welsch, U., Griffith, J., Mann, M., Reggiori, F., & Neupert, W. (2011). The mitochondrial contact site complex, a determinant of mitochondrial architecture. *EMBO J*, *30*(21), 4356-4370. https://doi.org/10.1038/emboj.2011.379

Heeren, J., & Scheja, L. (2021). Metabolic-associated fatty liver disease and lipoprotein metabolism. *Mol Metab*, *50*, 101238. https://doi.org/10.1016/j.molmet.2021.101238

Hernandez-Alvarez, M. I., Thabit, H., Burns, N., Shah, S., Brema, I., Hatunic, M., Finucane, F., Liesa, M., Chiellini, C., Naon, D., Zorzano, A., & Nolan, J. J. (2010). Subjects with early-onset type 2 diabetes show defective activation of the skeletal muscle PGC-1alpha/Mitofusin-2 regulatory

pathway in response to physical activity. *Diabetes Care*, *33*(3), 645-651. https://doi.org/10.2337/dc09-1305

Hinkle, P. C., Butow, R. A., Racker, E., & Chance, B. (1967). Partial resolution of the enzymes catalyzing oxidative phosphorylation. XV. Reverse electron transfer in the flavin-cytochrome beta region of the respiratory chain of beef heart submitochondrial particles. *J Biol Chem*, *242*(22), 5169-5173. https://www.ncbi.nlm.nih.gov/pubmed/4294331

Hinton, A., Vue, Z., & Marshall, A. (2023). Three-Dimensional Mitochondria Reconstructions of Murine Cardiac Muscle Changes in Size Across Aging. *Microsc Microanal*, *29*(29 Suppl 1), 1205-1206. https://doi.org/10.1093/micmic/ozad067.620

Hirosumi, J., Tuncman, G., Chang, L., Gorgun, C. Z., Uysal, K. T., Maeda, K., Karin, M., & Hotamisligil, G. S. (2002). A central role for JNK in obesity and insulin resistance. *Nature*, *420*(6913), 333-336. https://doi.org/10.1038/nature01137

Holland, W. L., Brozinick, J. T., Wang, L. P., Hawkins, E. D., Sargent, K. M., Liu, Y., Narra, K., Hoehn, K. L., Knotts, T. A., Siesky, A., Nelson, D. H., Karathanasis, S. K., Fontenot, G. K., Birnbaum, M. J., & Summers, S. A. (2007). Inhibition of ceramide synthesis ameliorates glucocorticoid-, saturated-fat-, and obesity-induced insulin resistance. *Cell Metab*, *5*(3), 167-179. https://doi.org/10.1016/j.cmet.2007.01.002

Hoppins, S., Collins, S. R., Cassidy-Stone, A., Hummel, E., Devay, R. M., Lackner, L. L., Westermann, B., Schuldiner, M., Weissman, J. S., & Nunnari, J. (2011). A mitochondrial-focused genetic interaction map reveals a scaffold-like complex required for inner membrane organization in mitochondria. *J Cell Biol*, *195*(2), 323-340. https://doi.org/10.1083/jcb.201107053

Horiguchi, M., Hata, S., Tsurudome, Y., & Ushijima, K. (2021). Characterizing the degeneration of nuclear membrane and mitochondria of adipose-derived mesenchymal stem cells from patients with type II diabetes. *J Cell Mol Med*, *25*(9), 4298-4306. https://doi.org/10.1111/jcmm.16484

Horvath, S. E., & Daum, G. (2013). Lipids of mitochondria. *Prog Lipid Res*, *52*(4), 590-614. https://doi.org/10.1016/j.plipres.2013.07.002

Hu, L., Ding, M., Tang, D., Gao, E., Li, C., Wang, K., Qi, B., Qiu, J., Zhao, H., Chang, P., Fu, F., & Li, Y. (2019). Targeting mitochondrial dynamics by regulating Mfn2 for therapeutic intervention in diabetic cardiomyopathy. *Theranostics*, *9*(13), 3687-3706. https://doi.org/10.7150/thno.33684

Huynen, M. A., Muhlmeister, M., Gotthardt, K., Guerrero-Castillo, S., & Brandt, U. (2016). Evolution and structural organization of the mitochondrial contact site (MICOS) complex and the mitochondrial intermembrane space bridging (MIB) complex. *Biochim Biophys Acta*, *1863*(1), 91-101. https://doi.org/10.1016/j.bbamcr.2015.10.009

Inigo, M., Deja, S., & Burgess, S. C. (2021). Ins and Outs of the TCA Cycle: The Central Role of Anaplerosis. *Annu Rev Nutr*, *41*, 19-47. https://doi.org/10.1146/annurev-nutr-120420-025558

Janer, A., Prudent, J., Paupe, V., Fahiminiya, S., Majewski, J., Sgarioto, N., Des Rosiers, C., Forest, A., Lin, Z. Y., Gingras, A. C., Mitchell, G., McBride, H. M., & Shoubridge, E. A. (2016). SLC25A46 is required for mitochondrial lipid homeostasis and cristae maintenance and is responsible for Leigh syndrome. *EMBO Mol Med*, *8*(9), 1019-1038. https://doi.org/10.15252/emmm.201506159

Jheng, H. F., Tsai, P. J., Guo, S. M., Kuo, L. H., Chang, C. S., Su, I. J., Chang, C. R., & Tsai, Y. S. (2012). Mitochondrial fission contributes to mitochondrial dysfunction and insulin resistance in skeletal muscle. *Mol Cell Biol*, *32*(2), 309-319. https://doi.org/10.1128/MCB.05603-11

Judge, A., & Dodd, M. S. (2020). Metabolism. *Essays Biochem*, *64*(4), 607-647. https://doi.org/10.1042/EBC20190041

Kashatus, J. A., Nascimento, A., Myers, L. J., Sher, A., Byrne, F. L., Hoehn, K. L., Counter, C. M., & Kashatus, D. F. (2015). Erk2 phosphorylation of Drp1 promotes mitochondrial fission and MAPK-driven tumor growth. *Mol Cell*, *57*(3), 537-551. https://doi.org/10.1016/j.molcel.2015.01.002

Kasuga, M., Zick, Y., Blithe, D. L., Crettaz, M., & Kahn, C. R. (1982). Insulin stimulates tyrosine phosphorylation of the insulin receptor in a cell-free system. *Nature*, *298*(5875), 667-669. https://doi.org/10.1038/298667a0

Kawaguchi, T., Yoshida, T., Harada, M., Hisamoto, T., Nagao, Y., Ide, T., Taniguchi, E., Kumemura, H., Hanada, S., Maeyama, M., Baba, S., Koga, H., Kumashiro, R., Ueno, T., Ogata, H., Yoshimura, A., & Sata, M. (2004). Hepatitis C virus down-regulates insulin receptor substrates 1 and 2 through up-regulation of suppressor of cytokine signaling 3. *Am J Pathol*, *165*(5), 1499-1508. https://doi.org/10.1016/S0002-9440(10)63408-6

Kim, T., Moore, J. F., Sharer, J. D., Yang, K., Wood, P. A., & Yang, Q. (2014). Carnitine Palmitoyltransferase 1b Deficient Mice Develop Severe Insulin Resistance After Prolonged High Fat Diet Feeding. *J Diabetes Metab*, *5*. https://doi.org/10.4172/2155-6156.1000401

Kishita, Y., Shimura, M., Kohda, M., Akita, M., Imai-Okazaki, A., Yatsuka, Y., Nakajima, Y., Ito, T., Ohtake, A., Murayama, K., & Okazaki, Y. (2020). A novel homozygous variant in MICOS13/QIL1 causes hepato-encephalopathy with mitochondrial DNA depletion syndrome. *Mol Genet Genomic Med*, *8*(10), e1427. https://doi.org/10.1002/mgg3.1427

Kondadi, A. K., Anand, R., Hansch, S., Urbach, J., Zobel, T., Wolf, D. M., Segawa, M., Liesa, M., Shirihai, O. S., Weidtkamp-Peters, S., & Reichert, A. S. (2020). Cristae undergo continuous cycles of membrane remodelling in a MICOS-dependent manner. *EMBO Rep*, *21*(3), e49776. https://doi.org/10.15252/embr.201949776

Kondadi, A. K., Anand, R., Hänsch, S., Urbach, J., Zobel, T., Wolf, D. M., Segawa, M., Liesa, M., Shirihai, O. S., Weidtkamp-Peters, S., & Reichert, A. S. (2020a). Cristae undergo continuous cycles of membrane remodelling in a MICOS-dependent manner. *EMBO Rep*, *21*(3), e49776. https://doi.org/10.15252/embr.201949776

Kondadi, A. K., Anand, R., & Reichert, A. S. (2019). Functional Interplay between Cristae Biogenesis, Mitochondrial Dynamics and Mitochondrial DNA Integrity. *Int J Mol Sci*, *20*(17). https://doi.org/10.3390/ijms20174311

Kondadi, A. K., Anand, R., & Reichert, A. S. (2020b). Cristae Membrane Dynamics - A Paradigm Change. *Trends Cell Biol*, *30*(12), 923-936. https://doi.org/10.1016/j.tcb.2020.08.008

Kondadi, A. K., & Reichert, A. S. (2024). Mitochondrial Dynamics at Different Levels: From Cristae Dynamics to Interorganellar Cross Talk. *Annu Rev Biophys*. https://doi.org/10.1146/annurev-biophys-030822-020736

Kong, D., Song, G., Wang, C., Ma, H., Ren, L., Nie, Q., Zhang, X., & Gan, K. (2013). Overexpression of mitofusin 2 improves translocation of glucose transporter 4 in skeletal muscle of high-fat diet-fed rats through AMP-activated protein kinase signaling. *Mol Med Rep*, *8*(1), 205-210. https://doi.org/10.3892/mmr.2013.1457

Koob, S., Barrera, M., Anand, R., & Reichert, A. S. (2015a). Data supporting the role of the non-glycosylated isoform of MIC26 in determining cristae morphology. *Data Brief*, *4*, 135-139. https://doi.org/10.1016/j.dib.2015.04.014

Koob, S., Barrera, M., Anand, R., & Reichert, A. S. (2015b). The non-glycosylated isoform of MIC26 is a constituent of the mammalian MICOS complex and promotes formation of crista junctions. *Biochim Biophys Acta*, *1853*(7), 1551-1563. https://doi.org/10.1016/j.bbamcr.2015.03.004

Koves, T. R., Ussher, J. R., Noland, R. C., Slentz, D., Mosedale, M., Ilkayeva, O., Bain, J., Stevens, R., Dyck, J. R., Newgard, C. B., Lopaschuk, G. D., & Muoio, D. M. (2008). Mitochondrial overload and incomplete fatty acid oxidation contribute to skeletal muscle insulin resistance. *Cell Metab*, *7*(1), 45-56. https://doi.org/10.1016/j.cmet.2007.10.013

Kreienkamp, R., & Gonzalo, S. (2020). Metabolic Dysfunction in Hutchinson-Gilford Progeria Syndrome. *Cells*, *9*(2). https://doi.org/10.3390/cells9020395

Kussmaul, L., & Hirst, J. (2006). The mechanism of superoxide production by NADH:ubiquinone oxidoreductase (complex I) from bovine heart mitochondria. *Proc Natl Acad Sci U S A*, *103*(20), 7607-7612. https://doi.org/10.1073/pnas.0510977103

Lamant, M., Smih, F., Harmancey, R., Philip-Couderc, P., Pathak, A., Roncalli, J., Galinier, M., Collet, X., Massabuau, P., Senard, J. M., & Rouet, P. (2006). ApoO, a novel apolipoprotein, is an original glycoprotein up-regulated by diabetes in human heart. *J Biol Chem*, *281*(47), 36289-36302. https://doi.org/10.1074/jbc.M510861200

Lane, A. N., & Fan, T. W. (2015). Regulation of mammalian nucleotide metabolism and biosynthesis. *Nucleic Acids Res*, *43*(4), 2466-2485. https://doi.org/10.1093/nar/gkv047

Lee, Y. H., Giraud, J., Davis, R. J., & White, M. F. (2003). c-Jun N-terminal kinase (JNK) mediates feedback inhibition of the insulin signaling cascade. *J Biol Chem*, *278*(5), 2896-2902. https://doi.org/10.1074/jbc.M208359200

Lenaers, G., Hamel, C., Delettre, C., Amati-Bonneau, P., Procaccio, V., Bonneau, D., Reynier, P., & Milea, D. (2012). Dominant optic atrophy. *Orphanet J Rare Dis*, *7*, 46. https://doi.org/10.1186/1750-1172-7-46

Lennicke, C., & Cocheme, H. M. (2021). Redox metabolism: ROS as specific molecular regulators of cell signaling and function. *Mol Cell*, *81*(18), 3691-3707. https://doi.org/10.1016/j.molcel.2021.08.018

Li, M., Chi, X., Wang, Y., Setrerrahmane, S., Xie, W., & Xu, H. (2022). Trends in insulin resistance: insights into mechanisms and therapeutic strategy. *Signal Transduct Target Ther*, *7*(1), 216. https://doi.org/10.1038/s41392-022-01073-0

Li, R., Jia, Z., & Trush, M. A. (2016). Defining ROS in Biology and Medicine. *React Oxyg Species (Apex)*, *1*(1), 9-21. https://doi.org/10.20455/ros.2016.803

Li, S., Brown, M. S., & Goldstein, J. L. (2010). Bifurcation of insulin signaling pathway in rat liver: mTORC1 required for stimulation of lipogenesis, but not inhibition of gluconeogenesis. *Proc Natl Acad Sci U S A*, *107*(8), 3441-3446. https://doi.org/10.1073/pnas.0914798107

Li, S., Han, S., Zhang, Q., Zhu, Y., Zhang, H., Wang, J., Zhao, Y., Zhao, J., Su, L., Li, L., Zhou, D., Ye, C., Feng, X. H., Liang, T., & Zhao, B. (2022). FUNDC2 promotes liver tumorigenesis by inhibiting MFN1-mediated mitochondrial fusion. *Nat Commun*, *13*(1), 3486. https://doi.org/10.1038/s41467-022-31187-6

Li, X., Xu, Z., Jiang, Z., Sun, L., Ji, J., Miao, J., Zhang, X., Li, X., Huang, S., Wang, T., & Zhang, L. (2014). Hypoglycemic effect of catalpol on high-fat diet/streptozotocin-induced diabetic mice by increasing skeletal muscle mitochondrial biogenesis. *Acta Biochim Biophys Sin (Shanghai)*, *46*(9), 738-748. https://doi.org/10.1093/abbs/gmu065

Li, Y., Soos, T. J., Li, X., Wu, J., Degennaro, M., Sun, X., Littman, D. R., Birnbaum, M. J., & Polakiewicz, R. D. (2004). Protein kinase C Theta inhibits insulin signaling by phosphorylating IRS1 at Ser(1101). *J Biol Chem*, *279*(44), 45304-45307. https://doi.org/10.1074/jbc.C400186200

Liesa, M., & Shirihai, O. S. (2013). Mitochondrial dynamics in the regulation of nutrient utilization and energy expenditure. *Cell Metab*, *17*(4), 491-506. https://doi.org/10.1016/j.cmet.2013.03.002

Lindh, R., Ahmad, F., Resjo, S., James, P., Yang, J. S., Fales, H. M., Manganiello, V., & Degerman, E. (2007). Multisite phosphorylation of adipocyte and hepatocyte phosphodiesterase 3B. *Biochim Biophys Acta*, *1773*(4), 584-592. https://doi.org/10.1016/j.bbamcr.2007.01.010

Lingappan, K. (2018). NF-kappaB in Oxidative Stress. *Curr Opin Toxicol*, *7*, 81-86. https://doi.org/10.1016/j.cotox.2017.11.002

Liu, Y., Rusinol, A., Sinensky, M., Wang, Y., & Zou, Y. (2006). DNA damage responses in progeroid syndromes arise from defective maturation of prelamin A. *J Cell Sci*, *119*(Pt 22), 4644-4649. https://doi.org/10.1242/jcs.03263

Locasale, J. W. (2018). New concepts in feedback regulation of glucose metabolism. *Curr Opin Syst Biol*, *8*, 32-38. https://doi.org/10.1016/j.coisb.2017.11.005

Lopez-Mejia, I. C., de Toledo, M., Chavey, C., Lapasset, L., Cavelier, P., Lopez-Herrera, C., Chebli, K., Fort, P., Beranger, G., Fajas, L., Amri, E. Z., Casas, F., & Tazi, J. (2014). Antagonistic functions of LMNA isoforms in energy expenditure and lifespan. *EMBO Rep*, *15*(5), 529-539. https://doi.org/10.1002/embr.201338126

Lopez-Vinas, E., Bentebibel, A., Gurunathan, C., Morillas, M., de Arriaga, D., Serra, D., Asins, G., Hegardt, F. G., & Gomez-Puertas, P. (2007). Definition by functional and structural analysis of two malonyl-CoA sites in carnitine palmitoyltransferase 1A. *J Biol Chem*, *282*(25), 18212-18224. https://doi.org/10.1074/jbc.M700885200

Loson, O. C., Song, Z., Chen, H., & Chan, D. C. (2013). Fis1, Mff, MiD49, and MiD51 mediate Drp1 recruitment in mitochondrial fission. *Mol Biol Cell*, *24*(5), 659-667. https://doi.org/10.1091/mbc.E12-10-0721

Lubeck, M., Derkum, N. H., Naha, R., Strohm, R., Driessen, M. D., Belgardt, B. F., Roden, M., Stuhler, K., Anand, R., Reichert, A. S., & Kondadi, A. K. (2023). MIC26 and MIC27 are bona fide subunits of the MICOS complex in mitochondria and do not exist as glycosylated apolipoproteins. *PLoS One*, *18*(6), e0286756. https://doi.org/10.1371/journal.pone.0286756

MacLean, A., Legendre, F., & Appanna, V. D. (2023). The tricarboxylic acid (TCA) cycle: a malleable metabolic network to counter cellular stress. *Crit Rev Biochem Mol Biol*, *58*(1), 81-97. https://doi.org/10.1080/10409238.2023.2201945

Mahley, R. W., Weisgraber, K. H., & Huang, Y. (2009). Apolipoprotein E: structure determines function, from atherosclerosis to Alzheimer's disease to AIDS. *J Lipid Res*, *50 Suppl*(Suppl), S183-188. https://doi.org/10.1194/jlr.R800069-JLR200

Mancini, G., Pirruccio, K., Yang, X., Bluher, M., Rodeheffer, M., & Horvath, T. L. (2019). Mitofusin 2 in Mature Adipocytes Controls Adiposity and Body Weight. *Cell Rep*, *26*(11), 2849-2858 e2844. https://doi.org/10.1016/j.celrep.2019.02.039

Mannella, C. A., Lederer, W. J., & Jafri, M. S. (2013). The connection between inner membrane topology and mitochondrial function. *J Mol Cell Cardiol*, *62*, 51-57. https://doi.org/10.1016/j.yjmcc.2013.05.001

Martinez Calejman, C., Trefely, S., Entwisle, S. W., Luciano, A., Jung, S. M., Hsiao, W., Torres, A., Hung, C. M., Li, H., Snyder, N. W., Villen, J., Wellen, K. E., & Guertin, D. A. (2020). mTORC2-AKT signaling to ATP-citrate lyase drives brown adipogenesis and de novo lipogenesis. *Nat Commun*, *11*(1), 575. https://doi.org/10.1038/s41467-020-14430-w

Martinez-Reyes, I., & Chandel, N. S. (2020). Mitochondrial TCA cycle metabolites control physiology and disease. *Nat Commun*, *11*(1), 102. https://doi.org/10.1038/s41467-019-13668-3

Mazumder, P. K., O'Neill, B. T., Roberts, M. W., Buchanan, J., Yun, U. J., Cooksey, R. C., Boudina, S., & Abel, E. D. (2004). Impaired cardiac efficiency and increased fatty acid oxidation in insulin-resistant ob/ob mouse hearts. *Diabetes*, *53*(9), 2366-2374. https://doi.org/10.2337/diabetes.53.9.2366

McClintock, D., Ratner, D., Lokuge, M., Owens, D. M., Gordon, L. B., Collins, F. S., & Djabali, K. (2007). The mutant form of lamin A that causes Hutchinson-Gilford progeria is a biomarker of cellular aging in human skin. *PLoS One*, *2*(12), e1269. https://doi.org/10.1371/journal.pone.0001269

Mehta, A., & Shapiro, M. D. (2022). Apolipoproteins in vascular biology and atherosclerotic disease. *Nat Rev Cardiol*, *19*(3), 168-179. https://doi.org/10.1038/s41569-021-00613-5

Meroni, M., Longo, M., Paolini, E., Tria, G., Ripolone, M., Napoli, L., Moggio, M., Fracanzani, A. L., & Dongiovanni, P. (2022). Expanding the phenotypic spectrum of non-alcoholic fatty liver disease and hypertriglyceridemia. *Front Nutr*, *9*, 967899. https://doi.org/10.3389/fnut.2022.967899

Merz, K. E., & Thurmond, D. C. (2020). Role of Skeletal Muscle in Insulin Resistance and Glucose Uptake. *Compr Physiol*, *10*(3), 785-809. https://doi.org/10.1002/cphy.c190029

Michalska, B. M., Kwapiszewska, K., Szczepanowska, J., Kalwarczyk, T., Patalas-Krawczyk, P., Szczepanski, K., Holyst, R., Duszynski, J., & Szymanski, J. (2018). Insight into the fission mechanism by quantitative characterization of Drp1 protein distribution in the living cell. *Sci Rep*, *8*(1), 8122. https://doi.org/10.1038/s41598-018-26578-z

Molina, A. J., Wikstrom, J. D., Stiles, L., Las, G., Mohamed, H., Elorza, A., Walzer, G., Twig, G., Katz, S., Corkey, B. E., & Shirihai, O. S. (2009). Mitochondrial networking protects beta-cells from nutrient-induced apoptosis. *Diabetes*, *58*(10), 2303-2315. https://doi.org/10.2337/db07-1781

Monzel, A. S., Enriquez, J. A., & Picard, M. (2023). Multifaceted mitochondria: moving mitochondrial science beyond function and dysfunction. *Nat Metab*, *5*(4), 546-562. https://doi.org/10.1038/s42255-023-00783-1

Mostofa, M. G., Tran, M., Gilling, S., Lee, G., Fraher, O., Jin, L., Kang, H., Park, Y. K., Lee, J. Y., Wang, L., & Shin, D. J. (2022). MicroRNA-200c coordinates HNF1 homeobox B and apolipoprotein O functions to modulate lipid homeostasis in alcoholic fatty liver disease. *J Biol Chem*, *298*(6), 101966. https://doi.org/10.1016/j.jbc.2022.101966

Mozdy, A. D., McCaffery, J. M., & Shaw, J. M. (2000). Dnm1p GTPase-mediated mitochondrial fission is a multi-step process requiring the novel integral membrane component Fis1p. *J Cell Biol*, *151*(2), 367-380. https://doi.org/10.1083/jcb.151.2.367

Murphy, M. P. (2009). How mitochondria produce reactive oxygen species. *Biochem J*, *417*(1), 1-13. https://doi.org/10.1042/BJ20081386

Myung, J., Gulesserian, T., Fountoulakis, M., & Lubec, G. (2003). Deranged hypothetical proteins Rik protein, Nit protein 2 and mitochondrial inner membrane protein, Mitofilin, in fetal Down syndrome brain. *Cell Mol Biol (Noisy-le-grand)*, *49*(5), 739-746. https://www.ncbi.nlm.nih.gov/pubmed/14528910

Naha, R., Strohm, R., Urbach, J., Wittig, I., Reichert, A. S., Kondadi, A. K., & Anand, R. (2023). SLP2 coordinates MICOS assembly and cristae morphogenesis via MIC13 and YME1L. In. bioRxiv.

Nakamura, K., Nemani, V. M., Azarbal, F., Skibinski, G., Levy, J. M., Egami, K., Munishkina, L., Zhang, J., Gardner, B., Wakabayashi, J., Sesaki, H., Cheng, Y., Finkbeiner, S., Nussbaum, R. L., Masliah, E., & Edwards, R. H. (2011). Direct membrane association drives mitochondrial fission by the Parkinson disease-associated protein alpha-synuclein. *J Biol Chem*, *286*(23), 20710-20726. https://doi.org/10.1074/jbc.M110.213538

Ngo, J., Choi, D. W., Stanley, I. A., Stiles, L., Molina, A. J. A., Chen, P. H., Lako, A., Sung, I. C. H., Goswami, R., Kim, M. Y., Miller, N., Baghdasarian, S., Kim-Vasquez, D., Jones, A. E., Roach, B., Gutierrez, V., Erion, K., Divakaruni, A. S., Liesa, M., . . . Shirihai, O. S. (2023). Mitochondrial morphology controls fatty acid utilization by changing CPT1 sensitivity to malonyl-CoA. *EMBO J*, *42*(11), e111901. https://doi.org/10.15252/embj.2022111901

Nouws, J., Te Brinke, H., Nijtmans, L. G., & Houten, S. M. (2014). ACAD9, a complex I assembly factor with a moonlighting function in fatty acid oxidation deficiencies. *Hum Mol Genet*, *23*(5), 1311-1319. https://doi.org/10.1093/hmg/ddt521

Osellame, L. D., Blacker, T. S., & Duchen, M. R. (2012). Cellular and molecular mechanisms of mitochondrial function. *Best Pract Res Clin Endocrinol Metab*, *26*(6), 711-723. https://doi.org/10.1016/j.beem.2012.05.003

Otera, H., Wang, C., Cleland, M. M., Setoguchi, K., Yokota, S., Youle, R. J., & Mihara, K. (2010). Mff is an essential factor for mitochondrial recruitment of Drp1 during mitochondrial fission in mammalian cells. *J Cell Biol*, *191*(6), 1141-1158. https://doi.org/10.1083/jcb.201007152

Ott, C., Dorsch, E., Fraunholz, M., Straub, S., & Kozjak-Pavlovic, V. (2015). Detailed analysis of the human mitochondrial contact site complex indicate a hierarchy of subunits. *PLoS One*, *10*(3), e0120213. https://doi.org/10.1371/journal.pone.0120213

Palmer, C. S., Osellame, L. D., Laine, D., Koutsopoulos, O. S., Frazier, A. E., & Ryan, M. T. (2011). MiD49 and MiD51, new components of the mitochondrial fission machinery. *EMBO Rep*, *12*(6), 565-573. https://doi.org/10.1038/embor.2011.54

Peifer-Weiss, L., Kurban, M., David, C., Lubeck, M., Kondadi, A. K., Nemer, G., Reichert, A. S., & Anand, R. (2023). A X-linked nonsense APOO/MIC26 variant causes a lethal mitochondrial disease with progeria-like phenotypes. *Clin Genet*, *104*(6), 659-668. https://doi.org/10.1111/cge.14420

Perdomo, G., Commerford, S. R., Richard, A. M., Adams, S. H., Corkey, B. E., O'Doherty, R. M., & Brown, N. F. (2004). Increased beta-oxidation in muscle cells enhances insulin-stimulated glucose metabolism and protects against fatty acid-induced insulin resistance despite intramyocellular lipid accumulation. *J Biol Chem*, *279*(26), 27177-27186. https://doi.org/10.1074/jbc.M403566200

Perez-Hernandez, C. A., Moreno-Altamirano, M. M. B., Lopez-Villegas, E. O., Butkeviciute, E., Ali, M., Kronsteiner, B., Dunachie, S. J., Dockrell, H. M., Smith, S. G., & Sanchez-Garcia, F. J. (2022). Mitochondrial Ultrastructure and Activity Are Differentially Regulated by Glycolysis-, Krebs Cycle-, and Microbiota-Derived Metabolites in Monocytes. *Biology (Basel)*, *11*(8). https://doi.org/10.3390/biology11081132

Petersen, M. C., Madiraju, A. K., Gassaway, B. M., Marcel, M., Nasiri, A. R., Butrico, G., Marcucci, M. J., Zhang, D., Abulizi, A., Zhang, X. M., Philbrick, W., Hubbard, S. R., Jurczak, M. J., Samuel, V. T., Rinehart, J., & Shulman, G. I. (2016). Insulin receptor Thr1160 phosphorylation mediates lipid-induced hepatic insulin resistance. *J Clin Invest*, *126*(11), 4361-4371. https://doi.org/10.1172/JCI86013

Petersen, M. C., & Shulman, G. I. (2018). Mechanisms of Insulin Action and Insulin Resistance. *Physiol Rev*, *98*(4), 2133-2223. https://doi.org/10.1152/physrev.00063.2017

Pfeiffer, K., Gohil, V., Stuart, R. A., Hunte, C., Brandt, U., Greenberg, M. L., & Schagger, H. (2003). Cardiolipin stabilizes respiratory chain supercomplexes. *J Biol Chem*, *278*(52), 52873-52880. https://doi.org/10.1074/jbc.M308366200

Phan, J., & Reue, K. (2005). Lipin, a lipodystrophy and obesity gene. *Cell Metab*, *1*(1), 73-83. https://doi.org/10.1016/j.cmet.2004.12.002

Philip-Couderc, P., Smih, F., Pelat, M., Vidal, C., Verwaerde, P., Pathak, A., Buys, S., Galinier, M., Senard, J. M., & Rouet, P. (2003). Cardiac transcriptome analysis in obesity-related hypertension. *Hypertension*, *41*(3), 414-421. https://doi.org/10.1161/01.HYP.0000057573.32425.95

Powell, D. J., Hajduch, E., Kular, G., & Hundal, H. S. (2003). Ceramide disables 3-phosphoinositide binding to the pleckstrin homology domain of protein kinase B (PKB)/Akt by a PKCzeta-dependent mechanism. *Mol Cell Biol*, *23*(21), 7794-7808. https://doi.org/10.1128/MCB.23.21.7794-7808.2003

Puigserver, P., Rhee, J., Donovan, J., Walkey, C. J., Yoon, J. C., Oriente, F., Kitamura, Y., Altomonte, J., Dong, H., Accili, D., & Spiegelman, B. M. (2003). Insulin-regulated hepatic gluconeogenesis through FOXO1-PGC-1alpha interaction. *Nature*, *423*(6939), 550-555. https://doi.org/10.1038/nature01667

Rabl, R., Soubannier, V., Scholz, R., Vogel, F., Mendl, N., Vasiljev-Neumeyer, A., Korner, C., Jagasia, R., Keil, T., Baumeister, W., Cyrklaff, M., Neupert, W., & Reichert, A. S. (2009). Formation of

cristae and crista junctions in mitochondria depends on antagonism between Fcj1 and Su e/g. *J Cell Biol*, *185*(6), 1047-1063. https://doi.org/10.1083/jcb.200811099

Rafikov, R., Sun, X., Rafikova, O., Louise Meadows, M., Desai, A. A., Khalpey, Z., Yuan, J. X., Fineman, J. R., & Black, S. M. (2015). Complex I dysfunction underlies the glycolytic switch in pulmonary hypertensive smooth muscle cells. *Redox Biol*, *6*, 278-286. https://doi.org/10.1016/j.redox.2015.07.016

Rampelt, H., Wollweber, F., Gerke, C., de Boer, R., van der Klei, I. J., Bohnert, M., Pfanner, N., & van der Laan, M. (2018). Assembly of the Mitochondrial Cristae Organizer Mic10 Is Regulated by Mic26-Mic27 Antagonism and Cardiolipin. *J Mol Biol*, *430*(13), 1883-1890. https://doi.org/10.1016/j.jmb.2018.04.037

Randle, P. J. (1998). Regulatory interactions between lipids and carbohydrates: the glucose fatty acid cycle after 35 years. *Diabetes Metab Rev*, *14*(4), 263-283. https://doi.org/10.1002/(sici)1099-0895(199812)14:4<263::aid-dmr233>3.0.co;2-c

Randle, P. J., Garland, P. B., Hales, C. N., & Newsholme, E. A. (1963). The glucose fatty-acid cycle. Its role in insulin sensitivity and the metabolic disturbances of diabetes mellitus. *Lancet*, *1*(7285), 785-789. https://doi.org/10.1016/s0140-6736(63)91500-9

Razak Hady, H., Blachnio-Zabielska, A. U., Szczerbinski, L., Zabielski, P., Imierska, M., Dadan, J., & Kretowski, A. J. (2019). Ceramide Content in Liver Increases Along with Insulin Resistance in Obese Patients. *J Clin Med*, *8*(12). https://doi.org/10.3390/jcm8122197

Rivera-Torres, J., Acin-Perez, R., Cabezas-Sanchez, P., Osorio, F. G., Gonzalez-Gomez, C., Megias, D., Camara, C., Lopez-Otin, C., Enriquez, J. A., Luque-Garcia, J. L., & Andres, V. (2013). Identification of mitochondrial dysfunction in Hutchinson-Gilford progeria syndrome through use of stable isotope labeling with amino acids in cell culture. *J Proteomics*, *91*, 466-477. https://doi.org/10.1016/j.jprot.2013.08.008

Roden, M. (2004). How free fatty acids inhibit glucose utilization in human skeletal muscle. *News Physiol Sci*, *19*, 92-96. https://doi.org/10.1152/nips.01459.2003

Rosen, P., Nawroth, P. P., King, G., Moller, W., Tritschler, H. J., & Packer, L. (2001). The role of oxidative stress in the onset and progression of diabetes and its complications: a summary of a Congress Series sponsored by UNESCO-MCBN, the American Diabetes Association and the German Diabetes Society. *Diabetes Metab Res Rev*, *17*(3), 189-212. https://doi.org/10.1002/dmrr.196

Rui, L., Yuan, M., Frantz, D., Shoelson, S., & White, M. F. (2002). SOCS-1 and SOCS-3 block insulin signaling by ubiquitin-mediated degradation of IRS1 and IRS2. *J Biol Chem*, *277*(44), 42394-42398. https://doi.org/10.1074/jbc.C200444200

Ruprecht, J. J., & Kunji, E. R. S. (2020). The SLC25 Mitochondrial Carrier Family: Structure and Mechanism. *Trends Biochem Sci*, *45*(3), 244-258. https://doi.org/10.1016/j.tibs.2019.11.001

Russell, B. E., Whaley, K. G., Bove, K. E., Labilloy, A., Lombardo, R. C., Hopkin, R. J., Leslie, N. D., Prada, C., Assouline, Z., Barcia, G., Bouchereau, J., Chomton, M., Debray, D., Dorboz, I., Durand, P., Gaignard, P., Habes, D., Jardel, C., Labarthe, F., . . . Schiff, M. (2019). Expanding and Underscoring the Hepato-Encephalopathic Phenotype of QIL1/MIC13. *Hepatology*, *70*(3), 1066-1070. https://doi.org/10.1002/hep.30627

Rustin, P., Bourgeron, T., Parfait, B., Chretien, D., Munnich, A., & Rotig, A. (1997). Inborn errors of the Krebs cycle: a group of unusual mitochondrial diseases in human. *Biochim Biophys Acta*, *1361*(2), 185-197. https://doi.org/10.1016/s0925-4439(97)00035-5

Ryu, D., Oh, K. J., Jo, H. Y., Hedrick, S., Kim, Y. N., Hwang, Y. J., Park, T. S., Han, J. S., Choi, C. S., Montminy, M., & Koo, S. H. (2009). TORC2 regulates hepatic insulin signaling via a mammalian phosphatidic acid phosphatase, LIPIN1. *Cell Metab*, *9*(3), 240-251. https://doi.org/10.1016/j.cmet.2009.01.007

Ryu, D., Seo, W. Y., Yoon, Y. S., Kim, Y. N., Kim, S. S., Kim, H. J., Park, T. S., Choi, C. S., & Koo, S. H. (2011). Endoplasmic reticulum stress promotes LIPIN2-dependent hepatic insulin resistance. *Diabetes*, *60*(4), 1072-1081. https://doi.org/10.2337/db10-1046

Saklayen, M. G. (2018). The Global Epidemic of the Metabolic Syndrome. *Curr Hypertens Rep*, *20*(2), 12. https://doi.org/10.1007/s11906-018-0812-z

Sangwung, P., Petersen, K. F., Shulman, G. I., & Knowles, J. W. (2020). Mitochondrial Dysfunction, Insulin Resistance, and Potential Genetic Implications. *Endocrinology*, *161*(4). https://doi.org/10.1210/endocr/bqaa017

Schmidinger, B., Weijler, A. M., Schneider, W. J., & Hermann, M. (2016). Hepatosteatosis and estrogen increase apolipoprotein O production in the chicken. *Biochimie*, *127*, 37-43. https://doi.org/10.1016/j.biochi.2016.04.017

Schubert, K. M., Scheid, M. P., & Duronio, V. (2000). Ceramide inhibits protein kinase B/Akt by promoting dephosphorylation of serine 473. *J Biol Chem*, *275*(18), 13330-13335. https://doi.org/10.1074/jbc.275.18.13330

Scott, I., & Youle, R. J. (2010). Mitochondrial fission and fusion. *Essays Biochem*, *47*, 85-98. https://doi.org/10.1042/bse0470085

Scrimieri, R., Locatelli, L., Cazzaniga, A., Cazzola, R., Malucelli, E., Sorrentino, A., Iotti, S., & Maier, J. A. (2023). Ultrastructural features mirror metabolic derangement in human endothelial cells exposed to high glucose. *Sci Rep*, *13*(1), 15133. https://doi.org/10.1038/s41598-023-42333-5

Sebastian, D., Hernandez-Alvarez, M. I., Segales, J., Sorianello, E., Munoz, J. P., Sala, D., Waget, A., Liesa, M., Paz, J. C., Gopalacharyulu, P., Oresic, M., Pich, S., Burcelin, R., Palacin, M., & Zorzano, A. (2012). Mitofusin 2 (Mfn2) links mitochondrial and endoplasmic reticulum function with insulin signaling and is essential for normal glucose homeostasis. *Proc Natl Acad Sci U S A*, *109*(14), 5523-5528. https://doi.org/10.1073/pnas.1108220109

Shao, X., Liu, Y., Zhou, M., Xu, M., Chen, Y., Huang, H., Lin, J., & Wang, Y. (2023). Dynamic evolution and mechanism of myocardial glucose metabolism in different functional phenotypes of diabetic cardiomyopathy - a study based on (18) F-FDG microPET myocardial metabolic imaging. *Diabetol Metab Syndr*, *15*(1), 64. https://doi.org/10.1186/s13098-023-01038-5

Sheka, A. C., Adeyi, O., Thompson, J., Hameed, B., Crawford, P. A., & Ikramuddin, S. (2020). Nonalcoholic Steatohepatitis: A Review. *JAMA*, *323*(12), 1175-1183. https://doi.org/10.1001/jama.2020.2298

Shen, H. M., & Liu, Z. G. (2006). JNK signaling pathway is a key modulator in cell death mediated by reactive oxygen and nitrogen species. *Free Radic Biol Med*, *40*(6), 928-939. https://doi.org/10.1016/j.freeradbiomed.2005.10.056

Shirendeb, U., Reddy, A. P., Manczak, M., Calkins, M. J., Mao, P., Tagle, D. A., & Reddy, P. H. (2011). Abnormal mitochondrial dynamics, mitochondrial loss and mutant huntingtin oligomers in Huntington's disease: implications for selective neuronal damage. *Hum Mol Genet*, *20*(7), 1438-1455. https://doi.org/10.1093/hmg/ddr024

Shirendeb, U. P., Calkins, M. J., Manczak, M., Anekonda, V., Dufour, B., McBride, J. L., Mao, P., & Reddy, P. H. (2012). Mutant huntingtin's interaction with mitochondrial protein Drp1 impairs mitochondrial biogenesis and causes defective axonal transport and synaptic degeneration in Huntington's disease. *Hum Mol Genet*, *21*(2), 406-420. https://doi.org/10.1093/hmg/ddr475

Shoelson, S. E., Lee, J., & Yuan, M. (2003). Inflammation and the IKK beta/I kappa B/NF-kappa B axis in obesity- and diet-induced insulin resistance. *Int J Obes Relat Metab Disord*, *27 Suppl 3*, S49-52. https://doi.org/10.1038/sj.ijo.0802501

Sies, H., Berndt, C., & Jones, D. P. (2017). Oxidative Stress. *Annu Rev Biochem*, *86*, 715-748. https://doi.org/10.1146/annurev-biochem-061516-045037

Signes, A., & Fernandez-Vizarra, E. (2018). Assembly of mammalian oxidative phosphorylation complexes I-V and supercomplexes. *Essays Biochem*, *62*(3), 255-270. https://doi.org/10.1042/EBC20170098

Sinha, S., Perdomo, G., Brown, N. F., & O'Doherty, R. M. (2004). Fatty acid-induced insulin resistance in L6 myotubes is prevented by inhibition of activation and nuclear localization of nuclear factor kappa B. *J Biol Chem*, *279*(40), 41294-41301. https://doi.org/10.1074/jbc.M406514200

Smeitink, J. A., Zeviani, M., Turnbull, D. M., & Jacobs, H. T. (2006). Mitochondrial medicine: a metabolic perspective on the pathology of oxidative phosphorylation disorders. *Cell Metab*, *3*(1), 9-13. https://doi.org/10.1016/j.cmet.2005.12.001

Sohn, J. H., Mutlu, B., Latorre-Muro, P., Liang, J., Bennett, C. F., Sharabi, K., Kantorovich, N., Jedrychowski, M., Gygi, S. P., Banks, A. S., & Puigserver, P. (2023). Liver mitochondrial cristae organizing protein MIC19 promotes energy expenditure and pedestrian locomotion by altering nucleotide metabolism. *Cell Metab*, *35*(8), 1356-1372 e1355. https://doi.org/10.1016/j.cmet.2023.06.015

Song, S., Attia, R. R., Connaughton, S., Niesen, M. I., Ness, G. C., Elam, M. B., Hori, R. T., Cook, G. A., & Park, E. A. (2010). Peroxisome proliferator activated receptor alpha (PPARalpha) and PPAR gamma coactivator (PGC-1alpha) induce carnitine palmitoyltransferase IA (CPT-1A) via independent gene elements. *Mol Cell Endocrinol*, *325*(1-2), 54-63. https://doi.org/10.1016/j.mce.2010.05.019

Stephan, T., Bruser, C., Deckers, M., Steyer, A. M., Balzarotti, F., Barbot, M., Behr, T. S., Heim, G., Hubner, W., Ilgen, P., Lange, F., Pacheu-Grau, D., Pape, J. K., Stoldt, S., Huser, T., Hell, S. W., Mobius, W., Rehling, P., Riedel, D., & Jakobs, S. (2020). MICOS assembly controls mitochondrial inner membrane remodeling and crista junction redistribution to mediate cristae formation. *EMBO J*, *39*(14), e104105. https://doi.org/10.15252/embj.2019104105

Strauss, M., Hofhaus, G., Schroder, R. R., & Kuhlbrandt, W. (2008). Dimer ribbons of ATP synthase shape the inner mitochondrial membrane. *EMBO J*, *27*(7), 1154-1160. https://doi.org/10.1038/emboj.2008.35

Summers, S. A., Kao, A. W., Kohn, A. D., Backus, G. S., Roth, R. A., Pessin, J. E., & Birnbaum, M. J. (1999). The role of glycogen synthase kinase 3beta in insulin-stimulated glucose metabolism. *J Biol Chem*, *274*(25), 17934-17940. https://doi.org/10.1074/jbc.274.25.17934

Takemura, G., Onoue, K., Kashimura, T., Kanamori, H., Okada, H., Tsujimoto, A., Miyazaki, N., Nakano, T., Sakaguchi, Y., & Saito, Y. (2016). Electron Microscopic Findings Are an Important Aid for Diagnosing Mitochondrial Cardiomyopathy With Mitochondrial DNA Mutation 3243A>G. *Circ Heart Fail*, *9*(7). https://doi.org/10.1161/CIRCHEARTFAILURE.116.003283

Talari, N. K., Mattam, U., Meher, N. K., Paripati, A. K., Mahadev, K., Krishnamoorthy, T., & Sepuri, N. B. V. (2023). Lipid-droplet associated mitochondria promote fatty-acid oxidation through a distinct bioenergetic pattern in male Wistar rats. *Nat Commun*, *14*(1), 766. https://doi.org/10.1038/s41467-023-36432-0

Tan, M., Mosaoa, R., Graham, G. T., Kasprzyk-Pawelec, A., Gadre, S., Parasido, E., Catalina-Rodriguez, O., Foley, P., Giaccone, G., Cheema, A., Kallakury, B., Albanese, C., Yi, C., & Avantaggiati, M. L. (2020). Inhibition of the mitochondrial citrate carrier, Slc25a1, reverts steatosis, glucose intolerance, and inflammation in preclinical models of NAFLD/NASH. *Cell Death Differ*, *27*(7), 2143-2157. https://doi.org/10.1038/s41418-020-0491-6

Tang, J., Zhang, K., Dong, J., Yan, C., Hu, C., Ji, H., Chen, L., Chen, S., Zhao, H., & Song, Z. (2020). Sam50-Mic19-Mic60 axis determines mitochondrial cristae architecture by mediating mitochondrial outer and inner membrane contact. *Cell Death Differ*, *27*(1), 146-160. https://doi.org/10.1038/s41418-019-0345-2

Thapa, D., Nichols, C. E., Lewis, S. E., Shepherd, D. L., Jagannathan, R., Croston, T. L., Tveter, K. J., Holden, A. A., Baseler, W. A., & Hollander, J. M. (2015). Transgenic overexpression of mitofilin

attenuates diabetes mellitus-associated cardiac and mitochondria dysfunction. *J Mol Cell Cardiol*, *79*, 212-223. https://doi.org/10.1016/j.yjmcc.2014.11.008

Tian, F., Wu, C. L., Yu, B. L., Liu, L., & Hu, J. R. (2017). Apolipoprotein O expression in mouse liver enhances hepatic lipid accumulation by impairing mitochondrial function. *Biochem Biophys Res Commun*, *491*(1), 8-14. https://doi.org/10.1016/j.bbrc.2017.06.128

Tilokani, L., Nagashima, S., Paupe, V., & Prudent, J. (2018). Mitochondrial dynamics: overview of molecular mechanisms. *Essays Biochem*, *62*(3), 341-360. https://doi.org/10.1042/EBC20170104

Turkieh, A., Caubere, C., Barutaut, M., Desmoulin, F., Harmancey, R., Galinier, M., Berry, M., Dambrin, C., Polidori, C., Casteilla, L., Koukoui, F., Rouet, P., & Smih, F. (2014). Apolipoprotein O is mitochondrial and promotes lipotoxicity in heart. *J Clin Invest*, *124*(5), 2277-2286. https://doi.org/10.1172/JCI74668

Turner, N., Bruce, C. R., Beale, S. M., Hoehn, K. L., So, T., Rolph, M. S., & Cooney, G. J. (2007). Excess lipid availability increases mitochondrial fatty acid oxidative capacity in muscle: evidence against a role for reduced fatty acid oxidation in lipid-induced insulin resistance in rodents. *Diabetes*, *56*(8), 2085-2092. https://doi.org/10.2337/db07-0093

Turpin, S. M., Nicholls, H. T., Willmes, D. M., Mourier, A., Brodesser, S., Wunderlich, C. M., Mauer, J., Xu, E., Hammerschmidt, P., Bronneke, H. S., Trifunovic, A., LoSasso, G., Wunderlich, F. T., Kornfeld, J. W., Bluher, M., Kronke, M., & Bruning, J. C. (2014). Obesity-induced CerS6-dependent C16:0 ceramide production promotes weight gain and glucose intolerance. *Cell Metab*, *20*(4), 678-686. https://doi.org/10.1016/j.cmet.2014.08.002

Turpin-Nolan, S. M., Hammerschmidt, P., Chen, W., Jais, A., Timper, K., Awazawa, M., Brodesser, S., & Bruning, J. C. (2019). CerS1-Derived C(18:0) Ceramide in Skeletal Muscle Promotes Obesity-Induced Insulin Resistance. *Cell Rep*, *26*(1), 1-10 e17. https://doi.org/10.1016/j.celrep.2018.12.031

Turrens, J. F., Alexandre, A., & Lehninger, A. L. (1985). Ubisemiquinone is the electron donor for superoxide formation by complex III of heart mitochondria. *Arch Biochem Biophys*, *237*(2), 408-414. https://doi.org/10.1016/0003-9861(85)90293-0

Utsumi, T., Matsuzaki, K., Kiwado, A., Tanikawa, A., Kikkawa, Y., Hosokawa, T., Otsuka, A., Iuchi, Y., Kobuchi, H., & Moriya, K. (2018). Identification and characterization of protein N-myristoylation occurring on four human mitochondrial proteins, SAMM50, TOMM40, MIC19, and MIC25. *PLoS One*, *13*(11), e0206355. https://doi.org/10.1371/journal.pone.0206355

Van Laar, V. S., Berman, S. B., & Hastings, T. G. (2016). Mic60/mitofilin overexpression alters mitochondrial dynamics and attenuates vulnerability of dopaminergic cells to dopamine and rotenone. *Neurobiol Dis*, *91*, 247-261. https://doi.org/10.1016/j.nbd.2016.03.015

Vanhorebeek, I., De Vos, R., Mesotten, D., Wouters, P. J., De Wolf-Peeters, C., & Van den Berghe, G. (2005). Protection of hepatocyte mitochondrial ultrastructure and function by strict blood glucose control with insulin in critically ill patients. *Lancet*, *365*(9453), 53-59. https://doi.org/10.1016/S0140-6736(04)17665-4

Vanisova, M., Stufkova, H., Kohoutova, M., Rakosnikova, T., Krizova, J., Klempir, J., Rysankova, I., Roth, J., Zeman, J., & Hansikova, H. (2022). Mitochondrial organization and structure are compromised in fibroblasts from patients with Huntington's disease. *Ultrastruct Pathol*, *46*(5), 462-475. https://doi.org/10.1080/01913123.2022.2100951

Villa-Bellosta, R., Rivera-Torres, J., Osorio, F. G., Acin-Perez, R., Enriquez, J. A., Lopez-Otin, C., & Andres, V. (2013). Defective extracellular pyrophosphate metabolism promotes vascular calcification in a mouse model of Hutchinson-Gilford progeria syndrome that is ameliorated on pyrophosphate treatment. *Circulation*, *127*(24), 2442-2451. https://doi.org/10.1161/CIRCULATIONAHA.112.000571

Visiedo, F., Bugatto, F., Sanchez, V., Cozar-Castellano, I., Bartha, J. L., & Perdomo, G. (2013). High glucose levels reduce fatty acid oxidation and increase triglyceride accumulation in human placenta. *Am J Physiol Endocrinol Metab*, *305*(2), E205-212. https://doi.org/10.1152/ajpendo.00032.2013

Vitali, D. G., Drwesh, L., Cichocki, B. A., Kolb, A., & Rapaport, D. (2020). The Biogenesis of Mitochondrial Outer Membrane Proteins Show Variable Dependence on Import Factors. *iScience*, *23*(1), 100779. https://doi.org/10.1016/j.isci.2019.100779

Vogel, F., Bornhovd, C., Neupert, W., & Reichert, A. S. (2006). Dynamic subcompartmentalization of the mitochondrial inner membrane. *J Cell Biol*, *175*(2), 237-247. https://doi.org/10.1083/jcb.200605138

von der Malsburg, K., Muller, J. M., Bohnert, M., Oeljeklaus, S., Kwiatkowska, P., Becker, T., Loniewska-Lwowska, A., Wiese, S., Rao, S., Milenkovic, D., Hutu, D. P., Zerbes, R. M., Schulze-Specking, A., Meyer, H. E., Martinou, J. C., Rospert, S., Rehling, P., Meisinger, C., Veenhuis, M., . . . van der Laan, M. (2011). Dual role of mitofilin in mitochondrial membrane organization and protein biogenesis. *Dev Cell*, *21*(4), 694-707. https://doi.org/10.1016/j.devcel.2011.08.026

Wai, T., Garcia-Prieto, J., Baker, M. J., Merkwirth, C., Benit, P., Rustin, P., Ruperez, F. J., Barbas, C., Ibanez, B., & Langer, T. (2015). Imbalanced OPA1 processing and mitochondrial fragmentation cause heart failure in mice. *Science*, *350*(6265), aad0116. https://doi.org/10.1126/science.aad0116

Wang, L. J., Hsu, T., Lin, H. L., & Fu, C. Y. (2020). Drosophila MICOS knockdown impairs mitochondrial structure and function and promotes mitophagy in muscle tissue. *Biol Open*, *9*(12). https://doi.org/10.1242/bio.054262

Wang, Q., Liu, Y., Zou, X., Wang, Q., An, M., Guan, X., He, J., Tong, Y., & Ji, J. (2008). The hippocampal proteomic analysis of senescence-accelerated mouse: implications of Uchl3 and mitofilin in cognitive disorder and mitochondria dysfunction in SAMP8. *Neurochem Res*, *33*(9), 1776-1782. https://doi.org/10.1007/s11064-008-9628-6

Wang, Q., Somwar, R., Bilan, P. J., Liu, Z., Jin, J., Woodgett, J. R., & Klip, A. (1999). Protein kinase B/Akt participates in GLUT4 translocation by insulin in L6 myoblasts. *Mol Cell Biol*, *19*(6), 4008-4018. https://doi.org/10.1128/MCB.19.6.4008

Wang, X., Su, B., Lee, H. G., Li, X., Perry, G., Smith, M. A., & Zhu, X. (2009). Impaired balance of mitochondrial fission and fusion in Alzheimer's disease. *J Neurosci*, *29*(28), 9090-9103. https://doi.org/10.1523/JNEUROSCI.1357-09.2009

Weber, T. A., Koob, S., Heide, H., Wittig, I., Head, B., van der Bliek, A., Brandt, U., Mittelbronn, M., & Reichert, A. S. (2013). APOOL is a cardiolipin-binding constituent of the Mitofilin/MINOS protein complex determining cristae morphology in mammalian mitochondria. *PLoS One*, *8*(5), e63683. https://doi.org/10.1371/journal.pone.0063683

Westermann, B. (2012). Bioenergetic role of mitochondrial fusion and fission. *Biochim Biophys Acta*, *1817*(10), 1833-1838. https://doi.org/10.1016/j.bbabio.2012.02.033

Wolf, D. M., Segawa, M., Kondadi, A. K., Anand, R., Bailey, S. T., Reichert, A. S., van der Bliek, A. M., Shackelford, D. B., Liesa, M., & Shirihai, O. S. (2019). Individual cristae within the same mitochondrion display different membrane potentials and are functionally independent. *EMBO J*, *38*(22), e101056. https://doi.org/10.15252/embj.2018101056

Yapa, N. M. B., Lisnyak, V., Reljic, B., & Ryan, M. T. (2021). Mitochondrial dynamics in health and disease. *FEBS Lett*, *595*(8), 1184-1204. https://doi.org/10.1002/1873-3468.14077

Yoo, H. C., Park, S. J., Nam, M., Kang, J., Kim, K., Yeo, J. H., Kim, J. K., Heo, Y., Lee, H. S., Lee, M. Y., Lee, C. W., Kang, J. S., Kim, Y. H., Lee, J., Choi, J., Hwang, G. S., Bang, S., & Han, J. M. (2020). A Variant of SLC1A5 Is a Mitochondrial Glutamine Transporter for Metabolic

Reprogramming in Cancer Cells. *Cell Metab*, *31*(2), 267-283 e212. https://doi.org/10.1016/j.cmet.2019.11.020

Yoon, Y., Krueger, E. W., Oswald, B. J., & McNiven, M. A. (2003). The mitochondrial protein hFis1 regulates mitochondrial fission in mammalian cells through an interaction with the dynamin-like protein DLP1. *Mol Cell Biol*, *23*(15), 5409-5420. https://doi.org/10.1128/MCB.23.15.5409-5420.2003

Yuan, M., Konstantopoulos, N., Lee, J., Hansen, L., Li, Z. W., Karin, M., & Shoelson, S. E. (2001). Reversal of obesity- and diet-induced insulin resistance with salicylates or targeted disruption of Ikkbeta. *Science*, *293*(5535), 1673-1677. https://doi.org/10.1126/science.1061620

Yunn, N. O., Kim, J., Ryu, S. H., & Cho, Y. (2023). A stepwise activation model for the insulin receptor. *Exp Mol Med*. https://doi.org/10.1038/s12276-023-01101-1

Zhang, G. E., Jin, H. L., Lin, X. K., Chen, C., Liu, X. S., Zhang, Q., & Yu, J. R. (2013). Anti-tumor effects of Mfn2 in gastric cancer. *Int J Mol Sci*, *14*(7), 13005-13021. https://doi.org/10.3390/ijms140713005

Zhang, L., Keung, W., Samokhvalov, V., Wang, W., & Lopaschuk, G. D. (2010). Role of fatty acid uptake and fatty acid beta-oxidation in mediating insulin resistance in heart and skeletal muscle. *Biochim Biophys Acta*, *1801*(1), 1-22. https://doi.org/10.1016/j.bbalip.2009.09.014

Zhang, M., Mileykovskaya, E., & Dowhan, W. (2002). Gluing the respiratory chain together. Cardiolipin is required for supercomplex formation in the inner mitochondrial membrane. *J Biol Chem*, *277*(46), 43553-43556. https://doi.org/10.1074/jbc.C200551200

8 Publications

8.1 Lubeck *et al.*, 2023a

Lubeck, M., Derkum, N. H., Naha, R., Strohm, R., Driessen, M. D., Belgardt, B. F., Roden, M., Stuhler, K., Anand, R., Reichert, A. S., & Kondadi, A. K. (2023).
MIC26 and MIC27 are bona fide subunits of the MICOS complex in mitochondria and do not exist as glycosylated apolipoproteins. *PLoS One*, *18*(6), e0286756. https://doi.org/10.1371/journal.pone.0286756

Author contribution Melissa Lubeck:
Conceptualization, performance, analysis, and visualization of all experiments except of mass spectrometry. Writing, review and editing of original draft together with A.K. Kondadi.

8.2 Peifer-Weiß *et al.*, 2023

Peifer-Weiß L., Kurban M., David C., **Lubeck M.**, Kondadi A. K., Nemer G., Reichert A. S., Anand R., (2023).
A X-linked nonsense APOO/MIC26 variant causes a lethal mitochondrial disease with progeria-like phenotypes. *Clin Genet*, 104(6):659-668. https://doi:10.1111/cge.14420

Author contribution Melissa Lubeck:
Investigation, methodology, analysis and visualization of **Fig. 3 A, C** and **D** and **Fig. S1**.

8.3 Lubeck *et al*., 2023b

Lubeck M., Naha R., Schaumkessel S., Westhoff P., Stefanski A., Petzsch P., Stühler K., Köhrer K., Weber A.P.M, Anand R., Reichert A.S., Kondadi A.K. (2023)
Mitochondrial Apolipoprotein MIC26 is a metabolic rheostat regulating central cellular fuel pathways. *bioRxiv,* https://doi.org/10.1101/2023.12.01.569567

Author contribution Melissa Lubeck:
Conceptualization, performance, analysis, and visualization of all experiments except of proteomic, transcriptomic and metabolomic measurements and primary data analysis and native PAGE. Writing, review and editing of original draft together with A.K. Kondadi.

9 Acknowledgements

Firstly, I would like to thank my supervisor Prof. Andreas Reichert for giving me the possibility to work on this interesting and challenging topic as well as his patient support, enthusiasm, and fruitful scientific discussions.

Further I want to thank Prof. Hadi Al-Hasani for his support and feedback as well as giving me the opportunity to be part of the great graduate school VIVID.

My special thanks to my supervisor Dr. Arun K. Kondadi for consistent support and guidance. Thank you for all the time you invested in my project as well as your continuous care and trust in me.

From the bottom of my heart, I want to thank all my colleges from BumbI for an amazing work environment. I want to thank Nick Derkum and Estelle David for their always motivated commitment in working on the MIC26 projects with me.
Special thanks to Andrea Borchardt, Gisela Pansegrau, Tanja Portugall and Sandra Schmidt for maintaining the whole lab and keeping everything (including us) under control and always providing a helping hand when required.
Furthermore, I especially want to thank Yulia Schaumkessel and Ritam Naha for over three years of scientific and emotional support in work and private belongings. You became real friends over the last years, and I could not image my PhD time without you.

Finally, I want to thank my family and friends for their support and love that encouraged and strengthened me to go through this time.
Mein größter Dank geht an meine Mama und meinen Partner Dennis. Danke Mama, dass du mich immer in allem, was ich mir vorgenommen habe, unterstützt, begleitet und vor allem an mich geglaubt hast. Danke an meinen Partner, dass du jeden Tag an meiner Seite bist, dir meine Probleme angehört, mich aufgebaut und motiviert hast nie aufzugeben.

10 Eidesstattliche Versicherung

Ich versichere an Eides Statt, dass die Dissertation von mir selbständig und ohne unzulässige fremde Hilfe unter Beachtung der „Grundsätze zur Sicherung guter wissenschaftlicher Praxis an der Heinrich-Heine-Universität Düsseldorf“ erstellt worden ist. Die aus fremden Quellen übernommenen Gedanken sind als solche kenntlich gemacht. Die Dissertation wurde in der vorgelegten oder in ähnlicher Form noch bei keiner anderen Institution eingereicht. Ich habe bisher keine erfolglosen Promotionsversuche unternommen.

Düsseldorf, den Melissa Lubeck